Boston University

OpenBU **http://open.bu.edu**

Theses & Dissertations Boston University Theses & Dissertations

2021

The role of autism gene NEXMIF in neuronal development, synapse formation, and behaviors

https://hdl.handle.net/2144/42973

Boston University

BOSTON UNIVERSITY

GRADUATE SCHOOL OF ARTS AND SCIENCES

Dissertation

THE ROLE OF AUTISM GENE NEXMIF IN NEURONAL DEVELOPMENT, SYNAPSE FORMATION, AND BEHAVIORS

By

MARGARET O'CONNOR

B.S., Rensselaer Polytechnic Institute, 2014
M.A., Boston University, 2017

Submitted in partial fulfillment of the

requirements for the degree of

Doctor of Philosophy

2021

© 2021 by
MARGARET O’CONNOR
All rights reserved

Approved by

First Reader _____

Hengye Man, M.D., Ph.D.
Professor of Biology

Second Reader _____

Xue Han, Ph.D.
Associate Professor of Biomedical Engineering

ACKNOWLEDGMENTS

I would like to thank everyone who supported me in this journey and helped to make this achievement possible. In particular, I am grateful for the guidance and support of my advisor Dr. Hengye Man. With your boundless curiosity and enthusiasm for science, you are the model of a great researcher. Thank you for being an inspiring and encouraging mentor and for all of the helpful discussions, suggestions, and insights that kept my work moving forward. I would also like to thank my committee members: Dr. Xue Han, Dr. Angela Ho, Dr. Cynthia Bradham, and Dr. Alberto Cruz-Martin. Thank you for your valuable advice and input throughout my graduate studies and for your comments during the preparation of this dissertation. Your unique perspectives and suggestions on my research have been very helpful and are greatly appreciated.

Thank you to all the members of the Man lab who have been with me on this journey. Guan, JP, Natasha, Yuda, Zach, Yuan, Qingming, Ouyang, Maggie H., Hui, Naveed, Aparna, Kathryn, Lucy, Rong, Yanmin, Xiaofei, Wen, and Yalin, thank you all for creating a helpful and friendly environment to work in. Guan, thank you for all your guidance and help in my early years as a newbie to science. JP and Natasha, thank you for welcoming me in as both mentors and friends. Yuda, thank you for sharing your drive and determination for excellence. Qingming, Hui, and Maggie H, thank you for all your expert help and for always being so cheerful. Zach and Yuan, thank you for your camaraderie through the ups and downs of this journey. Ouyang, we started in the lab together and you have stayed a great friend.

Thank you for commiserating and celebrating with me. To all the undergraduate students who helped me with this work, particularly Amanda, View, Bella, and Pedro, thank you for trusting me as your mentor and for all your hard work and contributions.

Thank you to all those in the Boston University Biology Department for their support. Dennis, Peter, Tom, Ana, Todd, Christina, and Meredith thank you for keeping everything running smoothly and always coming to my rescue when I needed something. Natalie and Diane, thank you for being great examples of strong women who can do it all. I am proud to be in your cohort. Thank you to all those who I taught with over the years. Niru, Mike, Ndidi, Chris, Cheryl, Quinn, and Kelly thank you for being great colleagues and friends. In particular, thank you to Jose for offering great advice, sharing technical tricks and experience, and being a great friend. Your rapport with both students and colleagues is a testament to your character, which I admire and look up to.

Thank you to all the friends who brought me joy outside of lab when I needed someone to lift me up. Nahomie and Katey, thank you for being great roommates and listening to all of my practice talks. Suzie, thank you for appearing in my life again in this last crazy year and being a wonderful listener and cheerleader. Clarke, you have been with me from the beginning of grad school and throughout it you have been a friend, teacher, and guide. Thank you for challenging me, encouraging me, and distracting me with many fun nights. James and Carlos, you are so much more than bandmates. Thank you for welcoming me into your

loving and amazing group. Thank you for listening to me on tough days and laughing with me on good ones. You guys are the thunder and lightning to my rain in a storm that I hope never ends.

Thank you to my loving family for cheering me on each step of the way. Team O, thank you for all the trivia nights where you listened to me ramble about the struggles of grad school. Grandma, the matriarch of the O'Connor clan, I am so glad I am able to share this achievement with you. Katie and Corey, thank you for your patience, love, and laughter. I especially would like to express my deepest thanks to my parents. Mom and Dad you always believed I would succeed even when I didn't believe it myself. Thank you for your constant support and encouragement. You have always been there for me, helping me get through the toughest moments and being the source of the brightest joys. Mom, thank you for always listening, for being my best buddy, and for your energetic spirit. Dad, thank you for teaching me the value of hard work, for being my rock I can always rely on, and for sharing your zest for life. I am so grateful to you both and would not have been able to do this without you.

THE ROLE OF AUTISM GENE NEXMIF IN NEURONAL DEVELOPMENT, SYNAPSE FORMATION, AND BEHAVIORS

MARGARET O'CONNOR

Boston University Graduate School of Arts and Sciences, 2021

Major Professor: Hengye Man, Professor of Biology

ABSTRACT

Autism spectrum disorders (ASDs) are a heterogeneous class of neurodevelopmental disorders that share the three core behavioral symptoms of impaired social interactions, communication deficits, and restrictive and repetitive behaviors. Our previous studies identified the novel X-linked ASD gene *NEXMIF* (*KIAA2022, KIDLIA*). Mutations in *NEXMIF* leading to loss of its protein product are responsible for the development of autistic features and intellectual disability in humans. However, the role NEXMIF plays in brain development and ASD remains largely unknown. Therefore, I investigated the behavioral impairments and cellular and molecular dysregulation that result from loss of NEXMIF in a transgenic mouse model. I found that male *NEXMIF*$^{-/y}$ hemizygous knockout (KO) mice replicate the behavioral alterations reported in affected humans and that cultured neurons from *NEXMIF*$^{-/y}$ KO brains show a significant decrease in neurite outgrowth, synaptic protein expression, and spine and synapse density. Loss of NEXMIF in cultured neurons also leads to altered expression of many genes including several involved in synaptic development and function. Reintroduction of

some of the downregulated genes in cultured neurons rescued the decreased spine density and synaptic AMPAR levels observed from loss of NEXMIF.

Several clinical reports have indicated that in females, haploinsufficiency of the X-linked *NEXMIF* gene causes symptoms similar to those observed in males lacking NEXMIF. Therefore, I examined the behavioral and molecular phenotypes in a transgenic mouse model of NEXMIF haploinsufficiency, female *NEXMIF*$^{+/-}$ mice. These animals displayed ASD-like behaviors, including impaired social interactions, repetitive self-grooming, and memory deficits. *NEXMIF* haploinsufficiency results in mosaic expression of the protein, resulting in two populations of neurons in the brain, those that express NEXMIF and those that do not. Interestingly, I found that both types of neurons demonstrated impairments in dendritic outgrowth, synaptic density, and the expression of important synaptic proteins. Together, these findings provide new insights into the cellular and molecular mechanisms of NEXMIF-dependent ASD and the role of NEXMIF in neurodevelopment, in both males and females.

TABLE OF CONTENTS

ACKNOWLEDGMENTS iv

TABLE OF CONTENTS ix

LIST OF TABLES xvii

LIST OF FIGURES xviii

LIST OF ABBREVIATIONS xxi

CHAPTER ONE: INTRODUCTION 1

1.1 Overview of brain development and neurodevelopment disorders 2

1.1.1 Basic structure and cellular organization of the brain 2

1.1.2 Neuronal morphology 3

1.1.3 Synaptic structure, function, and plasticity 6

1.1.4 Neuronal processes vulnerable to neurodevelopmental disorders 10

1.2 Autism spectrum disorder (ASD) 13

1.2.1 Introduction to ASD 13

1.2.2 ASD genes and genetics 14

1.2.3 Cellular and molecular alterations in ASD 16

1.2.3.1 Neurogenesis and migration in ASD 16

1.2.3.2 Neurite outgrowth and neuronal morphology in ASD 19

1.2.3.3 Synapse formation and function in ASD 21

1.2.4 Sex differences and the X chromosome in ASD 26

1.3 *NEXMIF* ASD gene and Thesis Rationale 29

1.3.1 Expression and Genetics 29

1.3.2 Clinical phenotypes 32

1.3.3 Cellular and molecular phenotypes 34

1.3.4 Thesis Rationale 35

CHAPTER TWO: MATERIALS AND METHODS 37

2.1 Materials 38

2.1.1 Plasmids 38

2.1.2 Antibodies 38

2.1.3 Drugs 38

2.1.4 Human brain tissue 38

2.1.5 Preparation and use of Aβ peptides 38

2.2 Cell culture 38

2.2.1 Primary culture of rat and mouse neurons 39

2.2.2 Culture of human embryonic kidney cell line (HEK293) 40

2.3 Plasmid transfection 40

2.4 Viral infection 41

2.4.1 Production of adenovirus and lentivirus 41

2.4.2 Intracerebroventricular viral injection 42
2.5 Cellular techniques 42
2.5.1 Immunocytochemistry 42
2.5.2 Immunohistochemistry 43
2.5.3 AMPA receptor internalization assay 44
2.5.4 AMPA receptor insertion assay 44
2.6 Biochemical techniques 45
2.6.1 Sample collection 45
2.6.2 Immunoprecipitation 46
2.6.3 Immunoblotting 47
2.6.4 Post-translational modification assays 47
2.6.5 GST assay 48
2.6.6 Synaptosome purification 49
2.7 Golgi impregnation 50
2.8 Acute brain slice preparation and LTP recording 51
2.9 Microscopy 52
2.10 Transgenic animals 53
2.10.1 Animal care and use 53
2.10.2 Genotyping 54

2.10.3 Novel object recognition test 55
2.10.4 Three chamber social test 55
2.10.5 Ultrasonic vocalization recordings 56
2.10.6 Marble burying 57
2.10.7 Grooming test 58
2.10.8 Open field test 58
2.10.9 Barnes maze spatial memory test 58
2.11 Statistical analysis 60
2.11.1 Sholl Analysis 61
CHAPTER THREE: INVESTIGATION OF BEHAVIORAL AND MOLECULAR PHENOTYPES IN NEXMIF KO MICE 67
3.1 Abstract 68
3.2 Introduction 69
3.3 Results 71
3.3.1 *NEXMIF*$^{-/y}$ mice show typical autistic features in social behavior† ... 71
3.3.2 Impaired spatial memory in *NEXMIF*$^{-/y}$ animals† 72
3.3.3 Impairments in communication by ultrasonic vocalization in *NEXMIF*$^{-/y}$ mice 73
3.3.4 Neurons from *NEXMIF*$^{-/y}$ mice show deficits in neurite extension ... 74

3.3.5 Loss of NEXMIF results in alterations in synaptic protein composition 76

3.3.6 Confirmation of synaptic impairment in neurons from *NEXMIF*$^{-/y}$ mice 77

3.3.7 Loss of NEXMIF results in deficits in synapse formation 78

3.3.8 Neurons from *NEXMIF*$^{-/y}$ animals show impairments in synaptic plasticity 79

3.3.9 Loss of NEXMIF leads to reduced expression of Nrgn and SynDig1† 80

3.3.10 Reintroduction of Nrgn and/or SynDig1 rescues synapse formation in NEXMIF null neurons 82

3.4 Discussion 83

CHAPTER FOUR: CHARACTERIZATION OF AUTISM-LIKE BEHAVIORS AND STUDY OF MOLECULAR DYSREGULATION IN HETEROZYGOUS NEXMIF FEMALE MICE 117

4.1 Abstract 118

4.2 Introduction 119

4.3 Results 121

4.3.1 *NEXMIF*$^{+/-}$ mice demonstrate autistic features in social behavior . 122

4.3.2 Increased repetitive behavior and hyperactivity in *NEXMIF*$^{+/-}$ mice 123

4.3.3 *NEXMIF*$^{+/-}$ mice show no changes in communication by ultrasonic vocalization 124

4.3.4 *NEXMIF*$^{+/-}$ mice show impairments in spatial memory 125

4.3.5 Heterozygous NEXMIF mice demonstrate mosaic expression of NEXMIF 127

4.3.6 Mosaic loss of NEXMIF impairs the development of neuronal morphology 128

4.3.7 NEXMIF haploinsufficiency results in reduced spine density 129

4.4 Discussion 131

CHAPTER FIVE: DISCUSSION, CONCLUSIONS, AND FUTURE PERSPECTIVES 160

5.1 Summary of findings 161

5.2 The role of NEXMIF in excitatory/inhibitory balance and epilepsy 163

5.3 Diversity in NEXMIF ASD phenotypes between males and females . 166

5.4 NEXMIF nuclear localization and its role in gene regulation 168

5.5 The role of NEXMIF in synapse formation and function..... 171

5.6 Conclusions and future perspectives 174

APPENDIX: ACETYLATION OF AMPA RECEPTORS REGULATES RECEPTOR TRAFFICKING AND RESCUES MEMORY DEFICITS IN ALZHEIMER'S DISEASE 176

A.1 Abstract 177

A.2 Introduction 177

A.3 Results 181

A.3.1 Aβ Induces a Reduction in AMPAR Acetylation 181

A.3.2 The Acetyltransferase p300 Causes GluA1 Acetylation† 183

A.3.3 p300-Mediated Acetylation Leads to AMPAR Stabilization 184

A.3.4 The Lysine Residues in the GluA1 C-Terminal Tail Are the Targets for p300-Mediated AMPAR Acetylation† 185

A.3.5 Acetylation of GluA1 Suppresses the Aβ-Induced Reduction of AMPAR Amount and Synaptic Accumulation 185

A.3.6 GluA1 Acetylation Mimetic Confers AMPAR Resistance to the Aβ-Induced Down-Regulation 186

A.3.7 AMPAR Acetylation Suppresses Aβ-Induced Receptor Endocytosis 187

A.3.8 Viral Brain Injection of GluA1-4KQ Restores GluA1 Expression and Synaptic Accumulation in APP/PS1 Mice† 188

A.3.9 Expression of GluA1 Acetylation Mimetic Rescues Deficits in Synaptic Plasticity in the APP/ PS1 Mice† 190

A.3.10 Expression of GluA1 Acetylation Mimetic Rescues Visual Episodic Memory Deficits in APP/ PS1 Mice† 191

A.4 Discussion 192

REFERENCES 210

CURICULUM VITAE 274

LIST OF TABLES

Table 2.1 Plasmids 63

Table 2.2 Antibodies 64

Table 2.3 Drugs 66

LIST OF FIGURES

Figure 3.1 NEXMIF knockout mice show impaired social behavior in the three-chamber social test† 88

Figure 3.2 NEXMIF knockout mice show impairments in Barnes maze spatial learning and memory† 90

Figure 3.4 Syllable classification of USV calls in NEXMIF mice 95

Figure 3.5 Neurons from *NEXMIF*$^{-/y}$ mice show a decrease in dendritic arborization 96

Figure 3.6 *NEXMIF*$^{-/y}$ neurons show impaired early axonal outgrowth 98

Figure 3.7 Altered synaptic protein composition in cultured neurons with shRNA mediated NEXMIF knockdown 100

Figure 3.8 Additional synaptic protein composition in cultured neurons with shRNA mediated NEXMIF knockdown 102

Figure 3.9 Aberrant synaptic protein composition and dendritic spines in NEXMIF KO mice 104

Figure 3.10 Reduced synaptic density from loss of NEXMIF 107

Figure 3.11 Synaptic plasticity fails in *NEXMIF*$^{-/y}$ neurons 109

Figure 3.12 Neurogranin and SynDig1 are among the most down-regulated genes from an RNAseq of neurons with loss of NEXMIF 112

Figure 3.13 Expression of neurogranin and SynDig1 is reduced from loss of NEXMIF† 113

Figure 3.14 Overexpression of neurogranin or SynDig1 can rescue synaptic deficits after loss of NEXMIF expression 116

Figure 4.1 NEXMIF heterozygous mice show abnormalities in social behaviors 138

Figure 4.2 NEXMIF heterozygous mice display aberrant marble burying behavior, increased repetitive grooming, and hyperactivity 141

Figure 4.3 NEXMIF heterozygous mice show normal communication behavior 143

Figure 4.4 NEXMIF heterozygous mice display defects in learning and memory in the Barnes maze test 146

Figure 4.5 Mosaic NEXMIF expression in the NEXMIF heterozygous mouse .. 149

Figure 4.6 Mosaic loss of NEXMIF results in a decrease in neurite outgrowth in primary neurons 151

Figure 4.7 Hippocampal neurons of NEXMIF heterozygous mice show abnormal dendritic arborization 154

Figure 4.8 NEXMIF haploinsufficiency leads to impaired axonal outgrowth 156

Figure 4.9 Aberrant dendritic spines and synapses in NEXMIF Het mice 159

Figure A.1. Aβ treatment induces a reduction in AMPAR acetylation 196

Figure A.2. Acetyltransferase p300 acetylates and stabilizes AMPARs 199

Figure A.3. Acetylation stabilizes AMPAR synaptic localization 202

Figure A.4. Acetylation blocks Aβ induced receptor internalization 204

Figure A.5. Viral brain injection of GluA1-4KQ restores GluA1 expression and synaptic accumulation† 206

Figure A.6. Overexpression of GluA1-4KQ rescues hippocampal LTP and the visual episodic memory deficit in APP/PS1 mice† 208

LIST OF ABBREVIATIONS

AAV ..... Adeno associated virus

Ace ..... Acetyl-

ACSF .....Artificial Cerebrospinal Fluid

AD .....Alzheimer's Disease

ADHD ..... Attention Deficit Hyperactivity Disorder

AHDC1 .....AT-Hook DNA Binding Motif Containing 1

AMPA ..... α-amino-3-hydroxy-5-methyl-4-isoxazolepropionic acid

AMPAR.....AMPA Receptor

ANOVA.....Analysis of Variance

APP/PS1 ..... Amyloid Precursor Protein/Presenilin 1

APV ..... (2R)-amino-5-phosphonovaleric acid

ARHGEF9.....Association with Rho Guanine Nucleotide Exchange Factor 9

ASD .....Autism Spectrum Disorder

ASPM ..... Assembly Factor for Spindle Microtubules

Aβ .....Amyloid beta

B2 ..... 5-[4-(4-Chlorobenzoyl)-1-piperazinyl]-8-nitroquinoline

BCA ..... Bicinchoninic Acid

BioGRID ..... Biological General Repository for Interaction Datasets

bp .....base pair

C646..... 4-[4-[[5-(4,5-Dimethyl-2-nitrophenyl)-2-furanyl]methylene]-4,5-dihydro-3-methyl-5-oxo-1H-pyrazol-1-yl] benzoic acid

CA .....Cornu Ammonis

$CaCl_2$ ..... Calcium Chloride

CALM1 ..... Calmodulin 1

CAMK .....Calcium/Calmodulin-Dependent Kinase

CAMKK1..... CaMK Kinase 1

CAMs..... Cell Adhesion Molecules

CBP .....CREB-binding protein

CDK19..... Cyclin Dependent Kinase 19

CDKL5.....Cyclin Dependent Kinase Like 5

CENPJ..... Centromere Protein J

CHD8..... Chromodomain Helicase DNA-Binding Protein 8

ChIPseq.....Chromatin Immunoprecipitation Sequencing

cm.....centimeter

CNTNAP2..... Contactin-Associated Protein-Like 2

Con.....Control

CREB .....Cyclic AMP Response Element Binding

Ct.....C-terminal

CTPB.....N-4-chloro-3-trifluoromethyl-phenyl)-2-ethoxy-6-pentadecyl-benzamide

Ctrl.....Control

Ctx..... Cortical

CYFIP1.....Cytoplasmic FMRP-Interacting Protein 1

DCX.....Doublecortin X

DIV .....Days In Vitro

DMEM .....Dulbecco's Modified Eagle Medium D

DMSO.....Dimethyl Sulfoxide

DNA..... Deoxyribonucleic Acid

DOCK4 ..... Dedicator Of Cytokinesis 4

DRNApred ..... DNA- and RNA-binding residues predictor

DTI.....Diffusion Tensor Imaging

DUF4683 ..... Domain of Unkown Function 4683

DYRK1A ..... Dual Specificity Tyrosine Phosphorylation Regulated Kinase 1A

E ..... Embryonic Day

E/I ..... Excitatory/Inhibitory ratio

EDTA..... Ethylenediaminetertraacetic Acid

FBS .....Fetal Bovine Serum

fEPSP.....Field Excitatory Postsynaptic Potential

FMR1..... Fragile X Mental Retardation Gene 1

GABA .....Gamma-Aminobutryic Acid

GABAR.....GABA Receptor

GAD65..... Glutamate Decarboxylase 65

GAPDH.....Glyceraldehyde 3-Phosphate Dehydrogenase

GFAP.....Glial Fibrillary Acidic Protein

GFP ..... Green Fluorescent Protein

GI..... Gastrointestinal

GluA1 .....Glutamate Receptor Subunit A1

GluA2 .....Glutamate Receptor Subunit A2

GO..... Gene Ontology

GS .....Goat Serum

GST ..... Glutathione S-Transferase

h .....hour

H_2O.....Water

HCl ..... Hydrochloric Acid

HDAC ..... Histone Deacetylase

HEK.....Human Embryonic Kidney

HEK293T ..... HEK Cell Line 293 Transformed

HEPES ..... 4-(2-hydroxyethyl)-1-piperazineethanesulfonic acid

Het ..... Heterozygous

HGNC ..... HUGO Gene Nomenclature Committee

Hip ..... Hippocampus

HPLC ..... High Performance Liquid Chromatography

HRP ..... Horseradish Peroxidase

HSP ..... Homeostatic Synaptic Plasticity

HUGO ..... Human Genome Organization

IACUC ..... Institutional Animal Care and Use Committee

IB ..... Immunoblotting

ICC ..... Immunocytochemistry

ID ..... Intellectual Disability

IHC ..... Immunohistochemistry

in ..... inches

IP ..... Immunoprecipitation

IPTG ..... Isopropyl β-D-1-thiogalactopyranoside

IQSEC2 ..... IQ Motif And Sec7 Domain 2

kb ..... kilobase

KCl..... Potassium Chloride

KD .....Knockdown

kDa ..... kilodaltons

kHz .....kilohertz

KIAA2022 ..... Kazusa Institute Gene AA2022

KIDLIA . KIAA2022 with Intellectual Disability and Language Impairment in Autism

KO ..... Knockout

L5 ..... Layer 5

LACF ..... Laboratory Animal Care Facility

LAP2α.....Lamina-associated polypeptide 2, isoform alpha

LB ..... Lysogeny Broth

LIS1 .....Lissencephaly 1

LOF .....Loss of Function

LTD.....Long-term Depression

LTP .....Long-term Potentiation

MAP2.....Microtubule-Associated Protein 2

MCHP1 ..... Microcephalin 1

MeCP2 ..... Methyl CpG Binding Protein 2

MEF2C .....Myocyte Enhancer Factor 2c

mEPSC.....Miniature Excitatory Postsynaptic Current

mg .....milligram

$MgCl_2$..... Magnesium Chloride

$MgSO_4$.....Magnesium Sulfate

min.....Minute

mIPSC .....Miniature Inhibitory Postsynaptic Current

ml..... milliliter

mm .....millimeter

mM ..... millimolar

mRNA..... Messenger Ribonucleic Acid

n ..... nano

NaCl .....Sodium Chloride

NaH_2PO_4 .....Sodium Phosphate Monobasic Monohydrate

$NaHCO_3$.....Sodium Bicarbonate

N-cadherin .....Neural-cadherin

NCK.....Non-Catalytic Region of Tyrosine Kinase

NCKAP1 ..... NCK-associated Protein 1

NDD.....Neurodevelopmental Disorder

NeuN .....Neuronal Nuclei Marker

NEUROD6 ..... Neuronal Differentiation 6

NEXMIF ..... Neurite Extension and Migration Factor

Ng ..... Neurogranin

NGF ..... Nerve Growth Factor

NIH ..... National Institute of Health

NLGN3 ..... Neuroligin 3

NLS ..... Nuclear Localization Sequence

NMDA ..... N-methyl-D-aspartate

NMDAR ..... NMDA Receptor

NOV ..... Nephroblastoma Overexpressed

NP40 ..... octylphenoxypolyethoxyethanol

Nrgn ..... Neurogranin

NRXN1 ..... Neurexin 1

ns ..... not significant

Nt ..... N-terminal

OCD ..... Obsessive Compulsive Disorder

OCT ..... Optimal Cutting Temperature

P ..... Postnatal Day

P/S ..... Penicillin/Streptomycin

p300 ..... E1A Binding Protein, 300 kDa

PAGE ..... Polyacrylamide Gel Electrophoresis

PAK1 ..... p21-Activated Kinase

PBS ..... Phosphate Buffered Saline

PCAF ..... p300/CBP-Associated Factor

PCDH ..... Protocadherin

PCR ..... Polymerase Chain Reaction

PEG ..... Polyethlyene Glycol

PEI ..... Polyethylenimine

PFC ..... Prefrontal Cortex

PRICKLE2 ..... Prickle Planar Cell Polarity Protein 2

PSD95 ..... Postsynaptic Density Protein 95 kDa

PTEN ..... Phosphate and Tensin Homolog

PVDF ..... Polyvinylidene Fluoride

qPCR ..... Quantitative Polymerase Chain Reaction

RELN ..... Reelin

REV3L ..... REV3 Like, DNA Directed Polymerase Zeta Catalytic Subunit

RGS14 ..... Regulator of G Protein Signaling 14

RhoA ..... Rho-family GTPase Ras homolog family member A

RING ..... Really Interesting New Gene

RIPA ..... Radio-Immunoprecipitation Assay

RNAseq ..... Ribonucleic Acid Sequencing

rpm ..... revolution per minute

RRE ..... Rev Response Element

RSV ..... Rous Sarcoma Virus

RT ..... Room Temperature

s ..... seconds

SCN1A ..... Sodium Voltage-Gated Channel Alpha Subunit 1

SCR ..... Scrambled

SD SynDig1

SDOC ..... Sodium Deoxycholate

SDS ..... Sodium Dodecyl Sulfate

SEM ..... Standard Error of the Mean

SFARI ..... Simmons Foundation Autism Research Initiative

SH3 ..... SRC homology 3

SHANK3 ..... SH3 and Multiple Ankyrin Repeat Domains Protein

shRNA ..... Short Hairpin Ribonucleic Acid

siRNA ..... Small Interfering Ribonucleic Acid

SIRT2 ..... Sirtuin 2

SLC17A7 .....Solute Carrier Family 17 Member 7, VGluT1

SLC6A8 .....Solute Carrier Family 6 Member 8

SVM-Prot.....Support Vector Machine Software

SynCAM ..... Synaptic Cell Adhesion Molecule

SynDig1 .....Synapse Differentiation Inducing 1

SYNGAP1..... Synaptic Ras GTPase Activating Protein 1

TAOK2.....Thousand-And-One Amino Acid Kinase 2

Tau1 .....Microtubule Associated Protein Tau

TBL1X .....Transducin Beta Like 1 X-Linked

TBST .....Tris-Buffered Saline with Tween 20

Tg .....Transgenic

TRF .....Telomeric Repeat Factor

TRIO..... Trio Rho Guanine Nucleotide Exchange Factor

TSC1 .....Tuberous Sclerosis Complex

TTX..... Tetrodotoxin

UBE3A.....Ubiquitin Protein Ligase E3A

USP46 .....Ubiquitin Specific Peptidase 46

USVs ..... Ultrasonic Vocalizations

VGat ..... Vesicular GABA Transporter

VGlut1 .....Vesicular Glutamate Transporter 1

VSVG .....Envelope Protein Env

WB.....Western Blot

WDFY3..... WD Repeat and FYVE Domain Containing 3

WDR62..... WD Repeat Domain 62

WT.....Wild type

Xa .....Active X Chromosome

XCI ..... X Chromosome Inactivation

Xi ..... Inactive X Chromosome

XLID .....X-linked Intellectual Disability

XLMR ..... X-linked Mental Retardation

Xpn .....XLMR Protein Related to Neurite Extension

α ..... Alpha

β .....Beta

γ.....Gamma

δ ..... Delta

μ .....Micro

CHAPTER ONE: INTRODUCTION

1.1 Overview of brain development and neurodevelopment disorders

1.1.1 Basic structure and cellular organization of the brain

The brain is the most complex organ in the body and is primarily made up of cells called neurons and glia. There are approximately 86 billion neurons in the human brain, which make trillions of connections, called synapses, resulting in a highly complex network (Azevedo et al., 2009). The normal development of this network is important for overall functioning of the brain.

The brain is organized into various regions based on anatomical structure and cognitive function. The neocortex makes up 80% of the of the volume of the brain and has characteristic folds and fissures (gyri and sulci) to increase its surface area (Azevedo et al., 2009; Kaas, 2013). Also known as the cerebral cortex, the neocortex is divided by the longitudinal fissure into two hemispheres, which remain connected by the corpus callosum. Each hemisphere is subdivided by the central sulcus and the lateral sulcus into four sections called the frontal, parietal, temporal, and occipital lobes.

The neurons of the cortex are organized into 6 distinct layers parallel to the surface of the brain. These layers vary in cell density and play different roles in overall brain function. For example, layer 5 (L5) is the main output layer while L4 is the main thalamic input layer and L2/3 form intracortical associations between the layers (Douglas and Martin, 2004; Feldmeyer, 2012; Schubert et al., 2007). Cortical neurons make connections with other neurons throughout the cortex but show particularly high interconnectedness with neurons within the same cortical

column. Columns are functional units of the cortex oriented perpendicular to the surface of the brain and are comprised of neurons from all 6 cortical layers (Bonhoeffer and Grinvald, 1991; Molnar, 2013; Rakic, 2008).

Other important brain regions include the hippocampus and the cerebellum. The hippocampus plays key roles in memory formation. The major components of the hippocampus include the dentate gyrus, which consists primarily of granule cells, and the cornu ammonis (CA), which consists primarily of pyramidal cells and is subdivided into four regions (CA1-CA4) (Wible, 2013). The cerebellum is located at the back of the brain and is important for movement. In humans, it is the next largest portion of the brain in volume after the cerebral cortex, and it too uses elaborate folding to increase its surface area (Ackerman, 1992; Herrup and Kuemerle, 1997). Thus, even in its complexity, the brain maintains organization within its structure to delegate and coordinate its various functions.

1.1.2 Neuronal morphology

Neurons have a complex morphology distinct from other cell types in the body. Proper development of neurons' two distinct domains, the axon and the dendrites, is crucial for normal nervous system function. The dendrites form a complex and highly branched arbor and are covered in small structures called spines that receive and integrate signals from presynaptic axons. The axon is a single, long process that extends from the cell body, or soma, of a neuron. The axon propagates signals to postsynaptic dendritic spines on a downstream neuron.

Neurons can be classified into many different subtypes based on a variety of criteria including morphological features, electrophysiological properties, gene expression, and connectivity (Van Aerde and Feldmeyer, 2015; Ascoli et al., 2008; Boudewijns et al., 2013; Donohue and Ascoli, 2008; Gentet, 2012; Gonchar et al., 2008; Kubota et al., 2011; Markram et al., 2004; Miyamae et al., 2017; Spruston, 2008; Tremblay et al., 2016). Most broadly, neurons can be classified based on the type of neurotransmitters they release, such as glutamate for glutamatergic neurons, or gamma-aminobutryric acid (GABA) for GABAergic neurons. Owning to the close relationship between form and function, the different subtypes of neurons maintain varied morphologies. One of the most abundant types of neurons in the cortex is excitatory pyramidal neurons, which are defined by the pyramidal shape of their soma and their distinct apical and basal dendritic arbors (Spruston, 2008). Even among pyramidal neurons there is diversity in their structure, for example with L2 pyramidal neurons maintaining particularly dense apical trees as compared to L3 or L5 pyramidal neurons and CA3 pyramidal neurons branching closer to the soma than CA1 pyramidal neurons (Van Aerde and Feldmeyer, 2015; Spruston, 2008). Likewise, there is variety in the morphology of inhibitory neurons, ranging from cerebellar Purkinje cells, which have a characteristic and extensively branched fan-shaped dendritic arbor, to chandelier cells, which have dense axonal branches with rows of axon terminal boutons resembling the candlesticks of a chandelier (Gentet, 2012; Markram et al., 2004; Sultan and Shi, 2018; Tremblay et al., 2016).

The stages of neurite growth in primary cultured neurons have been well characterized, making these neurons an excellent model for studying neurite development and growth (Dotti et al., 1988; Namba et al., 2015). Neurons cultured *in vitro* begin as a simple round soma, attach to a substrate, and form lamellipodia. Within 12 hours, neurons develop several immature neurites and select one neurite to elongate into the axon within 24 hours. After 5-7 days, the remaining neurites grow and branch to form the complex dendritic arbor. Both the axon and the dendrites continue to mature and, at 14 days *in vitro* (DIV), dendritic spines and synaptic connections to other neurons will form.

In vivo, excitatory neurons undergo radial migration through the cortex to form its six distinct layers. This process begins with neural progenitor cells at the ventricles undergoing asymmetrical division to self-renew the progenitor as well as produce a post-mitotic neuron. The fate of the daughter cells is highly controlled by chromatin regulators, which establish specific gene expression profiles for the renewed neural progenitor and the newly formed postmitotic neuron (Daynac and Petritsch, 2017; Homem et al., 2015; Kohwi and Doe, 2013; Lessard et al., 2007; Sokpor et al., 2017). These new neurons then migrate along radial glial scaffolds in an inside-out manner to their final destination in the brain, with the earliest neurons forming the deepest layers and the later neurons forming the outer layers (Cadwell et al., 2019; Hatanaka et al., 2016). Throughout this process, migrating neurons alter their morphology, undergoing a multipolar to bipolar transition (LoTurco and Bai, 2006). After arriving at their final destination, neurons will

undergo extensive dendritic outgrowth, followed by pruning, to create a mature structure (Riccomagno and Kolodkin, 2015). The particular morphology of the dendritic arbor is regulated for each neuronal subtype according to its particular function. The selective removal of unnecessary dendritic branches, known as pruning, is crucial for proper neural network formation. After this refinement period, dendrites begin to stabilize, though a small degree of dendritic plasticity is observed after early development (Wu et al., 1999). In contrast, cortical inhibitory interneurons undergo tangential migration. These neurons are formed from radial glial progenitor cells in the medial and caudal ganglionic eminences and migrate parallel to the ventricular surface to integrate into cortical circuits (Cadwell et al., 2019; Faux et al., 2012; Sultan and Shi, 2018).

1.1.3 Synaptic structure, function, and plasticity

Synapses are specialized structures, which connect neurons to form neural networks. Crucial for overall cognitive function, synapses transmit electrical signals from one neuron to the next using chemical neurotransmitters. Synapses are made up of a presynaptic axon terminal, the extracellular space between the neurons called the synaptic cleft, and the postsynaptic dendrite. Excitatory synapses are formed on the small, physical protrusions of dendrites called spines, while inhibitory synapses are generally formed on the dendritic shaft.

Formation of a functional synapse requires the presynaptic axon and the postsynaptic dendrite to come into close enough proximity to make contact. Axons are guided to recognize and grow towards their correct target by detecting

gradients of chemical cues and interacting with mechanical cues (Chédotal and Richards, 2010; Vitriol and Zheng, 2012). The axonal growth cone has receptors to detect molecular cues, such as netrins, neurotrophins, semaphorins, and Slits (Kolodkin and Tessier-Lavigne, 2011; McAllister, 2002; Raper and Mason, 2010). Additionally, axon pathfinding involves interactions with adhesive cues from the extracellular matrix or from neuronal surfaces expressing transmembrane proteins. These contact dependent cues include ephrins, laminin, fibronectin, and cell adhesion molecules (CAMs) (Kerstein et al., 2015; Raper and Mason, 2010).

Synaptogenesis continues after the initial contact of the axon and dendrite with mechanical changes, including stabilization of the connection and maturation of the pre- and postsynaptic structures, and recruitment of the functional molecular machinery. Synaptic adhesion molecules such as SynCAM, N-cadherin, neuroligin/neurexin, and protocadherin-γ localize to synaptic sites and help provide a physical link between the pre- and postsynaptic sites (Chamma and Thoumine, 2018; Missler et al., 2012; Waites et al., 2005; Weiner, 2006). The dynamic finger-like protrusions, called filopodia, which emerge from the dendritic shaft will mature into larger and more stable spines by the polymerization of actin into a stable core (Berry and Nedivi, 2017; Kilinc, 2018; Petzoldt and Sigrist, 2014). Mature spines have a mushroom shape with a large head for the postsynaptic synaptic machinery and a thin neck to act as a barrier for other intracellular components. In addition to the cytoskeleton, the pre- and postsynaptic sites organize a physical framework for their synaptic machinery using scaffolding molecules. The presynaptic active

zone makes use of proteins such as Bassoon, Piccolo, and RIM while the postsynaptic density includes proteins such as PSD-95, Shank, and Homer (Friedman et al., 2000; Petzoldt and Sigrist, 2014; Ziv and Fisher-Lavie, 2014). Functional synapses also require the recruitment of key molecules including synaptic vesicle exocytosis machinery such as SNARE proteins, neurotransmitter receptors such as NMDA and AMPA receptors, ion channels such as voltage-gated calcium channels, and calcium-binding molecules such as calcium calmodulin- dependent protein kinase II (CaMKII) (Munno and Syed, 2003; Waites et al., 2005).

In addition to synapse formation, synapse elimination is another key component of proper synapse development. In early development, there is an excess of synaptic growth and formation (Rakic et al., 1986). Later on, pruning occurs, in which many synapses are selectively eliminated in order to refine the connections for proper overall brain circuitry (Purves and Lichtman, 1980; Waites et al., 2005). One mechanism for synapse elimination is their activity-dependent engulfment by microglia, a type of glial cell in the brain capable of phagocytosis (Kim et al., 2017; Neniskyte and Gross, 2017; Paolicelli et al., 2011; Thion and Garel, 2018).

Once functional synapses are formed, they are capable of synaptic transmission. Transmission begins when an action potential reaches the axon terminal, causing an influx of Ca^{2+} and the subsequent exocytosis of synaptic vesicles containing neurotransmitters. The neurotransmitters are released into the

synaptic cleft and bind to neurotransmitter receptors on the surface of the dendritic spine. This initiates a signaling cascade to excite the post-synaptic neuron and propagate the signal with a new action potential (if the neurotransmitters are excitatory, such as glutamate) or to prevent excitation (if the neurotransmitters are inhibitory, such as GABA).

The strength of a synaptic connection can change in response to neuronal activity. This is a key feature of synaptic connections, known as synaptic plasticity, and is the molecular basis underlying learning and memory. There are two major types of synaptic plasticity: Hebbian plasticity and homeostatic synaptic plasticity (Davis, 2006; Marder and Goaillard, 2006; Turrigiano and Nelson, 2004).

Hebbian plasticity consists of long term alterations in synaptic strength. An enhancement in synaptic strength is known as long-term potentiation (LTP) and a reduction in strength, long-term depression (LTD). LTP can be induced by high frequency stimulation (50-100 Hz) and LTD by low frequency stimulation (0.1-1Hz). In this way, neurons are able to strengthen synaptic connections that are used frequently and spend fewer resources on connections that are not used often (Abraham et al., 2019; Bear and Malenka, 1994; Humeau and Choquet, 2019; Siegelbaum and Kandel, 1991).

Homeostatic synaptic plasticity (HSP) is a compensatory form of plasticity that balances other modulations in synaptic strength to maintain network stability using synaptic scaling. If unchecked, the self-reinforcing feedback of Hebbian plasticity could lead to runaway excitation and saturated synapses (in the case of

LTP) or synapse silencing and loss (in the case of LTD). This unstable state could change the overall excitability of the postsynaptic neuron and prevent it from effectively storing information through the differences in synaptic strengths (Turrigiano, 2012). HSP is therefore an important mechanism for maintaining the stability of the network at a set point while preserving the relative differences in synaptic strength (Keith and El-Husseini, 2008; Pozo and Goda, 2010). With prolonged increases in activity, HSP reduces synaptic strength with downscaling. In contrast, under chronic suppression of activity, HSP increases synaptic strength with upscaling. Thus, Hebbian and homeostatic plasticity work together to dynamically change synaptic strength in response to changes in activity.

In both forms of synaptic plasticity, changes in synaptic strength are mediated by changes in the expression of the excitatory glutamate receptor AMPAR at the postsynaptic surface (Diering and Huganir, 2018; Li et al., 2019a; Turrigiano, 2012). Strengthening of the synapse, such as in LTP and homeostatic up-scaling, involves insertion of more AMPARs into the synaptic surface, while weakening of the synapse, such as in LTD and homeostatic down-scaling, involves internalization of AMPARs from the surface (Li et al., 2019a; Lledo et al., 1998; Lüscher et al., 1999). This trafficking of AMPARs to and from the synaptic surface is a tightly regulated mechanism as this process is crucial for functional synaptic activity.

1.1.4 Neuronal processes vulnerable to neurodevelopmental disorders

Development of the brain is very complex and the appropriate regulation of each stage is necessary for proper cortical function. Disruption of various developmental processes can cause abnormalities in overall brain connectivity and lead to neurodevelopmental disorders (NDDs) including cortical malformations, intellectual disability, attention-deficit/hyperactivity disorder (ADHD), and autism spectrum disorder (ASD) (Morris-Rosendahl and Crocq, 2020; Parenti et al., 2020; Thapar and Rutter, 2015). As NDDs can be caused by impairments in various stages of development, they are heterogeneous in their clinical manifestations and finding a particular molecular mechanism underlying the pathology can be difficult. Some of the key developmental processes that are vulnerable to errors leading to NDDs include neurogenesis, neuronal migration, neurite extension and development, and synaptogenesis (Hu et al., 2014; Klingler et al., 2021; Zoghbi, 2003).

The first stage in neuronal development is neurogenesis. Asymmetric division of progenitor cells gives rise to neurons. Altered progenitor proliferation can change the number of neurons produced and ultimately the size of the brain. Changes in brain size are known as macrocephaly and microcephaly, where macrocephaly is an increase in brain size and microcephaly is a decrease in brain size. For example, microcephaly has been linked to mutations in genes associated with the cell cycle such as centrosome proteins (*CENPJ, MCHP1*) and spindle proteins (*ASPM, WDR62*) (Klingler et al., 2021; Pirozzi et al., 2018). When the

neural progenitors can't undergo normal cell division, there are fewer neurons formed resulting in a smaller brain.

After neuron proliferation, the next critical phase in brain development is neuronal migration. Neurons must migrate through the layers of the neocortex from their birthplace at the ventricular zone to their final destination at the cortical plate. Lissencephaly, a smooth brain, has been shown to be a cortical malformation associated with impairments in neural migration. Typically, the human brain has folds, known as gyri, creating grooves, known as sulci, which increases the surface area of the brain. In lissencephaly, there is a lack of cortical folding and often a thickening of the cortex. Lissencephaly has been linked to mutations in genes related to microtubule structural proteins or microtubule associated proteins (*LIS1, DCX*) (Hu et al., 2014; Kato and Dobyns, 2003; Tan et al., 2018). For neurons to migrate through the cortex, rapid and dynamic rearrangement of the cytoskeleton, including microtubules, is necessary. Thus, impairments in microtubule dynamics results in the inability of neurons to properly migrate.

Proper brain development involves the formation of functional neuronal connections, thus creating neural networks throughout the brain. This requires further maturation of the neurons with the development and maintenance of a complex dendritic arbor and dendritic spines. After growth of an extensive dendritic arbor and many spines, selective pruning is required to refine the neuronal connections. Therefore, in addition to errors in cytoskeletal elements (Lasser et al., 2018; Parato and Bartolini, 2021; Spence and Soderling, 2015; Yan et al.,

2016) and cell adhesion molecules (Cao and Tabuchi, 2017; Gnanapavan and Giovannoni, 2013; Parenti et al., 2020) required for the initial formation of neural circuits, impairments in pruning mechanisms, such as autophagy (Fleming and Rubinsztein, 2020; Lv and Ma, 2020; Neniskyte and Gross, 2017), can result in aberrant dendritic growth and synapse formation. This can lead to irregular network function, as observed in intellectual disability and ASD (Ameis and Catani, 2015; Betancur et al., 2009; Gilbert and Man, 2016; Lima Caldeira et al., 2019; Turner et al., 2006).

1.2 Autism spectrum disorder (ASD)

1.2.1 Introduction to ASD

Autism spectrum disorder (ASD) is a neurodevelopmental disorder with a strong genetic basis. ASDs are commonly characterized by impairments in communication, restrictive and repetitive behaviors, and deficits in social interactions (American Psychiatric Association, 2013; Chen et al., 2015a). In addition to the core ASD behavioral phenotypes, many ASDs also present with comorbid developmental, psychiatric, and physical phenotypes. Reports indicate that between about 25-70% of individuals with ASD are comorbid for intellectual disability (Chiurazzi et al., 2020; Idring et al., 2015; Maenner et al., 2020; La Malfa et al., 2004; Matson and Shoemaker, 2009). Many people with ASD also suffer from attention deficit/hyperactivity disorder (ADHD), obsessive compulsive disorder (OCD), and anxiety (Hartley et al., 2008; Simonoff et al., 2008). Other

common comorbidities include epilepsy, gastrointestinal (GI) issues, motor control problems, and sleep disorders (Limoges et al., 2005; Mannion and Leader, 2013; Nikolov et al., 2009).

The prevalence of ASDs is rising with current estimates reaching 1 in 54 individuals in the United States (Maenner et al., 2020). This increasing prevalence emphasizes the growing societal burden due to increased need for resources to care for and support individuals with a range of abilities and symptoms (Lavelle et al., 2014; Xu et al., 2019). As there is no cure for ASD, the costs of treatment and care become substantial as they accumulate over a lifetime (Agrawal et al., 2018; Buescher et al., 2014; Horlin et al., 2014). Therefore, scientific discoveries in the underlying mechanisms of ASD are essential to provide guidance for improved diagnosis and pharmacological intervention of the disorder.

1.2.2 ASD genes and genetics

ASDs are highly heterogeneous with hundreds of genetic variants implicated in its development. ASDs have a strong genetic component and are highly heritable, as seen in studies of families and twins, which indicate a high concordance rate of ASD. Different diagnostic methods result in varied estimates, but most studies agree that monozygotic twin concordance rates (~60%-90%) are much higher than dizygotic twin concordance rates (~5%-40%) (Castelbaum et al., 2020; Chen et al., 2015a; Colvert et al., 2015; Hu et al., 2019; McKernan et al., 2017; Tick et al., 2016). Additionally, the risk of ASD is higher in siblings of patients with ASD compared to that of the general population (McKernan et al., 2017; Ozonoff et al.,

2011). There also appears to be an increased inheritance of specific autistic traits and specific phenotypes (Hu et al., 2019).

However, most ASD associated genes account for no more than 1% of ASD cases (Abrahams and Geschwind, 2008; Fernandez and Scherer, 2017), emphasizing the vast genetic landscape underlying ASD pathology. Though these risk genes have diverse roles, many converge on similar developmental and molecular pathways including synapse structure and function, excitation/inhibition balance, axon and dendrite outgrowth, and neuronal connectivity (Varcin and Jeste, 2017). Genome-wide association and large-scale sequencing studies have demonstrated that the genetic variants associated with ASD risk genes can be categorized as *de novo* mutations, rare inherited variants, and copy number variations (Abrahams and Geschwind, 2008; Gaugler et al., 2014; Huguet et al., 2013; Iossifov et al., 2012; Krumm et al., 2015; Levy et al., 2011; Pinto et al., 2010; Ronemus et al., 2014; De Rubeis et al., 2014; Sanders et al., 2012; Sebat et al., 2007; Takata et al., 2016; Yu et al., 2013; Ziats and Rennert, 2016).

To make things more complicated, in addition to these monogenic disorders, ASD can occur from polygenic variation in which the sum of many small effects in risk alleles contribute together to manifest the disease (Iakoucheva et al., 2019; De La Torre-Ubieta et al., 2016; Weiner et al., 2017). Indeed, a clear, causative genetic variant has only been identified in about 25% of patients diagnosed with ASD (Fernandez and Scherer, 2017; Jeste and Geschwind, 2014; Quesnel-Vallières et al., 2019). Several studies have shown polygenic effects in

patients with ASD with more than one deleterious mutation (Guo et al., 2019; Huguet et al., 2013; Schaaf et al., 2011; Weiner et al., 2017; Ziats and Rennert, 2016). Thus, the variability in the genetics underlying ASD pathology makes studying the causative neurobiological pathways for potential treatments a major challenge.

1.2.3 Cellular and molecular alterations in ASD

Just as the genetic causes of ASD are diverse, the cellular and molecular phenotypes underlying the neuropathology can be quite varied. However, it has been observed that many risk genes converge on common molecular pathways and cellular phenotypes, which may help explain how similar behavioral phenotypes manifest from genetically heterogeneous individuals. Indeed, disruptions in the proliferation and positioning of the correct number of neurons, the growth of their neuronal processes, and the formation of the correct number of functional synapses can all lead to defects in neural network connectivity which contribute to ASD etiology (De La Torre-Ubieta et al., 2016).

1.2.3.1 Neurogenesis and migration in ASD

One recurring feature observed in ASD is an impairment in overall brain growth, leading to structural abnormalities such as micro- or macrocephaly (Chen et al., 2015a; Courchesne et al., 2011a; Donovan and Basson, 2017; Fombonne et al., 1999; Hazlett et al., 2011; Klingler et al., 2021; Lainhart et al., 1997). Microcephaly is defined as a head circumference below the 3rd percentile and

macrocephaly as that above the 97th percentile (Fombonne et al., 1999). Estimates of the prevalence of microcephaly in ASD range from 3-15% while reported rates of macrocephaly in ASD tend to be higher, ranging from 14-34% (Ben-Itzchak et al., 2013; Deutsch and Joseph, 2003; Fombonne et al., 1999; Grandgeorge et al., 2013; Lainhart et al., 2006; Miles et al., 2000; Sacco et al., 2007). Mutations in several ASD genes have been reported to cause macrocephaly including *PTEN*, *CHD8*, *PAK1*, and *WDFY3* (Abghari et al., 2019; Bernier et al., 2014; Butler et al., 2005; Buxbaum et al., 2007; Le Duc et al., 2019; Harms et al., 2018; Horn et al., 2019; McBride et al., 2010; Orrico et al., 2009; Prontera et al., 2014; Varga et al., 2009). Others have been linked to microcephaly including *DYRK1A*, *CDKL5*, and *TRIO* (Ba et al., 2016; Van Bon et al., 2016; Ji et al., 2015; Pengelly et al., 2016; Russo et al., 2009; Scala et al., 2005).

The changes in overall brain growth observed in ASD suggest underlying impairments in mechanisms such as neuron proliferation and differentiation. Indeed, a number of ASD-associated genes converge on neurogenesis as part of their underlying pathobiology (Courchesne et al., 2011b, 2019; Kaushik and Zarbalis, 2016; Marchetto et al., 2017; Mariani et al., 2015; Packer, 2016; Pinto et al., 2010; Stoner et al., 2014). For example, *CHD8* deficiency in mice has been shown to increase brain weight and volume and to increase proliferation during neurogenesis (Gompers et al., 2017; Katayama et al., 2016; Platt et al., 2017). Similarly, mice lacking *WDFY3* show macrocephaly and excess proliferation of neuronal progenitor cells (Le Duc et al., 2019; Orosco et al., 2014). Also,

conditional knockdown of BAF170 promoted indirect neurogenesis through the increased production of intermediate progenitors from radial glial cells, ultimately resulting in an increased number of neurons and an enlarged cortex (Tuoc et al., 2013). Loss of *PTEN* is well known for its connection to macrocephaly and has been shown to enhance pro-growth pathways leading to enhanced proliferation (Amiri et al., 2012; Chen et al., 2015b; Fraser et al., 2004; Gregorian et al., 2009; Groszer et al., 2001). Conversely, *PAK1* deficiency in mice reduces the number of neurons in several layers of the cortex and the pool of proliferating progenitor cells (Pan et al., 2015). Thus, altered neuronal proliferation can have a profound effect on brain size and overall cortical development in ASD.

Postmortem studies of brain tissue from individuals with ASD provide evidence to support impaired neuronal migration as an underlying neurobiological mechanism in ASD. Abnormalities in cytoarchitectural organization have been observed including ectopic cell clustering, cortical disorganization, aberrant laminar distribution of neurons, and irregular gray-white matter boundaries (Avino and Hutsler, 2010; Stoner et al., 2014; Wegiel et al., 2010). Further support for migration defects to play a role in ASD pathogenesis comes from the fact that several ASD risk genes have been implicated in neuronal migration. Of particular note is *RELN*, which is well known for its role in neuronal migration (Reiner et al., 2016; Wasser and Herz, 2017). Indeed, loss of *RELN* in humans has been shown to cause lissencephaly with cerebellar hypoplasia (Hong et al., 2000) and the *RELN* KO mouse, *reeler*¸ demonstrates layer disorganization throughout the

cortex due to abnormal neuron migration (Badea et al., 2007; Boyle et al., 2011; Curran and D'Arcangelo, 1998; D'Arcangelo et al., 1995; Hirotsune et al., 1995; Yabut et al., 2007). Additionally, loss of *CNTNAP2* in humans leads to abnormal neuron organization in clusters and ectopic neurons in the white matter (Alarcón et al., 2008; Rodenas-Cuadrado et al., 2014; Strauss et al., 2006; Whitehouse et al., 2011) and in mice leads to abnormal distribution of neurons in groups and ectopic neurons in the corpus callosum (Peñagarikano et al., 2011). Loss of *NCKAP1* has been shown to promote neuronal migration (Guo et al., 2020) while premature, ectopic expression inhibits neuronal migration (Yokota et al., 2007). Altered migration has also been observed from reduced expression of *PTEN* (Li et al., 2002), *PAK1* (Causeret et al., 2009), and *TRIO* (Peng et al., 2010). These studies support a likely role for impaired neuronal migration in improper positioning for circuit-level organization in ASD.

1.2.3.2 Neurite outgrowth and neuronal morphology in ASD

Disruptions in functional connectivity are considered a major defect in ASD (Carroll et al., 2021; Geschwind and Levitt, 2007; Hull et al., 2017). Indeed, functional imaging studies suggest there is local hyperconnectivity and long-range hypoconnectivity in ASD brains (Belmonte et al., 2004; Cooper et al., 2017; Damarla et al., 2010; Ebisch et al., 2011; Hull et al., 2017; Iidaka et al., 2019; Just et al., 2012; Di Martino et al., 2011; Mash et al., 2020; Maximo et al., 2014; Moseley et al., 2015; Müller et al., 2011; Vissers et al., 2012; Woodward et al., 2017). A likely mechanism underlying these impairments in functional connectivity is altered

structural connectivity as changes in neuronal morphogenesis and neurite outgrowth have a significant impact on circuit function during brain development (McFadden and Minshew, 2013). It has even been proposed that long-range hypoconnectivity in ASD is in part due to the hyperconnectivity caused by excessive local axonal and dendritic processes which outcompete inputs from more distal brain regions (Courchesne et al., 2007).

Evidence supporting altered neurite outgrowth as an underlying cellular phenotype in ASD comes from diffusion tensor imaging (DTI) and postmortem studies of ASD brains. DTI measurement of fiber tract microstructure in the brains of individuals with ASD demonstrate alterations in the morphology of white matter tracts, reflecting alterations in axon number, pathfinding, and arborization (Alexander et al., 2007; Ameis and Catani, 2015; Kana et al., 2014; Keller et al., 2007; Lee et al., 2007; Solso et al., 2016; Travers et al., 2012; Zikopoulos et al., 2010). Furthermore, Golgi staining of hippocampal neurons from patients with ASD showed reduced dendritic branching (Raymond et al., 1995), and MAP2 staining of the dorsolateral prefrontal cortex revealed reduced dendrite numbers in the individuals with ASD (Mukaetova-Ladinska et al., 2004). Additionally, several ASD genes have been implicated in the processes of neuronal morphogenesis, axon guidance, and dendritic arborization. It has been consistently shown that *PTEN* deficiency results in axon and dendrite overgrowth, as well as neuronal hypertrophy (Cupolillo et al., 2016; Fraser et al., 2008; Haws et al., 2014; Jaworski et al., 2005; Kwon et al., 2006; Weston et al., 2014; Wong et al., 2020). Loss of

TSC1 results in substantial changes in neuron morphogenesis, including ectopic axon formation (Choi et al., 2008; Floricel et al., 2007; Meikle et al., 2007; Uhlmann et al., 2002). Pak1/Pak3 double knockouts exhibit less complex neuronal morphology and introduction of a dominant negative form of *PAK1* caused a reduction in the dendritic branching (Hayashi et al., 2007; Huang et al., 2011). Overexpression of *UBE3A* in an ASD mouse model reduces dendritic branching (Khatri et al., 2018). Reduced neurite outgrowth is also observed from loss of *NCKAP1*, *MeCP2*, *CHD8*, *DOCK4*, *PRICKLE2*, and *TAOK2* (Armstrong et al., 1995; Calderon de Anda et al., 2012; Durak et al., 2016; Kishi and Macklis, 2004; Rietveld et al., 2015; Sowers et al., 2013; Ueda et al., 2008; Xiao et al., 2013; Xu et al., 2018; Yokota et al., 2007).

1.2.3.3 Synapse formation and function in ASD

Impaired synaptogenesis is one of the most commonly observed cellular phenotypes in ASD with alterations in synaptic structure and function considered a hallmark of ASD (Bagni and Zukin, 2019; Bourgeron, 2009, 2015; Carroll et al., 2021; Gilbert and Man, 2017; Guang et al., 2018; Phillips and Pozzo-Miller, 2014; Zoghbi and Bear, 2012). Indeed, dendritic spine density is increased on Golgi stained cortical neurons from ASD subjects (Hutsler and Zhang, 2010; Tang et al., 2014). Additionally, many ASD-associated genes have functions which converge at the synapse including those involved in actin dynamics, cell-cell adhesion, and synaptic scaffolding (Betancur et al., 2009; Joensuu et al., 2018; Lin et al., 2016; Martínez-Cerdeño, 2017; Penzes et al., 2011; Verma et al., 2019). For example, it

has been consistently shown that *PTEN* deficiency results in increased synapse number (Cupolillo et al., 2016; Fraser et al., 2008; Haws et al., 2014; Jaworski et al., 2005; Kwon et al., 2006; Weston et al., 2014). Loss of *TSC1* also leads to increased dendritic spine density (Tavazoie et al., 2005). *SHANK3* deficiency results in reduced spine density and, often, increased spine length, indicating less mature spines (Durand et al., 2012; Peça et al., 2011; Roussignol et al., 2005; Wang et al., 2011b; Zhou et al., 2016). Knockdown of *NCKAP1* using shRNA also resulted in reduced spine density (Yokota et al., 2007). Also, shRNA knockdown or haploinsufficiency of *CYFIP1* leads to an increase in the fraction of immature spines and filopodia (Pathania et al., 2014; De Rubeis et al., 2013). Similarly, *MeCP2* deficiency leads to reduced spine density in pyramidal cortical neurons and hippocampal CA1 neurons from affected humans and mouse models (Armstrong et al., 1995; Belichenko et al., 1994; Chapleau et al., 2009; Fukuda et al., 2005; Stuss et al., 2012; Tropea et al., 2009). Haploinsufficiency of *SYNGAP1* leads to premature spine maturation with more mature mushroom type spines and fewer less mature stubby type spines, as well as premature pruning (Aceti et al., 2015; Carlisle et al., 2008; Clement et al., 2012, 2013; Kim et al., 2003; Vazquez et al., 2004). The changes in spine number in ASD may be due to impairments in not only synapse formation but also synaptic elimination (Ram Venkataraman et al., 2017). There is evidence linking some ASD risk genes to synaptic pruning such as *FMR1*, *PCDH10*, and *MEF2C* (Pan et al., 2010; Pfeiffer et al., 2010; Tsai et al.,

2012). Thus, these findings indicate that multiple mechanisms may be involved in the synaptopathology of ASD.

Insight that synaptic functional abnormalities were a common underlying pathway in ASD was first gained by the phenotypic overlap ASD shares with similar monogenic diseases with synaptopathologies, such as fragile X syndrome and tuberous sclerosis complex, as well as the observation that somewhere between about 10-30% of patients with ASD have epilepsy (Besag, 2018; Bourgeron, 2009; Guang et al., 2018; Jokiranta et al., 2014; Mouridsen et al., 2011; Spence and Schneider, 2009; Tuchman et al., 2010; Zhang et al., 2019a). Mutations that lead to abnormal synaptic strength or number can lead to impairments in overall neuronal network connectivity. Indeed, an imbalance in the excitation to inhibition (E/I) ratio in the cortex, leading to altered excitability of cortical circuits, is considered to be a key underlying mechanism for ASD pathology (Ajram et al., 2017; Bozzi et al., 2018; Bruining et al., 2020; Canitano and Pallagrosi, 2017; Culotta and Penzes, 2020; Dickinson et al., 2016; Howell and Smith, 2019; Nelson and Valakh, 2015; Oliveira et al., 2018; Port et al., 2019; Rubenstein and Merzenich, 2003; Sohal and Rubenstein, 2019; Uzunova et al., 2016).

Many ASD susceptibility genes seem to converge on altered synaptic function and plasticity as the likely underlying pathology for ASD. Several demonstrate abnormalities in synaptic transmission including impairments in AMPAR-mediated excitatory synaptic transmission as measured by miniature excitatory postsynaptic currents (mEPSCs), $GABA_aR$-mediated miniature

inhibitory postsynaptic currents (mIPSCs), and basal synaptic transmission as measured by field excitatory postsynaptic potentials (fEPSPs). For example, *SHANK3* mutations show reductions in the amplitude and frequency of mEPSCs and the slope of fEPSPs (Bozdagi et al., 2010; Durand et al., 2012; Kouser et al., 2013; Peça et al., 2011; Yang et al., 2012; Yi et al., 2016). *SYNGAP1* deficiency also results in disrupted synaptic function as seen by an increase in the amplitude and frequency of mEPSC from increased AMPAR-mediated currents and an increase in fEPSPs at P14 (Clement et al., 2012; Llamosas et al., 2020; Ozkan et al., 2014; Vazquez et al., 2004; Wang et al., 2013). A transgenic mouse model of *NRXN1* KO showed reduced excitatory synaptic strength with a decrease in mEPSC frequency and fEPSP slope (Etherton et al., 2009). Expression of an ASD related mutation of *NLGN3*, R471C, increased the amplitude of mIPSC (Gutierrez et al., 2009) and a decreased fEPSP slope, while a *NLGN3* KO mouse showed increased mIPSC frequency and decreased mEPSC frequency (Etherton et al., 2011). Similarly, conditional knockout of *CYFIP1* leads to an increase in mIPSC amplitudes but no change in mEPSCs (Davenport et al., 2019). Furthermore, *CNTNAP2* KO mice show decreased mEPSC frequency and amplitude with no change in mIPSCs and *CNTNAP2* knockdown showed a reduced E/I ratio (Lazaro et al., 2019; Sacai et al., 2020). The imbalances between excitatory and inhibitory transmission observed in several of these studies demonstrate the importance of E/I balance for normal brain function and suggest a critical role for these genes in maintaining such a balance.

Impaired maintenance of experience-dependent synaptic plasticity is also a synaptic abnormality commonly observed in models of ASD-linked mutations (Hansel, 2019). As synaptic plasticity is the cellular mechanism underlying learning and memory consolidation, disturbances in plasticity are consistent with the high rates of intellectual disability and impairments in cognitive function observed in ASD (Verma et al., 2019). Deficiency in a number of ASD risk genes results in impaired LTP. These include *NLGN1* (Blundell et al., 2010; Chubykin et al., 2007; Kim et al., 2008), *SHANK3* (Bozdagi et al., 2010; Jaramillo et al., 2016; Kouser et al., 2013; Wang et al., 2011b; Yang et al., 2012), *SYNGAP1* (Clement et al., 2013; Kim et al., 2003; Komiyama et al., 2002; Ozkan et al., 2014; Vazquez et al., 2004), *FMR1* (Hu et al., 2008; Lauterborn et al., 2007; Lundbye et al., 2018; Shang et al., 2009; Tian et al., 2017; Zhao et al., 2005), and *MeCP2* (Asaka et al., 2006; Moretti et al., 2006; Weng et al., 2011). Interestingly, loss of some ASD risk genes result in enhanced mGluR-mediated LTD including *FMR1* (Hou et al., 2006; Huber et al., 2002; Tian et al., 2017; Till et al., 2015) and *SYNGAP1* (Barnes et al., 2015; Paul et al., 2019), whereas loss of other ASD risk genes decreases LTD such as in *MeCP2* (Moretti et al., 2006), *NLGN3* (Baudouin et al., 2012), *PTEN* (Takeuchi et al., 2013), and *TSC1* (Bateup et al., 2011). These abnormalities in LTD may also have consequences for synaptic pruning, underscoring the potential of aberrant synaptic plasticity to disturb synaptic connectivity (Hansel, 2019). Thus, the impaired synaptic function and plasticity which occur during the critical developmental period of synapse formation in ASD seem to result in abnormal

neuronal connectivity that persists into adulthood and leads to the observed alterations in behavior.

1.2.4 Sex differences and the X chromosome in ASD

It has been noted that ASD is more prevalent in males compared to females. Indeed, studies indicate that males are between 3-5 times more likely to be diagnosed with ASD than females (Fernell and Gillberg, 2010; Fombonne, 2009; Loomes et al., 2017; Nicholas et al., 2009). It is possible that a contributing factor to this gender bias is a bias in diagnosis. It has been suggested that current ASD diagnostic tools may overlook or misdiagnose females due to lack of sensitivity to the symptoms that manifest in women compared to men, thus contributing to the lower prevalence of ASD in women (Bargiela et al., 2016; Dworzynski et al., 2012; Giarelli et al., 2010; Lai and Baron-Cohen, 2015; Loomes et al., 2017; Mandy and Tchanturia, 2015; Murray et al., 2017; Navarro-Pardo et al., 2021; Trubanova et al., 2014).

Findings from recent studies support that there may also be a biological component to the gender bias. It has been proposed that there is a male vulnerability, or a female protective effect, in the development of ASD. This female protective model, also known as the multiple threshold liability model, states that multiple genetic variants contribute to the overall risk of developing ASD and females require a higher threshold of liability to manifest ASD (Jacquemont et al., 2014; Robinson et al., 2013; Werling et al., 2016; Zhang et al., 2020b). Supporting this hypothesis, there is evidence of a higher frequency of deleterious variants

disrupting more genes in females with ASD than in males with ASD (Desachy et al., 2015; Gilman et al., 2011; Jacquemont et al., 2014; Levy et al., 2011; Sanders et al., 2011; Satterstrom et al., 2020; Zhang et al., 2020b). There are a few theories to explain why females are able to withstand more mutations than males before developing ASD. One is the extreme male brain theory, in which differences in hormone exposure during development, specifically higher levels of fetal testosterone, may cause the gender differences seen in ASD (Auyeung et al., 2006; Baron-Cohen, 2002; Baron-Cohen et al., 2011; Baruah et al., 2018; McCarthy and Wright, 2017; Werling and Geschwind, 2013).

The differential inheritance of X-linked ASD genes provides another explanation for the male bias in ASD susceptibility. Males only carry one copy of the X chromosome, inherited from their mother, compared to the two copies in females. Thus, hemizygous loss of function (LOF) variants would result in a complete knockout of expression in males while females would still have another functional copy, contributing to the larger proportion of males observed in ASD. Indeed, there are several examples of ASD associated X-linked genes including *MeCP2, FMR1, NLGN3, SLC6A8, CDKL5, PCDH19, ARHGEF9, TBL1X, IQSEC2* (Amir et al., 1999; Carney et al., 2003; Jamain et al., 2003; Marco and Skuse, 2006; Reddy, 2005; Zipper et al., 2017). Although X-linked LOF mutations contribute to the male gender bias observed in ASD, statistically they alone cannot explain the overall male bias (Lim et al., 2013; Mandel and Chelly, 2004; Nava et al., 2012; Sanders et al., 2015; Stone et al., 2004; Werling et al., 2016; Zhang et

al., 2020b). Yet, they are still important to study for improving our understanding of the pathogenesis of ASD, particularly for affected females.

For females with ASD carrying a hemizygous LOF variant, epigenetic factors such as X chromosome inactivation (XCI) can play a key role in disease severity. One X chromosome is inactivated in each cell in females to balance the expression of X-linked genes between the sexes. XCI occurs early in development and which of the two X chromosomes will be inactivated is typically random, resulting in mosaic expression of paternally and maternally inherited X-linked genes. However, when one of the two X chromosomes is preferentially inactivated, the cellular mosaicism is skewed (Bittel et al., 2008; Gribnau and Barakat, 2017; Morleo and Franco, 2008; Payer, 2016; Ribeiro and MacDonald, 2020; Taherian et al., 2016; Tan et al., 1995; Tukiainen et al., 2017; Wu et al., 2014). This preferential inactivation is known as primary skewing. Secondary skewing can occur as a result of a genetic variant on one of the X chromosomes giving a survival advantage to cells expressing that variant or negative selection against cells expressing a deleterious variant. In this way, heterozygous females carrying X-linked mutations may have some protective compensation from skewed inactivation of the mutant allele. However, the opposite can also occur, where skewed inactivation of the wild type allele results in an increased risk, or severity, of disease. Thus, the varied XCI pattern in individual females can have a dramatic effect on disease pathogenesis for women and, indeed, skewed XCI has been observed in heterozygous women with various neurological disorders (Fieremans

et al., 2016; Godler et al., 2015; Heine-Suñer et al., 2003; Migeon, 2020; Plenge et al., 2002; Vacca et al., 2016; Zhang et al., 2020a; Zweier et al., 2013).

XCI skewing has also been observed in females heterozygous for several ASD risk genes (Braunschweig et al., 2004; Dibbens et al., 2008; Huppke et al., 2006; Jackson et al., 2019; Knudsen et al., 2006; Patel et al., 2020; Sikora et al., 2016; Snijders Blok et al., 2015; Young and Zoghbi, 2004a). Several studies have investigated the contribution of XCI patterning in ASD with inconsistent results. One study found an increase in skewing in females with ASD (33%) compared to female controls (11%) (Talebizadeh et al., 2005). However, another study using a larger sample of both affected girls and mothers of affected children found no significant excess of XCI skewing in females with ASD (Gong et al., 2008). A subsequent study in an Italian cohort of patients also failed to find any altered XCI pattern in the ASD females (Cannelli et al., 2011). These results overall suggest there is no correlation with XCI skewing and development of, or escape from, ASD; however, XCI patterns are assessed using peripheral blood cells which may not reflect the XCI patterning of the brain.

1.3 *NEXMIF* ASD gene and Thesis Rationale

1.3.1 Expression and Genetics

NEXMIF (also known as *KIDLIA, KIAA2022, or Xpn*) is an X-linked gene associated with ASD and X-linked intellectual disability (XLID). Located at Xq13.2, *NEXMIF* is a 192 kb gene containing 4 exons with a large 180 kb intron between

exons 1 and 2. Exon 3 spans over 4 kb and contains the majority of the coding region for the 170 kDa protein product, NEXMIF, made of 1516 amino acids.

Though little is known about NEXMIF's function and it has no significant homology to other proteins, work from our lab and others has established that NEXMIF is expressed in the nucleus of neurons in fetal and adult brains (Cantagrel et al., 2009; Gilbert and Man, 2016; Gilbert et al., 2020; Ishikawa et al., 2012; Magome et al., 2013). mRNA levels of NEXMIF are first detectable at embryonic day 10.5 (E10.5) with a peak at postnatal day 3 (P3) and decreased expression to low levels in adulthood (Cantagrel et al., 2009; Ishikawa et al., 2012). Using immunostaining, we are able to detect NEXMIF protein expression from the perinatal period into adulthood (Gilbert and Man, 2016; Gilbert et al., 2020; Ishikawa et al., 2012). NEXMIF is expressed in the nuclei of neurons, colocalizing with nuclear marker Hochest and neuronal marker NeuN, and purifying in nuclear, not cytosolic, fractions from cell lysates (Cantagrel et al., 2009; Gilbert and Man, 2016; Gilbert et al., 2020; Ishikawa et al., 2012; Magome et al., 2013). However, lacking colocalization with GFAP, NEXMIF is not expressed in glia (Cantagrel et al., 2009; Gilbert and Man, 2016; Ishikawa et al., 2012). NEXMIF expression is detected in the hippocampus, olfactory blub, cerebellum, and cerebral cortex (Cantagrel et al., 2009; Gilbert and Man, 2016; Ishikawa et al., 2012).

The first pathogenic variants in *NEXMIF* were observed in two male members of a family with autistic phenotypes and intellectual disability (Cantagrel et al., 2004). We followed this initial report with an investigation into the genetic

basis of the disorder in 8 male patients from 3 families with inherited autistic characteristics and intellectual disability, in which we established the novel gene *NEXMIF* as the etiological factor for the syndrome (Van Maldergem et al., 2013). Subsequently, dozens of pathogenic variants have been identified in 87 male and female patients from 78 families (Alarcon-Martinez et al., 2019; Athanasakis et al., 2014; Borlot et al., 2017; Cantagrel et al., 2004; Charzewska et al., 2015; Farach and Northrup, 2016; Kuroda et al., 2015; Lambert et al., 2018; de Lange et al., 2016; Lorenzo et al., 2018; Van Maldergem et al., 2013; Moysés-Oliveira et al., 2015; Panda et al., 2020; Samanta and Willis, 2020; Stamberger et al., 2020; Webster et al., 2017; Wu et al., 2020). Patients acquired these variants by *de novo* mutation or X-linked maternal inheritance. The genetic variants include nonsense mutations, frameshift mutations, and deleterious structural variants, all of which were predicted to decrease NEXMIF protein expression through nonsense-mediated decay leading to loss of function (Alarcon-Martinez et al., 2019; Athanasakis et al., 2014; Borlot et al., 2017; Cantagrel et al., 2004; Charzewska et al., 2015; Farach and Northrup, 2016; Kuroda et al., 2015; Lambert et al., 2018; de Lange et al., 2016; Lorenzo et al., 2018; Van Maldergem et al., 2013; Moysés-Oliveira et al., 2015; Panda et al., 2020; Samanta and Willis, 2020; Stamberger et al., 2020; Webster et al., 2017; Wu et al., 2020). Thus far, no missense pathogenic variants have been reported. The majority of mutations occur within the large exon 3 however, these span the length of exon 3, so no clear mutational hot spot with

clues to protein function has been identified (de Lange et al., 2016; Panda et al., 2020; Stamberger et al., 2020).

Given its spatiotemporal expression pattern and the increasing number of pathogenic variants identified, *NEXMIF* clearly plays an important role in early brain development.

1.3.2 Clinical phenotypes

Observations from our study, as well as others', revealed individuals with phenotypic *NEXMIF* variants demonstrate developmental delay and cognitive impairments (Alarcon-Martinez et al., 2019; Athanasakis et al., 2014; Borlot et al., 2017; Cantagrel et al., 2004; Charzewska et al., 2015; Farach and Northrup, 2016; Kuroda et al., 2015; Lambert et al., 2018; de Lange et al., 2016; Lorenzo et al., 2018; Van Maldergem et al., 2013; Moysés-Oliveira et al., 2015; Panda et al., 2020; Samanta and Willis, 2020; Stamberger et al., 2020; Webster et al., 2017; Wu et al., 2020). Often they have autistic features including impaired language, difficulty with social interactions, and repetitive stereotypies. Frequently, patients present with epilepsy, the majority showing generalized seizures including myoclonic, absence, atonic, and tonic-clonic seizures. Additional comorbidities include behavioral problems, such as hyperactivity, attention deficit disorder, and aggression, as well as gastroesophageal reflux, mild dysmorphic facial features, hypotonia, and microcephaly.

In general, males have more severe impairments than females, who range in phenotype from completely asymptomatic to severe intellectual disability and

drug-resistant epilepsy. Initially, only affected male were reported with their requisite related female carriers reporting as asymptomatic (Alarcon-Martinez et al., 2019; Cantagrel et al., 2004; Charzewska et al., 2015; Kuroda et al., 2015; Lambert et al., 2018; Lorenzo et al., 2018; Van Maldergem et al., 2013; Panda et al., 2020; Stamberger et al., 2020). Subsequently, several reports have identified symptomatic females (Athanasakis et al., 2014; Borlot et al., 2017; Farach and Northrup, 2016; Lambert et al., 2018; de Lange et al., 2016; Moysés-Oliveira et al., 2015; Samanta and Willis, 2020; Stamberger et al., 2020; Webster et al., 2017; Wu et al., 2020). Comparison of the individuals affected with *NEXMIF* variants across sex reveals males have a more severe degree of intellectual disability, while females have more frequently have epilepsy. Additionally, males have a more severe language impairment and more frequently show microcephaly. The onset of developmental delay is recognized earlier in males, with females being on average a greater age when their genetic diagnosis was established (Panda et al., 2020; Stamberger et al., 2020).

The differences between sexes and the phenotypic diversity observed in females might be explained by X chromosome inactivation (XCI). Located on the X chromosome, *NEXMIF* is subject to XCI (Cantagrel et al., 2004) and compared with the total loss of function from lack of protein expression in hemizygous males, heterozygous *NEXMIF* mutation in females combined with random XCI results in partial loss of function due to a decrease in protein expression. However, of the 32 female patients on which XCI analysis is available, 24 show a random XCI pattern,

4 are skewed, 2 are borderline skewed, and 2 are 100% skewed (Stamberger et al., 2020). And interestingly, comparing sisters with skewed versus random XCI (which occurs in 2 of the reported families) showed no correlation between XCI status and severity of the phenotype (Stamberger et al., 2020). Therefore, the hypothesis that the phenotypic variation is due to XCI pattern is not supported as there is not a genotype-phenotype correlation between the degree of skewed XCI and NEXMIF symptoms.

The severity of clinical phenotypes that occur from loss of NEXMIF function underscores its importance for normal brain development.

1.3.3 Cellular and molecular phenotypes

As a novel gene, *NEXMIF* initially had no formal name and was referred to as KIAA2022. In 2017, we worked with the HUGO Gene Nomenclature Committee (HGNC), aiming to assign the gene an official name. Because we, and others, had shown that the gene is involved in neurite growth and neuron migration, HGNC approved *NEXMIF* (Neurite EXtension and MIgration Factor) as the official name for the gene (Gilbert and Man, 2016; Gilbert et al., 2020; Ishikawa et al., 2012; Magome et al., 2013; Van Maldergem et al., 2013). Indeed, we have found that NEXMIF plays a role in neuronal morphogenesis, neuronal migration, and synapse formation.

We, and others, found that siRNA mediated knockdown of NEXMIF in cultured mouse neurons and PC12 cells resulted in reduced neurite and axon length and number (Ishikawa et al., 2012; Van Maldergem et al., 2013). We also

found that shRNA mediated knockdown in cultured neurons showed a decrease in dendritic growth and branching (Gilbert and Man, 2016). Additionally, our RNAi mediated knockdown of NEXMIF altered migration (Gilbert and Man, 2016; Magome et al., 2013). While our work, and that of others, supports a major role for NEXMIF in neuron development and brain function, further work is needed to fully understand its molecular mechanism of action underlying the phenotypes observed at both the clinical and cellular levels.

1.3.4 Thesis Rationale

NEXMIF is a novel X-linked ASD gene, however its role in brain development remains largely unknown. An increasing number of reports indicate that NEXMIF-dependent ASD results in severe ASD phenotypes, intellectual disability, and seizures in both males with complete loss-of-function and females with haploinsufficient loss-of-function. As a monogenetic cause of ASD with intellectual disability, NEXMIF represents an excellent opportunity to examine ASD pathogenesis at the cellular and molecular levels with clarity and certainty. To date, the molecular details underlying the lack, or haploinsufficiency, of NEXMIF in ASD remain unknown. The goal of my thesis is to systematically investigate the function of NEXMIF in neurobiology and to characterize the cellular and molecular dysregulation, and ASD behavioral impairments, which arise from loss of NEXMIF. First, I aimed to understand the cellular and molecular mechanisms underlying NEXMIF-dependent ASD pathogenesis. Second, I aimed to characterize behavioral phenotypes, and investigate phenotypic cellular mosaicism, due to

NEXMIF haploinsufficiency. Findings from this study provide important original knowledge of this new ASD gene and will help with the future development of strategies for clinical intervention in ASD.

CHAPTER TWO: MATERIALS AND METHODS

2.1 Materials

2.1.1 Plasmids

A list of plasmids used and their relevant information can be found in Table 2.1.

2.1.2 Antibodies

A list of antibodies used and their relevant information can be found in Table 2.2.

2.1.3 Drugs

A list of drugs used and their relevant information can be found in Table 2.3.

2.1.4 Human brain tissue

Human brain tissues from control and AD patients were provided by, and used with approval from, the Boston University Alzheimer's Disease Center. Samples were collected from both males and females aged from 54 to 96 years old.

2.1.5 Preparation and use of Aβ peptides

β-Amyloid (Aβ) [1-42] oligomeric peptides (Invitrogen, cat # 03-112) were prepared according to manufacturer's instructions. Briefly, lyophilized peptide was dissolved in HPLC grade water and diluted to 1 mg/ml with phosphate buffered saline (PBS). Peptides were then incubated at 37°C for at least 24 h. Aliquots were made and stored at -20°C. Aliquots were thawed once directly prior to use. Neuronal cultures were treated with Aβ oligomers or water at a comparable volume as a control.

2.2 Cell culture

2.2.1 Primary culture of rat and mouse neurons

Hippocampal and cortical brain tissues were dissected out of postnatal day 0-1 (P0- P1) mouse brains of transgenic NEXMIF mice and WT littermate controls or embryonic day 18 (E18) rats of either sex to be used for primary culture. Mice brains were individually digested, and rat brains collectively digested, in papain (1 mg/ml in Hanks balanced salt solution, Sigma-Aldrich; cat. # 4762) for 15 min at 37 °C, then triturated in a trituration buffer [0.1% DNase (cat. # PA5-22017 RRID: AB_11153259), 1% ovomucoid (Sigma-Aldrich; cat. # T2011)/1% bovine serum albumin (Sigma-Aldrich; cat. #05470) in Dulbecco's modified eagle medium (DMEM, Corning)] to fully dissociate neurons. Dissociated neurons were counted and plated on 18-mm circular coverslips (Carolina, Burlington, NC; cat. # 633013, No. 0) in 60-mm Petri dishes (five coverslips/dish) that had been coated in poly-l-lysine (Sigma-Aldrich; cat. # P2636; 100 µg/ml in borate buffer) overnight at 37°C then washed three times with sterile deionized water and left in plating medium [minimal essential medium (500 mL) containing 10% fetal bovine serum (FBS; Atlanta Biologicals, Flowery Branch, GA; cat. # S11550), 5% horse serum (HS; Atlanta Biologicals; cat. # S12150), 31 mg l-cysteine, 1% penicillin/streptomycin (P/S; Corning, Corning, NY; cat. # 30-002-CI), and l-glutamine (Corning; cat. # 25-005-CI) before cell plating. The day after plating, plating medium was replaced by feeding medium (neurobasal medium supplemented with 1% horse serum, 2% B-27, and 1% penicillin/streptomycin and l-glutamine) which was supplemented with

5′-fluoro-2′-deoxyuridine (10 µm; Sigma-Aldrich; cat. # F0503) after 7 d *in vitro* (DIV 7) to suppress glial growth.

2.2.2 Culture of human embryonic kidney cell line (HEK293)

An aliquot of frozen HEK293T cells (ATCC® CRL-3216™) stored at -80°C was thawed at 37°C for 2 min. The thawed cells were placed in a 10 cm Petri dish with 10 ml of pre-warmed culture media (DMEM with 10% fetal bovine serum and 1% penicillin/streptomycin. The cells were incubated 37°C with 5% CO_2 until at least 80% confluency was reached. Confluent cells were split by removing the culture media and incubating with 1 ml of trypsin-EDTA (Invitrogen) at 37°C for 1 min to free adherent cells from the surface of the dish. 10 ml of culture media was added to neutralize the trypsin and gently triturated to dissociate the cells into individual cells. Cells were then re-seeded at the desired density into a cell culture dish with pre-warmed culture media and maintained at 37°C until further use. To freeze cells for long-term storage, cells were isolated as described above, resuspended in DMEM with 10% FBS and 10% DMSO, aliquoted into cryovials (Nalgene), and frozen overnight at -20°C before transferring to -80°C.

2.3 Plasmid transfection

Neurons or HEK293T cells that were split and cultured overnight were transfected respectively with lipofectamine 2000 (Life Technologies) or polyethylenimine (PEI) reagent (Polysciences, Warrington, PA; cat. # 23966) along with the target plasmids. Target plasmids were mixed with lipofectamine 2000 (1:1 ratio) or PEI

(1:3 ratio) in 1X DMEM for 20 minutes at room temperature to form the transfection complex. The transfection complex was then incubated with the cells in culture medium for another 3-4-h at 37℃ in the cell culture incubator. Afterward, the medium with the transfection complex was replaced with fresh culture medium. For neurons, half of the fresh feeding medium was supplemented with conditioned feeding medium to minimize cell death. HEK 293T cells were cultured in the following medium: 1X DMEM with 10% FBS, 1% P/S and 1% L-Glutamine.

2.4 Viral infection

2.4.1 Production of adenovirus and lentivirus

For AAV GluA1 constructs, GFP-GluA1-WT and GFP-GluA1-4KQ in the adeno-associated virus vector (AAV2) (Addgene #50954) under the human synapsin 1 promoter were transfected in HEK293T cells along with viral packaging and envelope protein plasmids (XR2 and XX6.80) as described above. After incubation at 37°C for 72 h, the cells were scrapped from the dish surface and subjected to four freeze/thaw cycles to lyse the cells and release the virus. The lysate was centrifuged at 3000 g for 30 min at 4°C and the supernatant was combined with conditioned medium containing AAV from the culture dish, filtered through a 0.45-μm filter, and combined with PEG-it virus purification solution (System Bioscience) at a 1:4 dilution. This mixture was left at 4C overnight, followed by centrifugation at 1500 g for 30 min at 4°C .The viral particles were resuspended in 500 mL sterile 1x PBS, aliquoted, and stored at −80°C until use.

For lentiviral shRNA, two NEXMIF shRNA sequences (CAGGAGCTACTAAGAATCAC and CAGGTAGCTTTGAGGTGTCA), which recognize NEXMIF transcripts from mouse, rat and human, as well as a control scrambled shRNA sequence (CCGCAGGTATGCACGCGT) in the pLKO.1-TRC cloning vector (Addgene; cat. # 10878, RRID: SCR_005907) were transfected in HEK293T cells along with viral packaging and envelope protein plasmids (pRSV/REV, pMDLg/RRE, and pVSVG) as described above. After incubation at 37°C for 72 h, conditioned medium containing lentivirus was collected, centrifuged at 1000 × g for 10 min, filtered through a 0.45-μm filter, and combined with the PEG-it solution at a 1:4 dilution. This mixture was left at 4°C overnight, followed by centrifugation at 1500 g for 30 min at 4°C The viral particles were resuspended in 500 mL sterile 1x PBS, aliquoted, and stored at −80°C until use.

2.4.2 Intracerebroventricular viral injection

For AAV injection, the APP/PS1 mice were deeply anesthetized with isoflurane; AAV particles (1.0 μL at 0.1 μL/min) were injected into the lateral ventricle (1.8 mm antero-posterior, 1.06 mm medio-lateral, 2 mm dorso-ventral). After the injection, the mice were placed on a heating plate for recovery, and then were kept under standard laboratory conditions. The AAV of Control, GluA1-WT and GluA1-4KQ were constructed and prepared by Obio Technology (Shanghai, China).

2.5 Cellular techniques

2.5.1 Immunocytochemistry

Cortical or hippocampal neurons were fixed for 8 min in a 4% paraformaldehyde/4% sucrose solution at room temperature (RT). Cell membranes were permeabilized for 5 min in 0.3% Triton-X-100 (Fisher Biotech) in phosphate buffered saline (PBS) and rinsed three times in PBS. Cells were blocked in 10% goat serum in PBS for 1 h at RT. After blocking, cells were incubated with primary antibodies (in 5% goat serum PBS) for 2 h at RT, washed three times with PBS, and incubated with Alexa Fluor-conjugated fluorescent secondary antibodies (1:500, Life Technologies) for 1 h at RT. Cells were then mounted to microscopy glass slides with Prolong Gold anti-fade mounting reagent (Life Technologies) for subsequent visualization. Mounted coverslips were kept overnight in the dark at RT before imaging.

2.5.2 Immunohistochemistry

Adult mice underwent transcardial perfusion with ice cold PBS prior to collection of the brain. Brains were fixed in 4% paraformaldehyde for 4-6 h and cryoprotected in 30% sucrose/PBS. Brains were then placed in molds to be rapidly frozen in OCT (Tissue-Tek) and stored at -80°C until they were cut into 20 µm sections using a LEICA CM1850 cyrostat (LEICA Biosystems). Sections were mounted onto SuperFrost microscope slides (Fisher Scientific) and stored at −20°C until staining. To prepare for immunostaining, sections were hydrated in PBS for at least 2 h and underwent antigen retrieval by microwaving in sodium citrate buffer (10 mM, pH 6) at 800 watts for 1 min followed by 80 watts for 10 min. Sections were cooled to RT for 20 min and then blocked in 10% goat serum, 0.3% Triton X-100/PBS for 1 h.

Sections were then incubated in primary antibodies (5% goat serum PBS) overnight at 4°C, washed three times with PBS, and incubated in Alexa Fluor-conjugated fluorescent secondary antibodies (1:500, Life Technologies) for 1 h at RT. Brain slices were then washed three times with PBS, with the first wash containing Hoescht (1:10,000, Thermo Fisher) and mounted under a coverslip with Prolong Gold anti-fade mounting reagent (Life Technologies). Slides were allowed to dry at room temperature overnight and stored at −20°C for subsequent visualization.

2.5.3 AMPA receptor internalization assay

Neurons were incubated with an N-terminal specific GluA1 (GluA1Nt) antibody (Neuromab, 1:100) or GFP antibody (Synaptic Systems, 1:100) for GluA1-4KQ-GFP experiments at 37°C for 10 min and then washed twice with feeding medium to get rid of extra antibody. After replacing the treatment with the cells' original culture medium, cells were placed at 37°C for 20 min. Neurons were then fixed in 4% paraformaldehyde/4% sucrose solution for 8 min. Neurons were blocked with 10% GS and further incubated with a secondary antibody (Alexa Fluor dye 488 or HRP, 1:500, 1 h) to bind all the AMPARs remaining on the cell surface. Neurons were permeabilized with 0.3% Triton X-100/PBS for 5 min, blocked in 10% goat serum for 1 h and incubated with another secondary antibody of a different color (Alexa Fluor dye 555, 1:500, 1 h) to specifically label the internalized AMPARs.

2.5.4 AMPA receptor insertion assay

Neurons were incubated with GluA1Nt antibody (Neuromab, 1:80) at 37°C for 10 min and then washed twice with feeding medium to get rid of extra antibody. Neurons were further incubated with a secondary antibody (Alexa Fluor dye 488 or HRP, 1:100 in ACSF with no Mg^{2+}) for 45 min at RT to bind all the AMPARs initially on the cell surface. To induce insertion in chem-LTP assays, neurons were treated with 200 µM Glycine and 1 µM Strychnine, 20 µM Biccuculine, 1 µM TTX in ACSF with no Mg^{2+} for 3 min at 37°C. After replacing the treatment with the cells' original culture medium, cells were placed at 37°C for 20 min. Neurons were then fixed in 4% paraformaldehyde/4% sucrose solution for 8 min. Neurons were blocked with 10% GS and incubated again with GluA1Nt antibody (1:200, RT for 2 h) followed by a secondary antibody of a different color (Alexa Fluor dye 555, 1:500, 1 h) to specifically label the newly inserted AMPARs. Total surface AMPARs were calculated as the initial surface expressing AMPARs plus the newly inserted AMPARs.

2.6 Biochemical techniques

2.6.1 Sample collection

Brains regions were dissected on ice immediately after sacrificing animals at the appropriate time points. Tissues were lysed in RIPA buffer (50 mM Tris-Cl, 150 mM NaCl, 1% NP40, 1% sodium deoxycholate (SDOC)) with 1% SDS and a protease inhibitor cocktail (Complete tablets, Roche). Samples were homogeneneized mechanically with a pestle, followed by sonication (10X for 10 s

each), and head-to-toe rotation for at least 2 h at 4°C. Brain lysates were then centrifuged for 20 min at 13,000 rpm in a 4°C microcentrifuge to collect the supernatant fraction. Protein concentrations were determined with a BCA assay according to the manufacturer's protocol (Pierce) and were normalized to the same total protein concentration with RIPA lysis buffer cells. Each sample was given an equal volume of 2X Laemmli sample buffer (4% SDS, 10% 2-mercaptoethanol, 20% glycerol, 0.004% bromophenol blue, 0.125 M Tris HCl) and was boiled for 15 min at 95°C. Cultured cells were lysed in 2X Laemmli sample buffer and boiled for 15 min at 95°C. Samples were then stored at -20°C until use in immunoblotting assays.

2.6.2 Immunoprecipitation

Cultured neurons or brain tissues were lysed on ice in 1x radioimmunoprecipitation assay (RIPA) buffer (50 mM Tris-HCl [pH 7.4], 50 mM NaCl, 1% NP-40, 1% sodium deoxycholate [SDoC], and 0.1%-1% SDS) supplemented with protease inhibitor cocktail tablets (11697498001, Roche) to reduce protein degradation. For IP experiments, stringent RIPA buffer (1% SDS) was used to ensure specificity of immunoprecipitation. After collection, cells were lysed by pipetting, followed by 5 bursts of sonication. Samples were then rotated head-to-toe for 30 min and centrifuged at 13,000 rpm at 4°C for 20 min. The protein concentration of the supernatant was balanced using a BCA assay while the pellets were discarded. A small portion of each sample was saved as a total cell lysate while the remainder was incubated with specific antibodies for 1 h, rotating, at 4°C, then incubated

overnight after the addition of protein A-agarose beads (sc-2001, Santa Cruz Biotechnology). Agarose beads were rinsed at least three times with the lysis buffer used for that assay. The samples were finally boiled with Laemmli 2X sample buffer (4% SDS, 10% 8 2-mercaptoethanol, 20% glycerol, 0.004% bromophenol blue, and 0.125 M Tris HCl) for 10-15 min at 95°C before being used in immunoblotting assays.

2.6.3 Immunoblotting

SDS-polyacrylamide gel electrophoresis (SDS-PAGE) was performed to separate proteins of interest using standard procedures. Proteins were transferred to PVDF membranes and blocked for one hour in 10% milk prepared in Tris buffered saline supplemented with 0.05% Tween (TBST). Following blocking, membranes were probed with the appropriate primary antibody (in 5% milk in TBST) overnight at 4°C, then washed 3X in TBST for 5-10 min, and incubated with the appropriate secondary antibody tagged with horse radish peroxidase (HRP) for 1 h at RT. Membranes were washed 3x with TBST and visualized using a chemiluminescence detection system (GE Healthcare) and exposed on Fuji medical X-ray films (Fisher Scientific). The film was scanned and analyzed using ImageJ.

2.6.4 Post-translational modification assays

Acetylation assays were designed as in Wang et al., 2017, and ubiquitination assays as in Huo et al., 2015. To detect the post-translational modification signal

of endogenous AMPARs in brain (*in vivo*) or neuronal culture (*in vitro*), the GluA1 subunit was first immunoprecipitated from whole-brain extracts or homogenized cortical neuron lysates following the Immunoprecipitation procedure described above, using a specific antibody bound by Protein A-agarose beads. Lysis buffer (RIPA buffer with 1% SDS) was used to homogenize the brain tissue. The buffer was supplemented with a cocktail of deacetylase inhibitors (100 μM trichostatin A, 50 mM sodium butyrate, and 50 mM nicotinamide), to sufficiently block deacetylase activity, and deubiquitination inhibitors (5 μM ubiquitin aldehyde) as needed. The acetylation signal was then assessed by immunoblotting with an antibody that detects general acetylated lysine residues (1:1000; ab80178, Abcam or 32268, Santa Cruz). Ubiquitination signals were detected by immunoblotting with an antibody targeting ubiquitin (1:1000; ab19247, Abcam) and smear signals above 100 kDa were measured and quantified.

2.6.5 GST assay

The GST assay was adapted from Einarson et al., 2007. The BL21 E.coli bacteria were transformed with GST-GluA1-Cterm plasmid then grown at 37°C to show single colonies (diameter <1mm) before the experiments. For each experiment, one colony of transformed BL21 bacteria was inoculated into 2-ml aliquot of LB containing appropriate antibiotic selection then grew overnight at 37°C with shaking at 250 rpm. One liter of LB containing the antibiotic selection was then inoculated with the 2-mL aliquot of transformed BL21 bacteria and grown at 19°C with shaking for a few hours untill the OD600 reached 0.5-1.0. Isopropyl β-D-1-

thiogalactopyranoside (IPTG) was then added to the concentration of 0.1 mM to induce the expression of GST-GluA1-Cterm recombinant protein for another 3 hours. The bacteria were centrifuged at 3500 g for 20 min at 4°C to be concentrated then lysed in 20 mL of PBS for lysis with repeated sonication. Lysed bacteria were centrifuged again at 12,000 g for another 15 min at 4°C to keep the supernatant. GST-GluA1-Cterm recombinant protein in the supernatant was then purified with GST beads and resuspended in acetylation assay buffer [RIPA buffer (50 mM Tris-HCl pH 7.4, 150 mM NaCl, 1% NP-40, 1% SDOC, and 0.1% SDS) supplemented with a protease inhibitor cocktail (Roche, cat# 11697498001) and a protein deacetylase inhibitor cocktail (100 mM trichostatin A, 50 mM sodium butyrate, and 50 mM nicotinamide)]. Resuspended GST beads were equally divided into several aliquots for protein acetylation assay.

2.6.6 Synaptosome purification

For brain tissues, the hippocampus or cortex of APP/PS1 mice were washed with cool artificial cerebral spinal fluid (aCSF: 140 mM NaCl, 3 mM KCl, 10 mM HEPES, 2 mM $CaCl_2$, 1 mM $MgCl_2$, and 10 mM glucose) and suspended in 300 µL (per 30 mg tissue) solution A containing 0.32 M sucrose,1 mM $NaHCO_3$, 1 mM $MgCl_2$, 0.5 mM $CaCl_2 \cdot 2H_2O$, 10 mM sodium pyrophosphate, and protease inhibitors on ice. The suspension was collected and mixed up and down with a pipette up to 12 times, centrifuged at 710 g for 10 min, and the supernatant was collected. The pellet (P1) was re-suspended in 50 mL of solution A, and following pipetting up and down three times, centrifuged at 1,400 g for 10 min. The supernatant was

collected together with the previously collected supernatant as whole-cell lysate (S1, whole). S1 was further centrifuged at 13,800 g for 10 min; supernatant (S2, cytosolic fraction) and pellet (P2, containing synaptosome and mitochondria) were separated. Pellet was resuspended in RIPA buffer, sonicated on ice, and rotated at 4°C for 30 min.

For cultured neurons, synaptic fractions were purified using Syn-PER Synaptic Protein Extraction Reagent (87793, Thermo Scientific). The protein concentrations in whole, cytosolic, and crude synaptosomal fractions were measured by BCA assay. Samples were then boiled with 4X loading buffer for Western blotting detection.

2.7 Golgi impregnation

Whole brains from adult female C57BL/6J wild-type and NEXMIF Heterozygous mice were subjected to Golgi neuron staining using the FD Rapid GolgiStain Kit (FD Neurotechnologies, catalog #PK401) according to the manufacturer's instructions. Mice were sacrified in a 4% CO2 chamber and brains were collected and rinsed in cold PBS. Brains were immersed in a Golgi-Cox solution containing potassium dichromate, mercuric chloride, and potassium chromate. The solution was replaced after 1 d of immersion with fresh solution and stored at RT in the dark for 2 weeks. After immersion, the brains were rapidly frozen and stored at -80°C prior to cutting. Brain slices were sectioned in the coronal plane at 100 um thickness on a cryostat and were mounted on gelatin-coated slices (FD

Neurotechnologies, catalog #PO101) and air dried at RT before further processing. Sections were then rinsed in distilled water, incubated in staining solution for 10 min, and dehydrated with 50%, 75%, 95%, and finally 100% ethanol. Sections were defatted in xylene and mounted onto coverslips with Permount mounting medium (Thermo Fisher Scientific). Sections were stored at RT in the dark for subsequent visualization.

2.8 Acute brain slice preparation and LTP recording

Mice were decapitated under anesthesia with isoflurane, the brain was quickly removed and placed in ice-cold oxygenated artificial cerebral spinal fluid (aCSF) containing 119 mM NaCl, 2.5 mM KCl, 26.2 mM NaHCO3, 1 mM NaH2PO4, 11 mM glucose, 1.3 mM MgSO4, and 2.5 mM CaCl2 (pH 7.4). Horizontal 350 μm thick brain slices were cut in ice-cold aCSF using a vibrating microtome (Leica, VT1000S, Germany). Slices were transferred to a recovery chamber at least 1.5 h with oxygenated aCSF at room temperature until recordings were performed.

For LTP recording, acute brain slices were transferred to a recording chamber and submerged in aCSF. Slices were laid down in a chamber with an 8 × 8 microelectrode array (Parker Technology, China) on the bottom plane (each 50 × 50 μm in size, with an interpolar distance of 150 μm) and kept submerged in aCSF. Signals were acquired using the MED64 System (Alpha MED Sciences, Panasonic). The fEPSPs in CA1 neurons were recorded by stimulating CA3 neurons. LTP was induced by applying three trains of high-frequency stimulation

(HFS; 100 Hz, 1s duration). The LTP magnitude was quantified as the percentage change in the fEPSP slope (10%–90%) taken during the 60 min interval after LTP induction.

2.9 Microscopy

Exposure time for the fluorescence signals was adjusted manually so the signals were within a full dynamic range. Either the glow scale look-up table or the histogram was used to monitor the saturation level. Once the parameters were set, they were fixed and used throughout image acquisition for the experiment.

For ICC: fluorescent images were collected with a 40x air-objective (numerical aperture, 0.95) on a DS-Fi2 Color Camera on a Nikon Eclipse NiE using NIS-Elements software or with a either a 40× (numerical aperture, 1.3) or_63x (numerical aperture, 1.4) oil-immersion objective on a Zeiss Axiovert 200M using Axiovision 4.5 software. Neuron images were quantified in using NIH ImageJ software.

For IHC: Brain sections were imaged with 10x and 20x air-objectives using a Nikon C2+ Si spectral laser scanning confocal microscope using NIS-Elements software.

For Golgi staining: images were acquired using brightfield transmitted light with a 40x air-objective (numerical aperture, 0.95) on a DS-Qi1 Monochrome Cooled Digital Camera on a Nikon Eclipse NiE using NIS-Elements software. Each neuron was scanned by varying the depth of the Z plane to ensure that all parts of

the cell (especially dendrites) were intact. The number of basal spines on neurons was measured with ImageJ software.

2.10 Transgenic animals

2.10.1 Animal care and use

For NEXMIF mice: All the procedures involving animal use were in compliance with the policies of the Institutional Animal Care and Use Committee (IACUC) at Boston University. Mouse colonies were maintained in the Laboratory Animal Care Facility (LACF) at Boston University, Charles River Campus in a C57BL/6J genetic background. Female mice heterozygous for NEXMIF were crossed with wild-type male mice. All WT (*NEXMIF*$^{+/+}$) mice were randomized female littermate controls for experiments with the heterozygous mice (*NEXMIF*$^{+/-}$), or male littermate controls for experiments with the knockout mice (*NEXMIF*$^{-/y}$). Adult mice were used in all behavioral studies to avoid variability due to changes during adolescent periods. Transgenic mice were backcrossed to C57Bl/6J mice >10 times prior to use.

For APP/PS1 mice: All animal experiments were approved by the Animal Care and Use Committee of Huazhong University of Science and Technology, and performed in compliance with the National Institutes of Health Guide for the Care and Use of Laboratory Animals. The Tg(APPswe,PSEN1dE9)85Dbo (APP/PS1) mice and littermates were from Jackson Lab. The mice were kept under standard laboratory conditions: 12 h light and 12 h dark with water and food ad libitum.

2.10.2 Genotyping

DNA was isolated from tail snips for genotyping using the Hot Shot Method. A single tail snip was collected from each mouse at the time of weaning on postnatal day 21 (P21) and placed in an Eppendorf tube. Tail snips were incubated for 30 min at 95°C in 75 ul of alkaline lysis buffer (25 mM NaOH, 0.2 M EDTA). The tubes were allowed to cool at room temperature for 5 min before 75 ul of neutralization buffer (40 mM Tris-HCl, pH 5) was added. The tubes were vortexed to mix and 1 ul of DNA extract was used in the following PCR protocol run on a Biorad DNA engine Tetrad 2 Peltier Thermal Cycler:

	Initial Denaturation	94 °C	5 min
30 cycles {	Denature	98 °C	15 s
	Anneal	55 °C (WT) or 59 °C (KO)	30 s
	Extend	72 °C	1 min
	Final Extension	72 °C	5 min
	Hold	4 °C	∞

The resulting PCR fragments were run on a 1% agarose gel with ethidium bromide to label and visualize DNA under ultraviolet light.

Two sets of primers were used to genotype NEXMIF Het animals. One set (WT) was targeted against the deleted exon 4 region using the primers: 5'−AGGACTTGCTTAGGTTGCTTCATGGAA−3' and

5’−CTTAAATTGCTCTACCTCAAGACCACCA−3’ with an expected PCR fragment of 949 bp. The other set (KO) was targeted against the KO cassette using the primers: 5’−CACACCTCCCCCTGAACCTGAAAG −3’ and 5’−CCCACGAAGGGATCATACCCTGTA−3’ with an expected PCR fragment of 794 bp.

2.10.3 Novel object recognition test

The mice were put in to the arenas (50 cm × 50 cm ×50 cm wooden container) for 5 min to adapt to the empty arenas 24 h before the test. 70% ethanol was used to clean arenas between each habituation period. On the first training day, the mice re-entered the arenas from the same starting point and were granted 5 min to familiarize themselves with the A object and B object. The 70% ethanol was used to clean arenas and objects after each familiarization period. One hour after the familiarization period, B object was replaced with C object, and the mice were granted 5 min to explore both objects; Twenty-four hours after the familiarization period, C object was replaced with D object, and the mice were granted 5 min to explore both objects. The recognition index was calculated by TA/(TA+TB), TB/(TA+TB),TC/(TA+TC), TD/(TA+TD). The discrimination index was calculated by (TC-TA)/(TA+TC), (TD-TA)/(TA+TD). TA, TB, TC, TD were respectively the time mice exploring the object A, B, C, D.

2.10.4 Three chamber social test

A three-chambered box measuring 65 × 28 × 28 cm was constructed from 0.75 in thick white plastic board with 4 × 4 in cut-out doors in the walls to the center chamber allowing movement between chambers. A small wire cage was placed in each of the side chambers to later house stranger mice. For 3 d before the test, test mice were habituated to the apparatus with empty cages in both side chambers and allowed to move freely between all three chambers for 5 min each day. On the testing day, the side doors were blocked with white plastic boards and test mice were singly placed into the center chamber with a stranger WT mouse (Mouse 1) placed under the wire cage in either of the side chambers. Once the doors were unblocked, the test mouse was allowed to move freely within the apparatus for 5 min. The test mouse was then returned to the center chamber, the doors were blocked again, and a second mouse (Novel Mouse) was placed in the wire cage of the other side chamber. The center doors were unblocked again and the test mouse was allowed to move freely within the apparatus for another 5 min. Between test mice, the entire apparatus was wiped with 70% ethanol to eliminate odor cues. Animals' movement was analyzed for the time spent interacting with each mouse or empty cage (nose ≤ 2 cm) and the time spent in each chamber.

2.10.5 Ultrasonic vocalization recordings

To record USVs, pups were separated from the dam and littermates and isolated in a recording chamber. Mouse vocalizations were recorded every 2 days (P5, P7, P9) in a random order for each litter using a CM16/CMPA microphone (Avisoft Bioacoustics, Berlin, Germany) placed 15 cm above the pups. The recording

chamber was cleaned with 70% ethanol and dried between each pup. Audio recordings were done at a sampling rate of 300 kHz in 16-bit format. The microphone was connected to a pre-amplifer UltraSoundGate 116Hb (Avisoft Bioacoustics, Berlin, Germany) and digitized sonograms were stored in a computer. Recordings were analyzed using SASLab Pro 5.2.12 (Avisoft Bioacoustics, Berlin, Germany). Spectrograms were generated using fast Fourier transform (256 FFT length, 100% frame, FlatTop window, and 50% window overlap) and a high-pass filter was applied to eliminate background noise below 30 kHz. USVs were detected automatically (threshold: -47 ± 10 dB, hold time: 7 ms) followed by manual inspection to ensure all detected calls were legitimate. Several acoustic parameters of calls were measured including number of calls, mean call duration, total time spent calling, peak frequency, and peak amplitude. Calls were classified based on their acoustic features into the following groups; simple: short, flat, upward, downward, chevron, U shape, and complex: modulated, frequency jump, multiple jumps, harmonic.

2.10.6 Marble burying

The marble burying was conducted in a square plastic bin with a 3 in thick layer of fresh pine chip bedding. Twenty-five shiny glass marbles (0.25 in diameter) were arranged in a 5 × 5 grid on top of the bedding. Mice were singly placed into the bin and allowed to move freely and bury marbles for 30 min. The number of marbles buried after 5, 10, 15, 25 and 30 min were manually counted.

2.10.7 Grooming test

Grooming was assessed in the animal's home cage with a 3 in thick layer of fresh pine chip bedding. Mice were singly placed back into the cage and allowed to move freely for 20 min. Video recordings were captured from the side of the cage. The amount of time spent grooming and the number of grooming instances were manually quantified. The number of unsupported rearing instances was all quantified.

2.10.8 Open field test

The open field test was conducted in a chamber constructed from 0.75 in thick white plastic box with a base measuring 28 × 28 × 28 cm. Lights in the testing room were dimmed for comfort of the animal with only a small desk lamp in the corner for the experimenter. Mice were habituated to the testing room over three days and handled for 5 min each session. On the test day, each mouse was singly placed into the center of the box and allowed to freely explore the chamber for 15 min. Animals' movement was analyzed for the movement speed, entries to open center, and track lengths.

2.10.9 Barnes maze spatial memory test

The Barnes maze consisted of a 48 in diameter, 0.75 in thick, circular white plastic board with twenty 2 in diameter holes evenly distributed around the board 1 in from the edge. The maze was mounted 30 in above the ground on a pedestal that allowed it to rotate from the center. A plain curtain with a few shapes attached as

spatial cues surrounded the maze to simplify the cues for the mice. The escape cage beneath the escape hole consisted of a black plastic box with a ramp to allow for easy access.

For each session, the test mouse was placed in the center of the maze under an opaque container. The aversive stimuli of four bright ceiling lamps and a loud alarm were turned on when the mouse was released from the container and allowed to roam freely about the maze. The ceiling lights and loud noise remained on while the mouse was exploring the maze and turned off immediately after they entered the escape hole. The maze and escape cage were thoroughly cleaned with 70% ethanol between testing sessions to avoid any olfactory cues and the maze was rotated randomly after every mouse to avoid intra-maze odor or visual cues. The escape hole remained in the same location relative to the spatial cues.

On day 1 of the procedure, the mice were habituated to the maze. After 3 min of exploring the maze, the mouse was gently nudged into the escape hole. The mouse was then allowed to stay in the escape hole without the aversive stimuli for 2 min. All mice were adapted to the maze in this way. On days 2-5, the mice were trained 3 times each day (12 times total) to learn to enter the escape hole by themselves and ensure a strong memory for the escape hole location. For each training trial, if the mice did not enter the escape hole on their own after 3 min, they were gently nudged into the hole. After the entered the escape hole, the aversive stimuli were turned off and the mice remained in the escape chamber for

1 min. On days 6 and 10 (1 d and 5 d post-training), the mice were tested for their memory of the escape hole location. During the memory probes, the escape hole was covered and the mice were allowed to roam freely for 3 min. Recordings of the animals' movement were analyzed to test the spatial memory of the mice. Primary latency to the escape hole, distance traveled to the escape hole, percentage of erroneous nose pokes, and time spent in each quadrant of the maze were quantified.

2.11 Statistical analysis

Statistical analysis for parametric data was performed using the two-population student's t test, one-way ANOVA with Tukey post-hoc test, or repeated measures two-way ANOVA with Sidak's multiple comparison test as appropriate. Kolmogorov–Smirnov test was used to analyze cumulative probabilities of mEPSC frequency and amplitude. All data are expressed as mean ± SEM and were analyzed using GraphPad Prism 6 statistical software (USA, GraphPad Software). $p < 0.05$ is considered statistically significant. p values are presented as $p > 0.05$ (ns, not significant), $* p < 0.05$, $** p < 0.01$, and $*** p < 0.001$.

For Western blots: Values of band immunointensity were measured using ImageJ and normalized to their corresponding tubulin or GAPDH loading control in the same lane, or to the total amount of pulled-down protein for immunoprecipitation assays. Data was then normalized to the control group by dividing all conditions and their SEMs by the value of the control condition. Data

from multiple trials were averaged to obtain the mean for each experiment. Multiple means of the same conditions were averaged to obtain the standard error of the mean, as indicated by the error bars in histograms.

For ICC: Synaptic puncta were analyzed using NIH FIJI (ImageJ) Software. Images were manually thresholded to select synaptic puncta. To obtain intensity values, raw integrated density measurements were acquired using the Analyze Particles function. Colocalization of pre-synaptic and post-synaptic fluorescent puncta was assessed using the "Puncta Analyzer" plugin. Measurements from at least three segments of secondary dendrites from different neurites were analyzed to represent one neuron. Control conditions were normalized to 1 by dividing all conditions and their SEMs by the value of the control condition.

For IHC: Mosaic expression of NEXMIF in brain slices was analyzed using the Spots protocol in IMARIS 9.5.1 (Bitplane AG, Zurich, Switzerland). Images underwent deconvolution according to the parameters of the microscope objective used for capture. Neurons were identified and labelled based on NeuN expression. Neurons were then sorted as $NEXMIF^{+}$ and $NEXMIF^{-}$ based on NEXMIF expression.

For behavioral tests: Video recordings were captured with a Logitech c920 webcam during each test. Locomotion tracks were generated using idtracker.ai software (Romero-Ferrero et al., 2018). These tracks were used in custom scripts written in Python to quantify the desired aspects of the animals' movement.

2.11.1 Sholl Analysis

Complexity of dendritic arborization was quantified using IMARIS 9.5.1 (Bitplane AG, Zurich, Switzerland). The dendrites of each neuron were manually traced using the Filament Tracer AutoPath protocol. The tracings were used to obtain measurements of the total dendritic length, mean dendritic length, and dendritic complexity evaluated by Sholl analysis. Sholl analysis within IMARIS measured dendritic branching complexity by counting the number of intersections between the dendritic filaments and concentric circles set at 1 μm intervals from the soma. The Sholl value at each radius was then plotted versus the radius of its intersecting circle.

Table 2.1 Plasmids

Plasmid Name	Vector Backbone	Bacterial Resistance	Source	Catalog Number
pLKO scrambled shRNA	pLKO.1 TRC	Ampicillin	Addgene	10878
pLKO NEXMIF shRNA 365	pLKO.1 TRC	Ampicillin	Cloned In House	-
pLKO NEXMIF shRNA 368	pLKO.1 TRC	Ampicillin	Cloned In House	-
GFP Lentivirus	pLVX	Ampicillin	Weifeng Xub, MIT	-
Nrgn-GFP lentivirus	pLVX	Ampicillin	Weifeng Xu, MIT	-
SynDig1-HA	pHM6	Amipcillin	Elva Diaz, UC Davis	-
p300-myc	pCMVβ	Ampicillin	Addgene	30489
CBP-HA	pRc/RSV	Ampicillin	Addgene	16701
GCN5-flag	pAdEasy	Kanamycin	Addgene	14106
PCAF-flag	pCI	Ampicillin	Addgene	8941
GluA1-WT-GFP	pRK5	Ampicillin	Richard Huganir, John Hopkins	-
GluA1-4KQ-GFP	pRK5	Ampicillin	Cloned In House	-
GluA1-4KR-GFP	pRK5	Ampicillin	Cloned In House	-

Table 2.2 Antibodies

Primary Antibodies				
Name	**Dilution**	**Host**	**Source**	**Catalog Number**
Acetyl-Lysine	1:1000 (WB)	mouse	Santa Cruz	sc-32268
GABARα1	1:100 (ICC)	rabbit	Abcam	Ab33299
GAD65	1:100 (ICC)	mouse	Santa Cruz	sc-377145
GAPDH	1:5000 (WB)	mouse	Abcam	ab8245
Gephyrin	1:100 (ICC) 1:1000 (WB)	rabbit	Abcam	ab3220066
GluA1-C	1:100 (ICC)	rabbit	OriGene Tech	Custom-made
GluA1-N	1:100 (ICC)	mouse	Millipore	MAB2263
GluA2	1:1000 (WB)	mouse	Millipore	MAB397
HDAC1	1:1000 (WB)	mouse	Cell Signaling	5356P
MAP2	1:100 (ICC)	mouse	Abcam	ab70218
NEXMIF	1:100 (slice IHC) 1:500 (ICC)	rabbit	Sigma-Aldrich	HPA000404
NeuN	1:250 (slice IHC)	mouse	Millipore	MAB377
Neurogranin	1:1000 (WB)	rabbit	Abcam	ab23570
PSD-95	1:400 (ICC) 1:1000 (WB)	mouse	Synaptic Systems	124 011BT
Synapsin I	1:1000 (WB)	rabbit	Millipore	AB1543

SynDig1	1:1000 (WB)	mouse	Neuromab	75-251
Tau-1	1:100 (ICC)	mouse	Millipore	MAB3420
α-tubulin	1:5000 (WB)	rabbit	Sigma-Aldrich	20911
Ubiquitin	1:2000 (WB)	rabbit	Abcam	ab7780
VGlut1	1:250 (ICC)	mouse	Santa Cruz	sc-377425
VGat	1:200 (ICC)	mouse	Neuromab	75-457
Phalloidin	1:50 (ICC)	dye in methanol	Cell Signalling	8953
Hoechst	1:10000 (ICC)	dye in Water	Sigma-Aldrich	63493
Secondary Antibodies				
Name	**Dilution**	**Host**	**Source**	**Catalog Number**
Rb IgG-HRP	1:5000 (WB)	rabbit	BioRad	170-6515
Ms IgG-HRP	1:5000 (WB)	mouse	BioRad	170-6516
Rb Alexa Fluor 488	1:500 (ICC)	rabbit	Molecular Probes	A11094
Rb Alexa Fluor 555	1:500 (ICC)	rabbit	Molecular Probes	A21428
Ms Alexa Fluor 488	1:500 (ICC)	mouse	Molecular Probes	A21121
Ms Alexa Fluor 555	1:500 (ICC)	mouse	Molecular Probes	A21127

Table 2.3 Drugs

Drug Name	Solvent	Final Concentration	Source	Catalog Number
Glycine	Water	200 μM	Fisher	BP381-5
Strychnine	Water	1 μM	Sigma-Aldrich	s8753
Biccuculine	DMSO	20 μM	Sigma-Aldrich	14340
TTX	Water	1 μM	Tocris	1069
APV	Water	25 μM	Sigma-Aldrich	A5282
Aβ	PBS	0.5 μM	Invitrogen	03-112
C646	DMSO	20 mM	Millipore	SML0002
CTPB	DMSO	20 mM	Santa Cruz	sc-202558
B2	DMSO	2 mM	Santa Cruz	sc-202486
Trichostatin A	DMSO	100 μM	Sigma-Aldrich	T8552
Sodium butyrate	Water	50 mM	Sigma-Aldrich	B5887
Nicotinamide	Water	50 mM	Sigma-Aldrich	N3376
Ubiquitin aldehyde	50 mM HCl	5 μM	Boston Biochem	U-201

CHAPTER THREE: INVESTIGATION OF BEHAVIORAL AND MOLECULAR PHENOTYPES IN NEXMIF KO MICE

3.1 Abstract

Autism spectrum disorders (ASDs) comprise a heterogeneous class of disorders characterized by impaired social interactions, diminished language and communication, and the tendency for repetitive behaviors. Our previous work identified the novel ASD gene *NEXMIF* and provided the first study of the associated cellular phenotypes. However, the molecular mechanism underlying NEXMIF function in brain development and ASD remains largely unknown. Here we investigate the cellular and molecular mechanisms underlying NEXMIF dependent ASD using a transgenic NEXMIF mouse model established by our group. We show that loss of NEXMIF in *NEXMIF*$^{-/y}$ animals leads to ASD-like behavioral alterations as well as impairments in neuronal development, such as reduced neurite growth, decreased synapse formation, and impaired synaptic plasticity. We also show loss of NEXMIF leads to downregulation of neurogranin (Nrgn) and SynDig1, which play roles in synaptic development and function. Reintroduction of Nrgn or SynDig1 *in vitro* rescues the decreased spine density and synaptic AMPAR levels observed from loss of NEXMIF. These findings indicate the *NEXMIF*$^{-/y}$ mouse faithfully models the human condition and Nrgn and SynDig act as downstream regulators of NEXMIF function to affect synaptic development. Use of the *NEXMIF*$^{-/y}$ mouse, particularly for potential rescue of behavioral impairments by Nrgn and SynDig1 *in vivo,* will allow for a better understanding of the role NEXMIF plays in the brain and in the development of ASD.

3.2 Introduction

Autism spectrum disorders (ASD), estimated to affect 1 in 54 individuals in the United States (Maenner et al., 2020), are characterized by reduced social interactions, impaired language and communication, and stereotyped, repetitive behaviors (American Psychiatric Association, 2013; Chen et al., 2015a; Lord et al., 1989). ASD often presents with other co-morbid psychiatric and medical conditions such as intellectual disability (ID), epilepsy, gross and fine motor deficits, anxiety, gastrointestinal issues, and attention-deficit/ hyperactivity disorder (ADHD) (Chiurazzi et al., 2020; Reiersen and Todd, 2008; Storch et al., 2012; Towbin et al., 2005; Tye et al., 2019; Zafeiriou et al., 2007).

ASD is among the most heritable neuropsychiatric disorders, and the genetic influences implicated in ASD are highly heterogeneous (Fernandez and Scherer, 2017; Geschwind, 2011; Grove et al., 2019; Jeste and Geschwind, 2014; Krumm et al., 2015; Persico and Bourgeron, 2006; Pinto et al., 2010; Ziats and Rennert, 2016). Analysis of the Simons Foundation Autism Research Initiative (SFARI) gene database identifies a vast diversity of hundreds of ASD associated genes (Abrahams et al., 2013; Banerjee-Basu and Packer, 2010a). Amongst these genes, a large number play roles in the development and function of synapses, such as neuroligin 3 (*NLGN3*), neuroligin 4X (*NLGN4X*), neurexin 1 (*NRXN1*), and SH3 and multiple ankyrin repeat domains 3 (*SHANK3*) (Durand et al., 2007; Feng et al., 2006; Jamain et al., 2003; Tabuchi et al., 2007). These and other reports

show that synaptic dysregulation and imbalances in neuronal activity are among the most common cellular alterations in ASD (Bagni and Zukin, 2019; Berkel et al., 2010; Bourgeron, 2015; Pfeiffer et al., 2010; Romero-Garcia et al., 2019; Schwede et al., 2018; Zoghbi, 2003).

The *NEXMIF* gene (also known as *KIDLIA*, *KIAA2022*, or *Xpn*) is a novel gene, localized on the X chromosome at Xq13.2, with little known biological function. Previous studies have demonstrated that NEXMIF mRNA expression starts as early as E10.5, increases throughout development with a peak at P3, and continues at a lower level into adulthood (Cantagrel et al., 2009; Ishikawa et al., 2012). NEXMIF mRNA shows notably strong expression in the cortex, hippocampus, cerebellum, and olfactory bulb (Allen Institute for Brain Science, 2004; Cantagrel et al., 2009). At the protein level, NEXMIF is specifically distributed in the nucleus of post-mitotic neurons but not in glia. Strong protein expression can be detected from E17 through adulthood in mice (Gilbert and Man, 2016), indicating a role for NEXMIF in brain development.

The *NEXMIF* gene was first implicated in ASD as one of the candidate genes in two male members of a family who had autistic phenotypes and ID (Cantagrel et al., 2004). That original report and others established that individuals with mutations in *NEXMIF* show repetitive behaviors, impaired language, seizures, and ID, with several cases of microcephaly (Cantagrel et al., 2004, 2009; Van Maldergem et al., 2013). Multiple additional reports have confirmed the loss of NEXMIF by gene mutation or deletion in individuals diagnosed with ASD (Alarcon-

Martinez et al., 2019; Charzewska et al., 2015; Farach and Northrup, 2016; Kuroda et al., 2015; Lambert et al., 2018; de Lange et al., 2016; Lorenzo et al., 2018; Webster et al., 2017). *NEXMIF* has been listed as an ASD gene in the SFARI database. We have recently shown that NEXMIF knockdown in rat hippocampal neurons impairs neurite outgrowth *via* a disruption of N-cadherin/δ-catenin signaling and actin dynamics, and loss of NEXMIF caused defects in neuron migration *in vivo* (Gilbert and Man, 2016; Van Maldergem et al., 2013). However, to date little is known regarding the function of NEXMIF or the cellular and molecular mechanisms underlying the disorder caused by the loss of NEXMIF.

Therefore, we utilized our transgenic *NEXMIF*$^{-/y}$ knockout mouse to investigate the role of NEXMIF in neuronal and synaptic development. We hypothesized that NEXMIF is involved in synaptogenesis and that the absence of NEXMIF in neurons from *NEXMIF*$^{-/y}$ brains would result in synaptopathy, thus causing ASD-like behaviors in these animals.

3.3 Results

3.3.1 *NEXMIF*$^{-/y}$ mice show typical autistic features in social behavior†

Loss of NEXMIF expression in humans produces behavioral deficits typical of ASD, including repetitive behavior, decreased social behavior and ID (Cantagrel et al., 2004, 2009; Farach and Northrup, 2016; Kuroda et al., 2015; de Lange et al., 2016; Van Maldergem et al., 2013; Webster et al., 2017). We therefore sought to characterize the knockout *NEXMIF*$^{-/y}$ mouse (KO) to determine its suitability as

a model for studying the human disorder. First, we looked for any deficits in social behavior, one of the core ASD behavioral impairments. To do this, we used the three-chamber social task, a test broadly used for assessing mouse sociability and interest in social novelty (Crawley, 2007; Moy et al., 2009). Animals were habituated to the apparatus by allowing the animals to explore all three chambers, including the empty cages, prior to testing (**Fig. 3.1A-3.1C**). To examine sociability, first a stranger mouse (Mouse 1) was placed into one of the chambers and the test mouse was allowed to freely navigate within the three-chamber apparatus (**Fig. 3.1D**). Representative track lengths during the test show that *NEXMIF*$^{-/y}$ mice spent significantly less time interacting with Mouse 1 compared to the empty cage (**Fig. 3.1E**). A significant decrease in the preference index for Mouse 1 was observed, indicating an impairment in sociability (**Fig. 3.1F**). To examine the *NEXMIF*$^{-/y}$ animal's interest in social novelty, a second mouse (Novel Mouse) was placed into the empty cage after the test mouse had been allowed to interact with Mouse 1 (**Fig. 3.1G**). Strikingly, *NEXMIF*$^{-/y}$ animals showed no preference for the Novel Mouse as shown in the representative track lengths (**Fig. 3.1H**) with a preference index significantly smaller compared to the WT animals, indicating a lack of interest in social novelty (**Fig. 3.1I**).

3.3.2 Impaired spatial memory in *NEXMIF*$^{-/y}$ animals†

Humans with loss of function mutations or genetic deletions of *NEXMIF* show autistic phenotypes accompanied by severe ID. We therefore sought to investigate whether our *NEXMIF*$^{-/y}$ mouse showed learning and memory deficits to

recapitulate the human condition. To do this, we used the Barnes maze for spatial memory. In this task, mice were trained over a period of 4 days to learn the location of a target escape hole, using spatial cues placed within the testing room, on a board containing 20 holes around its circumference. *NEXMIF*$^{-/y}$ animals showed the ability to learn the target escape hole location during acquisition training periods (**Fig. 3.2A**). After spatial acquisition training, the target hole was covered and the number of nose pokes made at each hole location was quantified 24 h and 5 d later (**Fig. 3.2B**). In the 24 h probe for spatial memory, *NEXMIF*$^{-/y}$ animals did not show significant differences in the number of nose pokes made at the target hole (**Fig. 3.2C**). Probing spatial memory 5 d after training showed that *NEXMIF*$^{-/y}$ animals had impairments in memory of the target hole location, with significantly less nose pokes at the target and adjacent holes and a broader search of the board (**Fig. 3.2D**). Quantification of the primary latency to find the target hole showed that *NEXMIF*$^{-/y}$ animals took much longer to find the target hole and traveled much longer prior to making an initial nose poke at the target hole in both the 24 h and the 5 d tests (**Fig. 3.2E- 3.2F**). These findings suggest that loss of NEXMIF impairs spatial memory, which may be a contributing factor to the ID observed in humans with loss of NEXMIF and ASD with ID.

3.3.3 Impairments in communication by ultrasonic vocalization in *NEXMIF*$^{-/y}$ mice

To further assess the behavioral characteristics of this model, we tested *NEXMIF*$^{-/y}$ animals for impaired communication, a core ASD behavioral deficit present in

humans with NEXMIF variants. To examine the communication behavior, we recorded and analyzed ultrasonic vocalizations (USVs) in pups isolated from their mother and littermates. Pups at P5, P7, and P9 were placed in a recording chamber for 5 min in which a microphone recorded any vocalizations (**Fig. 3.3A**). Quantification of the number of calls showed that *NEXMIF*$^{-/y}$ animals made significantly fewer calls overall (**Fig. 3.3B**) and fewer calls within each minute of the 5-minute recording period, at all time points measured (**Fig. 3.3C-3.3E**). Calls made by the *NEXMIF*$^{-/y}$ animals were also of shorter length (**Fig. 3.3F**) resulting in a reduced total time spent calling (**Fig. 3.3G**). There was no change in average peak amplitude or peak frequency of vocalizations between the WT and KO animals (**Fig. 3.3H-3.3I**). Further analysis of the call syllable types (**Fig. 3.4A**) revealed that *NEXMIF*$^{-/y}$ animals generally made simpler USV calls than WT animals (**Fig. 3.4B**), making significantly more short and flat calls and fewer modulated and multiple jump calls (**Fig. 3.4C-3.4E**). These findings suggest that loss of NEXMIF results in an impairment in normal communication. In addition, we found that *NEXMIF*$^{-/y}$ animals demonstrate repetitive self-grooming, decreased marble burying, and increased activity in an open field (data not shown), further establishing this as an ASD model.

3.3.4 Neurons from *NEXMIF*$^{-/y}$ mice show deficits in neurite extension

Having established that the *NEXMIF*$^{-/y}$ mice are a good model of the human disorder, we wanted to use this model to investigate the molecular mechanisms underlying the observed behavioral phenotypes. To directly study the effect of

complete knockout of NEXMIF on neuron morphological development, we used primary mouse neurons cultured from *NEXMIF*$^{-/y}$ mice. To measure changes in dendritic arborization, *NEXMIF*$^{-/y}$ cortical neurons were fixed at DIV 8 and immunostained for MAP2 to label dendrites (**Fig. 3.5A**). At this time point, the dendrites are undergoing much of their initial branching. Sholl analysis revealed a significant reduction in dendritic branching complexity for neurons from *NEXMIF*$^{-/y}$ animals compared to those from male WT littermates (**Fig. 3.5B**). *NEXMIF*$^{-/y}$ neurons also showed a decrease in the total number of dendrites, number of branch points, number of terminal points, and the sum length of the dendrites compared to WT neurons (**Fig. 3.5C-3.5F**). We also assessed dendritic phenotypes at DIV 14, when a great deal of the dendritic extension has taken place (**Fig. 3.5G**). Similarly, DIV 14 *NEXMIF*$^{-/y}$ neurons have a dramatically reduced dendritic arbor with fewer dendrites, branch points, terminal points, and a decreased sum length of dendrites compared to WT neurons (**Fig. 3.5H-3.5L**). These findings are consistent with our earlier work using shRNA knockdown of NEXMIF in cultured rat neurons (Gilbert and Man, 2016).

We also examined the effect of NEXMIF knockout on axon extension. To do this, cortical neurons from *NEXMIF*$^{-/y}$ mice were fixed at DIV 3 and immunostained for Tau1 to label axons (**Fig 3.6A**). At this time point, the axon has recently differentiated from the other neurites. Tracing the axons revealed that axons from *NEXMIF*$^{-/y}$ neurons were shorter and branched less than those from WT neurons (**Fig. 3.6B-3.6C**). We also assessed axonal development after

several days of growth and branching at DIV 6 (**Fig 3.6D**). Interestingly, there was no difference in total axon length or number of branches between WT and *NEXMIF*$^{-/y}$ neurons at this later time point (**Fig. 3.6E-3.6D**). Together, these results support a role for NEXMIF in neurite formation and extension.

3.3.5 Loss of NEXMIF results in alterations in synaptic protein composition

To examine synaptic changes due to loss of NEXMIF, we first used an *in vitro* model using lentiviral-mediated shRNA knockdown of NEXMIF, and analyzed GluA1 and PSD-95 synaptic puncta *via* ICC at DIV 14 in primary hippocampal neurons (**Fig. 3.7A**). Strikingly, a 45% reduction in GluA1 puncta density and 20% reduction in GluA1 puncta intensity were observed after shRNA-mediated knockdown of NEXMIF compared to scrambled shRNA treatment (**Fig. 3.7B-3.7C**). Analysis of the immunostaining of PSD-95 showed a 60% reduction in puncta density with no change in synaptic intensity (**Fig. 3.7D-3.7E**). Analysis of GluA1 puncta in primary cortical neurons showed similar reductions in puncta density of 20% and in puncta intensity of 37%, (**Fig. 3.7F-3.7G**) while PSD-95 puncta showed a 45% reduction puncta density and a 40% reduction in puncta intensity (**Fig. 3.7H-3.7I**).

We then immunostained the presynaptic marker VGluT1 (**Fig. 3.8A**). After shRNA-mediated knockdown of NEXMIF, VGluT1 puncta density was reduced by 38% with no change in puncta intensity (**Fig. 3.8B-3.8C**). To examine changes in inhibitory GABAergic synaptic proteins, we used lentiviral-mediated shRNA knockdown of NEXMIF and immunostained for gephyrin (**Fig. 3.8D**). We found

that, compared to scrambled shRNA, knockdown of NEXMIF resulted in a 27% reduction in the intensity and a modest reduction in density of gephyrin puncta (**Fig. 3.8E-3.8F**). We further characterized the effect of loss of NEXMIF on GABAergic synaptic proteins by immunostaining for GAD65 (**Fig. 3.8G**). Analysis of GAD65 immunostaining revealed a significant reduction in both puncta intensity and puncta density (**Fig. 3.8H-3.8I**). Collectively, these results demonstrate a reduced in the level of synaptic proteins from loss of NEXMIF, which is suggestive of a change in synapses.

3.3.6 Confirmation of synaptic impairment in neurons from *NEXMIF$^{-/y}$* mice

To confirm the changes in synaptic proteins observed from transient knockdown of NEXMIF, we further examined synaptic development in neurons from the *NEXMIF$^{-/y}$* mice. We cultured cortical neurons from transgenic knockout *NEXMIF$^{-/y}$* mice and WT male littermates and immunostained them at DIV 14 for the excitatory postsynaptic receptor subunit GluA1 (**Fig. 3.9A**). Strikingly, in *NEXMIF$^{-/y}$* neurons, GluA1 puncta density was reduced by 70% and puncta intensity was reduced by 40% compared to that in WT neurons (**Fig. 3.9B-3.9C**). Similarly, in hippocampal neurons, GluA1 demonstrated deficits in *NEXMIF$^{-/y}$* neurons compared to WT neurons with a 55% decrease in puncta density and a 15% decrease in puncta intensity (**Fig 3.9D-3.9E**). Cortical neurons cultures from WT or *NEXMIF$^{-/y}$* mice were also immunostained at DIV 14 for the inhibitory postsynaptic receptor subunit GABARα1 (**Fig. 3.9F**). Analysis of GABARα1 immunostaining revealed a 60% reduction in puncta density and a 26% reduction

in puncta intensity in *NEXMIF*$^{-/y}$ neurons compared to WT neurons (**Fig. 3.9G-3.9H**). GABARα1 in hippocampal *NEXMIF*$^{-/y}$ neurons, however, showed no change in puncta intensity compared to WT neurons but maintained the 60% reduction in puncta density observed in cortical neurons (**Fig. 3.9I-3.9J**).

We also investigated spine density in our transgenic culture. Consistent with the phenotype we observed from Golgi staining of WT and *NEXMIF*$^{-/y}$ brain slices, Phalloidin staining for actin-rich spines in DIV 13 neurons cultured from WT or *NEXMIF*$^{-/y}$ mice showed a significant decrease in spine density for *NEXMIF*$^{-/y}$ neurons compared to WT neurons (**Fig. 3.9K-3.9L**).

3.3.7 Loss of NEXMIF results in deficits in synapse formation

To further investigate the effect of NEXMIF knockdown on synaptic formation, we quantified the number of functional synapses by colocalization of presynaptic axon terminals with postsynaptic spines. For excitatory glutamatergic synapses, we used lentiviral-mediated shRNA knockdown of NEXMIF and co-immunostained the presynaptic marker VGluT1 with the postsynaptic marker PSD-95 (**Fig. 3.10A**). After shRNA-mediated knockdown of NEXMIF, glutamatergic synapse density was reduced by 30% (**Fig. 3.10B**). To examine changes in GABAergic synapses, we co-immunostained gephyrin and VGAT to analyze colocalized GABAergic synaptic puncta (**Fig. 3.10C**). We found that, compared to scrambled shRNA, knockdown of NEXMIF resulted in a 60% reduction in GABAergic synapse density (**Fig. 3.10D**).

As these results are due to transient knockdown of NEXMIF expression, we confirmed the changes in synapse density in neurons cultured from *NEXMIF*$^{-/y}$ mice. Similar to the knockdown result, complete loss of NEXMIF in *NEXMIF*$^{-/y}$ neurons resulted in a significant decrease in the density of VGluT1 and PSD95 colocalized glutamatergic synaptic puncta compared to WT neurons (**Fig. 3.10G-3.10H**). Additionally, *NEXMIF*$^{-/y}$ neurons showed a significant decrease in the density of VGat and gephyrin colocalized GABAergic puncta compared to WT neurons (**Fig. 3.10I-3.10J**). These findings demonstrate that loss of NEXMIF expression has a profound effect on both glutamatergic and GABAergic synapse formation, with a large decrease in synapse number.

3.3.8 Neurons from *NEXMIF*$^{-/y}$ animals show impairments in synaptic plasticity

To determine the functional consequences of the impaired synapse development that occurs in *NEXMIF*$^{-/y}$ neurons, we investigated the AMPA receptor dynamics underlying both Hebbian and homeostatic synaptic plasticity in these neurons. First, we tested the ability of neurons from *NEXMIF*$^{-/y}$ mice to undergo LTP by using a standard protocol that chemically induces LTP (chem-LTP) by treating neurons with glycine (150 μM) (Lu et al., 2001). In DIV 14 neurons, an N-terminal specific GluA1 antibody was used to label surface expressing AMPARs before and after treatment to identify newly inserted AMPARs (**Fig. 3.11A**). As expected, neurons from WT mice showed an increase in GluA1 surface expression after chem-LTP (**Fig. 3.11B**). However, chem-LTP failed to increase the surface

expression of GluA1 in neurons from *NEXMIF*$^{-/y}$ mice (**Fig. 3.11B**). Additionally, we tested homeostatic synaptic plasticity (HSP) in *NEXMIF*$^{-/y}$ neurons using an established protocol that induces chronic inactivation to stimulate HSP. DIV 14 neurons were treated with TTX (1 μM) and APV (25 μM) for 24 h and then immunostained with an N-terminal specific GluA1 antibody to label the surface expressing AMPARs (**Fig. 3.11C**). When WT neurons had HSP induced, a significant increase in surface expressing GluA1 was observed (**Fig. 3.11D**). However, HSP induced *NEXMIF*$^{-/y}$ neurons failed to show an increase in GluA1 surface expression compared to those without HSP treatment (**Fig. 3.11D**).

3.3.9 Loss of NEXMIF leads to reduced expression of Nrgn and SynDig1†

Given the nuclear localization of NEXMIF, we hypothesized that NEXMIF may function as a transcriptional regulator. Therefore, our group performed an RNAseq to examine changes gene expression from loss of NEXMIF. Mouse neuronal cultures were infected with lentiviral NEXMIF shRNA or a scrambled control on DIV 0. Total RNA was collected at DIV 14 and analyzed in RNAseq for changes in gene expression. A total of 1,097 significantly up-regulated and 961 significantly down-regulated genes were identified, with more dramatic downregulation dominating (**Fig. 3.12A**). Ingenuity Pathway Analysis (IPA) identified glutamatergic signaling, synaptogenesis signaling, and synaptic plasticity processes such as LTP and LTD among the top dysregulated signaling pathways (**Fig. 3.12B**). Additionally, gene ontology (GO) enrichment analysis of the RNAseq dataset identified many synapse or neurodevelopment related genes

participating in processes such as neuron development and differentiation (**3.12C**). Among the top downregulated, genes, two emerged as top candidates for effecting synapse development downstream of NEXMIF. The first was neurogranin (Nrgn), the top downregulated gene, which is a calmodulin-binding protein enriched in dendritic spines and plays a role in synaptic plasticity and synaptogenesis (Díez-Guerra, 2010; Garrido-García et al., 2019; Ryoo et al., 2015; Zhabotinsky et al., 2006; Zhong and Gerges, 2010)**.** The second was SynDig1, which was in the top 10% of downregulated genes, is enriched in synapses, and promotes synapse formation (Díaz, 2012; Kalashnikova et al., 2010; Lovero et al., 2013). To confirm the reduced mRNA transcript levels of these candidates, we used lentiviral shRNA to knockdown NEXMIF in cultured neurons and performed qPCR on their cell lysates. Quantification of NEXMIF mRNA levels after shRNA treatment confirmed successful knockdown compared to use of a scrambled (SCR) shRNA control (**Fig. 3.13A**). Similar to the findings from RNAseq, shRNA knockdown of NEXMIF lead to a 72% decrease in Nrgn mRNA levels as well as a 60% decrease in SynDig1 mRNA levels (**Fig. 3.13B-3.13C**). To determine whether these decreases in mRNA lead to changes in protein expression, hippocampal brain lysates were collected from P30 WT and *NEXMIF*$^{-/y}$ mice for western blot analysis (**Fig. 3.13D**). Immunostaining of synaptic proteins revealed no change in total PSD95 levels but a significant decrease in total GluA1 levels (**Fig. 3.13E-3.13F**). Additionally, we observed a significant reduction in the

total protein expression of both Nrgn and SynDig1, confirming the findings from qPCR (**Fig. 3.13G-3.13H**).

3.3.10 Reintroduction of Nrgn and/or SynDig1 rescues synapse formation in NEXMIF null neurons

We next wanted to determine whether reintroduction of Nrgn or SynDig1 could rescue the synaptic deficits observed from loss of NEXMIF. To do this, we transfected rat hippocampal neuron cultures at DIV 9 with GFP or GFP and NEXMIF shRNA, together with an empty vector plasmid, Nrgn, SynDig1, or Nrgn and SynDig1. Neurons were then fixed and immunostained for GluA1 at DIV 16 (**Fig. 3.14A**). Similar to that observed previously, there was a decrease in the GluA1 puncta density in neurons with NEXMIF knockdown. However, neurons with co-transfection of Nrgn, SynDig1, or both showed a rescue of GluA1 puncta density to levels similar to those of the control neurons (**Fig. 3.14B**). We performed a similar transfection at DIV 6 in neurons that were fixed on DIV 14 and stained with Phalloidin to label actin-rich spines (**Fig. 3.14C**). As seen previously, loss of NEXMIF resulted in a significant decrease in spine density. Co-transfection with Nrgn, SynDig1, or both was able to significantly increase the spine density in these neurons compared to NEXMIF shRNA alone. However, only treatment with Nrgn was able to rescue spine density to a level similar to that of control neurons as neurons treated with SynDig1 or Nrgn and SynDig1 together only demonstrated partial rescue (**Fig. 3.14D**).

3.4 Discussion

In this study, we successfully established a mouse model for NEXMIF-dependent ASD and ID. The *NEXMIF*$^{-/y}$ mouse displays the characteristics observed in humans with loss of NEXMIF and can therefore be used as an animal model. *NEXMIF*$^{-/y}$ mice display significant impairments in the three-chamber social task, with decreased sociability and decreased interest in social novelty. *NEXMIF*$^{-/y}$ mice spent significantly less time interacting with a novel mouse. Additionally, *NEXMIF*$^{-/y}$ animals showed significant communication impairments shown by USVs, with increased use of simpler and shorter call types as well as fewer calls and less total time spent making calls. We also found significant impairments in the marble-burying test, with *NEXMIF*$^{-/y}$ animals burying significantly fewer marbles during the task, a phenotype that suggests a decreased interest in their surrounding environment. *NEXMIF*$^{-/y}$ mice also displayed significantly increased repetitive grooming and hyperactivity, common phenotypes observed in ASD mouse models (Kalueff et al., 2016; Silverman et al., 2010). *NEXMIF*$^{-/y}$ mice also displayed major deficits in spatial memory, which is consistent with findings of moderate-to-severe ID in humans with NEXMIF mutations, (Cantagrel et al., 2004, 2009; Kuroda et al., 2015; Lambert et al., 2018; Lorenzo et al., 2018; Van Maldergem et al., 2013). *NEXMIF*$^{-/y}$ mice were able to learn the target hole location over the course of the Barnes maze training but, showed impairments when probing their memory of the location 5 d later.

Our group has previously shown loss of NEXMIF impairs neurite outgrowth and actin dynamics (Gilbert and Man, 2016), work which helped in the naming of NEXMIF (neurite extension and migration factor). However, the previous findings were for loss of NEXMIF due to transient shRNA-mediated knockdown. Here we confirm the dysregulation of neurite formation in neurons from *NEXMIF*$^{-/y}$ mice. *NEXMIF*$^{-/y}$ neurons have less complex dendritic arbors with shorter dendrites and less branches than WT neurons at DIV 8 and DIV 14. *NEXMIF*$^{-/y}$ neurons also have shorter and less branched axons at DIV 3. Interestingly, this difference in axon size is no longer visible at DIV 6. This may indicate that loss of NEXMIF impairs initial axon specification but there is no deficit in axon extension. It would be interesting for future studies to examine the effect of loss of NEXMIF on the axon initial segment, for its roles in both neuronal polarity and excitability (Buffington and Rasband, 2011; Leterrier, 2018).

ASD is classified among other neurodevelopmental disorders, such as fragile X syndrome, Rett syndrome, and Angelman syndrome, as a synaptopathy due frequently observed alterations in synaptic structure and function among its cellular phenotypes (Bagni and Zukin, 2019; Guang et al., 2018; Phillips and Pozzo-Miller, 2014; Della Sala and Pizzorusso, 2014; Yang, 2020). Such irregularities in synaptogenesis and synaptic function are a shared underlying neurobiological mechanism that results in the social and cognitive deficits observed in these disorders (Carroll et al., 2021; Won et al., 2013; Zoghbi and Bear, 2012). We observed a major dysregulation in synaptic protein expression

with a reduction in both glutamatergic and GABAergic synaptic proteins including AMPARs, PSD-95, and gephyrin from neurons of NEXMIF knockdown and *NEXMIF*$^{-/y}$ brain tissue. Additionally, neurons from *NEXMIF*$^{-/y}$ mouse brains revealed significantly decreased spine and both glutamatergic and GABAergic synaptic densities. It will be valuable for future studies to explore changes in spine and synapse formation throughout developmental stages to clarify whether synaptic and spine deficits result from aberrant structural growth or pruning, and if NEXMIF plays a role in synapse maintenance and function after synaptogenesis.

In addition to these structural changes, we also observed functional changes in synaptic plasticity. Synaptic plasticity is mediated by exocytosis of AMPARs onto the synaptic surface from recycling endosomes (Ju et al., 2004; Park et al., 2004, 2006; Sutton et al., 2006). *NEXMIF*$^{-/y}$ neurons failed to enhance surface AMPAR expression in response to NMDAR-dependent chemical LTP. *NEXMIF*$^{-/y}$ neurons also failed to increase surface AMPAR expression in response to HSP treatments. These findings indicate impairments in both Hebbian and homeostatic synaptic plasticity. While the exact mechanisms remain to be elucidated, it is possible that loss of NEXMIF results in impaired exocytosis, or enhanced endocytosis, of AMPAR, thus preventing stable AMPAR insertion during both LTP and HSP. These major abnormalities in synapse formation and function may underlie the behavioral deficits of this animal model. Additional studies of LTD and AMPAR endocytosis in *NEXMIF*$^{-/y}$ neurons would be of interest to further our understanding of the role NEXMIF plays in synaptic plasticity.

Our previous work indicated that NEXMIF is distributed exclusively in the nucleus of neurons but not glia, indicating that NEXMIF may function as a transcriptional regulator (Gilbert and Man, 2016). Our RNAseq data from neurons with NEXMIF knockdown revealed a large population of genes being up- or down-regulated in expression. The significantly dysregulated genes include those involved in neuron development, glutamatergic signaling, synapse formation, and synaptic plasticity. This suggests that NEXMIF may function to enhance synaptic gene expression during development. Among the top down-regulated genes involved in synapse formation and function, we identified the candidate molecules neurogranin (Nrgn) and SynDig1 (Garrido-García et al., 2019; Kalashnikova et al., 2010; Zhabotinsky et al., 2006). We found that overexpression of either Nrgn or SynDig1 could rescue the density of AMPAR puncta and spines after loss of NEXMIF expression. Further studies to explore the potential rescue effect of Nrgn and SynDig1, particularly on synaptic plasticity and ASD-related behaviors, would be of interest. Additionally, future work to elucidate NEXMIF's role in the nucleus would help to clarify whether NEXMIF functions as a transcription factor or a component of regulatory complexes in gene expression.

In conclusion, neurons from the *NEXMIF*$^{-/y}$ mouse reveal potential roles for NEXMIF in multiple steps of neuron development including morphogenesis, synapse formation, and synaptic plasticity. Additionally, preliminary rescue experiments suggest downstream roles for Nrgn and SynDig1 in mediating NEXMIF's effects on synapse development. Further work is needed to elucidate

the direct function of NEXMIF as well as the mechanistic pathway leading from NEXMIF to each of its phenotypes. Future studies should make use of the *NEXMIF*$^{-/y}$ mouse for continued investigations of NEXMIF function and for ASD rescue approaches by molecular therapies, such as genetic restoration or signaling pathway intervention.

Figure 3.1

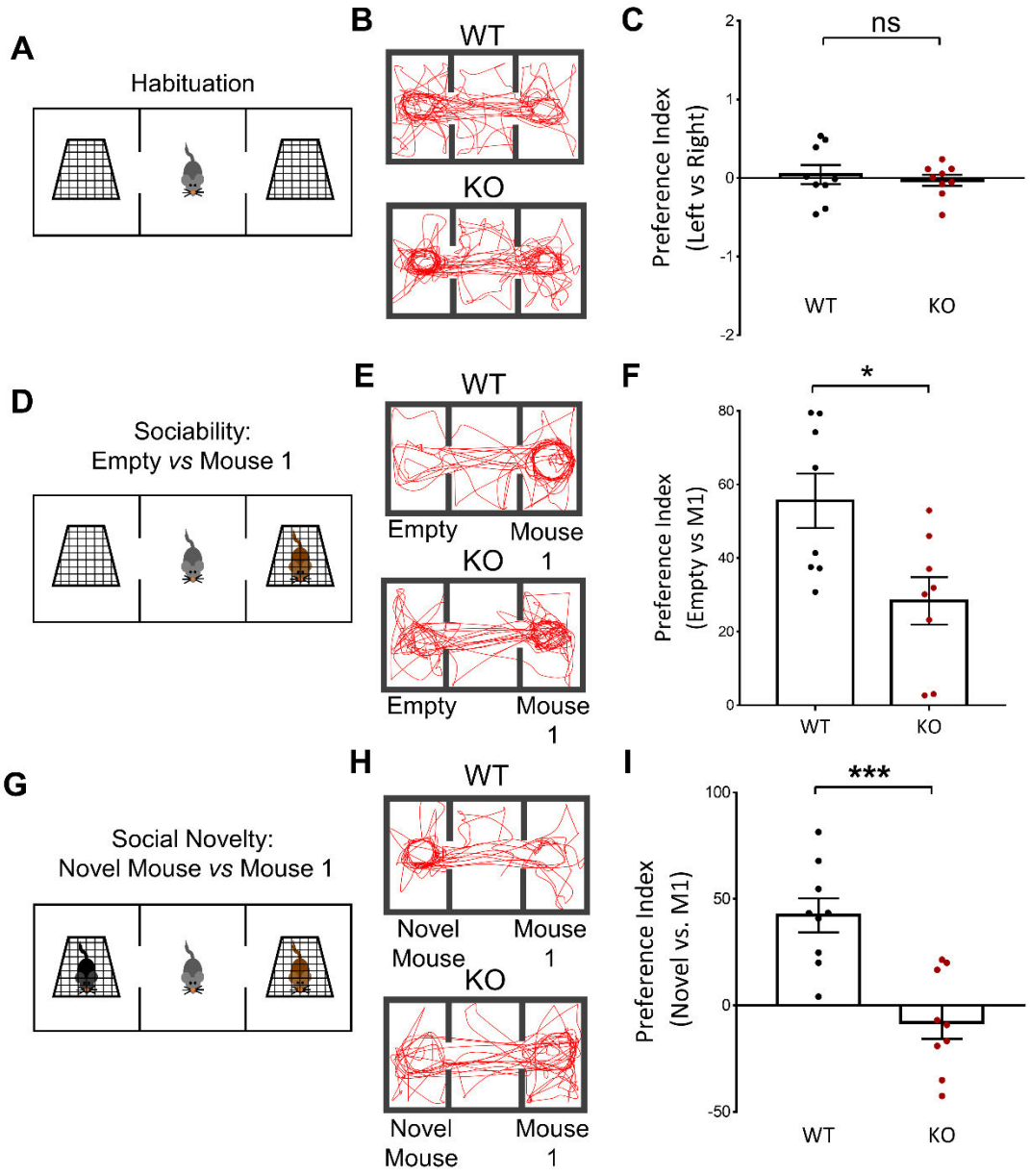


Figure 3.1 NEXMIF knockout mice show impaired social behavior in the three-chamber social test†

(A) Habituation to the three-chamber apparatus. Mice were released from the center chamber, with empty cages in the adjacent chambers, and allowed to move

freely within the apparatus for 5 min prior to beginning the sociability and social novelty tests. **(B)** Traces of animal track paths in the habituation phase for WT and KO mice. **(C)** Neither WT or KO animals showed any preference for either side chamber during habituation. (Left vs Right: WT: $t_{(32)} = 0.61$, $p = 0.55$; KO: $t_{(32)} = 0.29$, $p = 0.77$). **(D)** Paradigm for the sociability test. An unfamiliar mouse (Mouse 1) was placed into either of the side chambers and the test mouse was allowed to move freely within the apparatus. **(E)** Traces of animal track paths in the sociability test for WT and KO mice. **(F)** Quantification of the preference index (see methods) showed a decrease in preference for Mouse 1 in NEXMIF KO animals compared to WT controls. (WT = 55.57 $\pm$ 7.37, $n = 8$; KO = 28.38 $\pm$ 6.46, $n = 8$; $t_{(6)} = 2.71$, $p = 0.035$) **(G)** Paradigm for the social novelty test. A second mouse (Novel Mouse) was placed into the remaining empty chamber opposite to Mouse 1, and the test mouse was allowed to interact with both mice. **(H)** Traces of animal track paths in the social novelty test for WT and KO mice. **(I)** In the social novelty test, KO animals showed no preference for the novel animal. (WT = 42.30 $\pm$ 8.00, $n = 9$; KO = -7.93 $\pm$ 7.81, $n = 9$; $t_{(8)} = 3.84$, $p = 0.005$). WT: wild type littermate, KO: *NEXMIF*$^{-/y}$. Data are represented as mean ± SEM. *p<0.05, **p<0.01, ***p<0.001, ns = not significant. † *Contribution from James Gilbert.*

Figure 3.2

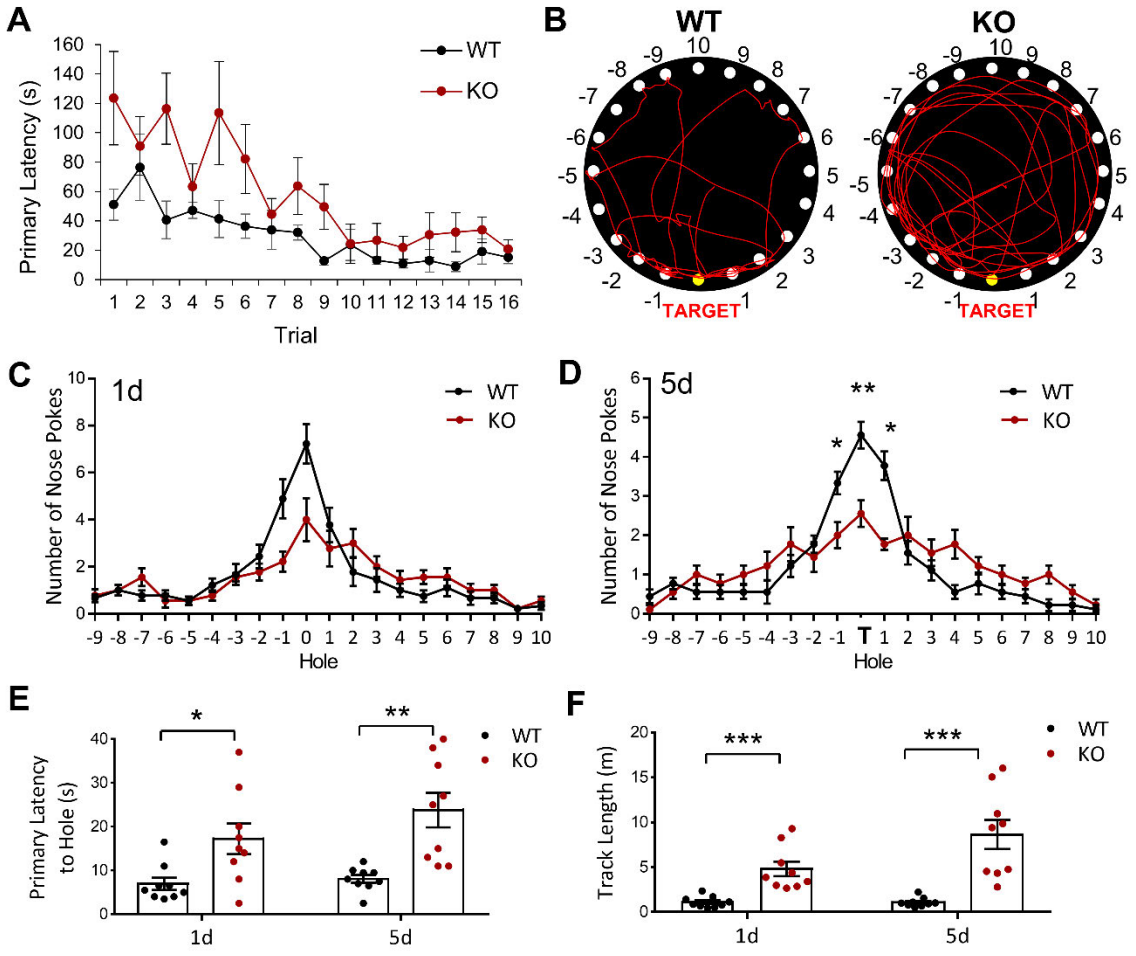


Figure 3.2 NEXMIF knockout mice show impairments in Barnes maze spatial learning and memory†

(A) Quantification of the primary latency (s) to find the target hole across all training trials (4 trials per day over 4 days) for WT and KO animals. **(B)** Traces of track paths in the Barnes spatial memory maze during the 5 d memory probe for WT and KO animals. **(C)** The distribution of nose pokes on the board showed no difference 24 h after training. **(D)** Quantification of the distribution of nose pokes

across different holes on the board showed a significant decrease for the target and adjacent holes in the 5 d memory probe. **(E, F)** Primary latency to the target hole (E) (24 h: WT = 6.94 ± 1.41 s, $n = 9$; KO = 17.22 ± 3.5 s, $n = 9$; $t_{(32)} = 2.64$, $p = 0.013$; 5 d: WT = 8.06 ± 0.90 s, $n = 9$; KO = 23.78 ± 3.91 s, $n = 9$; $t_{(32)} = 4.04$, $p = 0.00032$) and total track length (F) (24 h: WT = 0.11 ± 0.021 m, $n = 9$; KO = 0.48 ± 0.0.81 m, $n = 9$; $t_{(16)} = 4.41$, $p = 0.00044$; 5 d: WT = 0.11 ± 0.017 m, $n = 9$; KO = 0.86 ± 0.16 m, $n = 9$; $t_{(16)} = 4.65$, $p = 0.00027$) were increased in the KO animals probing both 1 d and 5 d after training. WT: wild type littermate, KO: *NEXMIF*$^{-/y}$. Data are represented as mean ± SEM. *p<0.05, **p<0.01, ***p<0.001, ns = not significant. † *Contribution from James Gilbert.*

Figure 3.3

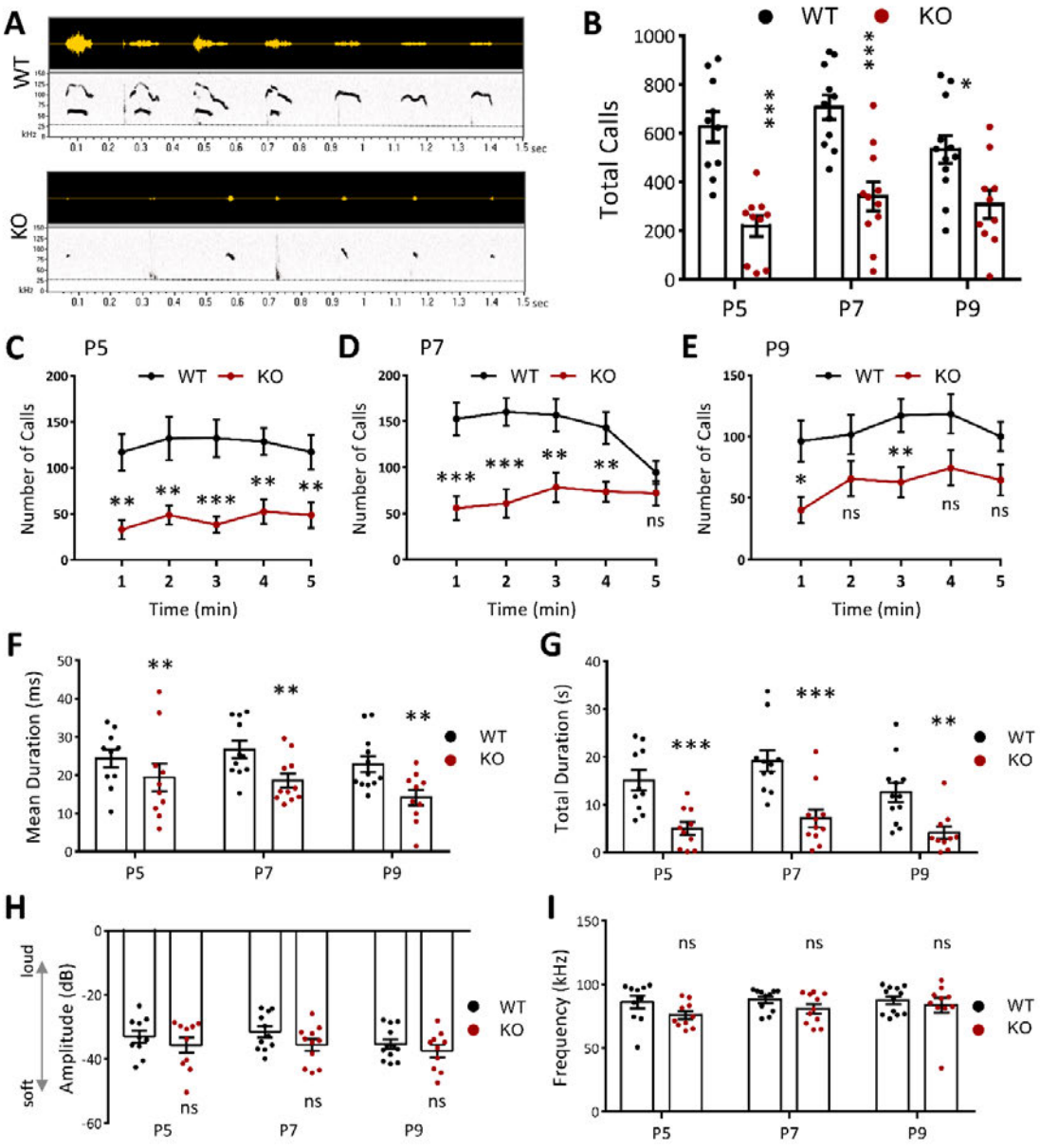


Figure 3.3 NEXMIF knockout mice show impairments in communication

(A) Representative vocalizations from P7 recordings for WT and KO mice. Top: the raw USV signals. Bottom: the associated spectrograms; all are 1.5 s in length. Dashed line depicts the 30 kHz frequency threshold for eliminating noise. **(B)**

Quantification of the call rate shows a decrease in the number of calls made by NEXMIF KO animals compared to WT controls at each developmental time point recorded. (P5: $t_{(18)} = 5.37$, $n = 10$, $p < 0.0001$; P7: $t_{(20)} = 4.71$, $n = 11$, $p = 0.00013$; P9: $t_{(20)} = 2.78$, WT: $n = 12$, KO: $n = 10$, $p = 0.012$). **(C-E)** Mean number of calls emitted across the 5 min recording period at each developmental time point P5 (C: WT, n =10; KO, n =10), P7, (D: WT, n =11; KO, n =11), and P9 (E: WT, n =12; KO, n =11). **(F, G)** NEXMIF KO mice showed a decreased mean call syllable duration (F) (P5: $t_{(16)} = 3.06$, $p = 0.0075$; P7: $t_{(20)} = 2.86$, $p = 0.0097$; P9: $t_{(20)} = 2.98$, $p = 0.0074$) and a decrease in total time spent calling (G) (P5: $t_{(18)} = 4.02$, $p = 0.0008$; P7: $t_{(20)} = 4.18$, $p = 0.00047$; P9: $t_{(20)} = 3.43$, $p = 0.0027$) at each time point. **(H, I)** Quantification of the peak amplitude (H) and peak frequency (I) of calls shows no change between NEXMIF WT and KO animals at any time point. WT: wild type littermate, KO: *NEXMIF*$^{-/y}$. Data are represented as mean ± SEM. *p<0.05, **p<0.01, ***p<0.001, ns = not significant.

Figure 3.4

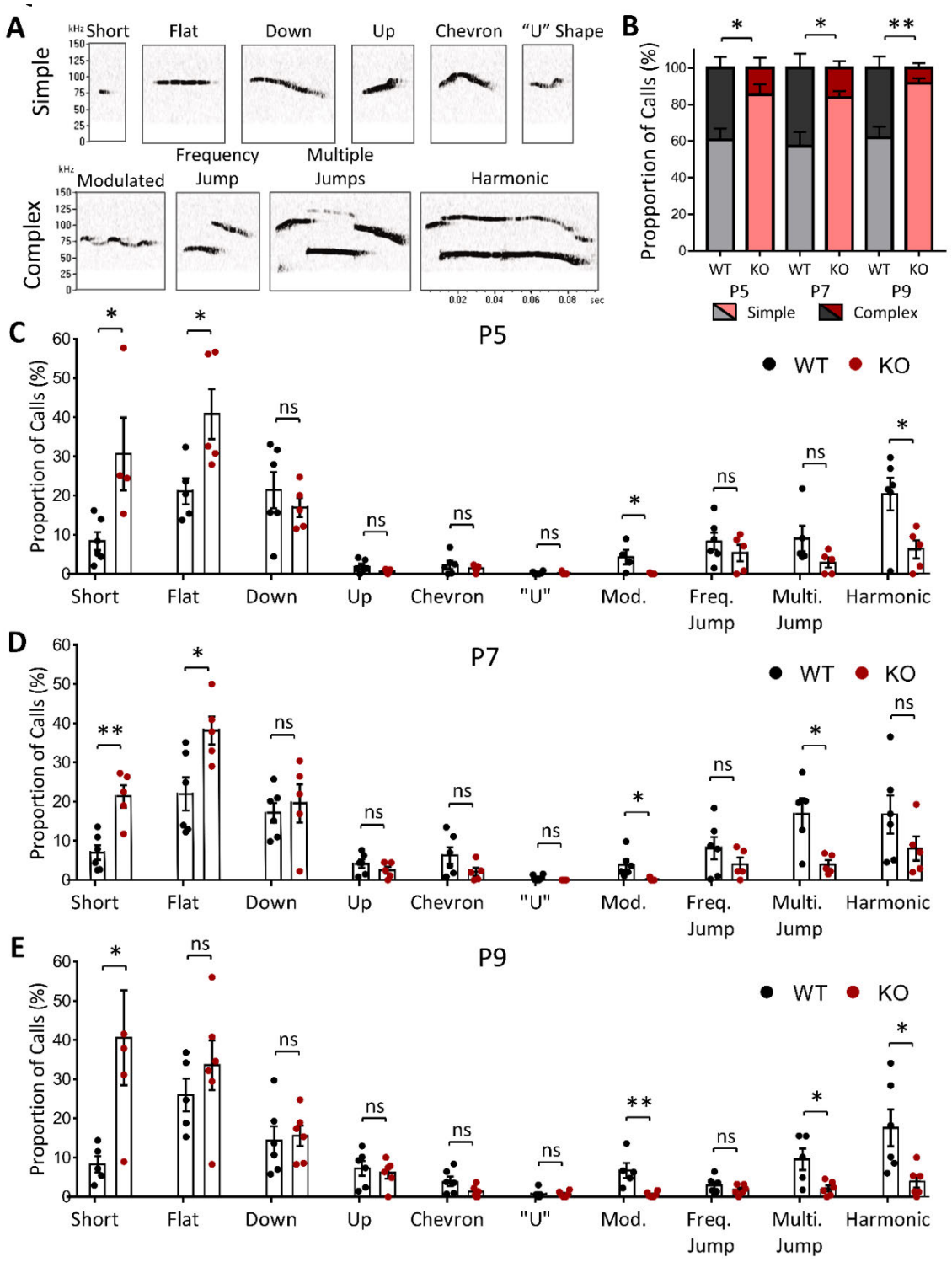

A
Simple
Short
Flat
Down
Up
Chevron
"U" Shape
Complex
Modulated
Frequency Jump
Multiple Jumps
Harmonic
kHz
sec
B
Proppportion of Calls (%)
WT
KO
P5
P7
P9
Simple
Complex
C
P5
D
P7
E
P9
Proportion of Calls (%)
WT
KO
Short
Flat
Down
Up
Chevron
"U"
Mod.
Freq. Jump
Multi. Jump
Harmonic
ns

Figure 3.4 Syllable classification of USV calls in NEXMIF mice

(A) Representative calls of each type used in syllable characterization. **(B)** KO animals showed an increase in Simple type calls and a decrease in Complex type calls compared to WT animals at each time point. (P7: WT = 57.12 ± 7.86%, n = 6; KO = 83.72 ± 3.69%, $n = 5$; $F_{(1,9)} = 19.27$, $p = 0.002$, ANOVA). **(C)** Call syllable classification at P5 shows an increase in short and flat calls and a decrease in modulated and harmonic calls made by KO animals compared to WT animals. **(D)** KO mice made significantly more short and flat calls compared to WT mice and significantly less modulated and multiple jump calls at P7. (P7: Short: $t_{(9)} = 4.9$, $p = 0.0018$; Flat: $t_{(9)} = 2.86$, $p = 0.019$; Mod.: $t_{(9)} = 2.60$, $p = 0.029$; Multi. Jump: $t_{(8)} = 3.14$, $p = 0.014$). **(E)** Call syllable classification at P9 shows an increase in short calls and decrease in modulated, multiple jump, and harmonic calls made by KO animals compared to WT animals. (WT, n =6; KO, n = 5). WT: wild type littermate, KO: *NEXMIF*$^{-/y}$. Data are represented as mean ± SEM. *p<0.05, **p<0.01, ***p<0.001, ns = not significant.

Figure 3.5

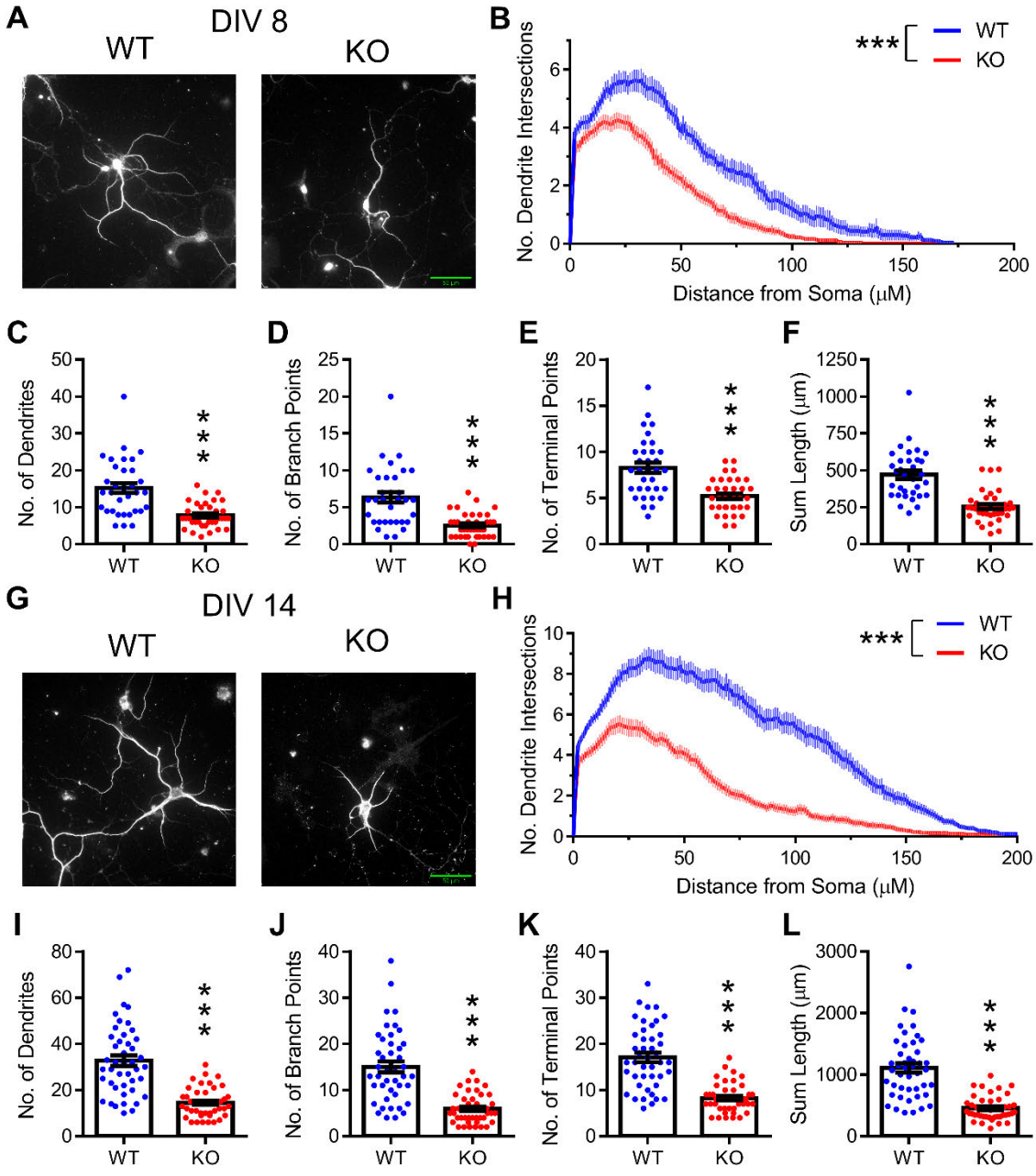


Figure 3.5 Neurons from *NEXMIF*$^{-/y}$ mice show a decrease in dendritic arborization

(A) Representative images of MAP2 immunostained primary cortical neurons from WT or *NEXMIF*$^{-/y}$ brains at DIV 8. **(B)** Sholl analysis reveals a decrease in dendritic arbor complexity for *NEXMIF*$^{-/y}$ neurons compared to WT neurons at DIV 8 (repeated measures two-way ANOVA followed by Bonferroni's multiple comparison test; $F_{(1,70)} = 28.47$, $p < 0.0001$ between genotypes; $F_{(173, 12110)} = 156.9$, $p < 0.0001$ between radius). **(C-F)** The number of dendrites (C) ($t_{(68)} = 5.375$, $p < 0.0001$), branch points (D) ($t_{(68)} = 5.244$, $p < 0.0001$), terminal points (E) ($t_{(68)} = 4.969$, $p < 0.0001$), and sum length of dendrites (F) ($t_{(68)} = 6.660$, $p < 0.0001$) were decreased in *NEXMIF*$^{-/y}$ neurons compared to WT neurons at DIV 8. $n = 34$ neurons/ group. **(G)** Representative images of MAP2 immunostained primary cortical neurons from WT or *NEXMIF*$^{-/y}$ brains at DIV 14. **(H)** Dendritic complexity is decreased in *NEXMIF*$^{-/y}$ neurons compared to WT neurons at DIV 14 as measured by Sholl analysis (repeated measures two-way ANOVA followed by Bonferroni's multiple comparison test; $F_{(1,89)} = 63.21$, $p < 0.0001$ between genotypes; $F_{(200, 17800)} = 166$, $p < 0.0001$ between radius). **(I-L)** The number of dendrites (I) ($t_{(87)} = 7.492$, $p < 0.0001$), branch points (J) ($t_{(87)} = 7.251$, $p < 0.0001$), terminal points (K) ($t_{(87)} = 7.918$, $p < 0.0001$), and the sum length of dendrites (L) ($t_{(88)} = 8.074$, $p < 0.0001$) were decreased in *NEXMIF*$^{-/y}$ neurons compared to WT neurons at DIV 14. $n = 44$ neurons/ group. Scale bars = 20 μm. WT: wild type littermate, KO: *NEXMIF*$^{-/y}$. Data are represented as mean ± SEM. $^{**}p<0.01$, $^{***}p<0.001$.

Figure 3.6

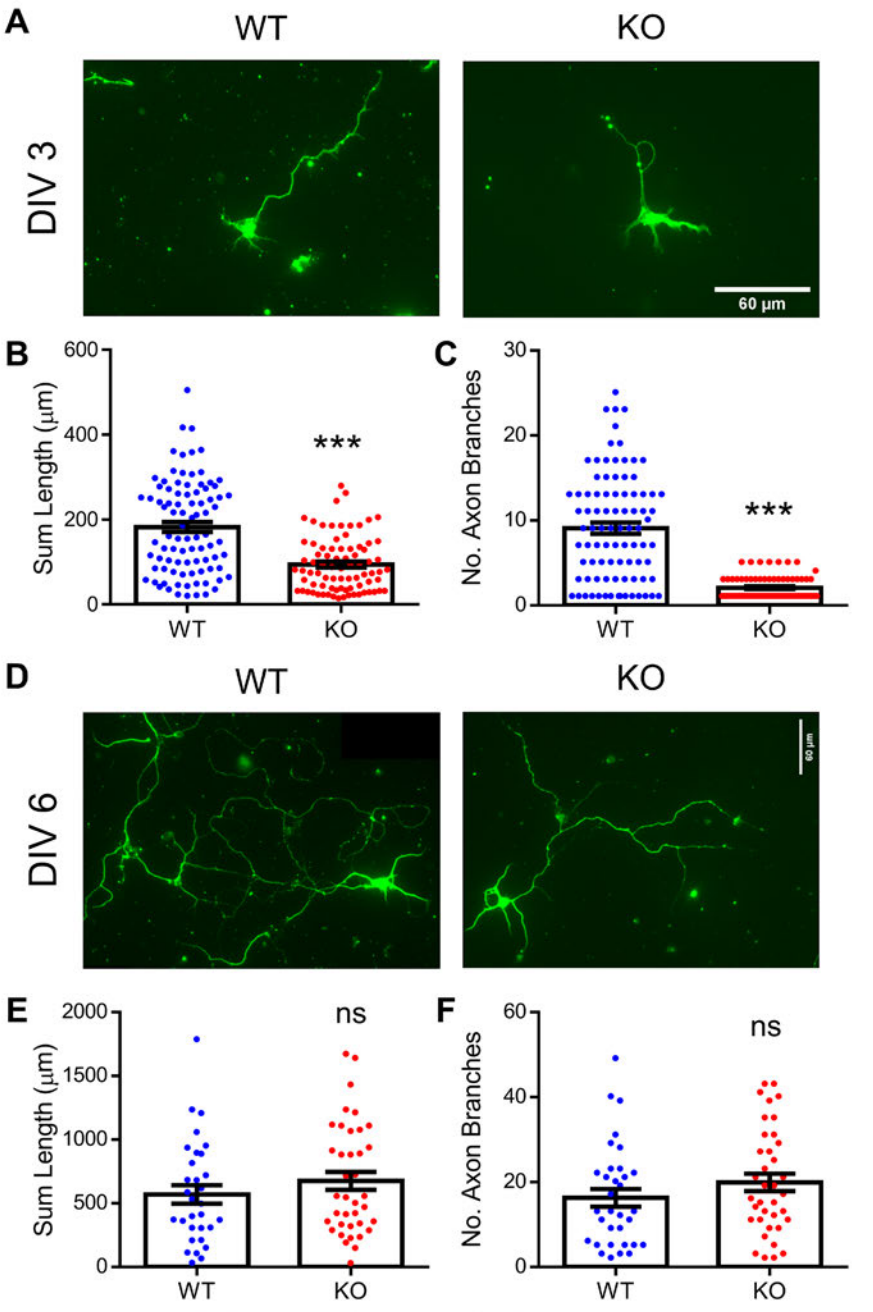


Figure 3.6 *NEXMIF*$^{-/y}$ neurons show impaired early axonal outgrowth

(A) Representative images of Tau immunostained primary cortical neurons from WT or *NEXMIF*$^{-/y}$ brains at DIV 3. **(B, C)** The sum length of axons (B) ($t_{(167)}$ = 6.295,

$p < 0.0001$) and the number of axon branches (C) ($t_{(153)} = 8.808$, $p < 0.0001$) were decreased in *NEXMIF*$^{-/y}$ neurons compared to WT neurons at DIV 3. n = 85 neurons/ group. **(D)** Representative images of Tau immunostained primary cortical neurons from WT or *NEXMIF*$^{-/y}$ brains at DIV 6. **(E, F)** Quantification of the sum length of axons (E) ($t_{(67)} = 1.040$, $p = 0.3022$) and the number of axon branches (F) ($t_{(68)} = 1.248$, $p = 0.2162$) showed no difference between WT and *NEXMIF*$^{-/y}$ neurons at DIV 6. n = 40-68 neurons/ group. Scale bars = 60 µm. WT: wild type littermate, KO: *NEXMIF*$^{-/y}$. Data are represented as mean ± SEM. $^{**}p<0.01$, $^{***}p<0.001$.

Figure 3.7

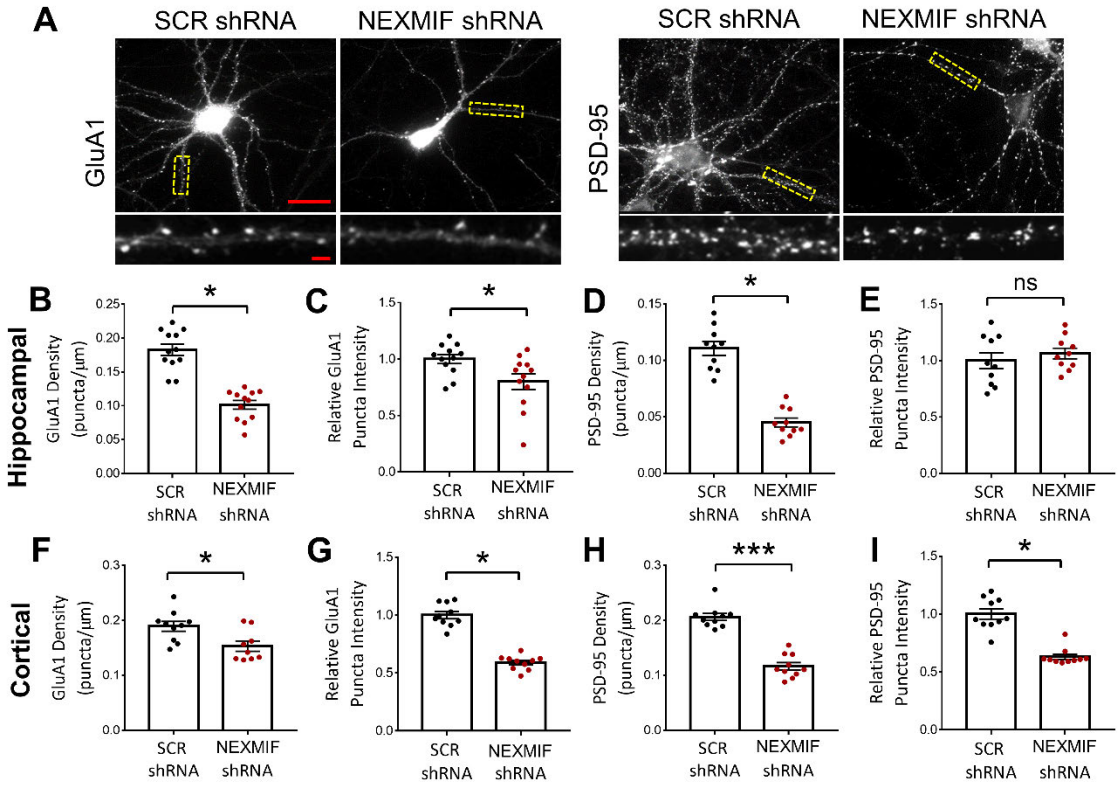


Figure 3.7 Altered synaptic protein composition in cultured neurons with shRNA mediated NEXMIF knockdown

(A)† Representative images of immunohistochemistry for GluA1 and PSD-95 at DIV15 in rat hippocampal cultures after infection with scrambled (SCR shRNA) or NEXMIF shRNA at DIV 0. Scale bars = 15 μm (full picture); 5 μm (enlarged area). **(B, C)**† Quantification of GluA1 immunostaining in hippocampal neurons showed a decrease in puncta density and puncta intensity. (Density: $t_{(22)} = 7.59$, $p < 0.0001$; Intensity: $t_{(22)} = 2.50$, $p = 0.021$; $n = 10–12$ cells). **(D, E)**† Quantification of PSD-95 immunostaining in hippocampal neurons showed a decrease in PSD-95 density with no significant change in PSD-95 intensity. (Density: $t_{(18)} = 9.05$, p <

0.0001; Intensity: $t_{(18)} = 0.75$, $p = 0.46$, n =10–12 cells). **(F, G)** Quantification of GluA1 immunostaining in cortical neurons showed a decrease in puncta density and intensity from shRNA mediated NEXMIF knockdown. **(H, I)** Quantification of PSD-95 immunostaining in cortical neurons showed a decrease in puncta density and intensity from shRNA mediated NEXMIF knockdown. n = 10 cells. Data are represented as mean ± SEM. *p<0.05, ***p<0.001, ns = not significant. † *With contributions from James Gilbert for A-E.*

Figure 3.8

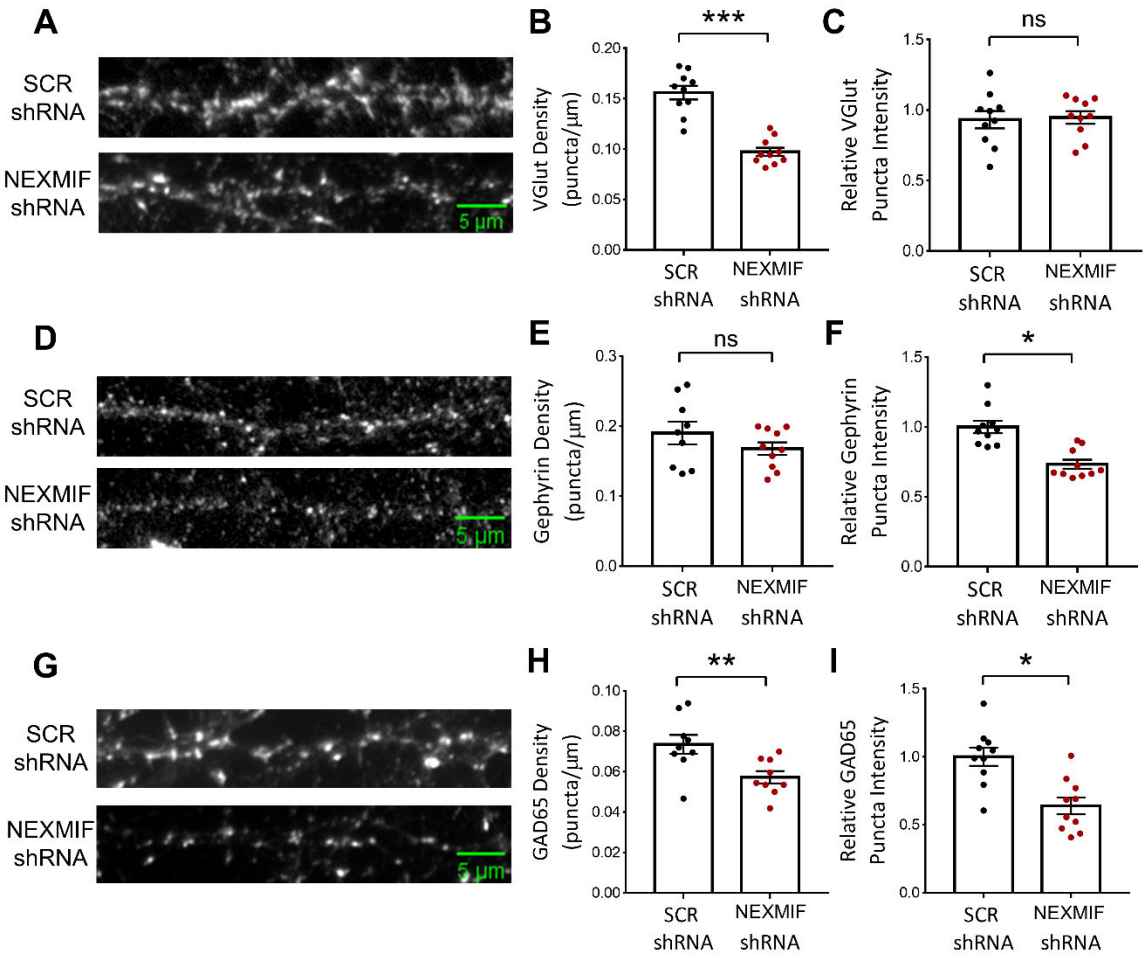


Figure 3.8 Additional synaptic protein composition in cultured neurons with shRNA mediated NEXMIF knockdown

(A) Representative images of immunocytochemistry for VGlut1 in DIV 15 rat hippocampal cultures after infection with scrambled (SCR shRNA) or NEXMIF shRNA at DIV 3. **(B, C)** Quantification of VGlut1 immunostaining showed a decrease in VGlut1 density with no significant change in VGlut1 intensity from shRNA mediated NEXMIF knockdown. **(D)** Representative images of immunocytochemistry for gephyrin in DIV 15 rat cortical cultures after infection with

SCR or NEXMIF shRNA at DIV 3. **(E, F)** Quantification of gephyrin immunostaining showed no change in puncta density and a decrease in puncta intensity from shRNA mediated NEXMIF knockdown. **(G)** Representative images of immunocytochemistry for GAD65 in DIV 15 rat cortical cultures after infection with SCR or NEXMIF shRNA at DIV 3. **(H, I)** Quantification of GAD65 immunostaining showed a decrease in both puncta density and intensity from shRNA mediated NEXMIF knockdown. *n* = 10 neurons/ group. Scale bars = 5 μm. Data are represented as mean ± SEM. *$p<0.05$, ** $p<0.01$, ***$p<0.001$, ns = not significant.

Figure 3.9

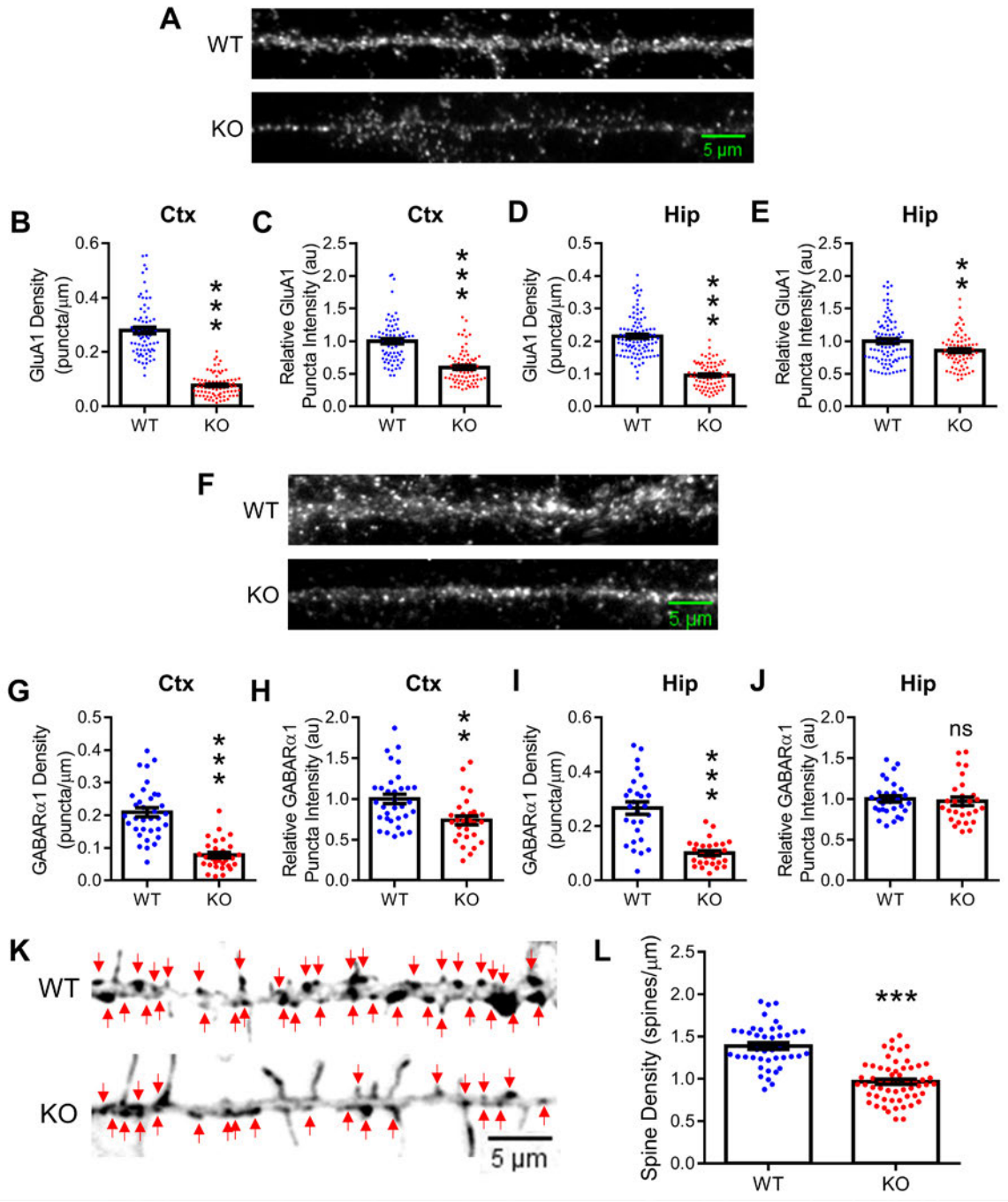


Figure 3.9 Aberrant synaptic protein composition and dendritic spines in NEXMIF KO mice

(A) Representative images of DIV 14 cortical neurons from WT and *NEXMIF*$^{-/y}$ mice immunostained with antibodies against GluA1. **(B, C)** Quantification of GluA1 immunostaining in cortical neurons showed a decrease in puncta density and intensity in *NEXMIF*$^{-/y}$ neurons compared to WT neurons. (Density: $t_{(154)} = 16.87$, $p < 0.0001$; Intensity: $t_{(147)} = 8.400$, $p < 0.001$, n = 74-80 neurons/ group). **(D, E)** Quantification of GluA1 immunostaining in hippocampal neurons showed a decrease in puncta density and puncta intensity in *NEXMIF*$^{-/y}$ neurons compared to WT neurons. (Density: $t_{(176)} = 14.94$, $p < 0.0001$; Intensity: $t_{(168)} = 3.004$, $p = 0.0031$, n = 73-99 neurons/ group). **(F)** Representative images of DIV 14 cortical neurons from WT and *NEXMIF*$^{-/y}$ mice immunostained for GABARα1. **(G, H)** Quantification of GABARα1 immunostaining in cortical neurons showed a decrease in puncta density and intensity in *NEXMIF*$^{-/y}$ neurons compared to WT neurons. (Density: $t_{(61)} = 7.728$, $p < 0.0001$; Intensity: $t_{(60)} = 3.317$, $p = 0.0015$, n = 29-34 neurons/ group). **(I, J)** Quantification of GABARα1 immunostaining in hippocampal neurons showed a decrease in puncta density with no significant change in puncta intensity in *NEXMIF*$^{-/y}$ neurons compared to WT neurons. (Density: $t_{(54)} = 6.783$, $p < 0.0001$; Intensity: $t_{(55)} = 0.4454$, $p = 0.6577$, n = 28-29 neurons/ group). **(K)** Representative images of DIV 13 primary cortical neurons from WT or *NEXMIF*$^{-/y}$ mice treated with actin dye Phalloidin to label spines. Spines marked by red arrows. **(L)** Spine density was decreased in *NEXMIF*$^{-/y}$ neurons compared to WT neurons. ($t_{(98)} = 8.618$, $p < 0.0001$, n = 42-58 dendrites from 12-

15 neurons/ group). Scale bars = 5 μm. WT: wild type littermate, KO: *NEXMIF*$^{-/y}$. Data are represented as mean ± SEM. ** p<0.01, ***p<0.001, ns = not significant.

Figure 3.10

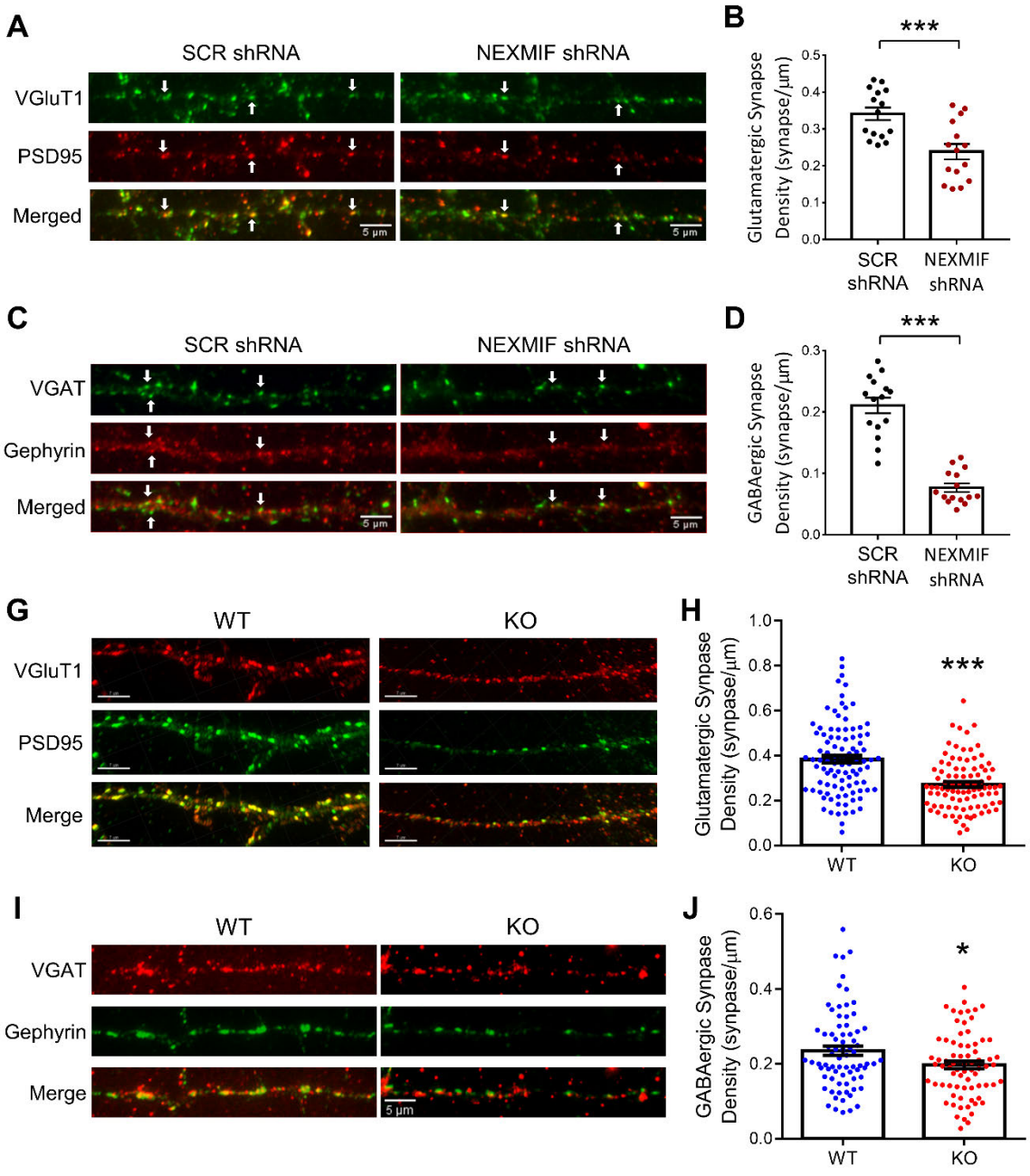


Figure 3.10 Reduced synaptic density from loss of NEXMIF

(A) Glutamatergic synapses were identified from colocalized VGluT1 and PSD95 puncta florescent signals in DIV 15 rat hippocampal cultures after infection with

scrambled (SCR shRNA) or NEXMIF shRNA at DIV 0. Scale bar = 5 μm **(B)** Quantification showed shRNA mediated NEXMIF knockdown resulted in a decrease in glutamatergic synapse density. ($t_{(28)} = 3.8$, $p = 0.0007$, n = 15 cells). **(C)** GABAergic synapses were identified from colocalized VGAT and gephyrin puncta florescent signals in DIV 15 rat hippocampal cultures after infection with SCR or NEXMIF shRNA at DIV 0. Scale bar = 5 μm **(D)** Quantification showed shRNA mediated NEXMIF knockdown resulted in a decrease in GABAergic synapse density. Examples of colocalization are marked by arrows. ($t_{(28)} = 9.26$, $p < 0.0001$, n = 15 cells). **(G)** Glutamatergic synapses were identified from colocalized VGluT1 and PSD95 puncta florescent signals in DIV 14 cortical neurons cultured from WT or *NEXMIF*$^{-/y}$ P0 mice. Scale bar = 7 μm **(H)** Quantification showed glutamatergic synapse density is decreased in *NEXMIF*$^{-/y}$ neurons compared to WT neurons. ($t_{(185)} = 5.429$, $p < 0.0001$, n = 90 dendrites from 30 neurons/ group). **(I)** GABAergic synapses were identified from colocalized VGAT and gephyrin puncta florescent signals in DIV 14 cortical neurons cultured from WT or *NEXMIF*$^{-/y}$ P0 mice. Scale bar = 5 μm. **(J)** Quantification showed GABAergic synapse density is decreased in *NEXMIF*$^{-/y}$ neurons compared to WT neurons. ($t_{(146)} = 2.381$, $p = 0.0185$, n = 73 dendrites from 25 neurons/ group). Data are represented as mean ± SEM. *p<0.05, ***p<0.001.

Figure 3.11

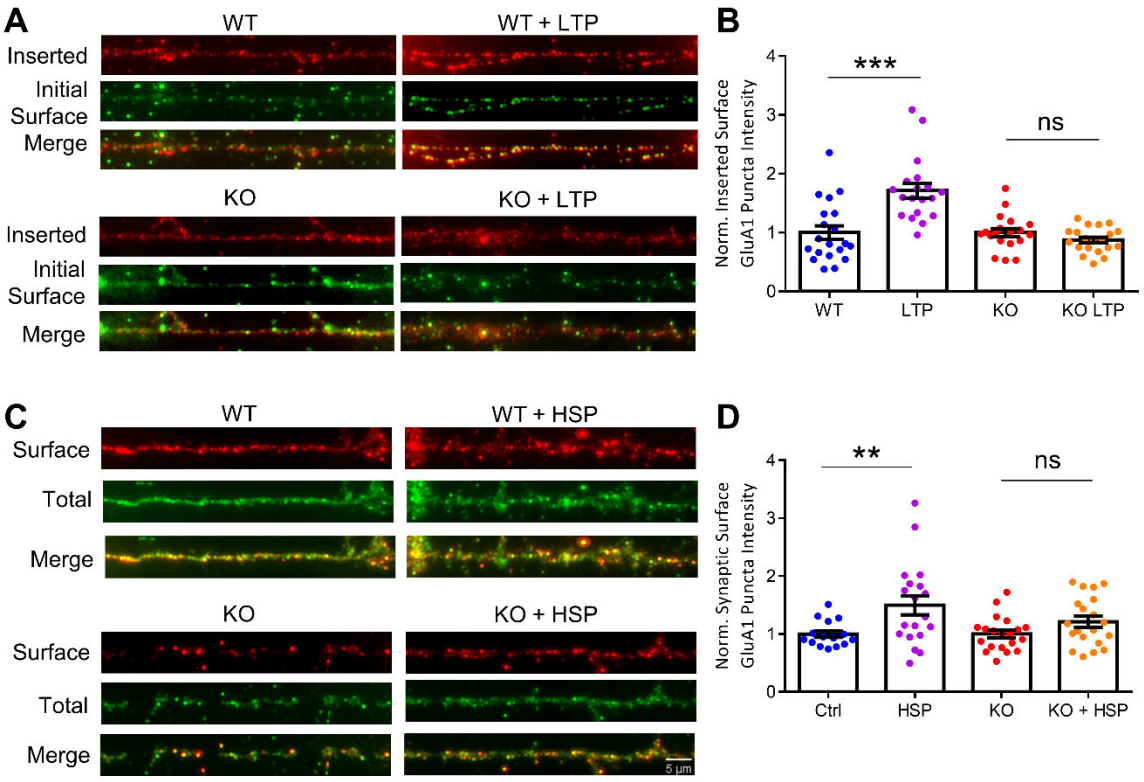


Figure 3.11 Synaptic plasticity fails in *NEXMIF*$^{-/y}$ neurons

(A) Representative images DIV 14 cortical neurons cultured from WT or *NEXMIF*$^{-/y}$ P0 mice immunostained for initial surface expressing GluA1 and newly inserted surface GluA1 after control or chem-LTP treatments. **(B)** Quantification of newly inserted surface GluA1 shows an increase in surface expression from chem-LTP treatment in WT neurons but not in *NEXMIF*$^{-/y}$ neurons. ($F_{(3, 74)} = 16.11$, $p < 0.0001$, n = 19-20 neurons/ group). **(C)** Representative images DIV 14 cortical neurons cultured from WT or *NEXMIF*$^{-/y}$ P0 mice immunostained for total and surface expressing GluA1 after control or homeostatic synaptic plasticity (HSP) treatments. **(B)** Quantification of surface GluA1 shows an increase in surface

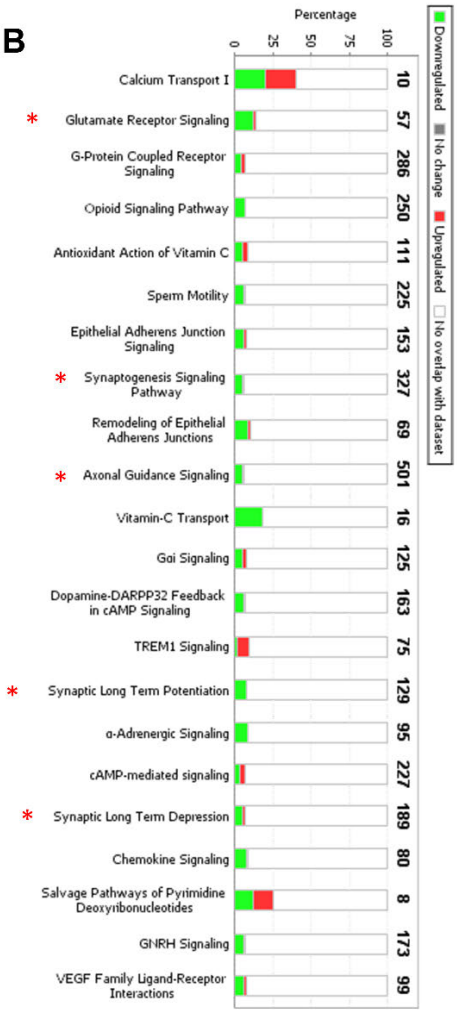
expression from HSP treatment in WT neurons but not in *NEXMIF*$^{-/y}$ neuronsc *n* = 15-20 neurons/ group). Scale bars = 5 μm. Data are represented as mean ± SEM. ** $p<0.01$, ***$p<0.001$, ns = not significant.

Figure 3.12

A

Gene	Fold Change	Adjusted p value	Location
NEXMIF	0.099	5.78E-36	Nucleus
NRGN	0.148	2.20E-07	Cytoplasm
NOV	0.150	1.16E-27	Extracellular
CDKL2	0.195	6.08E-24	Nucleus
CDK19	0.219	1.13E-20	Nucleus
CAMKV	0.260	7.06E-15	Membrane
RGS14	0.271	4.45E-07	Cytoplasm
SLC17A7	0.274	5.67E-15	Membrane
NEUROD6	0.282	2.16E-13	Nucleus
PCDHA1	0.328	5.17E-11	Membrane
PCDHA7	0.340	2.60E-10	Membrane
SYNDIG1	0.359	9.37E-10	Membrane
CALM1	0.366	4.24E-05	Cytoplasm
CAMK4	0.388	1.56E-07	Nucleus
CAMKK1	0.430	9.95E-07	Cytoplasm
GABRA5	0.409	2.64E-07	Membrane
GABRA4	0.460	1.20E-05	Membrane

B



C

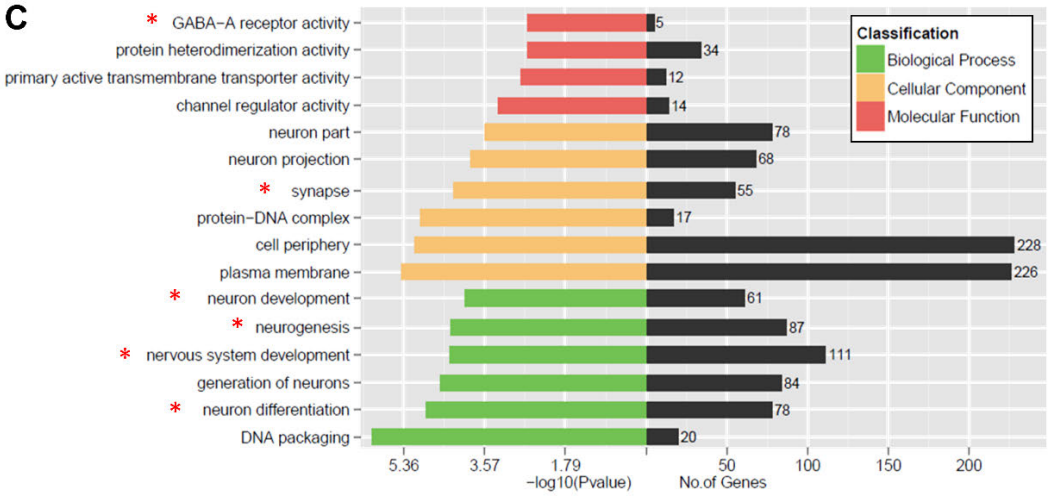


Figure 3.12 Neurogranin and SynDig1 are among the most down-regulated genes from an RNAseq of neurons with loss of NEXMIF

(A) Selected top downregulated genes identified in RNAseq after knockdown of NEXMIF in mouse cortical cultures ranked based on fold change. **(B)** Percentage of down-regulated (green) and up-regulated (red) signaling genes in Ingenuity Pathway Analysis after NEXMIF knockdown. Asterisk indicates those of particular interest. **(C)** Gene ontology enrichment analysis of top dysregulated molecular functions, cell components, and biological processes after knockdown of NEXMIF. Asterisk indicates those of particular interest.

Figure 3.13

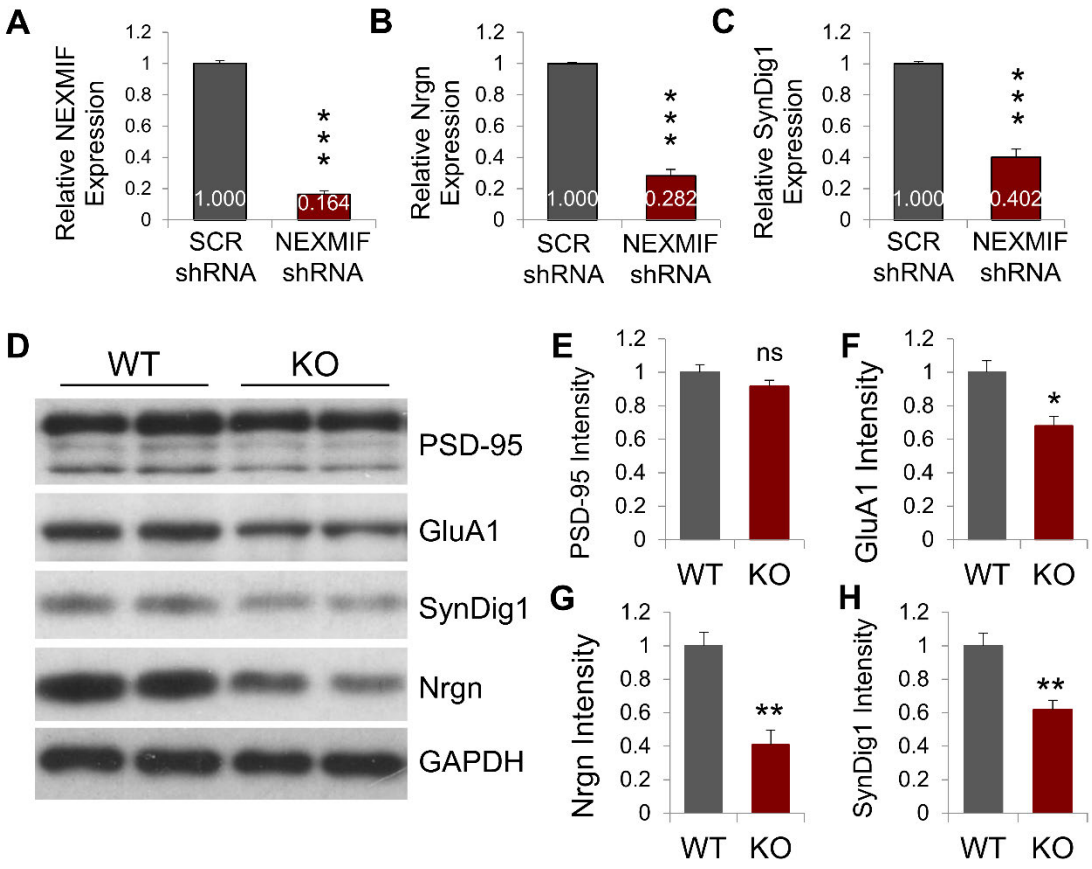


Figure 3.13 Expression of neurogranin and SynDig1 is reduced from loss of NEXMIF†

(A-C) qPCR after shRNA medicated knockdown of NEXMIF confirms decrease in mRNA transcripts of NEXMIF (A), Nrgn (B), and SynDig1 (C) compared to scrambled (SCR) shRNA. *n* = 3 neuron cultures performed in triplicate. **(D)** Western blot of synaptic-related proteins, PSD95 and GluA1, and candidate proteins, Nrgn and SynDig1, from P30 WT and NEXMIF KO hippocampal lysates. **(E-H)** Quantification of western blot data showed no change in PSD-95 (E) and a significant reduction in the total protein levels of GluA1 (F), Nrgn (G), and SynDig1

(H). *n* = 5 animals. Data are represented as mean ± SEM. *$p<0.05$, ** $p<0.01$, ***$p<0.001$, ns = not significant. † *Contribution from James Gilbert.*

Figure 3.14

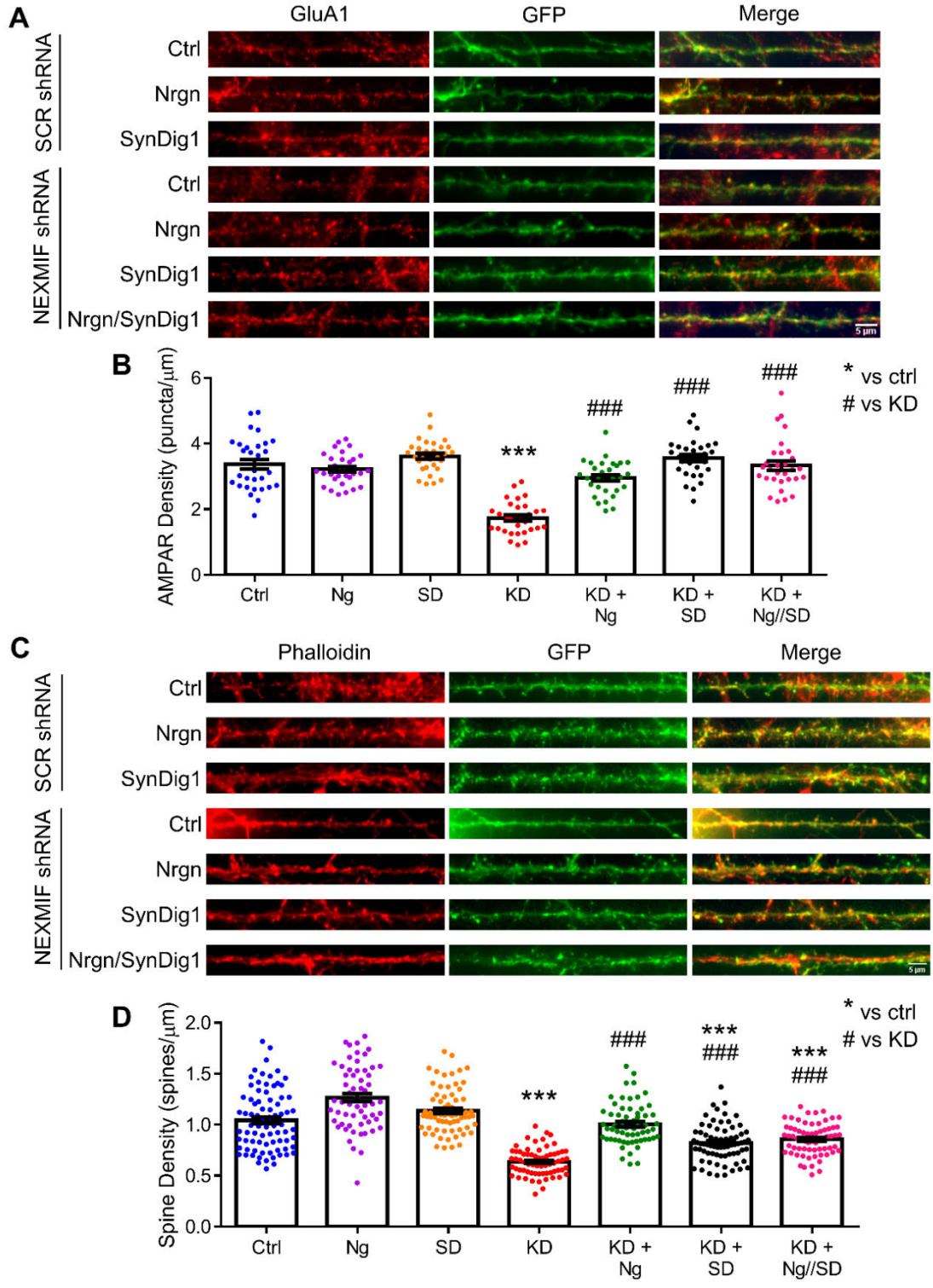

A
GluA1
GFP
Merge
SCR shRNA
NEXMIF shRNA
Ctrl
Nrgn
SynDig1
Nrgn/SynDig1
5 µm
B
AMPAR Density (puncta/µm)
* vs ctrl
# vs KD
Ctrl
Ng
SD
KD
KD + Ng
KD + SD
KD + Ng//SD
C
Phalloidin
GFP
Merge
D
Spine Density (spines/µm)

Figure 3.14 Overexpression of neurogranin or SynDig1 can rescue synaptic deficits after loss of NEXMIF expression

(A) Representative images of GluA1 staining in DIV 16 rat hippocampal neurons after transfection with scrambled (SCR) shRNA or NEXMIF shRNA, together with GFP and empty vector control, Nrgn, SynDig1, or both Nrgn and SynDig1 at DIV 9. **(B)** Overexpression of Nrgn alone, SynDig1 alone, and Nrgn and SynDig1 together was sufficient to rescue GluA1 puncta density. ($F_{(6, 203)}$ = 33.67, p < 0.0001, n = 30 dendrites from 10 neurons/ group). **(C)** Representative images of Phalloin staining of actin-rich spines in DIV 14 rat hippocampal neurons after transfection with SCR or NEXMIF shRNA, together with GFP and empty vector control, Nrgn, SynDig1, or both Nrgn and SynDig1 at DIV 6. **(D)** Overexpression of Nrgn alone was sufficient to rescue spine density while overexpression of SynDig1 alone or Nrgn and SynDig1 together achieved partial rescue. ($F_{(6, 467)}$ = 57.92, p < 0.0001, n = 59-79 dendrites from 15-20 neurons/ group). Scale bars = 5 µm. KD: NEXMIF shRNA mediated knockdown; Ng: Nrgn, neurogranin; SD: SynDig1. Data are represented as mean ± SEM. *** p<0.001 compared to control, ### p<0.001 compared to KD.

CHAPTER FOUR: CHARACTERIZATION OF AUTISM-LIKE BEHAVIORS AND STUDY OF MOLECULAR DYSREGULATION IN HETEROZYGOUS NEXMIF FEMALE MICE

4.1 Abstract

Autism spectrum disorder (ASD) is a neurodevelopmental disorder with a strong genetic basis. ASDs are commonly characterized by impairments in communication, restrictive and repetitive behaviors, and deficits in social interactions. Although ASD is a highly heterogeneous disease with many different genes implicated in its etiology, many ASD associated genes converge on common cellular defects, such as aberrant neuronal morphology and synapse dysregulation. Our previous work revealed that, in mice, a complete loss of the ASD-associated X-linked gene *NEXMIF* results in a reduction in dendritic complexity, a decrease in spine and synapse density, altered synaptic transmission, and ASD-like behaviors. Interestingly, human females of *NEXMIF* haploinsufficiency have recently been reported to demonstrate autistic features; however, the cellular and molecular basis for this haploinsufficiency-caused ASD remains unclear. Here we report that heterozygous female mice demonstrate behavioral impairments similar to those of knockout male mice. In the brains of *NEXMIF*$^{+/-}$ female mice, NEXMIF shows a mosaic expression pattern in neurons. In the mosaic mixture of neurons cultured from *NEXMIF*$^{+/-}$ mice, cells that lack NEXMIF have impairments in dendritic arborization and spine development. Remarkably, the NEXMIF-expressing neurons from *NEXMIF*$^{+/-}$ mice also demonstrate similar defects in dendritic growth and spine formation. These findings establish a novel mouse model of *NEXMIF* haploinsufficiency and provide new insights into the pathogenesis of NEXMIF dependent ASD.

4.2 Introduction

Autism spectrum disorders (ASD) comprise a heterogeneous class of disorders characterized by impaired social interactions, reduced communication, and restrictive interests and repetitive behaviors (American Psychiatric Association, 2013; Landa, 2008). In up to 25% of individuals diagnosed with ASD, an identifiable or genetic variant can be identified, providing valuable insights into the mechanisms involved in proper neurodevelopment (Fernandez and Scherer, 2017; Huguet et al., 2013). Of the hundreds of ASD related genes in the Simmons Foundation Autism Research Initiative (SFARI) database, a large number of rare genetic variants in protein-coding genes are causative for ASD (Abrahams et al., 2013; Banerjee-Basu and Packer, 2010b) however, none of these individually account for more than 1% of the total number of ASD diagnoses, demonstrating the complex landscape of autism genetics (Abrahams and Geschwind, 2008; Happé et al., 2006; Rylaarsdam and Guemez-Gamboa, 2019; Yoo, 2015).

NEXMIF was first implicated as one of the candidate genes in two male members of a family who showed autistic features with intellectual disabilities (ID) (Cantagrel et al., 2004). Since this original diagnosis, more cases have been reported, confirming that a loss of NEXMIF protein due to *NEXMIF* gene mutation or deletion leads to ASD (Alarcon-Martinez et al., 2019; Charzewska et al., 2015; Kuroda et al., 2015; Lambert et al., 2018; Lorenzo et al., 2018; Panda et al., 2020; Stamberger et al., 2020). The reported individuals affected with NEXMIF variants show repetitive behaviors, impaired language, ID, seizures, and several cases of

microcephaly. Interestingly, although only male cases were reported in earlier studies, recent clinical reports indicate that autistic characteristics are also observed in females with *NEXMIF* mutations (Athanasakis et al., 2014; Farach and Northrup, 2016; de Lange et al., 2016; Moysés-Oliveira et al., 2015; Stamberger et al., 2020; Webster et al., 2017; Wu et al., 2020). Due to infertility of affected males, females with inherited *NEXMIF* mutations are heterozygous and therefore haploinsufficient in NEXMIF. The pathogenicity of single copy *NEXMIF* gene mutation indicates that brain development and function are sensitive to the proper gene dosage of *NEXMIF*.

Notably, as an X-linked gene *NEXMIF* presents a particular genetic situation contributing to protein haploinsufficiency. In females, one of the two X chromosomes is inactivated (XCI) to balance gene dosage between sexes. XCI is typically random, and as a result, heterozygous female individuals become mosaics of cells expressing either the normal or mutant allele. This creates two populations of neurons in the brains of heterozygous females: those that express NEXMIF (NEXMIF^{+}) and those that have inactivated the X chromosome carrying the normal allele and thus do not express NEXMIF (NEXMIF^{-}). Under this condition, despite expression of the gene product remaining in a portion of neurons in the brain, the overall neural network can be compromised by the aberrant assembling of NEXMIF^{+} and NEXMIF^{-} neurons. Due to randomness of XCI, the extent of NEXMIF expression can vary in the affected individuals and at the level of specific organs or tissues, resulting in a broad range of disease

severity. In some X-linked gene disorders, one parental-specific X chromosome is preferentially inactivated, leading to skewed XCI activity. It has been reported that the majority of females with NEXMIF-dependent ASD had random XCI, suggesting a lack of compensatory regulation in XCI in these females (Athanasakis et al., 2014; Farach and Northrup, 2016; Lambert et al., 2018; de Lange et al., 2016; Moysés-Oliveira et al., 2019; Panda et al., 2020; Stamberger et al., 2020).

Here we characterize the behavioral and cognitive abnormalities of, and investigate the related cellular defects in, the NEXMIF heterozygote (*NEXMIF*$^{+/-}$) female mouse model. Female *NEXMIF*$^{+/-}$ mice demonstrate representative ASD behavioral phenotypes including reduced social interactions, repetitive behaviors, and impaired memory, but with intact development of communication. *NEXMIF* haploinsufficiency results in mosaic cellular expression of NEXMIF in the brains of these mice resulting in mixed coexistence of both NEXMIF^{+} and NEXMIF^{-} neurons due to random XCI. Haploinsufficient NEXMIF expression results in impairments in neuronal structural development in dendritic arborization and synaptic connectivity. These findings validate the mouse model for NEXMIF haploinsufficiency ASD, and provide new insights in our understanding of the role of NEXMIF in brain development and the pathobiological mechanisms underlying NEXMIF ASD in females.

4.3 Results

4.3.1 *NEXMIF*$^{+/-}$ mice demonstrate autistic features in social behavior

Individuals affected with *NEXMIF* mutations present with autistic behaviors, poor to absent speech, ID, and often epilepsy (de Lange et al., 2016; Van Maldergem et al., 2013; Panda et al., 2020; Stamberger et al., 2020; Webster et al., 2017). Additionally, *NEXMIF*$^{-/y}$ KO mice demonstrate decreased sociability, reduced communication, increased repetitive behaviors, and impaired spatial memory (Gilbert et al., 2020). We therefore sought to characterize the extent of behavioral changes that result from NEXMIF haploinsufficiency. We first examined the social behavior of the *NEXMIF*$^{+/-}$ mice using the three-chamber test, which assesses general sociability and preference for social novelty (Silverman et al., 2010). Animals were habituated to the three-chambered apparatus before testing by letting them explore all three areas (**Fig. 4.1A**). Neither female WT nor female *NEXMIF*$^{+/-}$ mice showed a preference for a particular side of the testing apparatus (**Fig. 4.1B-4.1D**). For the sociability test, an unfamiliar female mouse (Mouse 1) was placed into a cage in one of the side chambers and the test mouse was allowed to move throughout the three-chambers (**Fig. 4.1E**). WT mice spent a significant amount of time investigating and interacting with Mouse 1 relative to the empty chamber; however, *NEXMIF*$^{+/-}$ mice failed to show a preference toward Mouse 1 in either the amount of time spent in the chamber of Mouse 1 or in close proximity to the cage housing Mouse 1 (**Fig. 4.1F-4.1H**), indicating *NEXMIF*$^{+/-}$ mice have impairments in sociability. We then tested animals for preference for social novelty by placing a second unfamiliar female mouse (Novel Mouse) into

the remaining empty cage in the other side chamber and allowing the test mouse to roam freely (**Fig. 4.1I**). *NEXMIF*$^{+/-}$ mice showed no preference toward the Novel mouse (**Fig. 4.1J**) as demonstrated by similar times spent in either side chamber (**Fig. 4.1K**) and in close proximity to either mouse's cage (**Fig. 4.1L**), whereas the WT mice spent significantly more time in the side chamber with the Novel mouse (**Fig. 4.1K**) and in close proximity to the Novel mouse's cage (**Fig. 4.1L**). These findings indicate that the *NEXMIF*$^{+/-}$ mice have a lack of interest in social novelty.

4.3.2 Increased repetitive behavior and hyperactivity in *NEXMIF*$^{+/-}$ mice

We further investigated changes in the behavior of *NEXMIF*$^{+/-}$ mice using the marble burying test. We placed WT and *NEXMIF*$^{+/-}$ mice in a square cage with 25 evenly spaced marbles on top of fresh bedding. Over 30 min, the WT animals began to bury the marbles under the bedding with a digging behavior (**Fig. 4.2A**). The *NEXMIF*$^{+/-}$ animals however, buried significantly fewer marbles at all time-points after the first 10 min of observation (**Fig. 4.2B**). This finding is consistent with previous reports showing altered burying behaviors in ASD mice (Amodeo et al., 2019; Spencer et al., 2011; Sungur et al., 2014; Wang et al., 2018a, 2018b; Wong et al., 2019; Wurzman et al., 2015).

In our previous study, we found that the male *NEXMIF*$^{-/y}$ mice perform excessive self-grooming (Gilbert et al., 2020). This repetitive behavior has been observed in ASD and is linked to anxiety (Kalueff et al., 2016). We therefore assessed the grooming behavior in the *NEXMIF*$^{+/-}$ females. Similar to the *NEXMIF*$^{-/y}$ males, we found that *NEXMIF*$^{+/-}$ females spent a significantly longer time

grooming with a significantly greater number of grooming episodes (**Fig. 4.2C-4.2D**). We also investigated the rearing behavior of the mice, which has been linked to anxiety with increases in unsupported rearing indicating reduced anxiety (Sturman et al., 2018). We quantified unsupported rearing as the number of instances in which the mice reared up onto their hind legs without leaning on the wall of the cage. *NEXMIF*$^{+/-}$ mice performed significantly fewer rearing instances than the WT controls (**Fig. 4.2E**).

We next examined the *NEXMIF*$^{+/-}$ mice in the open field test. Consistent with the hyperactivity observed in *NEXMIF*$^{-/y}$ males, *NEXMIF*$^{+/-}$ females had a significant increase in their movement during the open field test compared to WT females, as shown by the representative traces (**Fig. 4.2F**). Quantification of the track lengths revealed that *NEXMIF*$^{+/-}$ mice traveled a further distance during the test (**Fig. 4.2G**) with a significantly greater maximum velocity, average velocity, and average acceleration (**Fig. 4.2H-4.2J**). Further quantification revealed that there is no change in time spent in the center of the open field between WT and *NEXMIF*$^{+/-}$ mice (**Fig. 4.2K**). All together, these results show that *NEXMIF*$^{+/-}$ mice are hyperactive with an increased level of anxiety.

4.3.3 *NEXMIF*$^{+/-}$ mice show moderate changes in communication by ultrasonic vocalization

Impaired or delayed communication is a defining phenotype in ASD (American Psychiatric Association, 2013), and indeed, both males and females affected with *NEXMIF* variants have shown poor or absent speech (Alarcon-Martinez et al.,

2019; Charzewska et al., 2015; Kuroda et al., 2015; de Lange et al., 2016; Lorenzo et al., 2018; Van Maldergem et al., 2013; Panda et al., 2020; Stamberger et al., 2020; Webster et al., 2017). In order to assess communication behavior in *NEXMIF*$^{+/-}$ mice, we recorded and analyzed their ultrasonic vocalizations. Wild type and *NEXMIF*$^{+/-}$ female pups were separated from their dam and littermates to induce calling and vocalizations were recorded for 5 mins. The same animals were tested at P5, P7, and P9. Both groups of animals made calls within the ultrasonic range as depicted in representative 1.5 s of recording at P5 (**Fig. 4.3A**). The total number of calls, the number of calls per minute, average duration of calls, total time spent calling, average peak amplitude of calls, and average peak frequency of calls (**Fig. 4.3B-4.3I**), as well as the frequency of call types (**Fig. 4.3J-4.3L**), were analyzed at all time points. Unlike their hemizygous KO male counterparts, which showed a dramatic reduction in ultrasonic vocalization (Gilbert et al., 2020), the *NEXMIF*$^{+/-}$ females showed moderate communication deficits compared to that WT controls. In line with this, it has been observed that in human NEXMIF patients, males have a more severe language impairment than females (Panda et al., 2020; Stamberger et al., 2020).

4.3.4 *NEXMIF*$^{+/-}$ mice show impairments in spatial memory

Intellectual disability is a comorbidity in individuals affected with *NEXMIF* variants, and consistently, the *NEXMIF*$^{-/y}$ KO mice show learning and memory deficits that recapitulate this human condition. To test whether haploinsufficient loss of *NEXMIF* is sufficient to result in this phenotype, we examined spatial memory

using the Barnes maze test. Mice were trained over 4 days to use spatial cues to locate a target escape hole on a circular maze containing 20 holes around its circumference. Over the acquisition training period, the *NEXMIF*$^{+/-}$ mice showed a reduction in the primary latency to the target hole, indicating their ability to learn its location (**Fig. 4.4A**). After training, the target hole was covered and the ability of the mice to remember its location was assessed both 1 d and 5 d later. *NEXMIF*$^{+/-}$ mice traveled a significantly longer distance than WT mice before making an initial nose poke at the target hole in the 5 d test but not the 1 d test (**Fig. 4.4B)**, as shown by representative traces (**Fig. 4.4C-4.4D**). *NEXMIF*$^{+/-}$ mice also took a longer amount of time than WT mice to find the target hole in the 5 d test, as measured by the primary latency (**Fig. 4.4E**). Quantification of the number of investigative nose pokes at the target hole versus incorrect holes showed that *NEXMIF*$^{+/-}$ mice made a significantly greater number of nose poke errors than WT mice in both the 1 d and 5 d tests (**Fig. 4.4F**). We separated the maze into four quadrants to allow quantification of the amount of time the animals spent looking for the target hole in the correct area (**Fig. 4.4G-4.4H**). This revealed that in both the 1 d and 5 d tests *NEXMIF*$^{+/-}$ mice did not spend significantly more time exploring the target quadrant of the maze as compared to the other three quadrants, in contrast to WT mice, which did spend more time in the target quadrant (**Fig. 4.4I-4.4J**). These findings indicate that *NEXMIF* haploinsufficiency causes defects in spatial memory, which may contribute to the cognitive impairments observed in females.

4.3.5 Heterozygous NEXMIF mice demonstrate mosaic expression of NEXMIF

Due to the random inactivation of either X chromosome, the X-linked gene *NEXMIF* is predicted to be expressed in a mosaic manner in heterozygous female mice, leading to either normal expression or complete loss of NEXMIF in individual neurons. This type of mosaic expression has been observed in other haploinsufficient X-linked genes (Compagni et al., 2003; Hayashi et al., 2017; Sikora et al., 2016; Smrt et al., 2011; Tan et al., 1995; Wu et al., 2014). To determine the NEXMIF expression pattern in the brain, we used a NEXMIF specific antibody to immunolabel NEXMIF both *ex vivo* and *in vivo*.

First, we generated primary neuronal cultures from *NEXMIF*$^{+/-}$ mice or WT littermate controls. These neuron cultures were maintained for 6 days (Days *in vitro* 6; DIV 6) and were probed for NEXMIF expression. As previously observed, NEXMIF was expressed in the nuclei as seen by colocalization with the nuclear dye Hoechst (**Fig. 4.5A)**. Consistent with random XCI, we found that some neurons from *NEXMIF*$^{+/-}$ mice expressed NEXMIF while others did not (**Fig. 4.5A**). Quantification of the *NEXMIF*$^{+/-}$ neurons revealed approximately 70% of cells expressed NEXMIF (**Fig. 4.5B**) to the same level as WT neurons (**Fig. 4.5C**), whereas the remaining 30% of cells were NEXMIF negative.

As the XCI patterning varies between individuals, we quantified the mosaic expression of NEXMIF *in vivo* from adult *NEXMIF*$^{+/-}$ mice and WT littermate controls. To do this we used immunohistochemistry to probe for NEXMIF, as well

as the neuronal marker NeuN, in brain slices of both the hippocampus (**Fig. 4.5D**) and L2/3 of the somatosensory cortex (**Fig. 4.5G and 4.5J**). We found mosaic expression of NEXMIF in both hippocampus (**Fig. 4.5E**) and somatosensory cortex (**Fig. 4.5H**) with NEXMIF expressed respectively in 60% and 65% of NeuN positive neurons from *NEXMIF*$^{+/-}$ brain slices. Consistent with the *in vitro* data, the level of NEXMIF expression in these NEXMIF positive neurons was similar to that of neurons from WT mice in both the hippocampus (**Fig. 4.5F**) and the somatosensory cortex (**Fig. 4.5I**). When the ratio of NEXMIF^{+} vs. NEXMIF^{-} neurons was analyzed in individual animals, we found no cases of skewing (>75:25 ratio) in our haploinsufficient mice (**Fig. 4.5K**).

4.3.6 Mosaic loss of NEXMIF impairs the development of neuronal morphology

One of the key phenotypes observed in neurons lacking NEXMIF is impairments in neurite extension (Gilbert and Man, 2016; Ishikawa et al., 2012; Van Maldergem et al., 2013). We therefore investigated the effect of mosaic loss of NEXMIF on the development of neuronal morphology. To do this, we cultured primary cortical neurons from WT or *NEXMIF*$^{+/-}$ brains and immunostained for MAP2 to label the dendrites at DIV 8 (**Fig. 4.6A**). Given the mosaic expression of NEXMIF in heterozygote females, we also immunostained for NEXMIF to identify neuron cell types in the *NEXMIF*$^{+/-}$ cultures. Consistent with our previous study of *NEXMIF* knockdown (Gilbert and Man, 2016), Sholl analysis revealed a decrease in dendritic arbor complexity for NEXMIF^{-} neurons in the *NEXMIF*$^{+/-}$ cultures (**Fig.**

4.6B). Further analysis demonstrated that the NEXMIF-lacking (NEXMIF^{-}) neurons had a significant reduction in total number of dendrites, number of branch points, and number of terminal points, as well as a decrease in the total sum length of dendrites (**Fig. 4.6C-4.6F**). Similar changes were also detected in NEXMIF^{-} neurons at DIV 14 (**Fig. 4.6G-4.6L**). Strikingly, NEXMIF-expressing (NEXMIF^{+}) neurons from the *NEXMIF*$^{+/-}$ culture also showed a reduction in dendritic morphology when compared to WT controls (**Fig. 4.6B and 4.6H-4.6L**). These impairments in dendrite morphology were also observed in primary hippocampal neurons from WT or *NEXMIF*$^{+/-}$ animals (**Fig. 4.7**).

To further examine the effect of NEXMIF haploinsufficiency on neurite extension, we examined axon outgrowth in primary neuronal cultures from WT or *NEXMIF*$^{+/-}$ brains. DIV 3 cortical (**Fig. 4.8A**) or hippocampal (**Fig. 4.8D**) were immunolabeled for Tau to label axons. Quantification of axonal length and the number of axon branches revealed reduced axonal outgrowth in both NEXMIF^{+} and NEXMIF^{-} neurons from the cortex (**Fig. 4.8B-4.8C**) and the hippocampus (**Fig. 4.8E-4.8F**). Collectively, this data demonstrates that in a mosaic network of mixed cell types, the loss of NEXMIF in some neurons not only causes developmental defects in those neurons themselves, but also *in trans* affects the neighboring neurons which have intact NEXMIF expression.

4.3.7 NEXMIF haploinsufficiency results in reduced spine density

Dysregulation of spine and synapse formation has been recognized as one of the most common cellular defects in ASD. Indeed, a dramatic reduction in spine

density was observed in the hippocampi of adult *NEXMIF*$^{-/y}$ KO mice (Gilbert et al., 2020). To determine possible changes in spine development in neurons from *NEXMIF*$^{+/-}$ mice *in vitro*, we cultured primary cortical neurons from WT or *NEXMIF*$^{+/-}$ brains and applied phalloidin at DIV 12 to label actin-rich spines (**Fig. 4.9A**). In line with the *NEXMIF*$^{-/y}$ results, we observed a significant decrease in spine density for NEXMIF^{-} neurons compared to neurons from WT brains (**Fig. 4.9B-4.9C**). Interestingly, NEXMIF^{+} neurons in the *NEXMIF*$^{+/-}$ culture showed a decrease in spine density similar to that of the NEXMIF^{-} neurons. By immunocytochemistry, we then examined the expression and localization of major synaptic proteins including GluA1, PSD95, VGlut1, GABARα1, gephyrin, and VGat. We found that puncta density of each of these synaptic proteins was significantly reduced in both NEXMIF^{+} and NEXMIF^{-} neurons from the *NEXMIF*$^{+/-}$ culture, as compared to neurons from the WT culture (**Fig. 4.9D**).

In order to observe changes in spine density *in vivo*, we performed Golgi staining on brains of adult WT and *NEXMIF*$^{+/-}$ mice. Because Golgi staining randomly labels neurons, the specific cell type regarding NEXMIF expression could not be determined. Therefore, the Golgi stained neurons were combined for structural analysis. Compared to WT controls, a significant decrease in spine density was detected in neurons from *NEXMIF*$^{+/-}$ brains (**Fig. 4.9E-4.9P**). This change was apparent in all brain regions measured, including L2/3 (**Fig. 4.9E-4.9G**) and L5 (**Fig. 4.9H-4.9J**) from the somatosensory cortex and CA1 (**Fig. 4.9K-4.9M**) and the dentate gyrus (**Fig. 4.9N-4.9P**) from the hippocampus. Closer

examination of this data revealed that the neurons from *NEXMIF*$^{+/-}$ brains did not fall into two distinct groups as predicted to result from the two subsets of NEXMIF^{+} and NEXMIF^{-} neurons, suggesting that the NEXMIF^{+} cells were likely also affected, as we found in cultured neurons (**Fig. 4.9A-4.9C**).

4.4 Discussion

In this study, we successfully established a haploinsufficient *NEXMIF*$^{+/-}$ mouse line. The behavioral phenotypes of the haploinsufficient female mice faithfully recapitulate those of the human disease. The *NEXMIF*$^{+/-}$ female mice demonstrated reduced sociability and preference for social novelty compared to wild-type female controls. They also showed significant changes in marble burying, grooming, and rearing behaviors. We also found that the *NEXMIF*$^{+/-}$ females displayed increased activity in an open field and significant impairments in spatial memory as measured by the Barnes Maze. In line with findings of milder communication phenotypes in females with NEXMIF-dependent ASD (Panda et al., 2020; Stamberger et al., 2020), NEXMIF KO male mice showed significant impairments in ultrasonic vocalizations from isolated pups, while *NEXMIF*$^{+/-}$ female mice showed moderate changes. Thus, our findings validify this transgenic line as a model for NEXMIF-dependent ASD in females.

We also investigated cellular and molecular phenotypes in the brains of *NEXMIF*$^{+/-}$ mice. We found the heterozygous brains demonstrate a mosaic mixture of wild-type and null mutant neurons caused by random X-inactivation in both the

hippocampus and the somatosensory cortex. In primary neuronal cultures from the brains of transgenic females, we found that both NEXMIF^{+} and NEXMIF^{-} neurons demonstrated aberrant dendritic arborization and reductions in spine and synapse density. Both groups of neurons also showed reductions in the puncta density of key synaptic proteins including GluA1, PSD95, and VGlut1 at excitatory synapses, and GABARα1, gephyrin, and VGat at inhibitory synapses. Thus, the loss of NEXMIF affects not only the mutant cells themselves, but also the neighboring NEXMIF^{+} cells. These surprising findings indicate a non-cell autonomous effect from loss of NEXMIF. It is possible that NEXMIF haploinsufficiency causes a reduction of secretory molecules in the extracellular milieu, leading to developmental defects in all cells.

Studies of humans with NEXMIF-dependent ASD have demonstrated a significant difference in disease phenotypes between hemizygous knockout male and heterozygous females. Males tend to have more severe impairments in language (58% nonverbal) and cognition (74% severe to profound ID) than females (10% nonverbal; 32% severe to profound ID) (Stamberger et al., 2020). Consistently, our data shows the *NEXMIF*$^{-/y}$ KO male mice have dramatic impairments in communication, while the haploinsufficient *NEXMIF*$^{+/-}$ females show only moderate changes. Interestingly, females are significantly more likely to have a seizure phenotype than males (Panda et al., 2020; Stamberger et al., 2020). We have observed seizures in both male and female mice, though the differences between male and female mice remain to be investigated. In

haploinsufficient females, variations in phenotypic severity could result from skewed XCI (Gribnau and Barakat, 2017; Heine-Suñer et al., 2003; Migeon, 2020; Ribeiro and MacDonald, 2020; Taherian et al., 2016; De Vries et al., 1996; Young and Zoghbi, 2004b; Zhang et al., 2020a). Of the 32 female NEXMIF patients who have been tested for XCI skewing, 25 showed random (<75:25) XCI patterning without skewing. Additionally, when comparing sisters within patient families, no correlation was found between extent of XCI skewing and disease phenotype, indicating skewing itself is unlikely to be responsible for phenotypic variations (Stamberger et al., 2020). Although these findings were from peripheral blood cells, it is in agreement with our findings in the female mouse model, which shows no signs of significant skewing in NEXMIF expression in the brains of heterozygous female mice.

In the brain, mosaic expression of NEXMIF could lead to structural and functional abnormalities *via* multiple potential mechanisms. While the most direct causal factor is the loss of NEXMIF in the NEXMIF^{-} neurons, the unbalanced NEXMIF expression among mosaic neurons in the brain can lead to further disruptions. To compensate for the overall reduction of NEXMIF in the brain, NEXMIF expression may be up regulated in NEXMIF^{+} cells. This global compensation would result in overexpression and a hyper-dosage of the protein in the NEXMIF^{+} neurons. Our findings indicate that this scenario did not occur in the NEXMIF haploinsufficient females. Second, if the effect of loss of NEXMIF is mediated, at least partially, *via* secretory signaling molecules, changes in NEXMIF

expression could affect all neurons in the brain. In fact, we found comparable defects in dendritic structure and spine formation in both NEXMIF^{+} and NEXMIF^{-} neurons. Interestingly, the impaired dendritic arborization phenotype became more severe in NEXMIF^{+} cortical neurons at DIV 14 than at DIV 8. It is possible that, at the early stage, a lack of NEXMIF only affects NEXMIF^{-} neurons, and at a later phase, the NEXMIF^{+} neurons are affected from neighboring NEXMIF^{-} neurons, probably due to changes in extracellular cues.

Given the mutual innervation between NEXMIF^{+} and NEXMIF^{-} neurons, the *trans* effects on NEXMIF^{+} neurons could also result from aberrant interneuronal communication. Not only might this account for the phenotypes in the NEXMIF^{+} neurons, but cell-cell interactions between wild type and mutant neurons in the brain of heterozygotes could disrupt the overall neuronal circuitry in a way that is different, and possibly more severe, than from the complete loss in KOs. Such a “cellular interference” or “metabolic interference” mechanism (Johnson, 1980) has been observed in other heterozygous X-linked diseases such as ARHGEF9 dependent ASD (Aarabi et al., 2019), *PCDH19* linked epilepsy and mental retardation (Dibbens et al., 2008; Hoshina et al., 2021), craniofrontonasal syndrome (Twigg et al., 2013; Wieland et al., 2004), and sporadic infantile epileptic encephalopathy (Depienne et al., 2009; Dibbens et al., 2008). This hypothesis might explain the greater percentage of females affected with NEXMIF variants (89%) who demonstrate an epileptic phenotype than affected males (65%) (Stamberger et al., 2020). We found that seizures were common in both the male

NEXMIF$^{-/y}$ and female *NEXMIF*$^{+/-}$ mice, but further studies are needed to compare the frequency, types, and severity of these seizures in our mouse models.

While a number of somatic gene mutations are known to lead to ASD in heterozygous females (Boccuto et al., 2013; Busch et al., 2019; Courchet et al., 2018; Dere et al., 2014; Gompers et al., 2017; Jaramillo et al., 2017), only a few X-linked genes, including *NEXMIF*, have been reported to be implicated in ASD by haploinsufficiency. For X-linked genes, heterozygous females generally have a milder disease phenotype, or are unaffected carriers, due to sufficient gene expression from their normal allele, which is not possible in their male counterparts. However, there are some cases of manifesting heterozygotes, in which heterozygous expression of an X-linked gene results in a more severe phenotype (Fuchs et al., 2018; Migeon, 2020; Taherian et al., 2016), such as in the heterozygous X-linked neurological disorders Rett syndrome (Gribnau and Barakat, 2017), fragile X syndrome (Godler et al., 2015; Marco and Skuse, 2006), *CASK* associated mental retardation (Moog et al., 2011; Patel et al., 2020), and loss of Pcdh19 (Hayashi et al., 2017; Pederick et al., 2018). In some cases, the disease phenotype results from XCI skewing which leads to biased silencing of the X chromosome containing the normal allele, but this seems not to be the case for NEXMIF patients. A number of computational studies have attempted to identify genes which cannot tolerate the loss of one of the two alleles (Dang et al., 2008; Huang et al., 2010; Shihab et al., 2017; Steinberg et al., 2015; Yang et al., 2021). It has been shown that haploinsufficient genes are enriched in several gene

ontology categories including transcription factors and phenotypes including neurodevelopmental disorders (Dang et al., 2008). Notably, *NEXMIF* is predicted to be a haploinsufficient gene (Steinberg et al., 2015).

In summary, our results show that the *NEXMIF*$^{+/-}$ animals recapitulate the phenotypes observed in the human disease, making it a useful model for further study of *NEXMIF* and ASD. NEXMIF is expressed in a mosaic pattern in the brains of these animals. Therefore, the heterozygous female mice provide a unique neural network intertwined by mutual innervation between and among the NEXMIF^{+} and NEXMIF^{-} neurons in a brain. Additionally, the heterozygous female model is of particular interest for future study for its potential to rescue the loss of NEXMIF from the endogenous normal NEXMIF allele by specific reactivation of the X chromosome with the wild type allele, as shown to be a promising strategy in Rett syndrome (Przanowski et al., 2018). The *NEXMIF*$^{+/-}$ line will therefore be of great value for further study of the mechanisms underlying NEXMIF-dependent ASD as well as the development of effective therapeutic approaches.

Figure 4.1

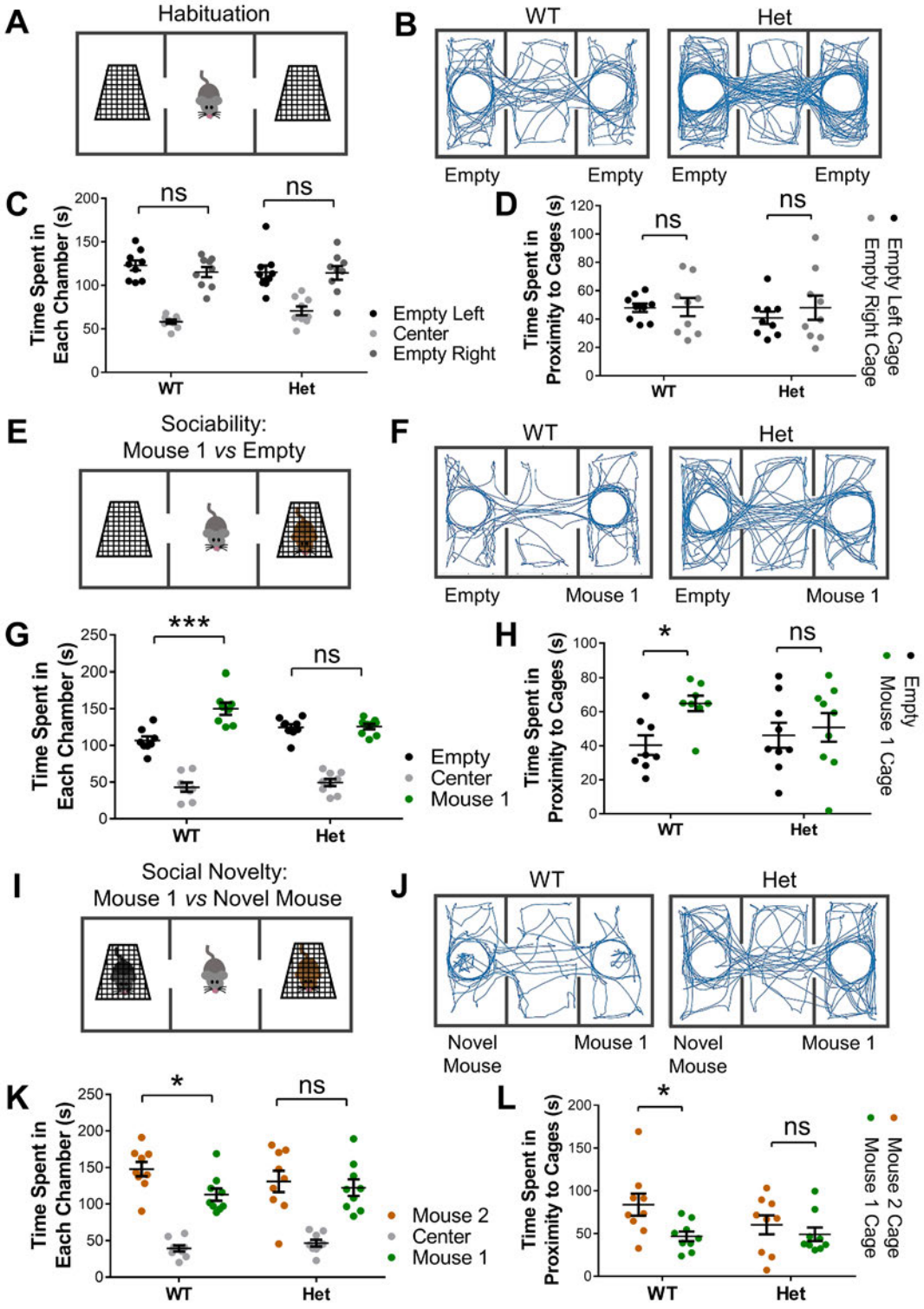

A
Habituation
B
WT
Het
Empty
Empty
Empty
Empty
C
ns
ns
Time Spent in Each Chamber (s)
Empty Left
Center
Empty Right
WT
Het
D
ns
ns
Time Spent in Proximity to Cages (s)
Empty Left Cage
Empty Right Cage
WT
Het
E
Sociability:
Mouse 1 vs Empty
F
WT
Het
Empty
Mouse 1
Empty
Mouse 1
G
***
ns
Time Spent in Each Chamber (s)
Empty
Center
Mouse 1
WT
Het
H
*
ns
Time Spent in Proximity to Cages (s)
Empty
Mouse 1 Cage
WT
Het
I
Social Novelty:
Mouse 1 vs Novel Mouse
J
WT
Het
Novel Mouse
Mouse 1
Novel Mouse
Mouse 1
K
*
ns
Time Spent in Each Chamber (s)
Mouse 2
Center
Mouse 1
WT
Het
L
*
ns
Time Spent in Proximity to Cages (s)
Mouse 2 Cage
Mouse 1 Cage
WT
Het

Figure 4.1 NEXMIF heterozygous mice show abnormalities in social behaviors

(A) Habituation to the three-chamber apparatus. Mice were released from the center chamber, with empty cages in the adjacent chambers, and allowed to move freely within the apparatus for 5 min each session for 3 d prior to beginning the sociability and social novelty tests. **(B)** Representative traces of animal track paths in the habituation phase for WT and *NEXMIF*$^{+/-}$ mice. **(C, D)** Neither WT nor *NEXMIF*$^{+/-}$ animals showed preference for either side chamber (C) (Left vs Right: WT: $t_{(32)} = 0.7979$, KO: $t_{(32)} = 0.0977$; $F_{(1, 32)} = 0.401$, $p = 0.5311$) or either empty cage (D) (Left vs Right: WT: $t_{(32)} = 0.059$, KO: $t_{(32)} = 0.849$; $F_{(1, 32)} = 0.4129$, $p = 0.5251$) during habituation. **(E)** Paradigm for the sociability test. An unfamiliar mouse (Mouse 1) was placed into either of the side chambers and the test mouse was allowed to move freely within the apparatus. **(F)** Representative traces of animal track paths in the sociability test for WT and *NEXMIF*$^{+/-}$ mice. **(G, H)** Het mice failed to demonstrate the sociability observed in WT mice, which show an increase in the time spent in the chamber (G) (Empty vs Mouse 1: WT: $t_{(30)} = 5.354$, KO: $t_{(30)} = 0.1375$; $F_{(1, 30)} = 15.92$, $p = 0.0004$) and in proximity to the cage (H) (Empty vs Mouse 1: WT: $t_{(30)} = 2.452$, KO: $t_{(30)} = 0.4959$; $F_{(1, 30)} = 4.514$, $p = 0.042$) with Mouse 1. **(I)** Paradigm for the social novelty test. A second mouse (Novel Mouse) was placed into the remaining empty chamber opposite to Mouse 1, and the test mouse was allowed to interact with both mice. **(J)** Representative traces of animal track paths in the social novelty test for WT and *NEXMIF*$^{+/-}$ mice.

(K, L) WT mice showed an increase in the time spent in the chamber (K) (Mouse 1 vs Mouse 2: WT: $t_{(30)} = 3.145$, KO: $t_{(30)} = 0.5769$; $F_{(1, 30)} = 7.205$, $p = 0.0117$) and in proximity to the cage (L) (Mouse 1 vs Mouse 2: WT: $t_{(30)} = 2.818$, KO: $t_{(30)} = 1.591$; $F_{(1, 30)} = 9.526$, $p = 0.0043$) with the Novel Mouse, but the *NEXMIF*$^{+/-}$ mice failed to demonstrate the preference for social novelty. Het, *NEXMIF*$^{+/-}$. $n = 9$ mice/ group. *$p<0.05$, **$p<0.01$, ns = not significant.

Figure 4.2

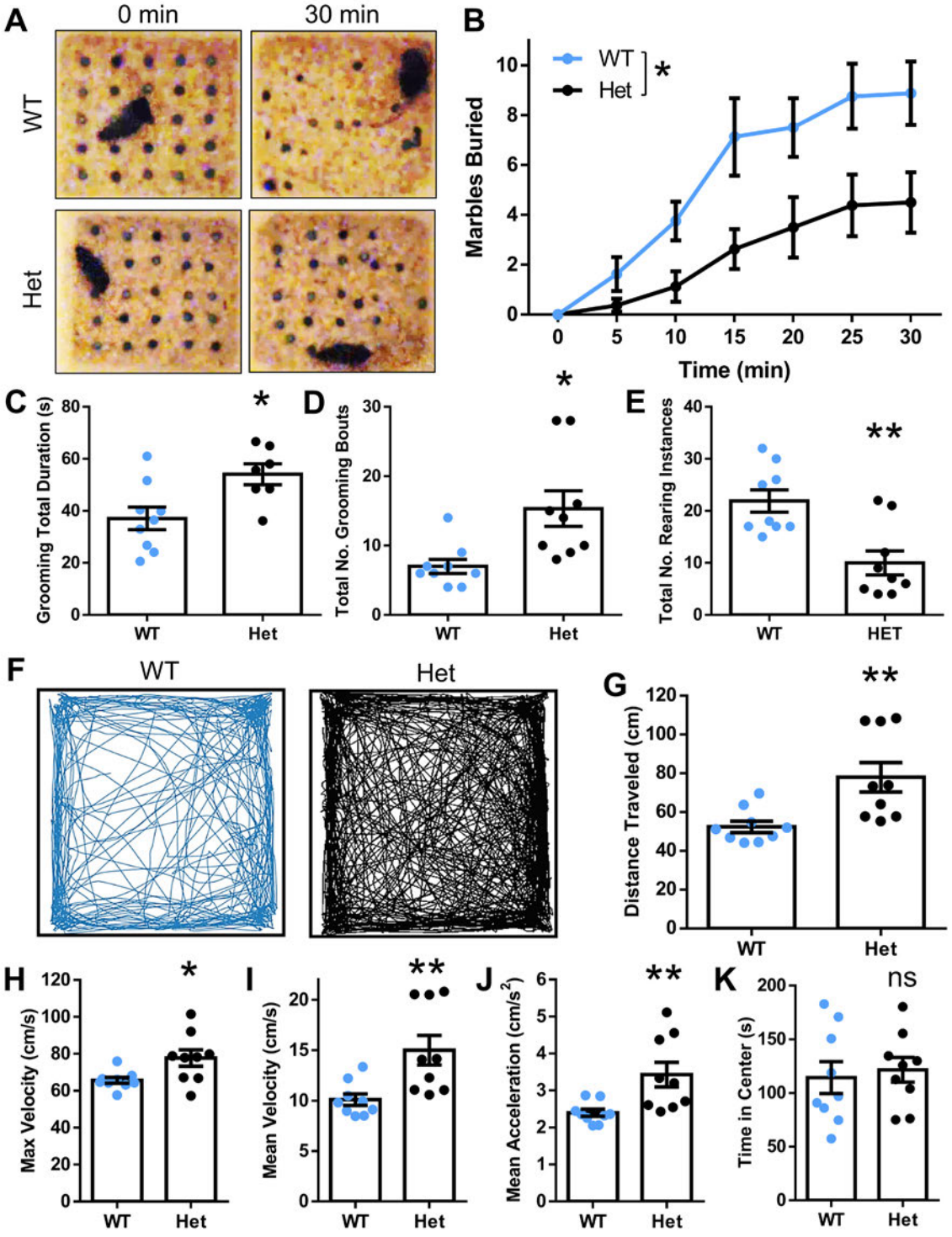

A
0 min
30 min
WT
Het
B
WT
Het
*
Marbles Buried
Time (min)
C
Grooming Total Duration (s)
*
WT
Het
D
Total No. Grooming Bouts
*
WT
Het
E
Total No. Rearing Instances
**
WT
HET
F
WT
Het
G
Distance Traveled (cm)
**
WT
Het
H
Max Velocity (cm/s)
*
WT
Het
I
Mean Velocity (cm/s)
**
WT
Het
J
Mean Acceleration (cm/s²)
**
WT
Het
K
Time in Center (s)
ns
WT
Het

Figure 4.2 NEXMIF heterozygous mice display aberrant marble burying behavior, increased repetitive grooming, and hyperactivity

(A, B) In the marble burying test, *NEXMIF*$^{+/-}$ animals buried significantly fewer marbles ($F_{(1,14)} = 7.924$, $p = 0.0138$ between genotypes; $F_{(6, 84)} = 31.02$, $p < 0.0001$ between time points). **(C, D)** *NEXMIF*$^{+/-}$ mice spent an increased amount of time grooming (C) ($t_{(14)} = 2.786$, $p = 0.0146$) and performed an increased number of grooming episodes (D) ($t_{(16)} = 3.021$, $p = 0.0081$). **(E)** *NEXMIF*$^{+/-}$ animals demonstrated a reduction in rearing behavior ($t_{(16)} = 3.757$, $p = 0.0017$). **(F)** Representative track paths of WT and *NEXMIF*$^{+/-}$ animals in the open field test. **(G-K)** *NEXMIF*$^{+/-}$ animals showed increased track lengths (G) ($t_{(16)} = 3.132$, $p = 0.0064$), increased max (H) ($t_{(16)} = 2.560$, $p = 0.0210$) and mean (I) ($t_{(16)} = 3.132$, $p = 0.0064$) speeds, increased mean acceleration (J) ($t_{(16)} = 2.966$, $p = 0.0091$), and no change in time spent in the central area (K) ($t_{(16)} = 0.3870$, $p = 0.7039$) in the open field test. $n = 9$ mice/ group. *$p<0.05$, **$p<0.01$, ns = not significant.

Figure 4.3

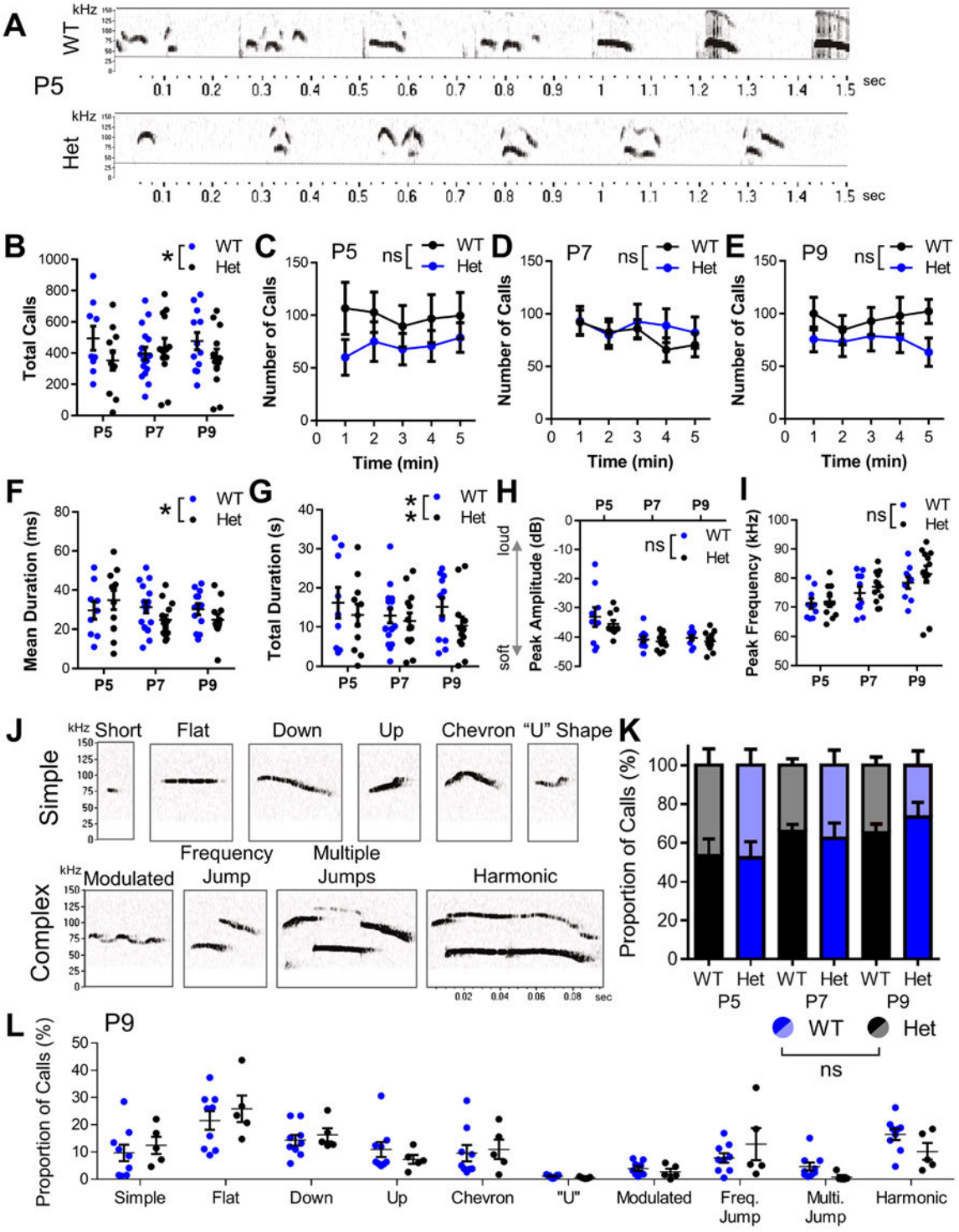

A
WT
P5
Het
kHz
sec
B
Total Calls
WT
Het
P5
P7
P9
C
P5
ns
Number of Calls
Time (min)
D
P7
E
P9
F
Mean Duration (ms)
G
Total Duration (s)
H
Peak Amplitude (dB)
loud
soft
I
Peak Frequency (kHz)
J
Simple
Short
Flat
Down
Up
Chevron
"U" Shape
Complex
Modulated
Frequency Jump
Multiple Jumps
Harmonic
K
Proportion of Calls (%)
L
Simple
Flat
Down
Up
Chevron
"U"
Modulated
Freq. Jump
Multi. Jump
Harmonic

Figure 4.3 NEXMIF heterozygous mice show moderate impairment in communication behavior

(A) Representative vocalizations from P5 recordings for WT and *NEXMIF*$^{+/-}$ mice. Top: the raw USV signals. Bottom: the associated spectrograms; all are 1.5 s in length. Dashed line depicts the 30 kHz frequency threshold for eliminating noise. **(B)** Quantification of the number of calls made by *NEXMIF*$^{+/-}$ animals compared to WT controls at each developmental time point recorded ($F_{(1,8)} = 5.959$, $p = 0.0405$ between genotypes; $F_{(2,16)} = 0.2021$, $p = 0.8191$ between time points). **(C-E)** Mean number of calls emitted across the 5 min recording period at each developmental time point P5 (C) ($F_{(1,8)} = 0.7084$, $p = 0.4244$ between genotypes; $F_{(4,32)} = 0.1688$, $p = 0.9527$ between time points), P7 (D) ($F_{(1,12)} = 0.1227$, $p = 0.7322$ between genotypes; $F_{(4,48)} = 1.353$, $p = 0.2643$ between time points), and P9 (E) ($F_{(1,11)} = 4.040$, $p = 0.0696$ between genotypes; $F_{(4,44)} = 0.3459$, $p = 0.8454$ between time points). **(F-G)** Quantification of the mean call syllable duration (F) ($F_{(1,8)} = 6.381$, $p = 0.0355$ between genotypes; $F_{(2,16)} = 0.8940$, $p = 0.4285$ between time points) and the total time spent calling (G) ($F_{(1,8)} = 14.28$, $p = 0.0054$ between genotypes; $F_{(2,16)} = 0.4545$, $p = 0.6427$ between time points) between WT and *NEXMIF*$^{+/-}$ mice. **(H-I)** *NEXMIF*$^{+/-}$ mice showed no change in peak amplitude of calls (H) ($F_{(1,8)} = 2.214$, $p = 0.1751$ between genotypes; $F_{(2,16)} = 9.698$, $p = 0.0017$ between time points), or peak frequency of calls (I) ($F_{(1,8)} = 0.1464$, $p = 0.7120$ between genotypes; $F_{(2,16)} = 1.721$, $p = 0.2104$ between time points). **(J)** Representative calls of each type used in syllable characterization. (**K)** WT and *NEXMIF*$^{+/-}$ mice

showed similar ratios of Simple vs Complex call types at each time point ($F_{(1,84)}$ = 0.0182, p = 0.8931). **(L)** *NEXMIF*$^{+/-}$ animals showed no change in frequency of particular call syllable types compared to WT animals at P9 (Simple: $t_{(12)}$ = 0.584, p = 0.570; Flat: $t_{(12)}$ = 0.733, p = 0.478; Down: $t_{(12)}$ = 0.606, p = 0.556; Up: $t_{(12)}$ = 0.927, p = 0.372; Chevron: $t_{(12)}$ = 0.295, p = 0.773; “U”: $t_{(12)}$ = 1.90, p = 0.0824; Modulated: $t_{(12)}$ = 0.829, p = 0.423; Freq. Jump: $t_{(12)}$ = 1.04, p = 0.318; Multi. Jump: $t_{(12)}$ = 1.86, p = 0.0874; Harmonic: $t_{(12)}$ = 1.76, p = 0.104). n = 9-16 animals. ns = not significant.

Figure 4.4

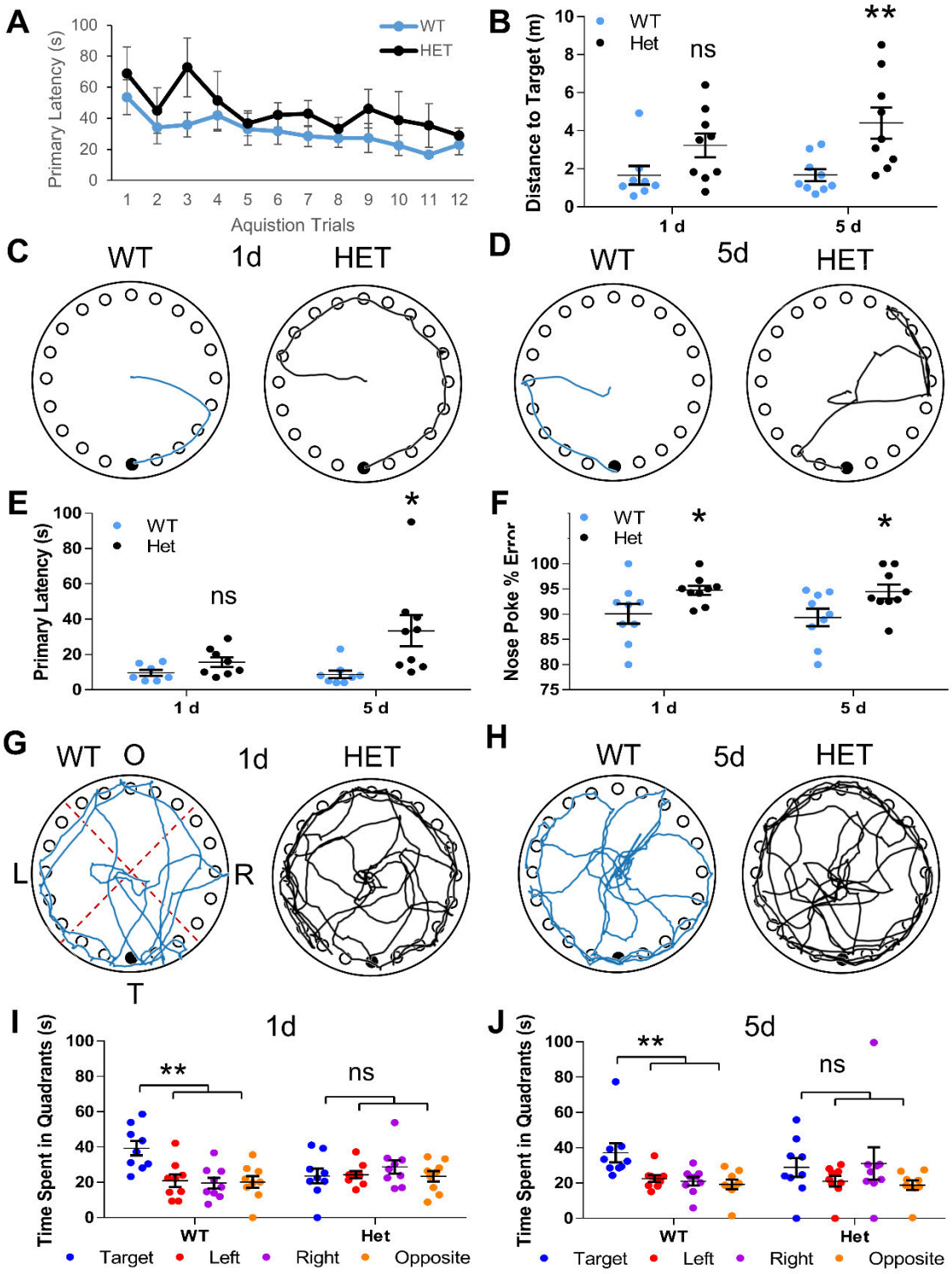
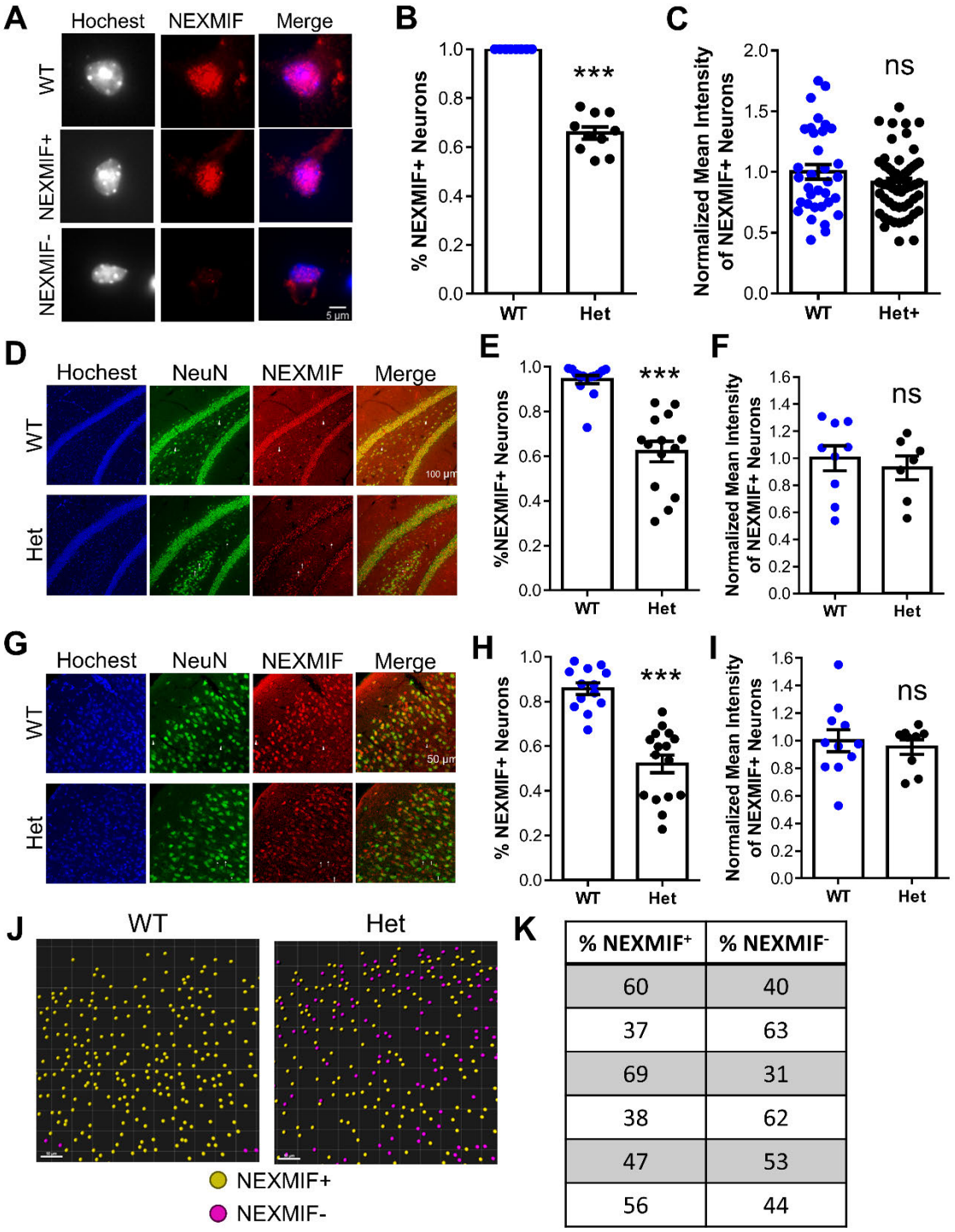

A
Primary Latency (s)
WT
HET
Aquistion Trials
B
Distance to Target (m)
WT
Het
ns
**
1 d
5 d
C
WT
1d
HET
D
WT
5d
HET
E
Primary Latency (s)
WT
Het
ns
*
1 d
5 d
F
Nose Poke % Error
WT
Het
*
*
1 d
5 d
G
WT
O
1d
HET
L
R
T
H
WT
5d
HET
I
Time Spent in Quadrants (s)
1d
**
ns
WT
Het
Target
Left
Right
Opposite
J
Time Spent in Quadrants (s)
5d
**
ns
WT
Het
Target
Left
Right
Opposite

Figure 4.4 NEXMIF heterozygous mice display defects in learning and memory in the Barnes maze test

(A) Quantification of the primary latency (s) to find the target hole across all training trials (3 trials per day over 4 days) for WT and *NEXMIF*$^{+/-}$ animals. **(B)** Total track length distance before initial contact with target hole was increased in *NEXMIF*$^{+/-}$ mice 5 d after training ($F_{(1,7)}$ = 15.63, p = 0.0055 between genotypes; $F_{(1,7)}$ = 3.519, p = 0.1028 between time points). **(C, D)** Representative traces of track paths to initial contact with target in the Barnes spatial memory maze during the 1 d (C) and 5 d (D) memory probe for WT and *NEXMIF*$^{+/-}$ animals. **(E)** Primary latency to the target hole was increased in the *NEXMIF*$^{+/-}$ animals in the test 5 d after training ($F_{(1,7)}$ = 7.828, p = 0.0266 between genotypes; $F_{(1,7)}$ = 0.7161, p = 0.4254 between time points). **(F)** *NEXMIF*$^{+/-}$ mice made a significantly higher number of nose poke errors in both the 1 d and 5 d memory tests than WT mice ($F_{(1,8)}$ = 11.35, p = 0.0098 between genotypes; $F_{(1,8)}$ = 0.2212, p = 0.6507 between time points). **(G, H)** Representative traces of track paths over 3 min test in the Barnes spatial memory maze during the 1 d (G) and 5 d (H) memory probe for WT and *NEXMIF*$^{+/-}$ animals. T, target; L, left; R, right; O, opposite. **(I, J)** *NEXMIF*$^{+/-}$ mice did not spend significantly more time in the target quadrant compared to the other maze quadrants, as WT controls do, in the tests at 1 d (I) (WT: Target v Left: $t_{(64)} = 3.810$, Target v Right: $t_{(64)} = 4.088$, Target v Opposite: $t_{(64)} = 3.967$; Het: Target v Left: $t_{(64)} = 0.1492$, Target v Right: $t_{(64)} = 1.050$, Target v Opposite: $t_{(64)} = 0.0424$; $F_{(3, 64)}$ = 3.347, $p = 0.0244$) and 5 d (J) (WT: Target v Left: $t_{(64)} = 2.218$,

Target v Right: $t_{(64)} = 2.442$, Target v Opposite: $t_{(64)} = 2.716$; Het: Target v Left: $t_{(64)} = 1.182$, Target v Right: $t_{(64)} = 0.3385$, Target v Opposite: $t_{(64)} = 1.524$; $F_{(3, 64)} = 3.41$, $p = 0.0227$) after training. n = 9 mice/ group. * $p<0.05$, ** $p<0.01$, ns = not significant.

Figure 4.5



K

% NEXMIF⁺	% NEXMIF⁻
60	40
37	63
69	31
38	62
47	53
56	44

Figure 4.5 Mosaic NEXMIF expression in the NEXMIF heterozygous mouse

(A-C) Immunostaining of NEXMIF in DIV 6 primary cortical neurons cultured from NEXMIF WT or *NEXMIF*$^{+/-}$ mouse brains shows colocalization with nuclear marker Hochest (A) and a lack of NEMXIF expression in some, but not all, neurons from *NEXMIF*$^{+/-}$ brains (B) ($t_{(18)} = 13.76$, $p < 0.0001$) with no change in the level of NEXMIF in the NEXMIF^{+} neurons (C) ($t_{(90)} = 1.366$, $p = 0.1752$). Scale bar = 5 µm. *n* = 10 experiments, 30-100 cells each. **(D-I)** Immunostaining of NEXMIF and neuronal marker NeuN in brain slices of adult female mice shows a reduction in NEXMIF-expressing neurons in Het hippocampus (D-F, scale bar = 100 µm; E: $t_{(26)} = 6.506$, $p < 0.0001$, F: $t_{(14)} = 0.5439$, $p = 0.5951$) and L2/3 of the somatosensory cortex (G-I, scale bar = 50 µm; H: $t_{(27)} = 6.693$, $p < 0.0001$, I: $t_{(18)} = 0.4492$, $p = 0.6587$). *n* = 13-16 slices, 60-800 cells each. **(J)** Representative mosaic distribution of NEXMIF-expressing (NEXMIF^{+}; yellow) and NEXMIF negative neurons (NEXMIF^{-}; pink) in the somatosensory cortex of WT and *NEXMIF*$^{+/-}$ mice. Scale bar = 50 µm. **(K)** Ratios of NEXMIF^{+} and NEXMIF^{-} neurons from the cortex of individual *NEXMIF*$^{+/-}$ mice. **p*<0.05, ***p*<0.01 ****p*<0.001, ns = not significant.

Figure 4.6

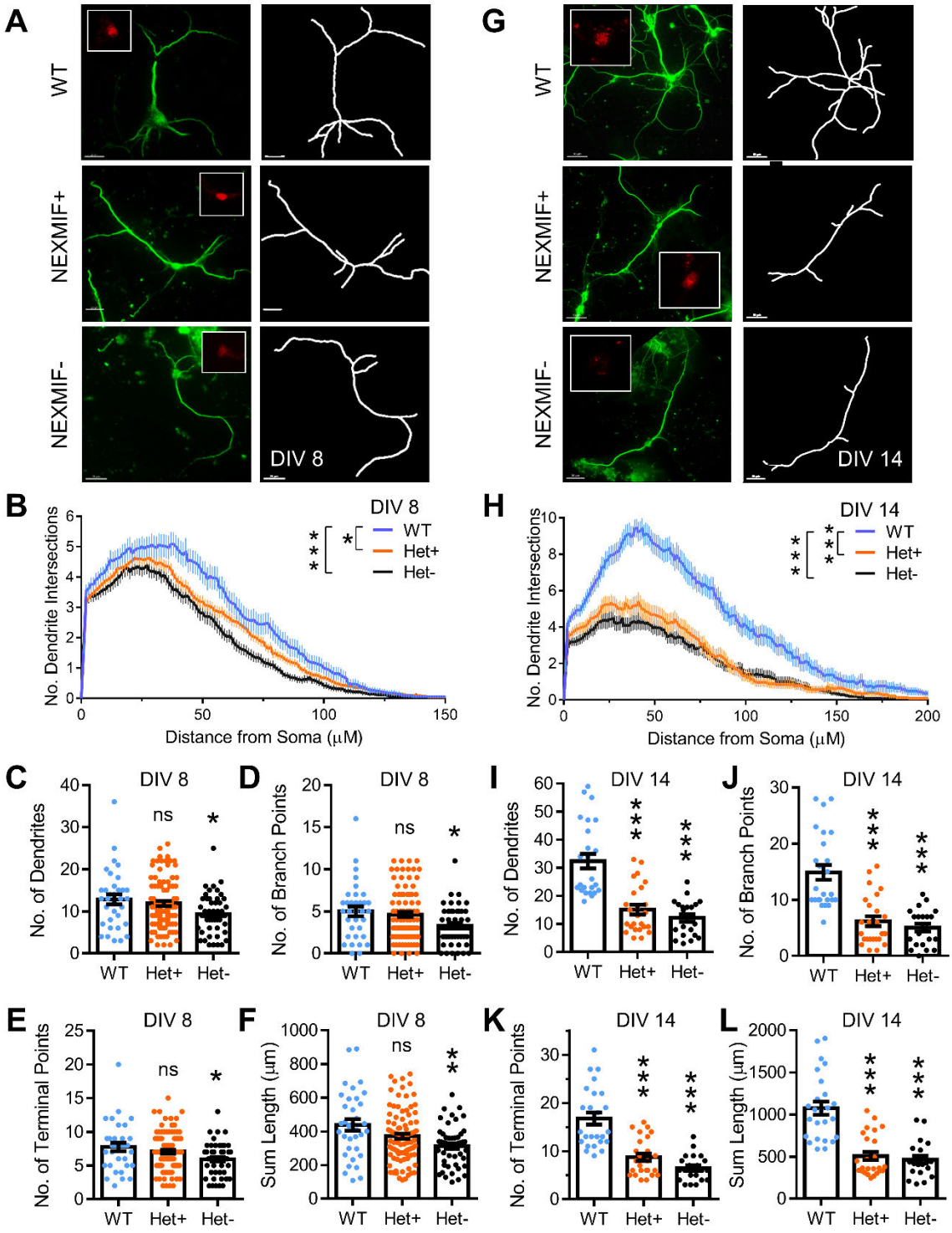

A
WT
NEXMIF+
NEXMIF-
DIV 8
G
DIV 14
B
DIV 8
WT
Het+
Het-
No. Dendrite Intersections
Distance from Soma (μM)
H
DIV 14
C
No. of Dendrites
D
No. of Branch Points
I
J
E
No. of Terminal Points
F
Sum Length (μm)
K
L
ns

Figure 4.6 Mosaic loss of NEXMIF results in a decrease in neurite outgrowth in primary neurons

(A) Representative images (left) and traces (right) of MAP2 immunostained primary cortical neurons from WT or *NEXMIF*$^{+/-}$ brains at DIV 8. Inset is immunostaining of NEXMIF, showing a mosaic mixture of NEXMIF^{+} and NEXMIF^{-} neurons. Scale bars = 20 µm. **(B)** Sholl analysis reveals a decrease in dendritic arbor complexity for both NEXMIF^{+} and NEXMIF^{-} neurons at DIV 8 ($F_{(2,172)}$ = 6.901, p = 0.0013 between genotypes; $F_{(150, 25800)}$ = 2.197, p < 0.0001 between radius). **(C-F)** The number of dendrites (C), branch points (D), terminal points (E), and the sum length of dendrites (F) were decreased in NEXMIF^{-} neurons at DIV 8. **(G)** Representative images and traces of cortical neurons at DIV 14. **(H)** Sholl analysis shows reduced complexity for both NEXMIF^{+} and NEXMIF^{-} neurons at DIV 14 ($F_{(2,68)}$ = 27.13, p < 0.0001 between genotypes; $F_{(200, 13600)}$ = 137.7, p < 0.0001 between radius). **(I-L)** The number of dendrites (I), branch points (J), terminal points (K), and the sum length of dendrites (L) were decreased in both NEXMIF^{+} and NEXMIF^{-} neurons at DIV 14. (No. of Dendrites: $F_{(2,40)}$ = 27.98, p < 0.0001 between genotypes; $F_{(1,20)}$ = 67.95, p < 0.0001 between time points; No. of Branch Points: $F_{(2,40)}$ = 22.04, p < 0.0001 between genotypes; $F_{(1,20)}$ = 27.88, p < 0.0001 between time points; No. of Terminal Points: $F_{(2,40)}$ = 28.42, p < 0.0001 between genotypes; $F_{(1,20)}$ = 34.27, p < 0.0001 between time points, Sum Length: $F_{(2,40)}$ = 29.77, p < 0.0001 between genotypes; $F_{(1,20)}$ = 55.22, p < 0.0001 between

time points). *n* = 30-90 cells/ group. Het+, NEXMIF^{+}/NEXMIF-expressing; Het-, NEXMIF^{-}/NEXMIF lacking. *p<0.05, **p<0.01 ***p<0.001, ns = not significant.

Figure 4.7

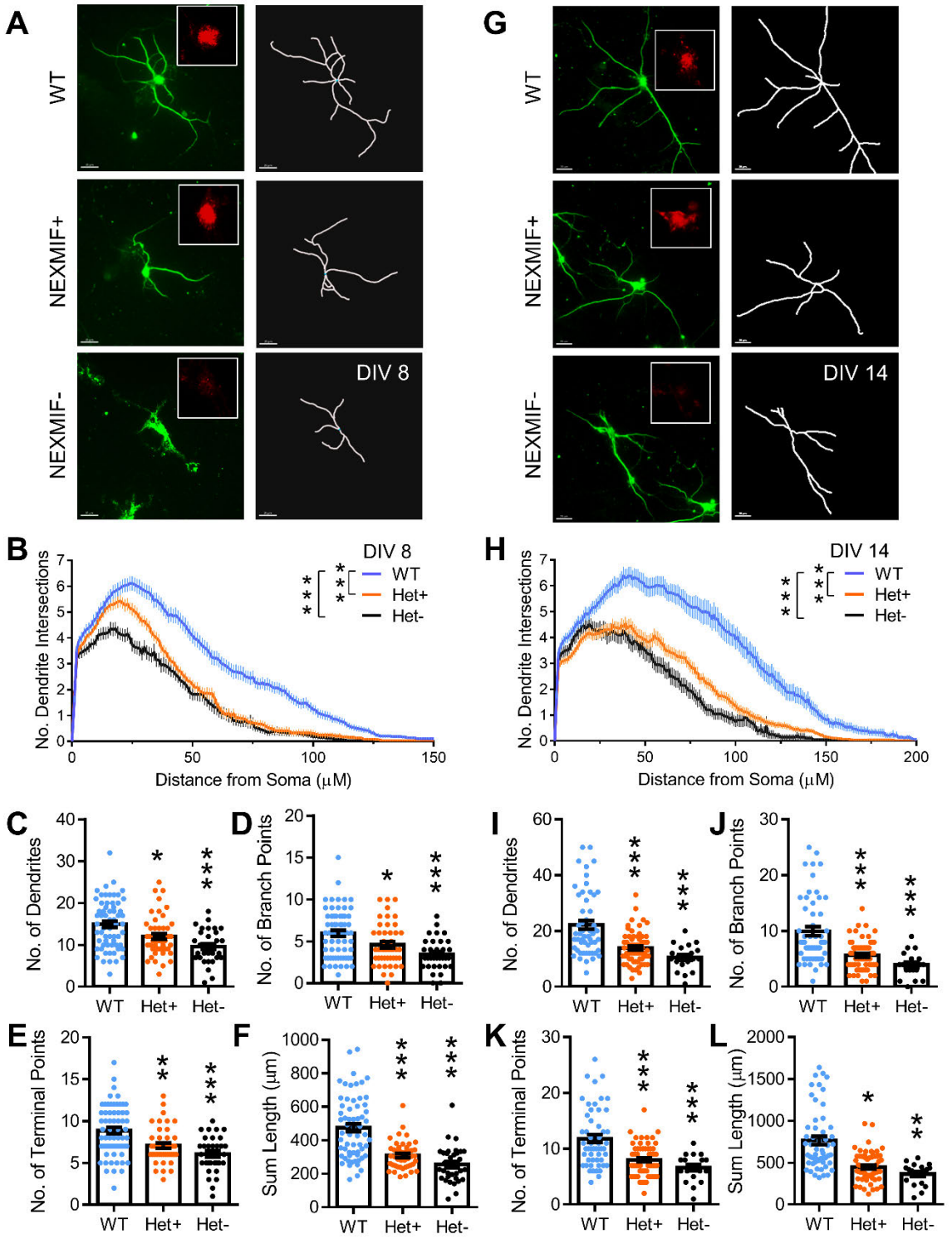

A
WT
NEXMIF+
NEXMIF-
DIV 8
G
DIV 14
B
DIV 8
WT
Het+
Het-
No. Dendrite Intersections
Distance from Soma (μM)
H
DIV 14
C
No. of Dendrites
D
No. of Branch Points
I
J
E
No. of Terminal Points
F
Sum Length (μm)
K
L

Figure 4.7 Hippocampal neurons of NEXMIF heterozygous mice show abnormal dendritic arborization

(A) Representative images (left) and traces (right) of MAP2 immunostained primary hippocampal neurons from WT or *NEXMIF*$^{+/-}$ brains at DIV 8. Inset is immunostaining of NEXMIF, showing a mosaic mixture of NEXMIF^{+} and NEXMIF^{-} neurons. Scale bars = 20 μm. **(B)** Sholl analysis reveals a decrease in dendritic arbor complexity for both NEXMIF^{+} and NEXMIF^{-} neurons at DIV 8 ($F_{(2,141)}$ = 29.35, p < 0.0001 between genotypes; $F_{(150, 21150)}$ = 350.5, p < 0.0001 between radius). **(C-F)** The number of dendrites (C), branch points (D), terminal points (E), and sum length of dendrites (F) were decreased in both groups of *NEXMIF*$^{+/-}$ neurons at DIV 8. **(G)** Representative images and traces of hippocampal neurons at DIV 14. **(H)** Sholl analysis shows reduced complexity for both NEXMIF^{+} and NEXMIF^{-} neurons at DIV 14 ($F_{(2,68)}$ = 27.13, p < 0.0001 between genotypes; $F_{(200, 13600)}$ = 137.7, p < 0.0001 between radius). **(I-L)** The number of dendrites (I), branch points (J), terminal points (K), and the sum length of dendrites (L) were decreased in both NEXMIF^{+} and NEXMIF^{-} neurons at DIV 14. (No. of Dendrites: $F_{(2,38)}$ = 46.72, p < 0.0001 between genotypes; $F_{(1,19)}$ = 25.77, p < 0.0001 between time points; No. of Branch Points: $F_{(2,38)}$ = 31.15, p < 0.0001 between genotypes; $F_{(1,19)}$ = 20.49, p = 0.0002 between time points; No. of Terminal Points: $F_{(2,38)}$ = 50.81, p < 0.0001 between genotypes; $F_{(1,19)}$ = 39.64, p < 0.0001 between time points, Sum Length: $F_{(2,38)}$ = 40.62, p < 0.0001 between genotypes; $F_{(1,19)}$ = 32.38,

$p < 0.0001$ between time points). $n = 20\text{-}70$ cells/ group. Het+, NEXMIF^{+}/NEXMIF-expressing; Het-, NEXMIF^{-}/NEXMIF lacking. *$p<0.05$, **$p<0.01$ ***$p<0.001$.

Figure 4.8

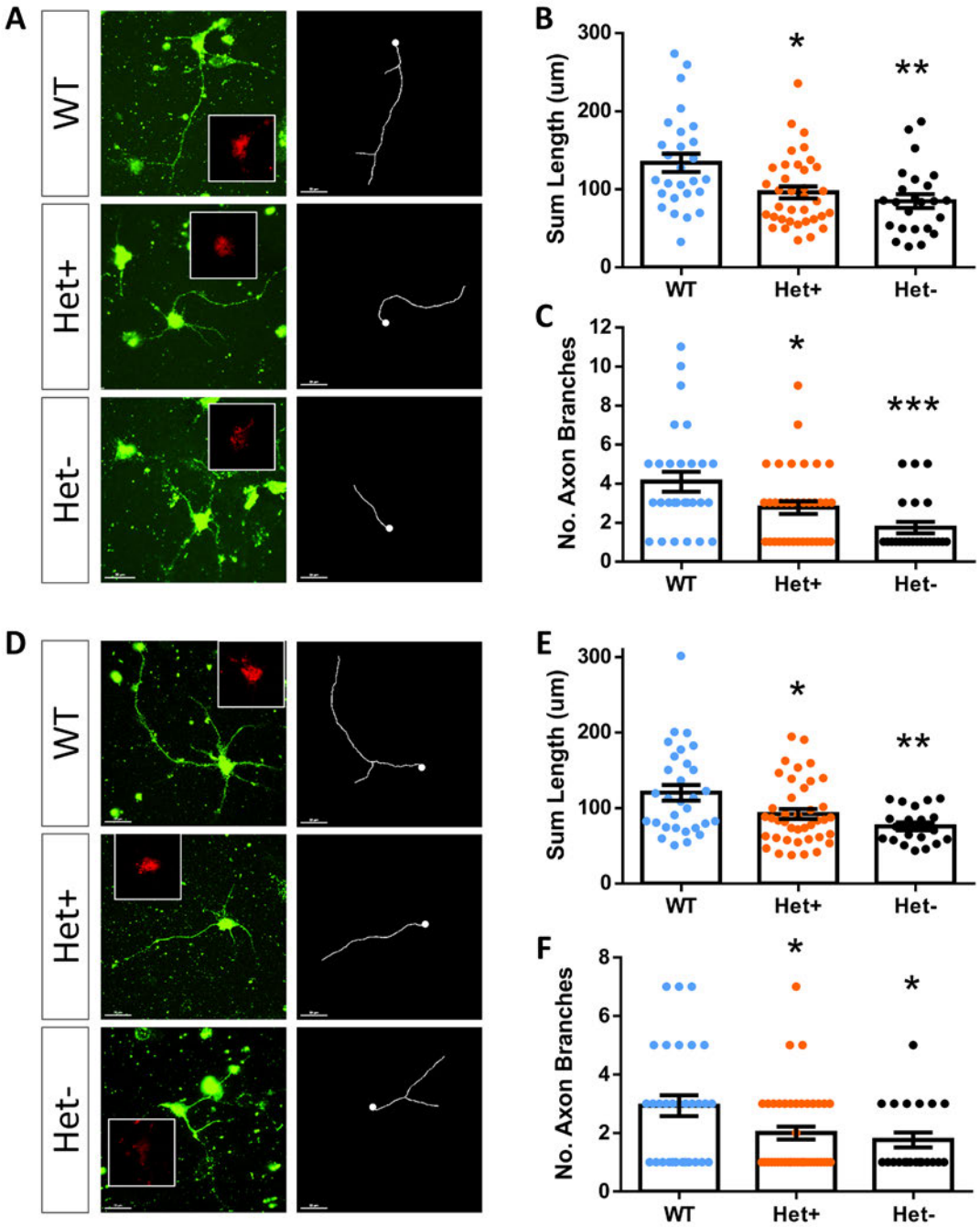


Figure 4.8 NEXMIF haploinsufficiency leads to impaired axonal outgrowth

(A) Representative images of Tau immunostained primary cortical neurons from WT or *NEXMIF*$^{+/-}$ brains at DIV 3. **(B, C)** The sum length of axons (B) ($F_{(2,84)}$ = 7.020, p = 0.0015) and the number of axon branches (C) ($F_{(2,85)}$ = 8.182, p = 0.0006) were decreased in only NEXMIF^{-} cortical neurons. n = 24-36 cells. **(D)** Representative images of Tau immunostained primary hippocampal neurons from WT or *NEXMIF*$^{+/-}$ brains at DIV 3. **(E, F)** The sum length of axons (E) ($F_{(2,87)}$ = 6.495, p = 0.0023) and the number of axon branches (F) ($F_{(2,90)}$ = 4.451, p = 0.0143) were decreased in both NEXMIF^{-} and NEXMIF^{+} hippocampal neurons. n = 21-41 cells.

Figure 4.9

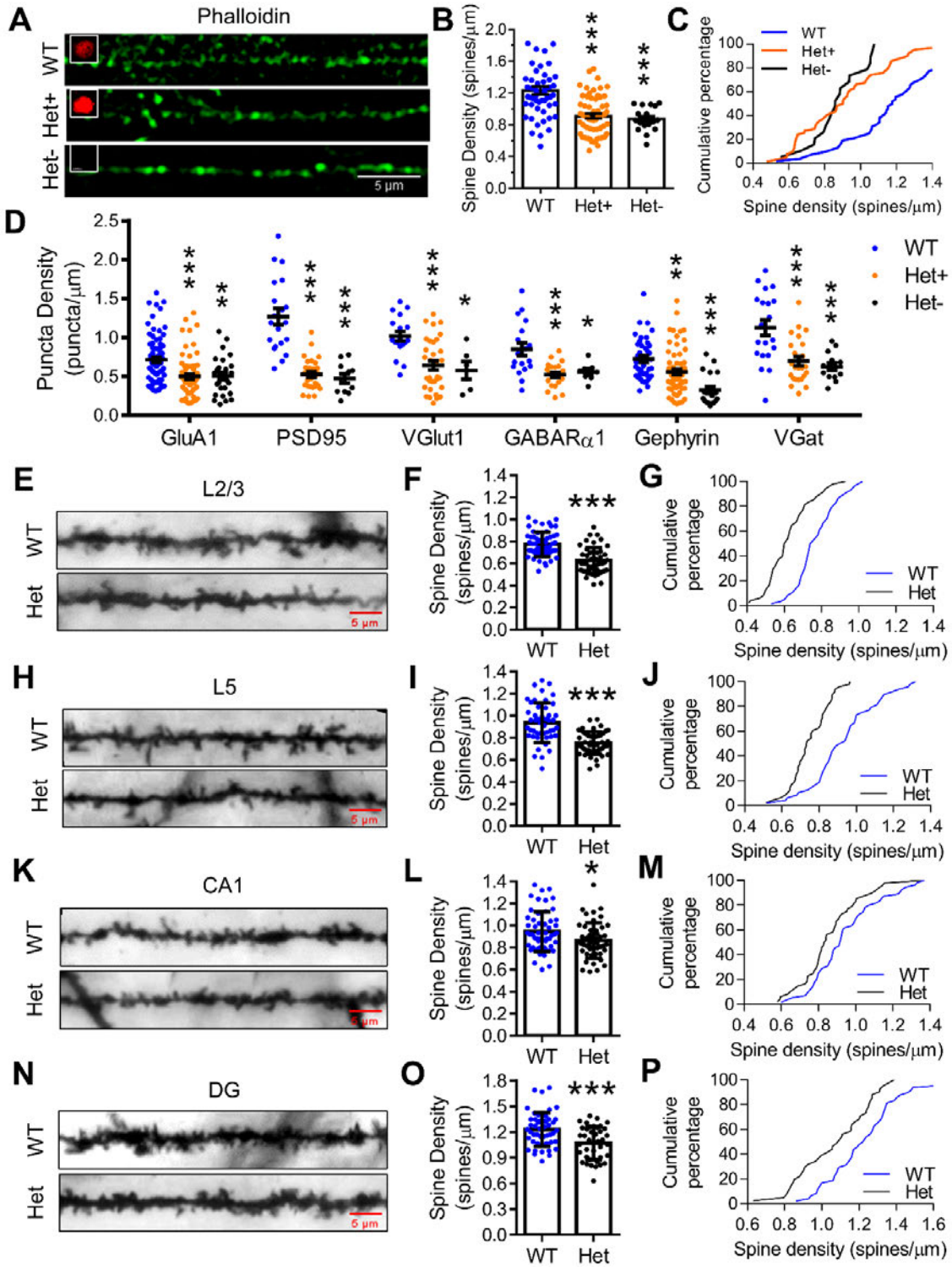

A
Phalloidin
WT
Het+
Het-
5 µm
B
Spine Density (spines/µm)
WT
Het+
Het-
C
Cumulative percentage
Spine density (spines/µm)
D
Puncta Density (puncta/µm)
GluA1
PSD95
VGlut1
GABARα1
Gephyrin
VGat
E
L2/3
F
G
H
L5
I
J
K
CA1
L
M
N
DG
O
P
Het

Figure 4.9 Aberrant dendritic spines and synapses in NEXMIF Het mice

(A) Representative images of DIV 12 primary cortical neurons from WT or *NEXMIF*$^{+/-}$ mice immunostained for NEXMIF and labelled for actin with Phalloidin. Inset is immunostaining of NEXMIF, showing a mosaic mixture of NEXMIF^{+} and NEXMIF^{-} neurons. Scale bar = 5 µm. **(B-C)** Spine density was decreased in both NEXMIF^{+} and NEXMIF^{-} neurons. ($F_{(2,130)}$ = 20.29, p < 0.0001, n = 19-60 dendrites/ group). **(D)** Quantification of puncta density of synaptic markers. DIV 12 cortical cultures of both NEXMIF^{+} and NEXMIF^{-} neurons were immunostained with antibodies against GluA1 ($F_{(2,171)}$ = 12.94, p < 0.0001), PSD95 ($F_{(2,56)}$ = 37.19, p < 0.0001), VGlut1 ($F_{(2,54)}$ = 9.754, p = 0.0002), GABARα1 ($F_{(2,45)}$ = 9.887, p = 0.0003), gephyrin ($F_{(2,123)}$ = 19.17, p < 0.0001), and VGat ($F_{(2,55)}$ = 12.12, p < 0.0001), respectively. n = 7-80 cells/ group. **(E-P)** Spines were analyzed from WT or *NEXMIF*$^{+/-}$ brain slices following Golgi staining. Spine density was decreased in L2/3 neurons of the somatosensory cortex (E-G) ($t_{(106)}$ = 6.727, p < 0.0001), L5 neurons of the somatosensory cortex (H-J) ($t_{(94)}$ = 6.114, p < 0.0001), CA1 neurons of the hippocampus (K-M) ($t_{(101)}$ = 2.422, p = 0.0172), and the dentate gyrus neurons (N-P) ($t_{(87)}$ = 3.866, p = 0.0002). Scale bar = 5 µm. n = 48-60 dendrites/ group. Het+, NEXMIF^{+}/NEXMIF-expressing; Het-, NEXMIF^{-}/NEXMIF lacking. *p<0.05, **p<0.01 ***p<0.001.

CHAPTER FIVE: DISCUSSION, CONCLUSIONS, AND FUTURE PERSPECTIVES

5.1 Summary of findings

NEXMIF is a novel X-linked ASD gene with loss of its protein product leading to autistic behavior and cognitive impairments in humans. This dissertation provides an investigation of the cellular and molecular dysregulation and ASD-like behavioral impairments that result from loss, and haploinsufficiency of, NEXMIF.

In Chapter 3, I report findings from the transgenic *NEXMIF*$^{-/y}$ knockout mouse. *NEXMIF*$^{-/y}$ mice showed autism-like behaviors including deficits in social behaviors, increased repetitive self-grooming, impaired communication, and deficient learning and memory. The *NEXMIF*$^{-/y}$ phenotype faithfully replicated the symptoms reported in humans with loss-of-NEXMIF (Alarcon-Martinez et al., 2019; Charzewska et al., 2015; Kuroda et al., 2015; Lambert et al., 2018; Lorenzo et al., 2018; Panda et al., 2020; Stamberger et al., 2020). Cultured hippocampal neurons from *NEXMIF*$^{-/y}$ brains, showed a significant decrease in neurite outgrowth, synaptic protein expression, spine and synapse density, and synaptic plasticity. Additionally, RNAseq after knockdown of NEXMIF demonstrated altered gene expression of many genes including those enriched at the synapse and involved in neuronal development and function. Among the top downregulated genes, neurogranin (Nrgn) and SynDig1 were identified as candidates for investigation due to their synaptic enrichment and roles in synaptogenesis and synaptic plasticity (Díaz, 2012; Díez-Guerra, 2010; Garrido-García et al., 2019; Kalashnikova et al., 2010; Lovero et al., 2013; Ryoo et al., 2015; Zhabotinsky et al., 2006; Zhong and Gerges, 2010). I have shown that overexpression of Nrgn or

SynDig1 *in vitro* was sufficient to rescue the decreased density of spines and synaptic AMPAR observed from loss of NEXMIF. These studies confirm the value of the mouse model for NEXMIF ASD and provide important original knowledge regarding the cellular defects that arise from NEXMIF-dependent ASD. Findings from the rescue experiments will help with the development of therapeutic strategies for clinical intervention of the disorders.

In addition, I investigated alterations in behavior due to *NEXMIF* haploinsufficiency and the underlying molecular alterations in transgenic *NEXMIF*$^{+/-}$ female mice. In Chapter 4, I discovered that *NEXMIF*$^{+/-}$ mice display reduced social interactions, repetitive behaviors, and impaired memory. Interestingly, *NEXMIF*$^{+/-}$ female mice show more moderate changes in communication than their male *NEXMIF*$^{-/y}$ counterparts, which is consistent with reports of milder communication phenotypes in human females affected with *NEXMIF* variants (Athanasakis et al., 2014; Farach and Northrup, 2016; de Lange et al., 2016; Moysés-Oliveira et al., 2015; Samanta and Willis, 2020; Stamberger et al., 2020; Webster et al., 2017; Wu et al., 2020). Furthermore, I have shown for the first time the cellular mosaicism of NEXMIF expression in the brains of *NEXMIF*$^{+/-}$ mice resulting in mixed coexistence of both NEXMIF^{+} and NEXMIF^{-} neurons due to random XCI. Surprisingly, both NEXMIF^{+} and NEXMIF^{-} neurons show impairments in neurite outgrowth and spine density. Additionally, both groups of neurons from *NEXMIF*$^{+/-}$ mice demonstrate reductions in synaptic proteins including the GluA1 subunit of AMPARs and PSD95. These findings

indicate that the female transgenic mouse of NEXMIF haploinsufficiency recapitulates autistic features of the human patients and that loss of NEXMIF impaired neuronal development both in *cis* and *trans* to neighboring cells. The unique neural network of mutually innervated NEXMIF^{+} and NEXMIF^{-} neurons and the potential to restore NEXMIF expression from the endogenous wild type allele make the *NEXMIF*$^{+/-}$ mouse a particularly interesting model for future study of *NEXMIF* and ASD.

5.2 The role of NEXMIF in excitatory/inhibitory balance and epilepsy

Reports indicate humans with ASD due to loss of NEXMIF show epilepsy as a comorbid phenotype (Cantagrel et al., 2004, 2009; Charzewska et al., 2015; Farach and Northrup, 2016; Lambert et al., 2018; de Lange et al., 2016; Lorenzo et al., 2018; Van Maldergem et al., 2013; Webster et al., 2017). The seizures vary in type but include generalized, tonic-clonic, absence, and myoclonic seizures. The onset of seizures also varied between patients but began as early as < 1 year old and as late as the teens. Some patients don't demonstrate seizures or have only had a single episode, while others could have up to hundreds of episodes per day. Our *NEXMIF*$^{-/y}$ and *NEXMIF*$^{+/-}$ mice also demonstrate severe seizures, typically in response to animal handling. This complex phenotype will require further studies for more detailed analysis but suggests dysregulated neuronal networks.

Several possible mechanisms could explain how loss of NEXMIF leads to epilepsy. First, loss of NEXMIF may lead to an abnormal ratio of excitatory to

inhibitory (E/I) neuronal activity. Disrupted E/I balance has been hypothesized as a mechanism underlying ASD pathology (Nelson and Valakh, 2015; Rubenstein and Merzenich, 2003; Sohal and Rubenstein, 2019). Such an imbalance can result from developmental changes such as synaptic transmission and plasticity, intrinsic neuronal excitability, and ratios of excitatory/inhibitory synaptic inputs or neuronal subtypes (Culotta and Penzes, 2020; Gao and Penzes, 2015; Lee et al., 2017). In my study, I observed decreases in both glutamatergic and GABAergic synapses from loss of NEXMIF. Interestingly, the RNAseq data shows significant downregulation of several GABA receptor subunits. Further work investigating the E/I ratio more directly, including studies of glutamatergic to GABAergic neuron ratios and electrophysiological recordings of excitatory and inhibitory synaptic currents, would help clarify whether loss of NEXMIF results in E/I imbalance.

Second, loss of NEXMIF may lead to hyperexcitability due to altered expression and/or distribution of ion channels. Such channelopathies have been implicated in the pathogenesis of ASD and over 25% of genes linked to epilepsy encode ion channels (Oyrer et al., 2018; Schmunk and Gargus, 2013; Zhang et al., 2019c). Our RNAseq dataset revealed downregulation of several potassium channels, as well as some chloride and calcium channels, after loss of NEXMIF. Loss of potassium channels, in particular, has been shown to increase neuronal excitability and enhance susceptibility of seizures (D'Adamo et al., 2013; Guglielmi et al., 2015; Köhling and Wolfart, 2016; Villa and Combi, 2016). Further studies including biochemical confirmation of reduced potassium channel protein

expression and electrophysiological recordings of resting membrane potential and action potential firing, would help to determine whether potassium channels play a role in hyperexcitability and epilepsy from loss of NEXMIF.

Third, in the case of NEXMIF haploinsufficiency, mosaic expression of NEXMIF may lead to epilepsy as a result of impaired interactions between $NEXMIF^{+}$ and $NEXMIF^{-}$ neurons. Indeed, the presence of two cell populations with different genotypes has been shown to lead to epilepsy, depending on the extent of mosaicism. For example, in mosaic parents of children with Dravet syndrome, parents with <45% mosaic expression of a *SCN1A* mutation were unaffected, while those with >45% expression of the mutation were affected with epilepsy correlated to the percent of mosaicism (Depienne 2010). Additionally, there is evidence that X-linked cellular mosaicism is an underlying cause of seizures. Mutation of the X-linked gene *PCDH19* causes epilepsy and intellectual disability in heterozygous females, but not hemizygous males, due to mismatched interactions between the mosaically expressed $PCDH19^{+}$ and $PCDH19^{-}$ neurons (Depienne 2009, Hoshina 2021, Hayashi 2017, Dibbens 2008). Further, mutations in the X-linked gene *CDKL5* cause seizures, autistic features, and neurodevelopmental impairment primarily in female heterozygotes and seizure-like events have been observed only in female heterozygotes of a transgenic *CDKL5* mouse model, not in hemizygous knockout males or homozygous knockout females (Terzic 2021). It is possible a similar cellular interference mechanism is the underlying cause for NEXMIF epilepsy as females heterozygous for NEXMIF seem to have a more severe

seizure phenotype than hemizygous males. Further investigations of a mosaic neural circuit, including electrophysiological recordings of basal synaptic transmission and synaptic plasticity from all four possible pairings of NEXMIF+ and NEXMIF- neurons, including mutual innervation between + to +, - to -, + to -, and - to + neurons, would help to elucidate the extent to which mosaicism contributes to synaptic dysfunction, neuronal hyperactivity, and the epileptic phenotype after loss of NEXMIF.

5.3 Diversity in NEXMIF ASD phenotypes between males and females

Pathogenic variants in *NEXMIF* have now been reported in dozens of patients who demonstrate developmental delay, autistic features, cognitive impairments, and epilepsy (Alarcon-Martinez et al., 2019; Athanasakis et al., 2014; Borlot et al., 2017; Cantagrel et al., 2004; Charzewska et al., 2015; Farach and Northrup, 2016; Kuroda et al., 2015; Lambert et al., 2018; de Lange et al., 2016; Lorenzo et al., 2018; Van Maldergem et al., 2013; Moysés-Oliveira et al., 2015; Panda et al., 2020; Samanta and Willis, 2020; Stamberger et al., 2020; Webster et al., 2017; Wu et al., 2020). Interestingly, males tend to demonstrate more severe language and cognitive impairments while females more frequently have epilepsy (Panda et al., 2020; Stamberger et al., 2020). The behavioral studies reported in this dissertation reveal the transgenic *NEXMIF* mouse model recapitulates the phenotypes observed in humans. Both hemizygous *NEXMIF*$^{-/y}$ and heterozygous *NEXMIF*$^{+/-}$ mice showed impairments in social behavior, repetitive self-grooming,

and deficit spatial memory. However, *NEXMIF*$^{-/y}$ mice had more dramatic impairments in communication than *NEXMIF*$^{+/-}$ mice, in line with the increased severity of language impairment in males than females. Both hemizygous *NEXMIF*$^{-/y}$ and heterozygous *NEXMIF*$^{+/-}$ mice have seizures although the frequency and severity of this phenotype remain to be investigated. It is possible that the differences in behavior are due to complete loss of NEXMIF versus mosaic loss of NEXMIF. However, XCI patterning does not seem to be a complete explanation for this difference as most female patients have random XCI and no correlation was found between XCI skewing and disease phenotype. This is in line with my data from the brains of *NEXMIF*$^{+/-}$ mice, which also show no sign of significant skewing in NEXMIF expression.

Given that males are generally 3-5 times more likely to be diagnosed with ASD than females, it is interesting to note that, to date, 72% of reported NEXMIF ASD patients are female (Fernell and Gillberg, 2010; Fombonne, 2009; Loomes et al., 2017; Nicholas et al., 2009). There are several hypotheses that could explain a skewed sex distribution for an X-linked disease. Firstly, mutations in *NEXMIF* could increase the risk of prenatal lethality in males. However, I observed that about 22% of pups born from our transgenic line were hemizygous *NEXMIF*$^{-/y}$ mice, similar to the expected frequency of about 25% given the wild-type male to heterozygous *NEXMIF*$^{+/-}$ female mating scheme. Second, a higher frequency of affected females could also be due to the statistically higher chance female have of a *de novo* mutation in *NEXMIF* as they have two copies compared to the

one copy in males. Or, thirdly, it is possible pathogenic *de novo* mutations in *NEXMIF* are more likely to occur in male germ cells, resulting in affected daughters but not sons (Thomas, 1996). This explanation has been applied to Rett syndrome (Girard et al., 2001; Zhu et al., 2010). Indeed, *NEXMIF* has several parallels with *MeCP2* as both are X-linked genes whose protein products localize to the nucleus and whose variants affect mostly females. However, it is difficult to make a conclusion about the inheritance of *NEXMIF* variants from our mouse model as the animals consistently inherited the mutant transgene from their mothers rather than *de novo*. Future work could be done to explore the likelihood of pathogenic *NEXMIF* mutations occurring at various developmental time points.

As the majority of affected individuals reported are female, it is reasonable to explore potential therapeutic approaches that are unique to haploinsufficiency. For example, specific reactivation of *NEXMIF* from the Xi chromosome in heterozygous *NEXMIF*$^{+/-}$ females would allow expression of wild-type NEXMIF in all unsilenced cells. This idea has recently shown promising results for reactivation of *MeCP2* in Rett Syndrome (Carrette et al., 2018; Przanowski et al., 2018). Investigations to confirm the feasibility of *NEXMIF* reactivation from the Xi chromosome in female heterozygous mice will help establish strategies to be used in future studies for treatment of the affected female individuals.

5.4 NEXMIF nuclear localization and its role in gene regulation

Much remains to be established about the direct function of NEXMIF and the mechanistic steps linking it to the structural and synaptic phenotypes I observe. NEXMIF has no significant homology with other known proteins (Cantagrel et al., 2004). Analysis of the NEXMIF protein sequence has only revealed a DUF4683 domain (Domain of Unknown Function 4683) (Lu et al., 2020) and two predicted nuclear localization (NLS) sequences (Kosugi et al., 2009). The presence of NLSs is consistent with NEXMIF's nuclear localization. While the function of NEXMIF within the nucleus remains unknown, it is possible NEXMIF acts as a component of a gene expression regulatory complex or a transcription factor. Our RNAseq analysis revealed significantly altered gene expression of a large number of genes, particularly those involved in neuronal and synaptic development, after loss of NEXMIF. Additionally, Support Vector Machine classification software tools (SVM-Prot and DRNApred) have predicted NEXMIF to be a DNA- and zinc-binding protein (Cai et al., 2003; Yan and Kurgan, 2017). Future work to confirm the DNA-binding capability of NEXMIF, including chromatin immunoprecipitation sequencing (ChIPseq), would help to clarify NEXMIF's role in the regulation of the genes identified in the RNAseq.

Although no significant homology with other known proteins has been identified for NEXMIF, recent studies of Xia-Gibbs syndrome revealed some small segments of similarity with the proteins REV3L and AHDC1 (Jiang et al., 2018; Khayat et al., 2021; Lange et al., 2016; Murdock et al., 2019). REV3L is the catalytic subunit of DNA polymerase zeta, specializing in translesion DNA

synthesis (Gan et al., 2008; Lange et al., 2016). Interestingly, the conversed region between REV3L and NEXMIF is within the DUF4683 of each protein, suggesting the function of this unknown domain is something shared between the two proteins, perhaps as a docking site for the recruitment of other DNA polymerase machinery. AHDC1 is a score 1 gene on the SFARI ASD gene database whose *de novo* truncating variants are linked with Xia-Gibbs syndrome, a neurodevelopmental disorder characterized by developmental delay, intellectual disability, seizures, hypotonia, and sleep apnea (Jiang et al., 2018; Khayat et al., 2021; Xia et al., 2014). AHDC1 contains AT-hook DNA binding motifs and is nuclear localized, though little is known about its function (Khayat et al., 2021). It shares small regions of similarity with both NEXMIF and REV3L and truncating mutations including these regions demonstrated unusual aggregation in the nucleolus, suggesting a role for these regions in proper localization within the nucleus (Khayat et al., 2021).

Further, *in silico* analysis has revealed potential binding partners for NEXMIF. A search on the BioGRID database of protein interactions indicated predicted interactions with the proteins RNF123, TRF1, and TRF2. RNF123 is a RING finger E3 ubiquitin ligase which has been shown to target nuclear envelope proteins, such as lamin B1 and LAP2α, for degradation (Chaturvedi et al., 2012; Khanna et al., 2018). As the BioGRID database predicts ubiquitination sites on 7 lysines within NEXMIF, it is possible RNF123 interacts with NEXMIF as the responsible E3 ligase for NEXMIF ubiquitination and its subsequent degradation.

TRF1 and TRF2 are part of the shelterin complex which binds duplex telomeric DNA to regulate telomere length and protect the ends of chromosomes (Arndt and MacKenzie, 2016; Giannone et al., 2010; De Lange, 2005; Lee et al., 2018). It is possible that the DNA-binding of NEXMIF is also at telomeres where it could interact with TRF1 and TRF2. This might indicate a role for NEXMIF in telomere maintenance and aging, which could be examined in older *NEXMIF*$^{-/y}$ mice. In addition to the previously mentioned ChIP-seq experiments to identify segments of NEXMIF-bound DNA, immunoprecipitation of NEXMIF followed by mass spectrometry would confirm RNF123, TRF1, and TRF2 as binding partners and possibly reveal other interacting proteins. It would be useful to design experiments to disrupt these protein-protein interactions to determine the role of the protein complexes and further our understanding of NEXMIF's function.

5.5 The role of NEXMIF in synapse formation and function

Altered synaptic structure and function has emerged as a common underlying pathology in ASD (Bagni and Zukin, 2019; Bourgeron, 2009, 2015; Carroll et al., 2021; Gilbert and Man, 2017; Guang et al., 2018; Phillips and Pozzo-Miller, 2014; Zoghbi and Bear, 2012). Indeed, I observed decreased synaptic density and expression of synaptic related proteins in *NEXMIF*$^{-/y}$ and *NEXMIF*$^{+/-}$ neurons. Additionally, Ingenuity Pathway Analysis of the dysregulated genes identified from NEXMIF knockdown RNAseq showed enrichment of genes involved in key synaptic processes, such as glutamatergic signaling, LTP, and LTD. My *in vitro*

studies showed *NEXMIF*$^{-/y}$ neurons failed to enhance surface AMPAR expression in response to either chemical LTP or HSP treatments. It is possible the loss of NEXMIF results in dysregulation of AMPAR trafficking or alters AMPAR stability at the synaptic surface, thus resulting in decreased surface expression. To assess basal AMPAR trafficking in *NEXMIF*$^{-/y}$ neurons, internalization and insertion assays could be performed. Additionally, we have shown that AMPARs are subject to acetylation which stabilizes their surface expression (Wang et al., 2017, Appendix). The level of AMPAR acetylation, versus its competing modification ubiquitination, could be measured in tissue from *NEXMIF*$^{-/y}$ mice. However, no significant change was observed in the gene expression of the related enzymes Nedd4, Sirt2, and p300 from analysis of the RNAseq dataset.

From the top downregulated genes enriched at the synapse in the RNAseq dataset, I chose to investigate the role of Nrgn and SynDig1 in synapse development after loss of NEXMIF. Nrgn and SynDig1 have been shown to play roles in synapse formation and function (Garrido-García et al., 2019; Kalashnikova et al., 2010; Zhabotinsky et al., 2006). I was able to show that overexpression of Nrgn or SynDig1 could rescue the density of AMPAR puncta and spines after loss of NEXMIF expression. This suggests decreased Nrgn and/or SynDig1 expression play a role in mediating the synaptic deficits observed after loss of NEXMIF. To further explore the downstream roles of Nrgn and SynDig1 in exerting NEXMIF's effects on the synapse, studies to measure synaptic plasticity after reintroduction of Nrgn and SynDig1 in *NEXMIF*$^{-/y}$ neurons would be of interest.

Furthermore, reintroduction at various time points in development could help to determine whether a specific stage is most sensitive to reversal of NEXMIF-dependent synaptic deficits, providing valuable insight into possible therapeutic interventions for future research.

In addition to Nrgn and SynDig1, there may be other potential targets participating downstream of NEXMIF, particularly those that might act as extracellular cues. My findings from *in vitro* study of *NEXMIF*$^{+/-}$ neurons revealed impaired neurite outgrowth, reduced density, and decreased puncta density of key synaptic proteins in both NEXMIF^{+} and NEXMIF^{-} neurons. This suggests that loss of NEXMIF in NEXMIF^{-} neurons results not only in direct changes to those cells, but also in impairments to NEXMIF^{+} neurons, an effect that might be due to altered extracellular cues from the NEXMIF^{-} neurons. Indeed, impairments in dendritic arborization appeared more severe for NEXMIF^{+} neurons at DIV 14 than at DIV 8, suggesting expression of key proteins during this developmental time period, such as those involved in synaptogenesis, may play a role in this phenotype. Our previous work using shRNA knockdown of NEXMIF proposed the mechanism for impaired dendritic outgrowth to be due to increased surface N-cadherin sequestering δ-catenin, resulting in increased RhoA activation and decreased actin dynamics at the growth cone (Gilbert and Man, 2016). Additionally, N-cadherin has been shown to stabilize filopodial F-actin, thus promoting maturation of dendritic filopodia to mushroom shaped spines (Chazeau et al., 2015). Thus, increased surface N-cadherin in NEXMIF^{-} neurons could be the source of aberrant

interneuronal communication with NEXMIF^{+} neurons. Indeed, the proposed underlying mechanism to impairments in *PCDH19* heterozygotes is that mosaic PCDH19 expression results in mismatched PCDH19^{+} and PCDH19^{-} synapses which prevent N-cadherin homophilic adhesion (Hoshina et al., 2021). To further investigate this hypothesis in the context of NEXMIF, the pre- and post-synaptic expression of N-cadherin, activity of RhoA, and actin dynamics in filopodia could be measured in *NEXMIF*$^{-/y}$ and NEXMIF^{-} neurons from *NEXMIF*$^{+/-}$ mice. Additionally, the RNAseq dataset showed that loss of NEXMIF resulted in downregulation of several protocadherins, including *PCDH19*. It would be interesting to explore whether reduced expression of protocadherins, due to loss of NEXMIF, could contribute to the observed impairments in synapse formation and function, particularly in *NEXMIF*$^{+/-}$ mice whose brains may not be able to properly mediate signals between NEXMIF^{+} protocadherin-expressing and NEXMIF^{-} protocadherin-deficient neurons.

5.6 Conclusions and future perspectives

In this dissertation, I examined behavioral and molecular phenotypes due to NEXMIF deficiency in *NEXMIF*$^{-/y}$ and *NEXMIF*$^{+/-}$ mice. I found that the *NEXMIF*$^{-/y}$ and *NEXMIF*$^{+/-}$ mice faithfully model the behavioral phenotypes observed in humans and that *NEXMIF*$^{-/y}$ and *NEXMIF*$^{+/-}$ neurons demonstrate impairments in neuronal and synaptic development. The work is the first to examine the molecular details of haploinsufficient NEXMIF expression, providing new insights into the

role of NEXMIF in proper development and maturation of the brain. Future studies will be necessary to dissect the detailed molecular mechanisms of NEXMIF function in different developmental processes including neuronal morphogenesis, migration, synaptogenesis, and network activity. *In vitro* studies utilizing NEXMIF mutants and truncations could help establish the NEXMIF nuclear localization signal, sites of post-translational modification, and functional domains, all of which would improve our understanding of NEXMIF's function. The *NEXMIF*$^{-/y}$ and *NEXMIF*$^{+/-}$ mouse models will also be useful tools for such mechanistic studies, as well as for future attempts to develop therapeutics which rescue the morphological and behavioral phenotypes. There are some comorbidities in humans with NEXMIF-dependent ASD that remain to be characterized in this model. Future work to assess the extent of attention deficit/hyperactivity and gastrointestinal issues would help to further establish this model. In particular, further studies are needed to compare the frequency, types, and severity of seizures in the *NEXMIF*$^{-/y}$ and *NEXMIF*$^{+/-}$ mice.

APPENDIX: ACETYLATION OF AMPA RECEPTORS REGULATES RECEPTOR TRAFFICKING AND RESCUES MEMORY DEFICITS IN ALZHEIMER'S DISEASE

A.1 Abstract

In Alzheimer's disease (AD), decreases in the amount and synaptic localization of AMPA receptors (AMPARs) result in weakened synaptic activity and dysfunction in synaptic plasticity, leading to impairments in cognitive functions. We have previously found that AMPARs are subject to lysine acetylation, resulting in higher AMPAR stability and protein accumulation. Here we report that AMPAR acetylation was significantly reduced in AD and neurons with Aβ incubation. We identified p300 as the acetyltransferase responsible for AMPAR acetylation, and found that enhancing GluA1 acetylation ameliorated Aβ-induced reductions in total and cell-surface AMPARs. Importantly, expression of acetylation mimetic GluA1 (GluA1-4KQ) in APP/PS1 mice rescued impairments in synaptic plasticity and memory. These findings indicate that Aβ-induced reduction in AMPAR acetylation and stability contributes to synaptopathy and memory deficiency in AD, suggesting that AMPAR acetylation may be an effective molecular target for AD therapeutics.

A.2 Introduction

Alzheimer's disease (AD) is the most common form of dementia characterized by impairments in learning and memory. A key hallmark of AD is the accumulation of amyloid-β (Aβ), which has been shown to cause loss of dendritic spines and dysregulation in synaptic functions, such as basal transmission and synaptic plasticity (Forner et al., 2019; Palop and Mucke, 2010; Rajmohan and Reddy, 2017; Selkoe, 2002; Sheng et al., 2012; Yu and Lu, 2012). Evidence suggests

these impairments in synaptic function are an early pathology which ultimately lead to the cognitive failures observed in AD (Baglietto-Vargas et al., 2018; Chen et al., 2000; Li et al., 2011; Ma and Klann, 2012; Oddo et al., 2003; Selkoe and Hardy, 2016).

AMPA receptors (AMPARs) mediate most of the excitatory synaptic transmission that underlies higher brain functions, including learning and memory. A change in the synaptic expression of AMPARs is the key mechanism underlying synaptic plasticity, the molecular basis for learning and memory. An increase in surface AMPARs through exocytosis leads to the expression of long-term potentiation (LTP), while internalization of AMPARs causes long-term depression (LTD) (Chidambaram et al., 2019; Collingridge et al., 2004; Derkach et al., 2007; Ju and Zhou, 2018; Kopec et al., 2006; Lledo et al., 1998; Lüscher et al., 1999; Makino and Malinow, 2009; Malinow and Malenka, 2002; Shepherd and Huganir, 2007; Song and Huganir, 2002). Consistent with impairments in synaptic function, a reduction in AMPARs has been observed in the brains of both human AD patients and mouse models of AD (Armstrong et al., 1994; Cantanelli et al., 2014; Carter et al., 2004; Chang et al., 2006; D'Amelio et al., 2011; Dewar et al., 1991; Du et al., 2020; Gao et al., 2016; Gong et al., 2009; Jacob et al., 2007; Monteiro-Fernandes et al., 2020; Samra and Ramtahal, 2012; Thorns et al., 1997; Wakabayashi et al., 1999; Yasuda et al., 1995). In line with this, incubation of neurons with Aβ results in down-regulation in AMPAR amounts (Guntupalli et al., 2016; Miyamoto et al.,

2016; Parameshwaran et al., 2008; Thomas et al., 2017; Wisniewski et al., 2011; Yu and Lu, 2012; Zhang et al., 2018).

The abundance of AMPARs in the post-synaptic domain is regulated by dynamic receptor trafficking. Enhanced receptor internalization and an ultimate reduction in AMPAR synaptic accumulation has been shown to be an early pathological feature of AD (Almeida et al., 2005; Baglietto-Vargas et al., 2018; Hsieh et al., 2006; Li et al., 2019b; Zhao et al., 2010). Overexpression of amyloid precursor protein (APP) or application of soluble oligomeric Aβ results in a reduction in surface expression of AMPARs (Alfonso et al., 2014; Gu et al., 2009; Miller et al., 2014; Roselli et al., 2005; Tanaka et al., 2019; Zhang et al., 2011) likely due to endocytosis of AMPARs from the synaptic surface (Hsieh et al., 2006; Miñano-Molina et al., 2011; Wang et al., 2011a; Zhang et al., 2017). The reduced stability of AMPARs may be a major contributing factor to the pathology of AD.

In AD, the reduction in AMPAR seems to result from reduced receptor stability. Indeed, treatment with Aβ increased AMPAR mobility(Opazo et al., 2018) and, in the presence of cycloheximide, shortened AMPAR half-life (Zhang et al., 2018). Studies have demonstrated that ubiquitination is a primary regulatory mechanism contributing to AMPAR stability (Guntupalli et al., 2017; Rodrigues et al., 2016; Zhang et al., 2018). AMPARs are subject to ubiquitination *via* the E3 ligase Nedd4 (Hou et al., 2011; Lin et al., 2011; Rodrigues et al., 2016; Schwarz et al., 2010) and deubiquitination by the deubiquitinase USP46 (Huo et al., 2015). Plasma membrane-inserted AMPARs are preferentially targeted for

ubiquitination(Lin et al., 2011), leading to receptor internalization and subsequent proteasomal degradation (Goo et al., 2015; Hou et al., 2011; Jarzylo and Man, 2012; Zhang et al., 2009).

We have recently demonstrated that AMPARs are also subject to lysine acetylation, a regulation that competes with ubiquitination because both processes target lysine residues. Acetylation confers AMPARs with higher levels of stability due to a suppression in AMPAR internalization and degradation (Wang et al., 2017). We have shown that inhibition of the AMPAR deacetylase, SIRT2, causes enhanced AMPAR acetylation and increased AMPAR accumulation at synapses (Wang et al., 2017). Because AMPAR reduction is a crucial first step leading to the cognitive deficits in AD, restoration of AMPARs at the synapse is predicted to improve synaptic strength and cognitive function in AD.

In this study, we find that AMPAR acetylation is altered under AD conditions. In Aβ-incubated neurons, and in brains of transgenic AD mice and AD patients, AMPARs show marked reduction in acetylation. We show that upregulation of AMPAR acetylation leads to a suppression in AMPAR internalization and an increase in total AMPAR amount. We identify p300 as the acetyltransferase responsible for AMPAR acetylation and find that activation of p300, or inhibition of AMPAR deacetylase SIRT2, results in an increase in AMPAR acetylation and blocks the Aβ-induced reduction in surface AMPAR expression. Importantly, we found that hippocampal expression of an acetylation mimetic of GluA1 was able to restore synaptic plasticity and rescue cognitive deficits in the

Tg(APPswe,PSEN1dE9)85Dbo (APP/PS1) mouse model. Together, these findings provide insights into the importance of AMPAR acetylation in the pathogenesis of cognitive dysfunction in AD.

A.3 Results

A.3.1 Aβ Induces a Reduction in AMPAR Acetylation

Our studies and the work of others have shown that AMPAR levels are reduced in AD (Armstrong et al., 1994; Carter et al., 2004; Dewar et al., 1991; Gong et al., 2009; Thorns et al., 1997; Yasuda et al., 1995; Zhang et al., 2018). In AD brains and Aβ-treated neurons, ubiquitination of AMPARs is up-regulated (Guntupalli et al., 2017; Rodrigues et al., 2016; Zhang et al., 2018), and studies have demonstrated proteasomal degradation of ubiquitinated AMPARs (Huo et al., 2015; Jarzylo and Man, 2012; Lin et al., 2011).Recently, we found that AMPARs are subject to another form of protein modification, i.e., acetylation, a modification that opposes receptor ubiquitination and functions to stabilize AMPARs (Wang et al., 2017). We therefore wondered whether this modification of AMPARs is altered in AD conditions, contributing to the aberrance in receptor expression. To this end, we first used immunostaining to confirm the effect of Aβ oligomers on the abundance of AMPAR expression. DIV 15 cultured rat hippocampal neurons were treated with Aβ (1 μM) for 24 h and labeled with specific antibodies against AMPAR subunit GluA1. Immunostaining against the GluA1 N-terminus under non-permeant conditions showed a reduction in the intensity of surface GluA1 puncta,

and antibodies against the GluA1 C-terminus under permeant conditions showed a similar reduction in total levels of GluA1 (**Fig. A.1A-A.1B**). To examine specifically the expression level of AMPARs at the synaptic sites, we purified synaptosomes from cultured cortical neurons. We found that the Aβ treatment resulted in a 62% reduction in the amount of GluA1 in the synaptosome, comparable to an overall 65% reduction from total cell lysate (**Fig. A.1C-A.1D**). In addition, we found that Aβ treatment did not affect the levels of PSD95 (**Fig. A.1E**). These findings indicate that Aβ incubation leads to a down-regulation of synaptic AMPARs in neurons.

We wondered whether AMPAR acetylation plays a role in Aβ-induced AMPAR down-regulation. Using DIV 15 primary cortical neurons treated with Aβ (1 μM) for 24 h, we isolated AMPAR GluA1 subunits *via* immunoprecipitation, and probed western blots with antibodies specific for lysine acetylation (Inuzuka et al., 2012; Wang et al., 2017). We found that, compared to the control, incubation with Aβ resulted in a significant reduction in acetylation signal in precipitated GluA1 (**Fig. A.1F-A.1G**). There was no significant difference in PSD95 levels (**Fig. A.1H**). To further determine the state of AMPAR acetylation in AD, we examined lysates from postmortem AD patient brains. GluA1 was precipitated from the prefrontal cortex lysates from patients and healthy controls. In line with our findings from Aβ-treated neurons, the AD patient brain homogenates showed a consistent decrease in the extent of GluA1 acetylation compared to the non-AD controls (**Fig. A.1I-A.1J**). We also observed a dramatic increase in GluA1 ubiquitination (**Fig. A.1K**).

Together these results demonstrate that AMPAR acetylation is decreased *in vitro* in Aβ-treated neurons and *ex vivo* in human AD brains.

A.3.2 The Acetyltransferase p300 Causes GluA1 Acetylation†

Our previous work has identified SIRT2 as the deacetylase responsible for the deacetylation of GluA1 (Wang et al., 2017), however, the enzyme(s) responsible for AMPAR acetylation remains unknown. We therefore sought to identify the acetyltransferase that catalyzes the conjugation of the acetyl group to the lysine residues at GluA1 C-terminus (GluA1ct). To this end, we purified GST-tagged GluA1ct and incubated it with several acetyltransferases including PCAF, p300, CBP, and GCN5, individually (**Fig. A.2A**). Interestingly, when the GluA1ct was probed for lysine acetylation, we observed a marked increase in GluA1 acetylation in assays that contained p300 and a trend of increase with the p300 homolog CBP (**Fig. A.2B**). However, this was not observed in assays containing PCAF or GCN5. This result indicates a specific role for the p300 family of acetyltransferases on AMPAR acetylation. p300 is well known for its role in histone acetylation for the regulation of gene expression, but it is also localized in the cytoplasm (Dancy and Cole, 2015; Kwok et al., 2006; Rotte et al., 2013; Shi et al., 2009). It is therefore possible for the endogenous p300 to acetylate AMPARs in neurons. To confirm the effect of p300 on AMPAR acetylation *in vivo*, we incubated primary cortical neurons with either the p300 inhibitor C646 (20 μM) (Bowers et al., 2010) or the p300 acetyltransferase activator CTPB (20 μM) (Balasubramanyam et al., 2003), for 24 h, and immunoprecipitated GluA1 for acetylation assays. Indeed, inhibition

of p300 by C646 caused a decrease in GluA1 acetylation whereas activation of p300 by CTPB increased acetylation of GluA1 (**Fig. A.2C**). Because an acetylation event often antagonizes protein ubiquitination due to competition for the same lysine residues, we examined changes in GluA1 ubiquitination. As expected, inhibition of p300 led to an increase while activation of p300 by CTPB caused a decrease in the level of GluA1 ubiquitination (**Fig A.2C).**

A.3.3 p300-Mediated Acetylation Leads to AMPAR Stabilization

Acetylation has been shown to cause stabilization of membrane proteins and expansion of protein's half-life (Alaei et al., 2018; Caron et al., 2005; Drazic et al., 2016; Mak et al., 2014). To determine whether acetylation by p300 confers AMPAR with enhanced stability, we transfected p300, together with GFP, in primary hippocampal neurons. Immunostainings showed an overexpression of p300 led to an increase in the total GluA1 puncta intensity (**Fig. A.2D-A.2E**). In addition, we transfected p300 with GFP-GluA1 into HEK293T cells and measured the total GluA1 levels by Western blotting analysis. In line with our findings in neurons, expression of p300 led to an increase in total GluA1 levels compared to the pcDNA control, while expression of PCAF did not affect the amount of GluA1 (**Fig. A.2F-A.2G**). These results showed that p300 acetyltransferase activity facilitates AMPAR acetylation and stabilization, supporting that p300 functions as the acetyltransferase for AMPAR acetylation.

A.3.4 The Lysine Residues in the GluA1 C-Terminal Tail Are the Targets for p300-Mediated AMPAR Acetylation†

Because the acetyl group is conjugated to lysine residues of the substrate during acetylation, the four lysine residues located in GluA1 C-terminal are potential candidate sites for p300-mediated acetylation. To confirm the acetylation sites, we mutated all four of the lysine residues in GluA1ct to arginine (GluA1-4KR). Arginine's side group mimics the charge of lysine's side group thus preserving structural integrity, but is incapable of being acetylated (Inuzuka et al., 2012). We transfected HEK293 cells with GFP-GluA1-4KR, together with either p300, PCAF, or control vector pcDNA, respectively and used the cell lysates to assess GluA1 protein levels to evaluate p300 effects on GluA1-4KR accumulation. Indeed, the previously observed increase in GluA1-WT levels from p300 overexpression was abolished in cells expressing GFP-GluA1-4KR (**Fig A.2F-A.2G**), indicating that the C-terminal lysine residues are required for p300-mediated GluA1 acetylation and stabilization.

A.3.5 Acetylation of GluA1 Suppresses the Aβ-Induced Reduction of AMPAR Amount and Synaptic Accumulation

Because acetylation reduces the rate of AMPAR turnover and increases AMPAR accumulation in neurons (Wang et al., 2017), we hypothesize that acetylation should lead to suppression of Aβ-induced AMPAR degradation. To test this idea, we incubated DIV 15 hippocampal neurons with Aβ alone, or with the SIRT2 inhibitor B2, for 24 h. We found that treatment with B2 (2 μM) alone resulted in an

increase in both total and surface GluA1 (**Fig. A.3A-A.3C**). Importantly, Aβ-induced reduction in AMPARs was blocked by co-incubation with B2 (**Fig. A.3A-A.3C).**

To examine the role of acetyltransferase activity in Aβ-induced AMPAR reductions, DIV 15 hippocampal neurons were incubated with p300 acetyltransferase activator CTPB (20 μM), together with or without Aβ, for 24 hr. We found that activation of p300 by CTPB resulted in an increase in total and surface GluA1 puncta (**Fig. A.3D-A.3F**). Similar to the effect of Sirt2 inhibition, activation of p300 resulted in a blockade of the Aβ-induced AMPAR reduction (**Fig. A.3D-A.3F**). To directly test the effect of the acetyltransferase, primary neurons were transfected with p300 at DIV 8, which were then incubated with Aβ at DIV14 for 24 hrs. Consistently, we found that compared to control neurons expressing GFP, which showed a reduction in GluA1 by Aβ treatment, no changes were detected on GluA1 puncta intensity in neurons overexpressing p300 (**Fig. A.3G).**

A.3.6 GluA1 Acetylation Mimetic Confers AMPAR Resistance to the Aβ-Induced Down-Regulation

It has been shown that substitution of lysine with glutamine mimics constitutive acetylation as glutamine's hydrophilic and uncharged structure imitates that of an acetylated lysine (Kim et al., 2006). We therefore mutated the four lysine residues of GluA1 to glutamine (GluA1-4KQ) and used the construct as a GluA1 acetylation mimetic (Wang et al., 2017). We transfected DIV 8 hippocampal neurons with GFP-GluA1-WT or GFP-GluA1-4KQ and compared their expression after one

week. Consistent with the effect of acetylation, we found that, compared to GFP-GluA1-WT, GFP-GluA1-4KQ retained significantly higher levels of surface expression relative to the total expressed at the synapse (**Fig. A.3H-A.3I**). To determine whether this acetylation mimetic was also able to block the effect of Aβ on AMPAR levels, we treated GFP-GluA1-WT or GFP-GluA1-4KQ transfected DIV 14 neurons with Aβ for 24 h. While Aβ incubation reduced the surface expression of GFP-GluA1-WT, the expression of acetyl-mimetic GFP-GluA1-4KQ was not changed in the presence of Aβ oligomers (**Fig. A.3H-A.3I**). These results demonstrate that acetylated AMPARs become resistant to Aβ-induced downregulation.

A.3.7 AMPAR Acetylation Suppresses Aβ-Induced Receptor Endocytosis

Our previous work and studies of others' have shown that Aβ exposure causes AMPAR ubiquitination and internalization (Guntupalli et al., 2017; Miñano-Molina et al., 2011; Zhang et al., 2018). We wondered whether the acetylation of AMPARs also plays a role in the regulation of Aβ-induced internalization. To test this idea, we incubated DIV 14 hippocampal neurons with Aβ alone, or with CTPB, for 24 h and performed internalization assays. We found that CTPB treatment (20 μM) suppressed AMPAR internalization at basal conditions, indicated by a reduction of the ratio of internalized to surface GluA1 (**Fig. A.4A-A.4B**). Furthermore, while treatment with Aβ alone (1 μM) resulted in an increase in AMPAR internalization as expected, co-incubation with CTPB abolished the Aβ effect on AMPAR trafficking (**Fig. A.4A-A.4B**). It was possible that CTPB affected AMPAR trafficking

via off-target effects of p300 activity. To directly determine the role of AMPAR acetylation in Aβ-induced receptor internalization, we examined receptor internalization using the GluA1 acetylation mimetic. DIV 8 cultured neurons were transfected with GFP-GluA1-WT or GFP-GluA1-4KQ, which were then treated with Aβ or vehicle control for 24 h before performing internalization assays on DIV 15. We found that the basal internalization of GFP-GluA1-4KQ was reduced compared to GFP-GluA1 (**Fig. A.4C-A.4D**). Importantly, while Aβ treatment enhanced the internalization of GFP-GluA1, not significant effect was observed in cells expressing GFP-GluA1-4KQ (**Fig. A.4C-A.4D**). These results indicate that modulation of AMPARs by direct acetylation causes suppression of both basal and Aβ-induced AMPAR internalization.

A.3.8 Viral Brain Injection of GluA1-4KQ Restores GluA1 Expression and Synaptic Accumulation in APP/PS1 Mice†

In AD, AMPARs have a facilitated turnover rate, leading to a reduction in the total amount and synaptic accumulation of AMPARs. As we found that acetylation was able to stabilize AMPARs and rescue the effect of Aβ treatment *in vitro*, we wanted to know the role AMPAR acetylation plays *in vivo* and in AD conditions. As a widely used model of AD, the APP/PS1 mouse produces high levels of Aβ in the brain and demonstrates typical molecular and behavioral phenotypes of AD (McClean and Hölscher, 2014; Reinders et al., 2016; Reiserer et al., 2007; Sun et al., 2019; Trinchese et al., 2004). To determine whether AMPAR acetylation is altered in this AD animal model, we isolated GluA1 from hippocampal brain tissues of 11 month

old APP/PS1 mouse by immunoprecipitation and probed for acetylation and ubiquitination (**Fig. A.5A**). Indeed, consistent with our findings from rat primary neurons and human AD brains, this mouse model showed a significant reduction in the level of GluA1 acetylation, as well as an increase in GluA1 ubiquitination (**Fig. A.5B-A.5C**). A reduction in GluA1 acetylation was also observed in APP/PS1 mice at 5 months old (**Fig. A.5D**). The APP/PS1 mouse also showed significant reduction in the total amount of AMPAR subunit GluA1 (**Fig. A.5A and A.5D**).

A reduction in AMPAR synaptic accumulation and the consequential suppression in synaptic strength is believed to be an early pathobiology in AD (Baglietto-Vargas et al., 2018; Hsieh et al., 2006; Kamenetz et al., 2003; Li et al., 2019b; Lin et al., 2019; Sun et al., 2019; Ting et al., 2007). We therefore wanted to know whether stabilization of AMPARs by acetylation confers positive effects towards AD conditions. To examine the role of AMPAR acetylation for memory impairments in the AD animals, we injected AAV viruses expressing either GFP-GluA1-WT or GFP-GluA1-4KQ into the bilateral ventricles of 11-month-old APP/PS1 mice. Another group of APP/PS1 mice were injected with a virus expressing only GFP as a control (APP/PS1-con). Six weeks after bilateral injection of the viruses, brain tissues were collected for examination. Brain slices revealed strong GFP signals, indicating efficient viral expression of the constructs (**Fig. A.5E**). Western blots of APP/PS1 hippocampal brain lysates showed a significant reduction in synaptic proteins including GluA1, GluA2, synapsin I, and PSD95 (**Fig. A.5F).** These changes in synaptic proteins are consistent with the

known loss of synapses in the AD mouse (McClean and Hölscher, 2014; Shi et al., 2017). In APP/PS1 mice injected with either GFP-GluA1-WT or GFP-GluA1-4KQ, we found a specific increase in GluA1 compared to APP/PS1 controls however, compared with GluA1-WT, GluA1-4KQ overexpression rescued GluA1 more significantly in APP/P1 mice **(Fig. A.5F)**. These results indicate the successful expression of the viral GluA1 and GluA1-4KQ AMPAR subunits at the synaptic sites of these brain regions.

A.3.9 Expression of GluA1 Acetylation Mimetic Rescues Deficits in Synaptic Plasticity in the APP/ PS1 Mice†

Synaptic plasticity serves as the molecular basis for learning and memory (Humeau and Choquet, 2019; Lüscher and Malenka, 2012; Nabavi et al., 2014; Parkinson and Hanley, 2018), which is known to be impaired in AD conditions (Colom-Cadena et al., 2020; Lambert et al., 1998; Li and Selkoe, 2020; Sánchez-Rodríguez et al., 2019; Shankar et al., 2008; Styr and Slutsky, 2018; Walsh et al., 2002). We wanted to know whether the improved synaptic expression of AMPARs by viral injection of GluA1-4KQ had any effect on synaptic function. Using hippocampal brain slices, we examined the expression of long-term potentiation (LTP) by recordings of field excitatory postsynaptic potentials (fEPSPs). Consistent with previous reports, recordings from APP/PS1 mice showed a significant reduction in LTP expression when compared to the wild type mice (Gelman et al., 2018; Gengler et al., 2010; Da Silva et al., 2016; Trinchese et al., 2004; Vargas et al., 2014; Vyas et al., 2020) (**Fig. A.6A-A.6B**). However, APP/PS1

mice expressing viral GFP-GluA1-4KQ had substantially improved LTP, while expression of GFP-GluA1-WT showed some rescue but to a lesser extent (**Fig. A.6A-A.6B**). These results indicate that restoration of AMPAR stability and synaptic accumulation rescues synaptic plasticity.

A.3.10 Expression of GluA1 Acetylation Mimetic Rescues Visual Episodic Memory Deficits in APP/ PS1 Mice†

To examine the effect of GluA1 expression on cognitive function in the AD mice, we first performed the novel object recognition test to assess visual episodic memory in the virally-injected APP/PS1 mice. Animals were first habituated to the apparatus by allowing them to explore the cage prior to the test. The animals were then allowed to familiarize themselves with the initial objects A and B. The preference index from the familiarization period showed a lack of preference for either of the objects (data not shown). 1 h and 24 h later, animals were brought back to the cage with object B being replaced with object C and then object D (**Fig. A.6C**). As measured by the discrimination index, APP/PS1 mice struggled to remember the familiar object and thus failed to discriminate between the objects (**Fig. A.6D**). In the familiarization stage, none of the animals showed a particular preference of either of the objects (**Fig. A.6E**). During the 1 h and 24 h tests, APP/PS1 mice spent similar amounts of time with familiar object A and either of the novel objects C or D, respectively, indicating impairments in short-term and long-term memory (**Fig. A.6F-A.6G**). APP/PS1 mice expressing viral GluA1 spent significantly more time with the novel object compared to the familiar object in both

the 1 h and 24 h tests (**Fig. A.6F-A.6G**). While viral expression of GluA1-WT led to modest improvements in memory, more robust rescue effects were observed in animals expressing the acetylation mimetic GluA1-4KQ, at both 1 h and 24 h after training (**Fig. A.6D**). These findings indicate that addition of acetylated and thus stabilized AMPARs is capable of correcting the impairments in memory capacity in AD mice.

A.4 Discussion

One of the earliest pathological features of AD is an impairment in synaptic function partly due to a reduction in AMPA receptors at the synapse (Almeida et al., 2005; Baglietto-Vargas et al., 2018; Chang et al., 2006; Dong et al., 2015; Li et al., 2019b; Marttinen et al., 2018). It has been shown that soluble Aβ oligomers promote AMPAR internalization and degradation (Guntupalli et al., 2017; Miñano-Molina et al., 2011). This is consistent with studies of our own, and those of others, which show an increase in ubiquitination of AMPARs in AD (Guntupalli et al., 2017; Rodrigues et al., 2016; Zhang et al., 2018) (as reviewed by (Harris et al., 2020; Moraes et al., 2020; Zhu and Tsai, 2020)). Findings from our recent work have revealed for the first time that AMPARs are also subject to acetylation, a new form of AMPAR regulation that antagonizes receptor ubiquitination due to competition for the same lysine residues (Wang et al., 2017). In this study, we further investigated the molecular mechanism involved in AMPAR acetylation and examined the role of AMPAR acetylation in cognitive deficits in AD.

We found that in brain lysates from AD patients, a reduction in total AMPAR amount is accompanied with a decrease in acetylation of AMPARs. The change in AMPAR acetylation was also observed in the brains of APP/PS1 AD mice. Consistently, treatment of neuronal cultures with soluble Aβ oligomers led to a significant reduction in the level of AMPAR acetylation.

In our previous work, SIRT2 was identified as the deacetylase for AMPAR deacetylation (Wang et al., 2017) however, the related acetyltransferase remained unknown. In this study, we discovered that p300 functions as the acetyltransferase responsible for AMPAR acetylation. Though p300 is generally known for its role in acetylation of nuclear histone proteins, it also localizes in the cytosol where it acetylates various substrates (Aslan et al., 2015; Dancy and Cole, 2015; Kwok et al., 2006; Rotte et al., 2013; Sebti et al., 2014; Shi et al., 2009). Our results demonstrate that p300 acetyltransferase activity triggers acetylation of AMPARs, resulting in a reduced rate in receptor internalization and degradation, leading to an increase in AMPAR cell-surface expression and elevated accumulation at the synapse.

The implication of AMPAR acetylation in brain function may vary depending on the basal levels of AMPAR protein amount and the extent of AMPAR acetylation. In this study, an increase in AMPAR acetylation led to improvements in memory in the APP/PS1 AD mice. Under AD conditions, a dramatic reduction in overall AMPAR amount is a major factor in causing synaptic weakening and impairments in cognition. Therefore, reintroduction of the acetylated and stabilized

AMPARs restores the level of AMPARs and synaptic activity, leading to rescue of AD-related memory deficits. Interestingly, over-stabilization of AMPARs *via* enhanced receptor acetylation seems to have different effect on brain function. Indeed, wild type mice expressing the stabilized acetylation mimetic GluA1, as well as knockout mice lacking the deacetylase SIRT2, showed impairments in synaptic plasticity and memory (Wang et al., 2017). This memory impairment likely results from excessive over-stabilization of acetylated AMPARs at synapses. In normal non-AD animals, a dramatic increase in AMPAR acetylation disrupts receptor trafficking and turnover, which is probably the cause for synaptic dysregulation and memory deficits (Wang et al., 2017).

Given their crucial role in interneuronal communication and brain function, AMPARs have been identified as a therapeutic target for several neurological disorders, (Hettinger et al., 2018; Lee et al., 2016; Lynch, 2006; Paula-Lima et al., 2013; Swanson, 2009; Zhang et al., 2019b). Our findings provide further support for potential strategies targeting AMPARs for the treatment of AD-related cognitive dysfunctions. Thus far, the main treatment focus has been the use of positive allosteric modulators of AMPARs known as Ampakines (Bernard et al., 2010; Black, 2005; Fernandes et al., 2018; Ward et al., 2010), a few of which have gone to clinical trial. However, while compounds showed some success in animal models (Bretin et al., 2017; Giralt et al., 2017; Lauterborn et al., 2016), they have had low clinical success (Bernard et al., 2019; Trzepacz et al., 2013; Wezenberg et al., 2007). Due to a lack of chemical diversity among the Ampakines, alternative

strategies for AMPAR-based treatment are being considered (Chang et al., 2012; Hao et al., 2015; Lee et al., 2016; Zhao et al., 2019). Our results provide a basis for pharmacological manipulation of AMPAR acetylation as a potential therapeutic strategy. On a broader level, because ubiquitination, a modulation antagonizing acetylation and resulting in receptor degradation, is enhanced in AD (Gadhave et al., 2016; Liu et al., 2019; Tramutola et al., 2018), manipulation of both of these opposing processes should be considered for more efficient management of AD.

In conclusion, our results show that the acetylation of AMPARs leads to a blockage of Aβ induced reduction of AMPARs at the synapse by preventing receptor internalization, resulting in significant improvements in memory for the transgenic AD mice. These findings encourage future efforts to identify novel compounds that enhance AMPAR acetylation as potential therapeutic tools for AD patients.

Figure A.1

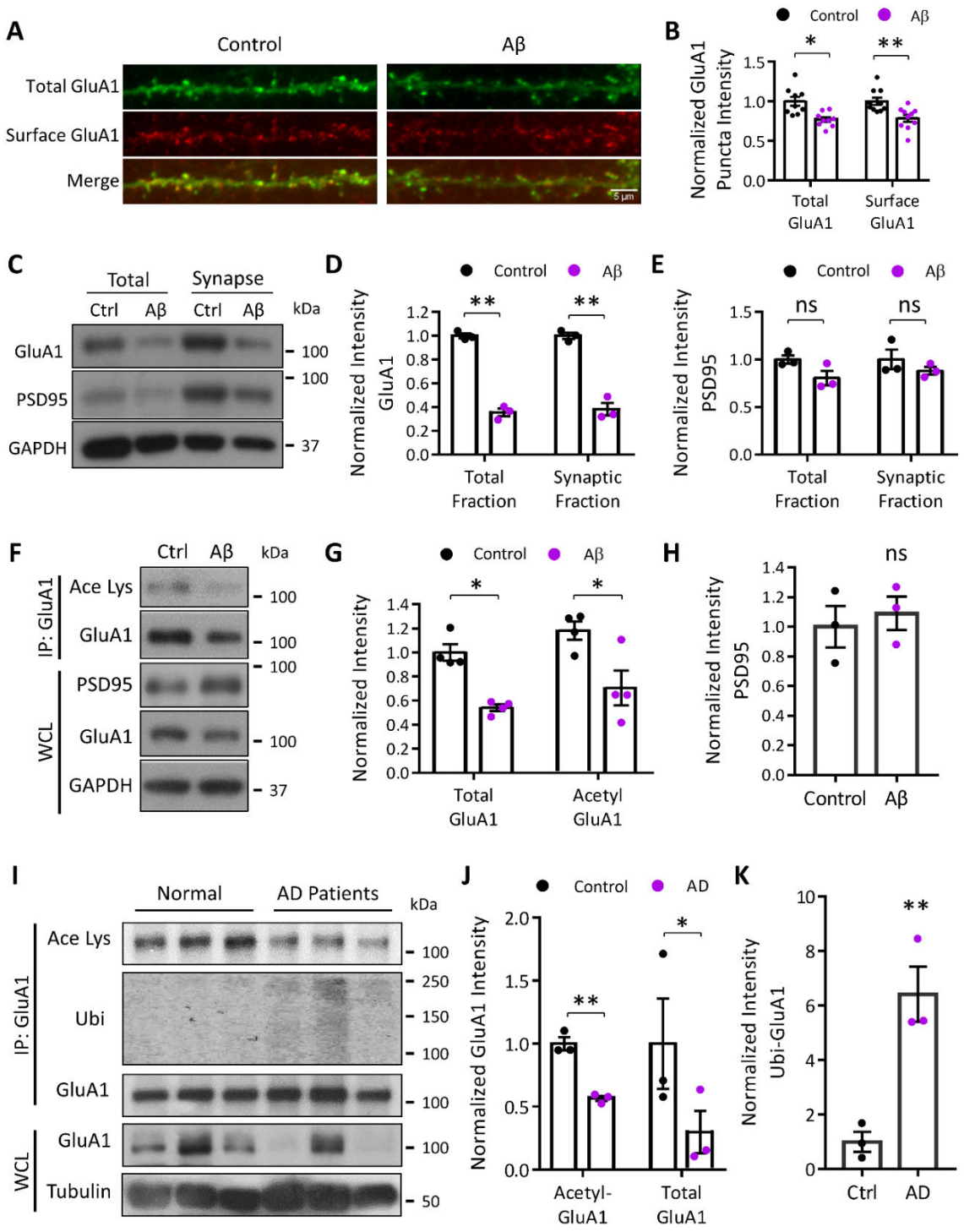


Figure A.1. Aβ treatment induces a reduction in AMPAR acetylation

(A) Hippocampal neurons were treated with Aβ (1μM) for 24 h and probed for synaptic GluA1 using immunocytochemistry (Total GluA1: Green; Surface GluA1: Red) (scale bar, 5 μm). **(B)** Quantitative analysis of the GluA1 puncta intensity showed a decrease in both surface (Ctrl, *n* = 10 cells, 548 puncta; Aβ, *n* = 11 cells, 511 puncta; $t_{(34)}$ = 3.453, *p* = 0.0015) and total intensities (Ctrl, *n* = 10 cells, 597 puncta; Aβ, *n* = 11 cells, 652 puncta; $t_{(34)}$ = 3.539, *p* = 0.0012). **(C)** Synaptosome purification of cultured cortical neurons incubated with Aβ (*n* = 3 experiments). **(D)** Quantification showed a decrease in synaptically localized, as well as total, GluA1 levels. (Synaptic: $t_{(8)}$ = 12.30, *p* < 0.0001; Total: $t_{(8)}$ = 12.85, *p* < 0.0001). **(E)** Quantification shows no change in PSD95 levels. (Synaptic: $t_{(8)}$ = 1.186, *p* = 0.2695; Total: $t_{(8)}$ = 1.940, *p* = 0.0883). **(F)** GluA1 acetylation levels were assessed *via* acetylation assays using cultured cortical neurons incubated with Aβ (*n* = 4 experiments). **(G)** Quantitative analysis showed that application of Aβ reduced acetylated and total GluA1 levels. GluA1 acetylation was measured by normalizing the acetyl-lysine signal to the amount of GluA1 in IP. (Acetylated: $t_{(12)}$ = 1.93, *p* = 0.0018; Total: $t_{(12)}$ = 2.87, *p* = 0.031). **(H)** Quantification shows no change in PSD95 levels. ($t_{(4)}$ = 0.4946, *p* = 0.6468). **(I)†** Acetylation assays from prefrontal cortical brain homogenates from AD patient and healthy control brains (*n* = 3 brains). **(J)†** Quantification showed reduced acetylation of GluA1 in AD patients' brains compared to those of controls. (Acetylated: $t_{(4)}$ = 8.014, *p* = 0.0013; Total: $t_{(8)}$ = 2.478, *p* = 0.038). **(K)†** Quantification showed a significant increase in GluA1 ubiquitination in AD brains compared to those of controls. ($t_{(4)}$ = 5.0352, *p* =

0.00731). * $p < 0.05$, ** $p < 0.01$, *** $p < 0.001$. Data are mean ± SEM. † *With contributions from Guan Wang for I-K.*

Figure A.2

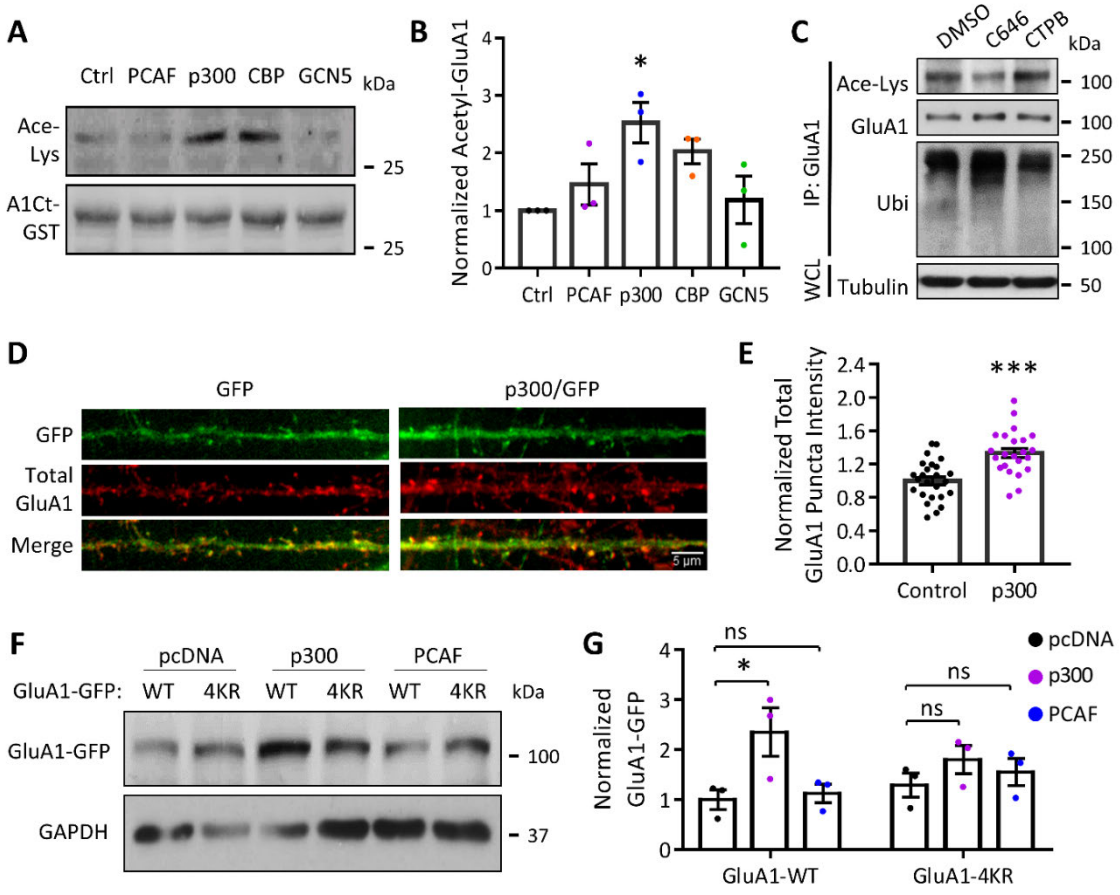


Figure A.2. Acetyltransferase p300 acetylates and stabilizes AMPARs

(A)† Acetylation assays from *in vitro* reactions with purified acetyltransferases. **(B)**† Quantification shows that incubation with p300, but not CBP, PCAF, or GCN5 increased GluA1 acetylation. ($F_{(4,10)}$ = 4.263, p = 0.0286, n = 3 experiments). **(C)**† Inhibition of p300 acetyltransferase activity by C646 (40 µM, 4 h) led to reduced acetylation while activation by CTPB (20 µM, 4 h) led to increased acetylation. **(D)** GluA1 puncta levels were assessed by immunocytochemistry following overexpression of p300 (Total GluA1: Red) (scale bar, 5 µm). **(E)** Quantitative

analysis showed overexpression of p300 increased total GluA1 puncta intensity. (Ctrl, n = 25 cells, 2407 puncta; p300, n = 23 cells, 2164 puncta; $t_{(46)} = 4.539$, $p < 0.0001$). **(F-G)†** In HEK293T cells, overexpression of p300 increases GluA1 intensity. Additionally, expression of GluA1-4KR mutant abolishes p300-induced GluA1-WT up-regulation, indicating the lysine-dependence of p300 effect (WT: pcDNA v p300: $t_{(12)} = 3.255$, $p = 0.0205$, pcDNA v PCAF: $t_{(12)} = 0.3032$, $p = 0.9873$; 4KR: pcDNA v p300: $t_{(12)} = 1.230$, $p = 0.5648$, pcDNA v PCAF: $t_{(12)} = 0.630$, $p = 0.9145$; $F_{(2,12)} = 5.601$, $p = 0.0191$; n = 3 experiments). * $p < 0.05$, ** $p < 0.01$, *** $p < 0.001$. Data are mean ± SEM. † *With contributions from Guan Wang for A-C and F-G.*

Figure A.3

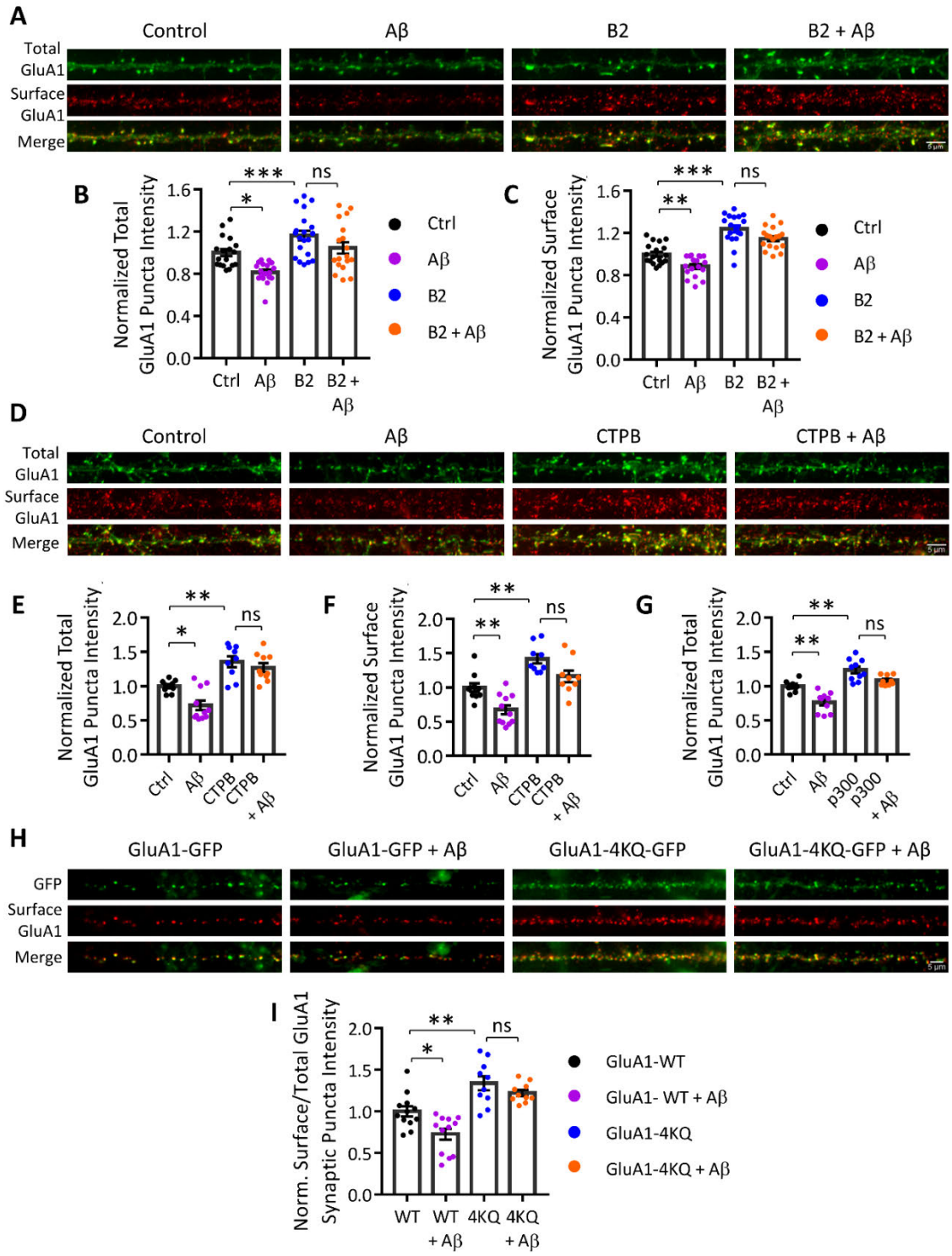

A
Control
Aβ
B2
B2 + Aβ
Total GluA1
Surface GluA1
Merge
B
Normalized Total GluA1 Puncta Intensity
Ctrl
Aβ
B2
B2 + Aβ
C
Normalized Surface GluA1 Puncta Intensity
D
Control
Aβ
CTPB
CTPB + Aβ
E
F
G
Normalized Total GluA1 Puncta Intensity
Normalized Surface GluA1 Puncta Intensity
CTPB
p300
H
GluA1-GFP
GluA1-GFP + Aβ
GluA1-4KQ-GFP
GluA1-4KQ-GFP + Aβ
GFP
I
Norm. Surface/Total GluA1 Synaptic Puncta Intensity
GluA1-WT
GluA1- WT + Aβ
GluA1-4KQ
GluA1-4KQ + Aβ
WT
4KQ

Figure A.3. Acetylation stabilizes AMPAR synaptic localization

(A) Cultured hippocampal neurons were treated with B2, to inhibit SIRT2 (Total GluA1: Green; Surface GluA1: Red) (scale bar, 5 μm). **(B-C)** Quantification showed B2 treatment increased GluA1 puncta localization and blocked Aβ induced reduction in GluA1 as measured by GluA1 (*B*) total and (*C*) surface puncta intensity. (Ctrl, n = 17 cells, 21,486 puncta; Aβ, n = 19 cells, 25,742 puncta; B2, n = 17 cells, 14,838 puncta; B2 + Aβ, n = 17 cells, 11,524 puncta; Total: $F_{(3, 70)}$ = 12.22, p < 0.0001; Surface: $F_{(3, 68)}$ = 36.33, p < 0.0001). **(D)** CTPB treatment, to activate acetyltransferase activity of p300, followed by immunocytochemistry probing of GluA1 (Total GluA1: Green; Surface GluA1: Red) (scale bar, 5 μm). **(E-F)** Quantification showed CTPB treatment increased GluA1 puncta localization and blocked Aβ induced reduction in GluA1 puncta intensity as measured by GluA1 (*E*) total and (*F*) surface puncta intensity. (Ctrl, n = 10 cells, 2615 puncta; Aβ, n = 11 cells, 3964 puncta; CTPB, n = 8 cells, 4383 puncta; CTPB + Aβ, n = 8 cells, 3363 puncta; Total: $F_{(3, 36)}$ = 21.78, p < 0.0001; Surface: $F_{(3, 35)}$ = 19.80, p < 0.0001). **(G)** Overexpression of p300 increased total GluA1 puncta intensity and blocked Aβ induced reduction. (Ctrl, n = 7 cells, 336 puncta; Aβ, n = 10 cells, 332 puncta; p300, n = 10 cells, 337 puncta; p300 + Aβ, n = 9 cells, 351 puncta; $F_{(3, 32)}$ = 24.44, p < 0.0001). **(H)** Aβ treatment of hippocampal neurons overexpressing GluA1-WT-GFP or GluA1-4KQ-GFP acetylation mimetic (Surface GluA1: Red) (scale bar, 5 μm). **(I)** Quantitative analysis of surface expressing exogenous GluA1 normalized to total puncta expressing exogenous GluA1 showed GluA1-4KQ-GFP

increased GluA1 surface expression and blocked Aβ induced decrease in surface GluA1 levels. (GluA1-WT, n = 8 cells, 798 puncta; GluA1-WT + Aβ, n = 9 cells, 943 puncta; GluA1-4KQ, n = 9 cells, 901 puncta; GluA1-4KQ + Aβ, n = 8 cells, 862 puncta; $F_{(3, 40)} = 17.75$, $p < 0.0001$). * $p < 0.05$, ** $p < 0.01$, *** $p < 0.001$. Data are mean ± SEM.

Figure A.4

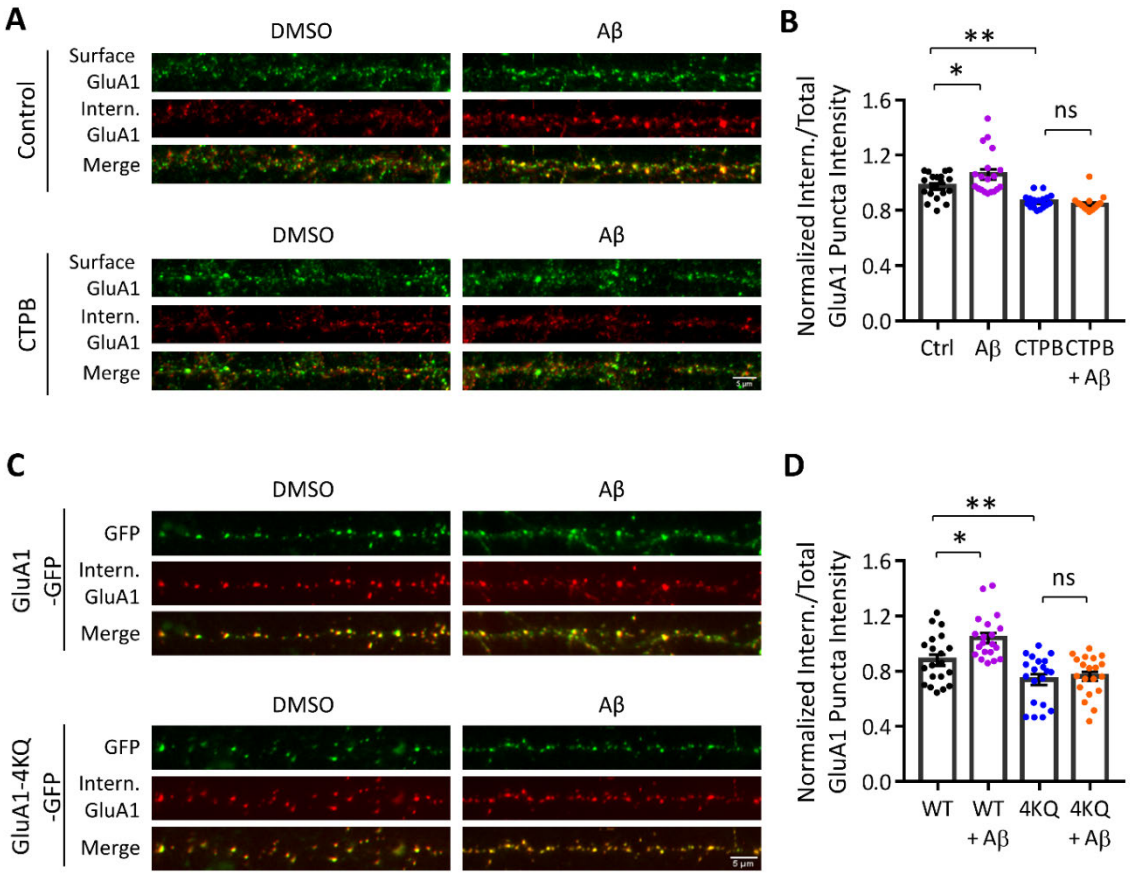


Figure A.4. Acetylation blocks Aβ induced receptor internalization

(A) Internalization assay of hippocampal neurons treated with CTPB, to activate acetyltransferase activity of p300, or CTPB with Aβ (Surface GluA1: Green; Internalized GluA1: Red) (scale bar, 5 μm). **(B)** Quantification of the puncta intensity of internalized GluA1 to initial surface total GluA1 (internalized + remaining surface) showed CTPB treatment blocked Aβ induced internalization of GluA1. (Ctrl, *n* = 19 cells, 2095 puncta; Aβ, *n* = 19 cells, 2124 puncta; CTPB, *n* = 19 cells, 6230 puncta; CTPB + Aβ, *n* = 19 cells, 3341 puncta; $F_{(3, 72)} = 20.91$, *p* <

0.0001). **(C)** Internalization assay of hippocampal neurons overexpressing GluA1-WT or GluA1-4KQ with or without Aβ (Internalized GluA1: Red) (scale bar, 5 μm). **(D)** Quantitative analysis of the puncta intensity of internalized GluA1-GFP or GluA1-4KQ-GFP to total GluA1-GFP or GluA1-4KQ-GFP expressed at that puncta. Quantification showed Aβ induced internalization of GluA1 is suppressed by overexpression of GluA1-4KQ. (GluA1-WT, n = 26 cells, 2637 puncta; GluA1-WT + Aβ, n = 20 cells, 2161 puncta; GluA1-4KQ, n = 20 cells, 1897 puncta; GluA1-4KQ + Aβ, n = 20 cells, 3018 puncta; $F_{(3, 76)} = 14.01$, $p < 0.0001$). * $p < 0.5$, ** $p < 0.01$, *** $p < 0.001$. Data are mean ± SEM.

Figure A.5

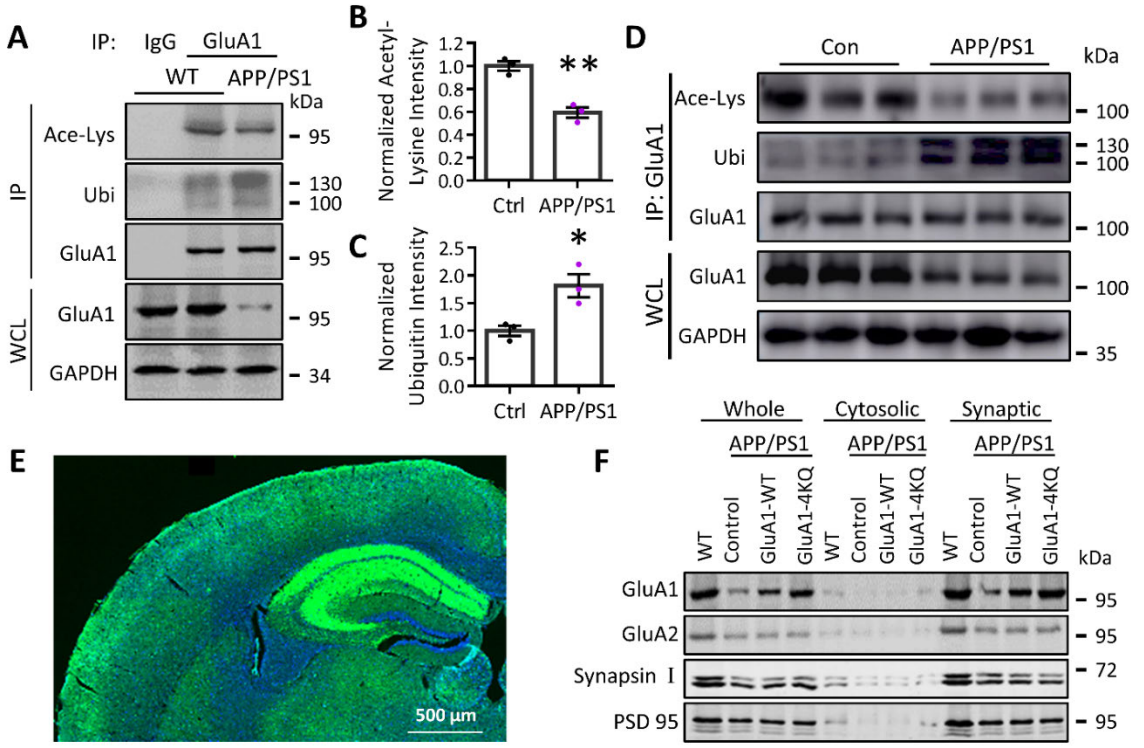


Figure A.5. Viral brain injection of GluA1-4KQ restores GluA1 expression and synaptic accumulation†

(A) Hippocampal tissue from 11-month wild type and APP/PS1 mouse brains was homogenized and immunoprecipitated with antibody against GluA1. GluA1 acetylation and ubiquitination levels were detected through probing the immunoprecipitated GluA1 with anti-Acetyl-Lysine or ubiquitin antibodies, respectively. **(B)** Quantitative analysis of the GluA1 acetylation levels showed a reduction in AMPAR acetylation in APP/PS1 mice. ($t_{(4)}$ = 6.652, p = 0.0027, n = 3 experiments). **(C)** Quantification analysis of the GluA1 ubiquitination levels showed an increase in AMPAR ubiquitination in APP/PS1 mice ($t_{(4)}$ = 3.594, p = 0.0229, n

= 3 experiments). **(D)** GluA1 acetylation and ubiquitination levels were detected through probing GluA1 immunoprecipitated from hippocampal tissue from 5-month old wild-type mice or APP/PS1 mice with anti-Acetyl-Lysine or ubiquitin antibodies, respectively (*n* = 3 brains). **(E)** AAV expression was observed (green) 6 weeks after injection. Cell nuclei were stained with Hoechst (blue) to show the cortex and hippocampus (scale bar, 500 μm). **(F)** GluA1, GluA2, synapsin I, and PSD95 were detected by Western blotting in whole cell lysates, cytosolic fractions and synaptosomal fractions of mouse hippocampus. * $p < 0.05$, ** $p < 0.01$, *** $p < 0.001$. Data are mean ± SEM. † *Contribution from Yang-Ping Shentu and Rong Liu.*

Figure A.6

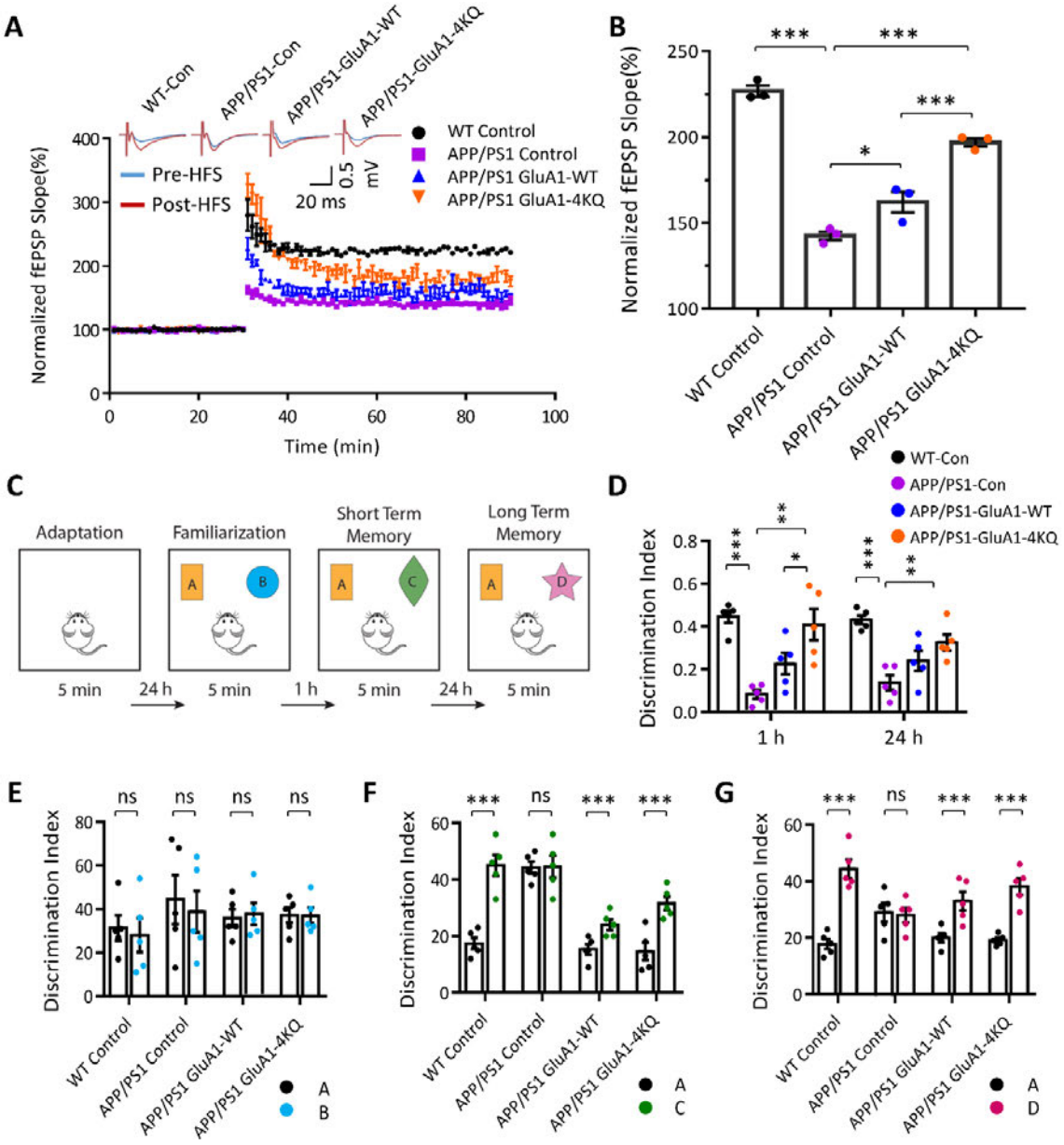


Figure A.6. Overexpression of GluA1-4KQ rescues hippocampal LTP and the visual episodic memory deficit in APP/PS1 mice†

(A) LTP recordings of fEPSP in acute hippocampal slices from AAV- injected wild-type mice or APP/PS1 mice. **(B)** Quantitative analysis of the normalized fEPSP

slope. ($F_{(3, 8)}$ = 95.08, p < 0.0001, n = 2 animals per condition, 3 brain slices per animal). **(C)** The experimental design of novel object recognition test (NOR). One day before the memory acquisition, the mice were habituated to the arenas for 5 min, as indicated in the first box. The second box showed the acquisition trial. The third and fourth box showed the test trial conducted 1 h and 24 h after the acquisition trial. **(D)** The discrimination index of 1 h test trial and 24 h test trial. (n = 5 animals). **(E)** The recognition index between objects A and B in the acquisition trial. (WT: $t_{(32)}$ = 0.3497, p = 0.99, APP/PS1 Con: $t_{(32)}$ = 0.5760, p = 0.97, APP/PS1 GluA1-WT: $t_{(32)}$ = 0.2057, p = 0.99, APP/PS1 GluA1-4KR: $t_{(32)}$ = 0.0206, p = 0.99; $F_{(3,32)}$ = 1.023, p = 0.3953) **(F)** The recognition index between objects A and C in the test trial 1 h after the acquisition trial. (WT: $t_{(32)}$ = 7.083, p < 0.0001, APP/PS1 Con: $t_{(32)}$ = 0.1026, p = 0.99, APP/PS1 GluA1-WT: $t_{(32)}$ = 2.207, p = 0.1314, APP/PS1 GluA1-4KR: $t_{(32)}$ = 4.363, p = 0.0005; $F_{(3,32)}$ = 31.77, p < 0.0001) **(G)** The recognition index between objects A and D in the test trial 24 h after the acquisition trial (WT: $t_{(32)}$ = 7.275, p < 0.0001, APP/PS1 Con: $t_{(32)}$ = 0.2735, p = 0.99, APP/PS1 GluA1-WT: $t_{(32)}$ = 3.555, p = 0.0048, APP/PS1 GluA1-4KR: $t_{(32)}$ = 5.196, p < 0.0001; $F_{(3,32)}$ = 1.061, p = 0.3793). * p < 0.05, ** p < 0.01, *** p < 0.001. Data are mean ± SEM. † *Contribution from Yang-Ping Shentu and Rong Liu.*

REFERENCES

Aarabi, M., Kessler, E., Madan-Khetarpal, S., Surti, U., Bellissimo, D., Rajkovic, A., and Yatsenko, S.A. (2019). Autism spectrum disorder in females with ARHGEF9 alterations and a random pattern of X chromosome inactivation. *European Journal of Medical Genetics*, *62*, 239–242.

Abghari, F.Z., Moradi, Y., and Akouchekian, M. (2019). PTEN gene mutations in patients with macrocephaly and classic autism: A systematic review. *Medical Journal of the Islamic Republic of Iran*, *33*, 52–59.

Abraham, W.C., Jones, O.D., and Glanzman, D.L. (2019). Is plasticity of synapses the mechanism of long-term memory storage? *Science of Learning*, *4*, 1–10.

Abrahams, B.S., and Geschwind, D.H. (2008). Advances in autism genetics: On the threshold of a new neurobiology. *Nature Reviews Genetics*, *9*, 341–355.

Abrahams, B.S., Arking, D.E., Campbell, D.B., Mefford, H.C., Morrow, E.M., Weiss, L.A., Menashe, I., Wadkins, T., Banerjee-Basu, S., and Packer, A. (2013). SFARI Gene 2.0: A community-driven knowledgebase for the autism spectrum disorders (ASDs). *Molecular Autism*, *4*, 36.

Aceti, M., Creson, T.K., Vaissiere, T., Rojas, C., Huang, W.C., Wang, Y.X., Petralia, R.S., Page, D.T., Miller, C.A., and Rumbaugh, G. (2015). Syngap1 haploinsufficiency damages a postnatal critical period of pyramidal cell structural maturation linked to cortical circuit assembly. *Biological Psychiatry*, *77*, 805–815.

Ackerman, S. (1992). Major Structures and Functions of the Brain. In Discovering the Brain, (National Academies Press (US)), p. 194.

Van Aerde, K.I., and Feldmeyer, D. (2015). Morphological and physiological characterization of pyramidal neuron subtypes in rat medial prefrontal cortex. *Cerebral Cortex*, *25*, 788–805.

Agrawal, S., Rao, S.C., Bulsara, M.K., and Patole, S.K. (2018). Prevalence of autism spectrum disorder in preterm infants: A meta-Analysis. *Pediatrics*, *142*.

Ajram, L.A., Horder, J., Mendez, M.A., Galanopoulos, A., Brennan, L.P., Wichers, R.H., Robertson, D.M., Murphy, C.M., Zinkstok, J., Ivin, G., et al. (2017). Shifting brain inhibitory balance and connectivity of the prefrontal cortex of adults with autism spectrum disorder. *Translational Psychiatry*, *7*, e1137.

Alaei, S.R., Abrams, C.K., Bulinski, J.C., Hertzberg, E.L., and Freidin, M.M. (2018). Acetylation of C-terminal lysines modulates protein turnover and stability of Connexin-32. *BMC Cell Biology*, *19*, 22.

Alarcon-Martinez, T., Khan, A., and Myers, K.A. (2019). Torpedo Maculopathy Associated with NEXMIF Mutation. *Molecular Syndromology*,.

Alarcón, M., Abrahams, B.S., Stone, J.L., Duvall, J.A., Perederiy, J. V., Bomar, J.M., Sebat, J., Wigler, M., Martin, C.L., Ledbetter, D.H., et al. (2008). Linkage, Association, and Gene-Expression Analyses Identify CNTNAP2 as an Autism-Susceptibility Gene. *American Journal of Human Genetics*, *82*, 150–159.

Alexander, A.L., Lee, J.E., Lazar, M., Boudos, R., DuBray, M.B., Oakes, T.R., Miller, J.N., Lu, J., Jeong, E.K., McMahon, W.M., et al. (2007). Diffusion tensor imaging of the corpus callosum in Autism. *NeuroImage*, *34*, 61–73.

Alfonso, S., Kessels, H.W., Banos, C.C., Chan, T.R., Lin, E.T., Kumaravel, G., Scannevin, R.H., Rhodes, K.J., Huganir, R., Guckian, K.M., et al. (2014). Synapto-depressive effects of amyloid beta require PICK1. *European Journal of Neuroscience*, *39*, 1225–1233.

Allen Institute for Brain Science (2004). Allen Mouse Brain Atlas.

Almeida, C.G., Tampellini, D., Takahashi, R.H., Greengard, P., Lin, M.T., Snyder, E.M., and Gouras, G.K. (2005). Beta-amyloid accumulation in APP mutant neurons reduces PSD-95 and GluR1 in synapses. *Neurobiology of Disease*, *20*, 187–198.

Ameis, S.H., and Catani, M. (2015). Altered white matter connectivity as a neural substrate for social impairment in Autism Spectrum Disorder. *Cortex*, *62*, 158–181.

American Psychiatric Association (2013). Diagnostic and Statistical Manual of Mental Disorders. (American Psychiatric Association), p.

Amir, R.E., Van Den Veyver, I.B., Wan, M., Tran, C.Q., Francke, U., and Zoghbi, H.Y. (1999). Rett syndrome is caused by mutations in X-linked MECP2, encoding methyl- CpG-binding protein 2. *Nature Genetics*, *23*, 185–188.

Amiri, A., Cho, W., Zhou, J., Birnbaum, S.G., Sinton, C.M., McKay, R.M., and Parada, L.F. (2012). Pten deletion in adult hippocampal neural stem/progenitor cells causes cellular abnormalities and alters neurogenesis. *Journal of Neuroscience*, *32*, 5880–5890.

Amodeo, D.A., Pahua, A.E., Zarate, M., Taylor, J.A., Peterson, S., Posadas, R., Oliver, B.L., and Amodeo, L.R. (2019). Differences in the expression of restricted repetitive behaviors in female and male BTBR T + tf/J mice. *Behavioural Brain Research*, *372*, 112028.

Armstrong, D., Dunn, J.K., Antalffy, B., and Trivedi, R. (1995). Selective Dendritic Alterations in the Cortex of Rett Syndrome. *Journal of Neuropathology and*

Experimental Neurology, *54*, 195–201.

Armstrong, D.M., Ikonomovic, M.D., Sheffield, R., and Wenthold, R.J. (1994). AMPA-selective glutamate receptor subtype immunoreactivity in the entorhinal cortex of non-demented elderly and patients with Alzheimer's disease. *Brain Research*, *639*, 207–216.

Arndt, G.M., and MacKenzie, K.L. (2016). New prospects for targeting telomerase beyond the telomere. *Nature Publishing Group*,.

Asaka, Y., Jugloff, D.G.M., Zhang, L., Eubanks, J.H., and Fitzsimonds, R.M. (2006). Hippocampal synaptic plasticity is impaired in the Mecp2-null mouse model of Rett syndrome. *Neurobiology of Disease*, *21*, 217–227.

Ascoli, G.A., Alonso-Nanclares, L., Anderson, S.A., Barrionuevo, G., Benavides-Piccione, R., Burkhalter, A., Buzsáki, G., Cauli, B., DeFelipe, J., Fairén, A., et al. (2008). Petilla terminology: Nomenclature of features of GABAergic interneurons of the cerebral cortex. *Nature Reviews Neuroscience*, *9*, 557–568.

Aslan, J.E., Rigg, R.A., Nowak, M.S., Loren, C.P., Baker-Groberg, S.M., Pang, J., David, L.L., and Mccarty, O.J.T. (2015). Lysine acetyltransfer supports platelet function. *Journal of Thrombosis and Haemostasis*, *13*, 1908–1917.

Athanasakis, E., Licastro, D., Faletra, F., Fabretto, A., Dipresa, S., Vozzi, D., Morgan, A., d'Adamo, A.P., Pecile, V., Biarnés, X., et al. (2014). Next generation sequencing in nonsyndromic intellectual disability: From a negative molecular karyotype to a possible causative mutation detection. *American Journal of Medical Genetics Part A*, *164*, 170–176.

Auyeung, B., Baron-Cohen, S., Chapman, E., Knickmeyer, R., Taylor, K., and Hackett, G. (2006). Foetal testosterone and the child systemizing quotient. In European Journal of Endocrinology, Supplement, (European Society of Endocrinology), pp. S123–S130.

Avino, T.A., and Hutsler, J.J. (2010). Abnormal cell patterning at the cortical gray-white matter boundary in autism spectrum disorders. *Brain Research*, *1360*, 138–146.

Azevedo, F.A.C., Carvalho, L.R.B., Grinberg, L.T., Farfel, J.M., Ferretti, R.E.L., Leite, R.E.P., Filho, W.J., Lent, R., and Herculano-Houzel, S. (2009). Equal numbers of neuronal and nonneuronal cells make the human brain an isometrically scaled-up primate brain. *Journal of Comparative Neurology*, *513*, 532–541.

Ba, W., Yan, Y., Reijnders, M.R.F., Schuurs-Hoeijmakers, J.H.M., Feenstra, I., Bongers, E.M.H.F., Bosch, D.G.M., De Leeuw, N., Pfundt, R., Gilissen, C., et al.

(2016). TRIO loss of function is associated with mild intellectual disability and affects dendritic branching and synapse function. *Human Molecular Genetics*, *25*, 892–902.

Badea, A., Nicholls, P.J., Johnson, G.A., and Wetsel, W.C. (2007). Neuroanatomical phenotypes in the Reeler mouse. *NeuroImage*, *34*, 1363–1374.

Baglietto-Vargas, D., Prieto, G.A., Limon, A., Forner, S., Rodriguez-Ortiz, C.J., Ikemura, K., Ager, R.R., Medeiros, R., Trujillo-Estrada, L., Martini, A.C., et al. (2018). Impaired AMPA signaling and cytoskeletal alterations induce early synaptic dysfunction in a mouse model of Alzheimer's disease. *Aging Cell*, *17*, e12791.

Bagni, C., and Zukin, R.S. (2019). A Synaptic Perspective of Fragile X Syndrome and Autism Spectrum Disorders. *Neuron*, *101*, 1070–1088.

Balasubramanyam, K., Swaminathan, V., Ranganathan, A., and Kundu, T.K. (2003). Small molecule modulators of histone acetyltransferase p300. *The Journal of Biological Chemistry*, *278*, 19134–19140.

Banerjee-Basu, S., and Packer, A. (2010a). SFARI Gene: an evolving database for the autism research community. *Disease Models & Mechanisms*, *3*, 133–135.

Banerjee-Basu, S., and Packer, A. (2010b). SFARI Gene: An evolving database for the autism research community. *DMM Disease Models and Mechanisms*, *3*, 133–135.

Bargiela, S., Steward, R., and Mandy, W. (2016). The Experiences of Late-diagnosed Women with Autism Spectrum Conditions: An Investigation of the Female Autism Phenotype. *Journal of Autism and Developmental Disorders*, *46*, 3281–3294.

Barnes, S.A., Wijetunge, L.S., Jackson, A.D., Katsanevaki, D., Osterweil, E.K., Komiyama, N.H., Grant, S.G.N., Bear, M.F., Näger, U.V., Kind, P.C., et al. (2015). Convergence of hippocampal pathophysiology in syngap+/- and fmr1-/y mice. *Journal of Neuroscience*, *35*, 15073–15081.

Baron-Cohen, S. (2002). The extreme male brain theory of autism. *Trends in Cognitive Sciences*, *6*, 248–254.

Baron-Cohen, S., Lombardo, M. V., Auyeung, B., Ashwin, E., Chakrabarti, B., and Knickmeyer, R. (2011). Why are Autism Spectrum conditions more prevalent in Males? *PLoS Biology*, *9*.

Baruah, A., Singla, K., NarwAt, P., Das, N., and Chapadgaonkar, S.S. (2018).

Gender Bias in Autism Spectrum Disorders-A Review. *Journal of Clinical and Diagnostic Research*, *12*, 1–07.

Bateup, H.S., Takasaki, K.T., Saulnier, J.L., Denefrio, C.L., and Sabatini, B.L. (2011). Loss of Tsc1 in vivo impairs hippocampal mGluR-LTD and increases excitatory synaptic function. *Journal of Neuroscience*, *31*, 8862–8869.

Baudouin, S.J., Gaudias, J., Gerharz, S., Hatstatt, L., Zhou, K., Punnakkal, P., Tanaka, K.F., Spooren, W., Hen, R., De Zeeuw, C.I., et al. (2012). Shared synaptic pathophysiology in syndromic and nonsyndromic rodent models of autism. *Science*, *338*, 128–132.

Bear, M.F., and Malenka, R.C. (1994). Synaptic plasticity: LTP and LTD. *Current Opinion in Neurobiology*, *4*, 389–399.

Belichenko, P. V., Belichenko, P. V., Oldfors, A., Hagberg, B., and Dahlström, A. (1994). Rett syndrome: 3-D confocal microscopy of cortical pyramidal dendrites and afferents. *NeuroReport*, *5*, 1509–1513.

Belmonte, M.K., Allen, G., Beckel-Mitchener, A., Boulanger, L.M., Carper, R.A., and Webb, S.J. (2004). Autism and abnormal development of brain connectivity. In Journal of Neuroscience, (Society for Neuroscience), pp. 9228–9231.

Ben-Itzchak, E., Ben-Shachar, S., and Zachor, D.A. (2013). Specific neurological phenotypes in autism spectrum disorders are associated with sex representation. *Autism Research*, *6*, 596–604.

Berkel, S., Marshall, C.R., Weiss, B., Howe, J., Roeth, R., Moog, U., Endris, V., Roberts, W., Szatmari, P., Pinto, D., et al. (2010). Mutations in the SHANK2 synaptic scaffolding gene in autism spectrum disorder and mental retardation. *Nature Genetics*, *42*, 489–491.

Bernard, K., Danober, L., Thomas, J.-Y., Lebrun, C., Muñoz, C., Cordi, A., Desos, P., Lestage, P., and Morain, P. (2010). DRUG FOCUS: S 18986: A Positive Allosteric Modulator of AMPA-Type Glutamate Receptors Pharmacological Profile of a Novel Cognitive Enhancer. *CNS Neuroscience & Therapeutics*, *16*, e193–e212.

Bernard, K., Gouttefangeas, S., Bretin, S., Galtier, S., Robert, P., Holthoff-Detto, V., Cummings, J., and Pueyo, M. (2019). A 24-week double-blind placebo-controlled study of the efficacy and safety of the AMPA modulator S47445 in patients with mild to moderate Alzheimer's disease and depressive symptoms. *Alzheimer's & Dementia: Translational Research & Clinical Interventions*, *5*, 231–240.

Bernier, R., Golzio, C., Xiong, B., Stessman, H.A., Coe, B.P., Penn, O., Witherspoon, K., Gerdts, J., Baker, C., Vulto-Van Silfhout, A.T., et al. (2014). Disruptive CHD8 mutations define a subtype of autism early in development. *Cell*, *158*, 263–276.

Berry, K.P., and Nedivi, E. (2017). Spine Dynamics: Are They All the Same? *Neuron*, *96*, 43–55.

Besag, F.M.C. (2018). Epilepsy in patients with autism: Links, risks and treatment challenges. *Neuropsychiatric Disease and Treatment*, *14*, 1–10.

Betancur, C., Sakurai, T., and Buxbaum, J.D. (2009). The emerging role of synaptic cell-adhesion pathways in the pathogenesis of autism spectrum disorders. *Trends in Neurosciences*, *32*, 402–412.

Bittel, D.C., Theodoro, M.F., Kibiryeva, N., Fischer, W., Talebizadeh, Z., and Butler, M.G. (2008). Comparison of X-chromosome inactivation patterns in multiple tissues from human females. *Journal of Medical Genetics*, *45*, 309–313.

Black, M.D. (2005). Therapeutic potential of positive AMPA modulators and their relationship to AMPA receptor subunits. A review of preclinical data. *Psychopharmacology*, *179*, 154–163.

Blundell, J., Blaiss, C.A., Etherton, M.R., Espinosa, F., Tabuchi, K., Walz, C., Bolliger, M.F., Südhof, T.C., and Powell, C.M. (2010). Neuroligin-1 deletion results in impaired spatial memory and increased repetitive behavior. *Journal of Neuroscience*, *30*, 2115–2129.

Boccuto, L., Lauri, M., Sarasua, S.M., Skinner, C.D., Buccella, D., Dwivedi, A., Orteschi, D., Collins, J.S., Zollino, M., Visconti, P., et al. (2013). Prevalence of SHANK3 variants in patients with different subtypes of autism spectrum disorders. *European Journal of Human Genetics*, *21*, 310–316.

Van Bon, B.W.M., Coe, B.P., Bernier, R., Green, C., Gerdts, J., Witherspoon, K., Kleefstra, T., Willemsen, M.H., Kumar, R., Bosco, P., et al. (2016). Disruptive de novo mutations of DYRK1A lead to a syndromic form of autism and ID. *Molecular Psychiatry*, *21*, 126–132.

Bonhoeffer, T., and Grinvald, A. (1991). Iso-orientation domains in cat visual cortex are arranged in pinwheel-like patterns. *Nature*, *353*, 429–431.

Borlot, F., Regan, B.M., Bassett, A.S., Stavropoulos, D.J., and Andrade, D.M. (2017). Prevalence of pathogenic copy number variation in adults with pediatric-onset epilepsy and intellectual disability. *JAMA Neurology*, *74*, 1301–1311.

Boudewijns, Z.S.R.M., Groen, M.R., Lodder, B., Mcmaster, M.T.B., Kalogreades, L., Haan, R. De, Narayanan, R.T., Meredith, R.M., Mansvelder, H.D., and de Kock, C.P.J. (2013). Layer-specific high-frequency spiking in the prefrontal cortex of awake rats. *Frontiers in Cellular Neuroscience*, *7*, 99.

Bourgeron, T. (2009). A synaptic trek to autism. *Current Opinion in Neurobiology*, *19*, 231–234.

Bourgeron, T. (2015). From the genetic architecture to synaptic plasticity in autism spectrum disorder. *Nature Reviews Neuroscience*, *16*, 551–563.

Bowers, E.M., Yan, G., Mukherjee, C., Orry, A., Wang, L., Holbert, M.A., Crump, N.T., Hazzalin, C.A., Liszczak, G., Yuan, H., et al. (2010). Virtual ligand screening of the p300/CBP histone acetyltransferase: identification of a selective small molecule inhibitor. *Chemistry & Biology*, *17*, 471–482.

Boyle, M.P., Bernard, A., Thompson, C.L., Ng, L., Boe, A., Mortrud, M., Hawrylycz, M.J., Jones, A.R., Hevner, R.F., and Lein, E.S. (2011). Cell-type-specific consequences of reelin deficiency in the mouse neocortex, hippocampus, and amygdala. *The Journal of Comparative Neurology*, *519*, 2061–2089.

Bozdagi, O., Sakurai, T., Papapetrou, D., Wang, X., Dickstein, D.L., Takahashi, N., Kajiwara, Y., Yang, M., Katz, A.M., Scattoni, M., et al. (2010). Haploinsufficiency of the autism-associated Shank3 gene leads to deficits in synaptic function, social interaction, and social communication. *Molecular Autism*, *1*, 15.

Bozzi, Y., Provenzano, G., and Casarosa, S. (2018). Neurobiological bases of autism-epilepsy comorbidity: a focus on excitation/inhibition imbalance. *European Journal of Neuroscience*, *47*, 534–548.

Braunschweig, D., Simcox, T., Samaco, R.C., and LaSalle, J.M. (2004). X-Chromosome inactivation ratios affect wild-type MeCP2 expression within mosaic Rett syndrome and Mecp2-/+ mouse brain. *Human Molecular Genetics*, *13*, 1275–1286.

Bretin, S., Louis, C., Seguin, L., Wagner, S., Thomas, J.-Y., Challal, S., Rogez, N., Albinet, K., Iop, F., Villain, N., et al. (2017). Pharmacological characterisation of S 47445, a novel positive allosteric modulator of AMPA receptors. *PLOS ONE*, *12*, e0184429.

Bruining, H., Hardstone, R., Juarez-Martinez, E.L., Sprengers, J., Avramiea, A.E., Simpraga, S., Houtman, S.J., Poil, S.S., Dallares, E., Palva, S., et al. (2020). Measurement of excitation-inhibition ratio in autism spectrum disorder using critical brain dynamics. *Scientific Reports*, *10*, 1–15.

Buescher, A.V.S., Cidav, Z., Knapp, M., and Mandell, D.S. (2014). Costs of autism spectrum disorders in the United Kingdom and the United States. *JAMA Pediatrics*, *168*, 721–728.

Buffington, S.A., and Rasband, M.N. (2011). The axon initial segment in nervous system disease and injury. *European Journal of Neuroscience*, *34*, 1609–1619.

Busch, R.M., Srivastava, S., Hogue, O., Frazier, T.W., Klaas, P., Hardan, A., Martinez-Agosto, J.A., Sahin, M., Eng, C., Warfield, S.K., et al. (2019). Neurobehavioral phenotype of autism spectrum disorder associated with germline heterozygous mutations in PTEN. *Translational Psychiatry*, *9*, 1–9.

Butler, M.G., Dazouki, M.J., Zhou, X.P., Talebizadeh, Z., Brown, M., Takahashi, T.N., Miles, J.H., Wang, C.H., Stratton, R., Pilarski, R., et al. (2005). Subset of individuals with autism spectrum disorders and extreme macrocephaly associated with germline PTEN tumour suppressor gene mutations. *Journal of Medical Genetics*, *42*, 318–321.

Buxbaum, J.D., Cai, G., Chaste, P., Nygren, G., Goldsmith, J., Reichert, J., Anckarsäter, H., Rastam, M., Smith, C.J., Silverman, J.M., et al. (2007). Mutation screening of the PTEN gene in patients with autism spectrum disorders and macrocephaly. *American Journal of Medical Genetics, Part B: Neuropsychiatric Genetics*, *144*, 484–491.

Cadwell, C.R., Bhaduri, A., Mostajo-Radji, M.A., Keefe, M.G., and Nowakowski, T.J. (2019). Development and Arealization of the Cerebral Cortex. *Neuron*, *103*, 980–1004.

Cai, C.Z., Han, L.Y., Ji, Z.L., Chen, X., and Chen, Y.Z. (2003). SVM-Prot: Web-based support vector machine software for functional classification of a protein from its primary sequence. *Nucleic Acids Research*, *31*, 3692–3697.

Calderon de Anda, F., Rosario, A.L., Durak, O., Tran, T., Gräff, J., Meletis, K., Rei, D., Soda, T., Madabhushi, R., Ginty, D.D., et al. (2012). Autism spectrum disorder susceptibility gene TAOK2 affects basal dendrite formation in the neocortex. *Nature Neuroscience*, *15*, 1022–1031.

Canitano, R., and Pallagrosi, M. (2017). Autism spectrum disorders and schizophrenia spectrum disorders: Excitation/inhibition imbalance and developmental trajectories. *Frontiers in Psychiatry*, *8*, 1.

Cannelli, N., Tabolacci, E., Rendeli, C., Neri, G., and Gurrieri, F. (2011). No correlation between X chromosome inactivation pattern and autistic spectrum disorders in an Italian cohort of patients. *Open Journal of Genetics*, *01*, 34–37.

Cantagrel, V., Lossi, A.-M., Boulanger, S., Depetris, D., Mattei, M.-G., Gecz, J., Schwartz, C.E., Van Maldergem, L., and Villard, L. (2004). Disruption of a new X linked gene highly expressed in brain in a family with two mentally retarded males. *Journal of Medical Genetics*, *41*, 736–742.

Cantagrel, V., Haddad, M.-R., Ciofi, P., Andrieu, D., Lossi, A.-M., Van Maldergem, L., Roux, J.-C., Villard, L., Maldergem, L. van, Roux, J.-C., et al. (2009). Spatiotemporal expression in mouse brain of Kiaa2022, a gene disrupted in two patients with severe mental retardation. *Gene Expression Patterns*, *9*, 423–429.

Cantanelli, P., Sperduti, S., Ciavardelli, D., Stuppia, L., Gatta, V., and Sensi, S.L. (2014). Age-dependent modifications of AMPA receptor subunit expression levels and related cognitive effects in 3xTg-AD mice. *Frontiers in Aging Neuroscience*, *6*, 200.

Cao, X., and Tabuchi, K. (2017). Functions of synapse adhesion molecules neurexin/neuroligins and neurodevelopmental disorders. *Neuroscience Research*, *116*, 3–9.

Carlisle, H.J., Manzerra, P., Marcora, E., and Kennedy, M.B. (2008). SynGAP regulates steady-state and activity-dependent phosphorylation of cofilin. *Journal of Neuroscience*, *28*, 13673–13683.

Carney, R.M., Wolpert, C.M., Ravan, S.A., Shahbazian, M., Ashley-Koch, A., Cuccaro, M.L., Vance, J.M., and Pericak-Vance, M.A. (2003). Identification of MeCP2 mutations in a series of females with autistic disorder. *Pediatric Neurology*, *28*, 205–211.

Caron, C., Boyault, C., and Khochbin, S. (2005). Regulatory cross-talk between lysine acetylation and ubiquitination: role in the control of protein stability. *BioEssays*, *27*, 408–415.

Carrette, L.L.G., Wang, C.-Y., Wei, C., Press, W., Ma, W., Kelleher, R.J., and Lee, J.T. (2018). A mixed modality approach towards Xi reactivation for Rett syndrome and other X-linked disorders. *Proceedings of the National Academy of Sciences of the United States of America*, *115*, E668–E675.

Carroll, L., Braeutigam, S., Dawes, J.M., Krsnik, Z., Kostovic, I., Coutinho, E., Dewing, J.M., Horton, C.A., Gomez-Nicola, D., and Menassa, D.A. (2021). Autism Spectrum Disorders: Multiple Routes to, and Multiple Consequences of, Abnormal Synaptic Function and Connectivity. *Neuroscientist*, *27*, 10–29.

Carter, T.L., Rissman, R.A., Mishizen-Eberz, A.J., Wolfe, B.B., Hamilton, R.L., Gandy, S., and Armstrong, D.M. (2004). Differential preservation of AMPA receptor subunits in the hippocampi of Alzheimer's disease patients according to Braak

stage. *Experimental Neurology*, *187*, 299–309.

Castelbaum, L., Sylvester, C.M., Zhang, Y., Yu, Q., and Constantino, J.N. (2020). On the Nature of Monozygotic Twin Concordance and Discordance for Autistic Trait Severity: A Quantitative Analysis. *Behavior Genetics*, *50*, 263–272.

Causeret, F., Terao, M., Jacobs, T., Nishimura, Y. V., Yanagawa, Y., Obata, K., Hoshino, M., and Nikolić, M. (2009). The p21-activated kinase is required for neuronal migration in the cerebral cortex. *Cerebral Cortex*, *19*, 861–875.

Chamma, I., and Thoumine, O. (2018). Dynamics, nanoscale organization, and function of synaptic adhesion molecules. *Molecular and Cellular Neuroscience*, *91*, 95–107.

Chang, E.H., Savage, M.J., Flood, D.G., Thomas, J.M., Levy, R.B., Mahadomrongkul, V., Shirao, T., Aoki, C., and Huerta, P.T. (2006). AMPA receptor downscaling at the onset of Alzheimer's disease pathology in double knockin mice. *Proceedings of the National Academy of Sciences of the United States of America*, *103*, 3410–3415.

Chang, P.K.-Y., Verbich, D., and McKinney, R.A. (2012). AMPA receptors as drug targets in neurological disease - advantages, caveats, and future outlook. *European Journal of Neuroscience*, *35*, 1908–1916.

Chapleau, C.A., Calfa, G.D., Lane, M.C., Albertson, A.J., Larimore, J.L., Kudo, S., Armstrong, D.L., Percy, A.K., and Pozzo-Miller, L. (2009). Dendritic spine pathologies in hippocampal pyramidal neurons from Rett syndrome brain and after expression of Rett-associated MECP2 mutations. *Neurobiology of Disease*, *35*, 219–233.

Charzewska, A., Rzońca, S., Janeczko, M., Nawara, M., Smyk, M., Bal, J., and Hoffman-Zacharska, D. (2015). A duplication of the whole *KIAA2022* gene validates the gene role in the pathogenesis of intellectual disability and autism. *Clinical Genetics*, *88*, 297–299.

Chaturvedi, P., Khanna, R., and Parnaik, V.K. (2012). Ubiquitin ligase RNF123 Mediates Degradation of Heterochromatin Protein 1α and β in Lamin A/C Knock-Down Cells. *PLoS ONE*, *7*, e47558.

Chazeau, A., Garcia, M., Czöndör, K., Perrais, D., Tessier, B., Giannone, G., and Thoumine, O. (2015). Mechanical coupling between transsynaptic N-cadherin adhesions and actin flow stabilizes dendritic spines. *Molecular Biology of the Cell*, *26*, 859–873.

Chédotal, A., and Richards, L.J. (2010). Wiring the brain: The biology of neuronal

guidance. *Cold Spring Harbor Perspectives in Biology*, *2*.

Chen, J.A., Peñagarikano, O., Belgard, T.G., Swarup, V., and Geschwind, D.H. (2015a). The Emerging Picture of Autism Spectrum Disorder: Genetics and Pathology. *Annual Review of Pathology: Mechanisms of Disease*, *10*, 111–144.

Chen, Q.-S., Kagan, B.L., Hirakura, Y., and Xie, C.-W. (2000). Impairment of hippocampal long-term potentiation by Alzheimer amyloid β-peptides. *Journal of Neuroscience Research*, *60*, 65–72.

Chen, Y., Huang, W.C., Séjourné, J., Clipperton-Allen, A.E., and Page, D.T. (2015b). Pten mutations alter brain growth trajectory and allocation of cell types through elevated β-Catenin signaling. *Journal of Neuroscience*, *35*, 10252–10267.

Chidambaram, S.B., Rathipriya, A.G., Bolla, S.R., Bhat, A., Ray, B., Mahalakshmi, A.M., Manivasagam, T., Thenmozhi, A.J., Essa, M.M., Guillemin, G.J., et al. (2019). Dendritic spines: Revisiting the physiological role. *Progress in Neuro-Psychopharmacology and Biological Psychiatry*, *92*, 161–193.

Chiurazzi, P., Kiani, A.K., Miertus, J., Barati, S., Manara, E., Paolacci, S., Stuppia, L., Gurrieri, F., and Bertelli, M. (2020). Genetic analysis of intellectual disability and autism. *Acta Biomedica*, *91*, 1–5.

Choi, Y.J., Di Nardo, A., Kramvis, I., Meikle, L., Kwiatkowski, D.J., Sahin, M., and He, X. (2008). Tuberous sclerosis complex proteins control axon formation. *Genes and Development*, *22*, 2485–2495.

Chubykin, A.A., Atasoy, D., Etherton, M.R., Brose, N., Kavalali, E.T., Gibson, J.R., and Südhof, T.C. (2007). Activity-Dependent Validation of Excitatory versus Inhibitory Synapses by Neuroligin-1 versus Neuroligin-2. *Neuron*, *54*, 919–931.

Clement, J.P., Aceti, M., Creson, T.K., Ozkan, E.D., Shi, Y., Reish, N.J., Almonte, A.G., Miller, B.H., Wiltgen, B.J., Miller, C.A., et al. (2012). Pathogenic SYNGAP1 mutations impair cognitive development by disrupting maturation of dendritic spine synapses. *Cell*, *151*, 709–723.

Clement, J.P., Ozkan, E.D., Aceti, M., Miller, C.A., and Rumbaugh, G. (2013). SYNGAP1 links the maturation rate of excitatory synapses to the duration of critical-period synaptic plasticity. *Journal of Neuroscience*, *33*, 10447–10452.

Collingridge, G.L., Isaac, J.T.R., and Wang, Y.T. (2004). Receptor trafficking and synaptic plasticity. *Nature Reviews Neuroscience*, *5*, 952–962.

Colom-Cadena, M., Spires-Jones, T., Zetterberg, H., Blennow, K., Caggiano, A., Dekosky, S.T., Fillit, H., Harrison, J.E., Schneider, L.S., Scheltens, P., et al. (2020).

The clinical promise of biomarkers of synapse damage or loss in Alzheimer's disease. *Alzheimer's Research and Therapy*, *12*, 1–12.

Colvert, E., Tick, B., McEwen, F., Stewart, C., Curran, S.R., Woodhouse, E., Gillan, N., Hallett, V., Lietz, S., Garnett, T., et al. (2015). Heritability of autism spectrum disorder in a UK population-based twin sample. *JAMA Psychiatry*, *72*, 415–423.

Compagni, A., Logan, M., Klein, R., and Adams, R.H. (2003). Control of skeletal patterning by EphrinB1-EphB interactions. *Developmental Cell*, *5*, 217–230.

Cooper, R.A., Richter, F.R., Bays, P.M., Plaisted-Grant, K.C., Baron-Cohen, S., and Simons, J.S. (2017). Reduced hippocampal functional connectivity during episodic memory retrieval in autism. *Cerebral Cortex*, *27*, 888–902.

Courchesne, E., Pierce, K., Schumann, C.M., Redcay, E., Buckwalter, J.A., Kennedy, D.P., and Morgan, J. (2007). Mapping Early Brain Development in Autism. *Neuron*, *56*, 399–413.

Courchesne, E., Campbell, K., and Solso, S. (2011a). Brain growth across the life span in autism: Age-specific changes in anatomical pathology. *Brain Research*, *1380*, 138–145.

Courchesne, E., Mouton, P.R., Calhoun, M.E., Semendeferi, K., Ahrens-Barbeau, C., Hallet, M.J., Barnes, C.C., and Pierce, K. (2011b). Neuron number and size in prefrontal cortex of children with autism. *JAMA - Journal of the American Medical Association*, *306*, 2001–2010.

Courchesne, E., Pramparo, T., Gazestani, V.H., Lombardo, M. V., Pierce, K., and Lewis, N.E. (2019). The ASD Living Biology: from cell proliferation to clinical phenotype. *Molecular Psychiatry*, *24*, 88–107.

Courchet, V., Roberts, A.J., Carmine, P. Del, Lewis, T.L., Polleux, F., and Courchet, J. (2018). Haploinsufficiency of autism candidate gene NUAK1 impairs cortical development and behavior. *BioRxiv*, 262725.

Crawley, J.N. (2007). Mouse Behavioral Assays Relevant to the Symptoms of Autism. *Brain Pathology*, *17*, 448–459.

Culotta, L., and Penzes, P. (2020). Exploring the mechanisms underlying excitation/inhibition imbalance in human iPSC-derived models of ASD. *Molecular Autism*, *11*, 1–11.

Cupolillo, D., Hoxha, E., Faralli, A., De Luca, A., Rossi, F., Tempia, F., and Carulli, D. (2016). Autistic-Like Traits and Cerebellar Dysfunction in Purkinje Cell PTEN Knock-Out Mice. *Neuropsychopharmacology*, *41*, 1457–1466.

Curran, T., and D'Arcangelo, G. (1998). Role of Reelin in the control of brain development. In Brain Research Reviews, (Elsevier), pp. 285–294.

D'Adamo, M.C., Catacuzzeno, L., Di Giovanni, G., Franciolini, F., and Pessia, M. (2013). K+ channelepsy: progress in the neurobiology of potassium channels and epilepsy. *Frontiers in Cellular Neuroscience*, *7*, 134.

D'Amelio, M., Cavallucci, V., Middei, S., Marchetti, C., Pacioni, S., Ferri, A., Diamantini, A., De Zio, D., Carrara, P., Battistini, L., et al. (2011). Caspase-3 triggers early synaptic dysfunction in a mouse model of Alzheimer's disease. *Nature Neuroscience*, *14*, 69–79.

D'Arcangelo, G., Miao, G.G., Chen, S.C., Scares, H.D., Morgan, J.I., and Curran, T. (1995). A protein related to extracellular matrix proteins deleted in the mouse mutant reeler. *Nature*, *374*, 719–723.

Damarla, S.R., Keller, T.A., Kana, R.K., Cherkassky, V.L., Williams, D.L., Minshew, N.J., and Just, M.A. (2010). Cortical underconnectivity coupled with preserved visuospatial cognition in autism: Evidence from an fMRI study of an embedded figures task. *Autism Research*, *3*, 273–279.

Dancy, B.M., and Cole, P.A. (2015). Protein lysine acetylation by p300/CBP. *Chemical Reviews*, *115*, 2419–2452.

Dang, V.T., Kassahn, K.S., Marcos, A.E., and Ragan, M.A. (2008). Identification of human haploinsufficient genes and their genomic proximity to segmental duplications. *European Journal of Human Genetics*, *16*, 1350–1357.

Davenport, E.C., Szulc, B.R., Drew, J., Taylor, J., Morgan, T., Higgs, N.F., López-Doménech, G., and Kittler, J.T. (2019). Autism and Schizophrenia-Associated CYFIP1 Regulates the Balance of Synaptic Excitation and Inhibition. *Cell Reports*, *26*, 2037-2051.e6.

Davis, G.W. (2006). Homeostatic control of neural activity: From phenomenology to molecular design. *Annual Review of Neuroscience*, *29*, 307–323.

Daynac, M., and Petritsch, C.K. (2017). Regulation of asymmetric cell division in mammalian neural stem and cancer precursor cells. In Results and Problems in Cell Differentiation, (Springer Verlag), pp. 375–399.

Depienne, C., Bouteiller, D., Keren, B., Cheuret, E., Poirier, K., Trouillard, O., Benyahia, B., Quelin, C., Carpentier, W., Julia, S., et al. (2009). Sporadic Infantile Epileptic Encephalopathy Caused by Mutations in PCDH19 Resembles Dravet Syndrome but Mainly Affects Females. *PLoS Genetics*, *5*, 1000381.

Dere, E., Dahm, L., Lu, D., Hammerschmidt, K., Ju, A., Tantra, M., KÃ¤stner, A., Chowdhury, K., and Ehrenreich, H. (2014). Heterozygous Ambra1 Deficiency in Mice: A Genetic Trait with Autism-Like Behavior Restricted to the Female Gender. *Frontiers in Behavioral Neuroscience*, *8*, 181.

Derkach, V.A., Oh, M.C., Guire, E.S., and Soderling, T.R. (2007). Regulatory mechanisms of AMPA receptors in synaptic plasticity. *Nature Reviews Neuroscience*, *8*, 101–113.

Desachy, G., Croen, L.A., Torres, A.R., Kharrazi, M., Delorenze, G.N., Windham, G.C., Yoshida, C.K., and Weiss, L.A. (2015). Increased female autosomal burden of rare copy number variants in human populations and in autism families. *Molecular Psychiatry*, *20*, 170–175.

Deutsch, C.K., and Joseph, R.M. (2003). Brief Report: Cognitive Correlates of Enlarged Head Circumference in Children with Autism.

Dewar, D., Chalmers, D.T.T., Graham, D.I.I., and McCulloch, J. (1991). Glutamate metabotropic and AMPA binding sites are reduced in Alzheimer's disease: an autoradiographic study of the hippocampus (Elsevier).

Díaz, E. (2012). SynDIG1 regulation of excitatory synapse maturation. *The Journal of Physiology*, *590*, 33–38.

Dibbens, L.M., Tarpey, P.S., Hynes, K., Bayly, M.A., Scheffer, I.E., Smith, R., Bomar, J., Sutton, E., Vandeleur, L., Shoubridge, C., et al. (2008). X-linked protocadherin 19 mutations cause female-limited epilepsy and cognitive impairment. *Nature Genetics*, *40*, 776–781.

Dickinson, A., Jones, M., and Milne, E. (2016). Measuring neural excitation and inhibition in autism: Different approaches, different findings and different interpretations. *Brain Research*, *1648*, 277–289.

Diering, G.H., and Huganir, R.L. (2018). The AMPA Receptor Code of Synaptic Plasticity. *Neuron*, *100*, 314–329.

Díez-Guerra, F.J. (2010). Neurogranin, a link between calcium/calmodulin and protein kinase C signaling in synaptic plasticity. *IUBMB Life*, *62*, 597–606.

Dong, Z., Han, H., Li, H., Bai, Y., Wang, W., Tu, M., Peng, Y., Zhou, L., He, W., Wu, X., et al. (2015). Long-term potentiation decay and memory loss are mediated by AMPAR endocytosis. *The Journal of Clinical Investigation*, *125*, 234–247.

Donohue, D.E., and Ascoli, G.A. (2008). A comparative computer simulation of dendritic morphology. *PLoS Computational Biology*, *4*, 1000089.

Donovan, A.P.A., and Basson, M.A. (2017). The neuroanatomy of autism - a developmental perspective. *Journal of Anatomy*, *230*, 4–15.

Dotti, C.G., Sullivan, C. a, and Banker, G. a (1988). The establishment of polarity by hippocampal neurons in culture. *The Journal of Neuroscience : The Official Journal of the Society for Neuroscience*, *8*, 1454–1468.

Douglas, R.J., and Martin, K.A.C. (2004). Neuronal circuits of the neocortex. *Annual Review of Neuroscience*, *27*, 419–451.

Drazic, A., Myklebust, L.M., Ree, R., and Arnesen, T. (2016). The world of protein acetylation. *Biochimica et Biophysica Acta - Proteins and Proteomics*, *1864*, 1372–1401.

Du, Y., Fu, M., Huang, Z., Tian, X., Li, J., Pang, Y., Song, W., Tian Wang, Y., and Dong, Z. (2020). TRPV1 activation alleviates cognitive and synaptic plasticity impairments through inhibiting AMPAR endocytosis in APP23/PS45 mouse model of Alzheimer's disease. *Aging Cell*, *19*.

Le Duc, D., Giulivi, C., Hiatt, S.M., Napoli, E., Panoutsopoulos, A., Harlan De Crescenzo, A., Kotzaeridou, U., Syrbe, S., Anagnostou, E., Azage, M., et al. (2019). Pathogenic WDFY3 variants cause neurodevelopmental disorders and opposing effects on brain size. *Brain*, *142*, 2617–2630.

Durak, O., Gao, F., Kaeser-Woo, Y.J., Rueda, R., Martorell, A.J., Nott, A., Liu, C.Y., Watson, L.A., and Tsai, L.H. (2016). Chd8 mediates cortical neurogenesis via transcriptional regulation of cell cycle and Wnt signaling. *Nature Neuroscience*, *19*, 1477–1488.

Durand, C.M., Betancur, C., Boeckers, T.M., Bockmann, J., Chaste, P., Fauchereau, F., Nygren, G., Rastam, M., Gillberg, I.C., Anckarsäter, H., et al. (2007). Mutations in the gene encoding the synaptic scaffolding protein SHANK3 are associated with autism spectrum disorders. *Nature Genetics*, *39*, 25–27.

Durand, C.M., Perroy, J., Loll, F., Perrais, D., Fagni, L., Bourgeron, T., Montcouquiol, M., and Sans, N. (2012). SHANK3 mutations identified in autism lead to modification of dendritic spine morphology via an actin-dependent mechanism. *Molecular Psychiatry*, *17*, 71–84.

Dworzynski, K., Ronald, A., Bolton, P., and Happé, F. (2012). How different are girls and boys above and below the diagnostic threshold for autism spectrum disorders? *Journal of the American Academy of Child and Adolescent Psychiatry*, *51*, 788–797.

Ebisch, S.J.H., Gallese, V., Willems, R.M., Mantini, D., Groen, W.B., Romani, G.L.,

Buitelaar, J.K., and Bekkering, H. (2011). Altered intrinsic functional connectivity of anterior and posterior insula regions in high-functioning participants with autism spectrum disorder. *Human Brain Mapping*, *32*, 1013–1028.

Etherton, M.R., Blaiss, C.A., Powell, C.M., and Südhof, T.C. (2009). Mouse neurexin-1α deletion causes correlated electrophysiological and behavioral changes consistent with cognitive impairments. *Proceedings of the National Academy of Sciences of the United States of America*, *106*, 17998–18003.

Etherton, M.R., Tabuchi, K., Sharma, M., Ko, J., and Südhof, T.C. (2011). An autism-associated point mutation in the neuroligin cytoplasmic tail selectively impairs AMPA receptor-mediated synaptic transmission in hippocampus. *EMBO Journal*, *30*, 2908–2919.

Farach, L.S., and Northrup, H. (2016). *KIAA2022* nonsense mutation in a symptomatic female. *American Journal of Medical Genetics Part A*, *170*, 703–706.

Faux, C., Rakic, S., Andrews, W., and Britto, J.M. (2012). Neurons on the move: Migration and lamination of cortical interneurons. *NeuroSignals*, *20*, 168–189.

Feldmeyer, D. (2012). Excitatory neuronal connectivity in the barrel cortex. *Frontiers in Neuroanatomy*, *6*, 24.

Feng, J., Schroer, R., Yan, J., Song, W., Yang, C., Bockholt, A., Cook, E.H., Skinner, C., Schwartz, C.E., and Sommer, S.S. (2006). High frequency of neurexin 1β signal peptide structural variants in patients with autism. *Neuroscience Letters*, *409*, 10–13.

Fernandes, D., Silva, J., Sotiropoulos, I., and Bretin, S. (2018). A novel modulator of AMPA receptors against Alzheimer's Disease pathology: the first in vivo evidence. *European Neuropsychopharmacology*, *28*, S56–S57.

Fernandez, B.A., and Scherer, S.W. (2017). Syndromic autism spectrum disorders: Moving from a clinically defined to a molecularly defined approach. *Dialogues in Clinical Neuroscience*, *19*, 353–371.

Fernell, E., and Gillberg, C. (2010). Autism spectrum disorder diagnoses in Stockholm preschoolers. *Research in Developmental Disabilities*, *31*, 680–685.

Fieremans, N., Van Esch, H., Holvoet, M., Van Goethem, G., Devriendt, K., Rosello, M., Mayo, S., Martinez, F., Jhangiani, S., Muzny, D.M., et al. (2016). Identification of Intellectual Disability Genes in Female Patients with a Skewed X-Inactivation Pattern. *Human Mutation*, *37*, 804–811.

Fleming, A., and Rubinsztein, D.C. (2020). Autophagy in Neuronal Development

and Plasticity. *Trends in Neurosciences*, *43*, 767–779.

Floricel, F., Higaki, K., Maki, H., Nanba, E., Ninomiya, H., and Ohno, K. (2007). Antisense suppression of TSC1 gene product, hamartin, enhances neurite outgrowth in NGF-treated PC12h cells. *Brain and Development*, *29*, 502–509.

Fombonne, E. (2009). Epidemiology of pervasive developmental disorders. *Pediatric Research*, *65*, 591–598.

Fombonne, E., Rogé, B., Claverie, J., Courty, S., and Frémolle, J. (1999). Microcephaly and macrocephaly in autism. *Journal of Autism and Developmental Disorders*, *29*, 113–119.

Forner, S., Martini, A.C., Prieto, G.A., Dang, C.T., Rodriguez-Ortiz, C.J., Reyes-Ruiz, J.M., Trujillo-Estrada, L., da Cunha, C., Andrews, E.J., Phan, J., et al. (2019). Intra- and extracellular β-amyloid overexpression via adeno-associated virus-mediated gene transfer impairs memory and synaptic plasticity in the hippocampus. *Scientific Reports*, *9*, 1–11.

Fraser, M.M., Zhu, X., Kwon, C.H., Uhlmann, E.J., Gutmann, D.H., and Baker, S.J. (2004). Pten loss causes hypertrophy and increased proliferation of astrocytes in vivo. *Cancer Research*, *64*, 7773–7779.

Fraser, M.M., Bayazitov, I.T., Zakharenko, S.S., and Baker, S.J. (2008). Phosphatase and tensin homolog, deleted on chromosome 10 deficiency in brain causes defects in synaptic structure, transmission and plasticity, and myelination abnormalities. *Neuroscience*, *151*, 476–488.

Friedman, H.V., Bresler, T., Garner, C.C., and Ziv, N.E. (2000). Assembly of new individual excitatory synapses: Time course and temporal order of synaptic molecule recruitment. *Neuron*, *27*, 57–69.

Fuchs, C., Gennaccaro, L., Trazzi, S., Bastianini, S., Bettini, S., Martire, V. Lo, Ren, E., Medici, G., Zoccoli, G., Rimondini, R., et al. (2018). Heterozygous CDKL5 Knockout Female Mice Are a Valuable Animal Model for CDKL5 Disorder. *Neural Plasticity*, *2018*.

Fukuda, T., Itoh, M., Ichikawa, T., Washiyama, K., and Goto, Y.I. (2005). Delayed maturation of neuronal architecture and synaptogenesis in cerebral cortex of Mecp2-deficient mice. *Journal of Neuropathology and Experimental Neurology*, *64*, 537–544.

Gadhave, K., Bolshette, N., Ahire, A., Pardeshi, R., Thakur, K., Trandafir, C., Istrate, A., Ahmed, S., Lahkar, M., Muresanu, D.F., et al. (2016). The ubiquitin proteasomal system: a potential target for the management of Alzheimer's

disease. *Journal of Cellular and Molecular Medicine*, *20*, 1392–1407.

Gan, G.N., Wittschieben, J.P., Wittschieben, B., and Wood, R.D. (2008). DNA polymerase zeta (pol) in higher eukaryotes. *Cell Research*, *18*, 174–183.

Gao, R., and Penzes, P. (2015). Common Mechanisms of Excitatory and Inhibitory Imbalance in Schizophrenia and Autism Spectrum Disorders. *Current Molecular Medicine*, *15*, 146–167.

Gao, L., Tian, M., Zhao, H.-Y., Xu, Q.-Q., Huang, Y.-M., Si, Q.-C., Tian, Q., Wu, Q.-M., Hu, X.-M., Sun, L.-B., et al. (2016). TrkB activation by 7, 8-dihydroxyflavone increases synapse AMPA subunits and ameliorates spatial memory deficits in a mouse model of Alzheimer's disease. *Journal of Neurochemistry*, *136*, 620–636.

Garrido-García, A., de Andrés, R., Jiménez-Pompa, A., Soriano, P., Sanz-Fuentes, D., Martínez-Blanco, E., and Díez-Guerra, F.J. (2019). Neurogranin Expression Is Regulated by Synaptic Activity and Promotes Synaptogenesis in Cultured Hippocampal Neurons. *Molecular Neurobiology*, *56*, 7321–7337.

Gaugler, T., Klei, L., Sanders, S.J., Bodea, C.A., Goldberg, A.P., Lee, A.B., Mahajan, M., Manaa, D., Pawitan, Y., Reichert, J., et al. (2014). Most genetic risk for autism resides with common variation. *Nature Genetics*, *46*, 881–885.

Gelman, S., Palma, J., Tombaugh, G., and Ghavami, A. (2018). Differences in Synaptic Dysfunction between rTg4510 and APP/PS1 Mouse Models of Alzheimer's Disease. *Journal of Alzheimer's Disease*, *61*, 195–208.

Gengler, S., Hamilton, A., and Hölscher, C. (2010). Synaptic Plasticity in the Hippocampus of a APP/PS1 Mouse Model of Alzheimer's Disease Is Impaired in Old but Not Young Mice. *PLoS ONE*, *5*.

Gentet, L.J. (2012). Functional diversity of supragranular GABAergic neurons in the barrel cortex. *Frontiers in Neural Circuits*, *6*, 52.

Geschwind, D.H. (2011). Genetics of autism spectrum disorders. *Trends in Cognitive Sciences*, *15*, 409–416.

Geschwind, D.H., and Levitt, P. (2007). Autism spectrum disorders: developmental disconnection syndromes. *Current Opinion in Neurobiology*, *17*, 103–111.

Giannone, R.J., McDonald, H.W., Hurst, G.B., Shen, R.-F., Wang, Y., and Liu, Y. (2010). The Protein Network Surrounding the Human Telomere Repeat Binding Factors TRF1, TRF2, and POT1. *PLoS ONE*, *5*, e12407.

Giarelli, E., Wiggins, L.D., Rice, C.E., Levy, S.E., Kirby, R.S., Pinto-Martin, J., and

Mandell, D. (2010). Sex differences in the evaluation and diagnosis of autism spectrum disorders among children. *Disability and Health Journal*, *3*, 107–116.

Gilbert, J., and Man, H.-Y. (2016). The X-Linked Autism Protein KIAA2022/KIDLIA Regulates Neurite Outgrowth via N-Cadherin and d-Catenin Signaling. *ENeuro*, *3*, ENEURO.0238-16.2016.

Gilbert, J., and Man, H.-Y. (2017). Fundamental Elements in Autism: From Neurogenesis and Neurite Growth to Synaptic Plasticity. *Frontiers in Cellular Neuroscience*, *11*, 359.

Gilbert, J., O'Connor, M., Templet, S., Moghaddam, M., Di Via Ioschpe, A., Sinclair, A., Zhu, L.-Q., Xu, W., and Man, H.-Y. (2020). NEXMIF/KIDLIA Knock-out Mouse Demonstrates Autism-Like Behaviors, Memory Deficits, and Impairments in Synapse Formation and Function. *The Journal of Neuroscience*, *40*, 237–254.

Gilman, S.R., Iossifov, I., Levy, D., Ronemus, M., Wigler, M., and Vitkup, D. (2011). Rare De Novo Variants Associated with Autism Implicate a Large Functional Network of Genes Involved in Formation and Function of Synapses. *Neuron*, *70*, 898–907.

Giralt, A., Gómez-Climent, M.Á., Alcalá, R., Bretin, S., Bertrand, D., María Delgado-García, J., Pérez-Navarro, E., Alberch, J., and Gruart, A. (2017). The AMPA receptor positive allosteric modulator S 47445 rescues in vivo CA3-CA1 long-term potentiation and structural synaptic changes in old mice. *Neuropharmacology*, *123*, 395–409.

Girard, M., Couvert, P., Carrié, A., Tardieu, M., Chelly, J., Beldjord, C., and Bienvenu, T. (2001). Parental origin of de novo MECP2 mutations in Rett syndrome. *European Journal of Human Genetics*, *9*, 231–236.

Gnanapavan, S., and Giovannoni, G. (2013). Neural cell adhesion molecules in brain plasticity and disease. *Multiple Sclerosis and Related Disorders*, *2*, 13–20.

Godler, D.E., Inaba, Y., Schwartz, C.E., Bui, Q.M., Shi, E.Z., Li, X., Herlihy, A.S., Skinner, C., Hagerman, R.J., Francis, D., et al. (2015). Detection of skewed X-chromosome inactivation in Fragile X syndrome and X chromosome aneuploidy using quantitative melt analysis. *Expert Reviews in Molecular Medicine*, *17*.

Gompers, A.L., Su-Feher, L., Ellegood, J., Copping, N.A., Riyadh, M.A., Stradleigh, T.W., Pride, M.C., Schaffler, M.D., Wade, A.A., Catta-Preta, R., et al. (2017). Germline Chd8 haploinsufficiency alters brain development in mouse. *Nature Neuroscience*, *20*, 1062–1073.

Gonchar, Y., Wang, Q., and Burkhalter, A. (2008). Multiple distinct subtypes of

GABAergic neurons in mouse visual cortex identified by triple immunostaining. *Frontiers in Neuroanatomy*, *1*, 3.

Gong, X., Bacchelli, E., Blasi, F., Toma, C., Betancur, C., Chaste, P., Delorme, R., Durand, C.M., Fauchereau, F., Botros, H.G., et al. (2008). Analysis of X chromosome inactivation in autism spectrum disorders. *American Journal of Medical Genetics Part B: Neuropsychiatric Genetics*, *147B*, 830–835.

Gong, Y., Lippa, C.F., Zhu, J., Lin, Q., and Rosso, A.L. (2009). Disruption of glutamate receptors at Shank-postsynaptic platform in Alzheimer's disease. *Brain Research*, *1292*, 191–198.

Goo, M.S., Scudder, S.L., and Patrick, G.N. (2015). Ubiquitin-dependent trafficking and turnover of ionotropic glutamate receptors. *Frontiers in Molecular Neuroscience*, *8*, 60.

Grandgeorge, M., Lemonnier, E., and Jallot, N. (2013). Autism spectrum disorders: Head circumference and body length at birth are both relative. *Acta Paediatrica, International Journal of Paediatrics*, *102*, 901–907.

Gregorian, C., Nakashima, J., Belle, J. Le, Ohab, J., Kim, R., Liu, A., Smith, K.B., Groszer, M., Garcia, A.D., Sofroniew, M. V., et al. (2009). Pten deletion in adult neural stem/progenitor cells enhances constitutive neurogenesis. *Journal of Neuroscience*, *29*, 1874–1886.

Gribnau, J., and Barakat, T.S. (2017). X-chromosome inactivation and its implications for human disease. *BioRxiv*, 76–95.

Groszer, M., Erickson, R., Scripture-Adams, D.D., Lesche, R., Trumpp, A., Zack, J.A., Kornblum, H.I., Liu, X., and Wu, H. (2001). Negative regulation of neural stem/progenitor cell proliferation by the Pten tumor suppressor gene in vivo. *Science*, *294*, 2186–2189.

Grove, J., Ripke, S., Als, T.D., Mattheisen, M., Walters, R.K., Won, H., Pallesen, J., Agerbo, E., Andreassen, O.A., Anney, R., et al. (2019). Identification of common genetic risk variants for autism spectrum disorder. *Nature Genetics*, *51*, 431–444.

Gu, Z., Liu, W., and Yan, Z. (2009). B-amyloid impairs AMPA receptor trafficking and function by reducing Ca2+/calmodulin-dependent protein kinase II synaptic distribution. *Journal of Biological Chemistry*, *284*, 10639–10649.

Guang, S., Pang, N., Deng, X., Yang, L., He, F., Wu, L., Chen, C., Yin, F., and Peng, J. (2018). Synaptopathology involved in autism spectrum disorder. *Frontiers in Cellular Neuroscience*, *12*, 470.

Guglielmi, L., Servettini, I., Caramia, M., Catacuzzeno, L., Franciolini, F., D'Adamo, M.C., and Pessia, M. (2015). Update on the implication of potassium channels in autism: K(+) channelautism spectrum disorder. *Frontiers in Cellular Neuroscience*, *9*, 34.

Guntupalli, S., Widagdo, J., and Anggono, V. (2016). Amyloid- β -Induced Dysregulation of AMPA Receptor Trafficking. *Neural Plasticity*, *2016*, 1–12.

Guntupalli, S., Jang, S.E., Zhu, T., Huganir, R.L., Widagdo, J., and Anggono, V. (2017). GluA1 subunit ubiquitination mediates amyloid-β-induced loss of surface α-amino-3-hydroxy-5-methyl-4-isoxazolepropionic acid (AMPA) receptors. *The Journal of Biological Chemistry*, *292*, 8186–8194.

Guo, H., Duyzend, M.H., Coe, B.P., Baker, C., Hoekzema, K., Gerdts, J., Turner, T.N., Zody, M.C., Beighley, J.S., Murali, S.C., et al. (2019). Genome sequencing identifies multiple deleterious variants in autism patients with more severe phenotypes. *Genetics in Medicine*, *21*, 1611–1620.

Guo, H., Zhang, Q., Dai, R., Yu, B., Hoekzema, K., Tan, J., Tan, S., Jia, X., Chung, W.K., Hernan, R., et al. (2020). NCKAP1 Disruptive Variants Lead to a Neurodevelopmental Disorder with Core Features of Autism. *American Journal of Human Genetics*, *107*, 963–976.

Gutierrez, R.C., Hung, J., Zhang, Y., Kertesz, A.C., Espina, F.J., and Colicos, M.A. (2009). Altered synchrony and connectivity in neuronal networks expressing an autism-related mutation of neuroligin 3. *Neuroscience*, *162*, 208–221.

Hansel, C. (2019). Deregulation of synaptic plasticity in autism. *Neuroscience Letters*, *688*, 58–61.

Hao, J.-R., Sun, N., Lei, L., Li, X.-Y., Yao, B., Sun, K., Hu, R., Zhang, X., Shi, X.-D., and Gao, C. (2015). L-Stepholidine rescues memory deficit and synaptic plasticity in models of Alzheimer's disease via activating dopamine D1 receptor/PKA signaling pathway. *Cell Death & Disease*, *6*, e1965–e1965.

Happé, F., Ronald, A., and Plomin, R. (2006). Time to give up on a single explanation for autism. *Nature Neuroscience*, *9*, 1218–1220.

Harms, F.L., Kloth, K., Bley, A., Denecke, J., Santer, R., Lessel, D., Hempel, M., and Kutsche, K. (2018). Activating Mutations in PAK1, Encoding p21-Activated Kinase 1, Cause a Neurodevelopmental Disorder. *American Journal of Human Genetics*, *103*, 579–591.

Harris, L.D., Jasem, S., and Licchesi, J.D.F. (2020). The ubiquitin system in Alzheimer's disease. In Advances in Experimental Medicine and Biology,

(Springer), pp. 195–221.

Hartley, S.L., Sikora, D.M., and McCoy, R. (2008). Prevalence and risk factors of maladaptive behaviour in young children with autistic disorder. In Journal of Intellectual Disability Research, (John Wiley & Sons, Ltd), pp. 819–829.

Hatanaka, Y., Zhu, Y., Torigoe, M., Kita, Y., and Murakami, F. (2016). From migration to settlement: The pathways, migration modes and dynamics of neurons in the developing brai. *Proceedings of the Japan Academy Series B: Physical and Biological Sciences*, *92*, 1–19.

Haws, M.E., Jaramillo, T.C., Espinosa, F., Widman, A.J., Stuber, G.D., Sparta, D.R., Tye, K.M., Russo, S.J., Parada, L.F., Stavarache, M., et al. (2014). PTEN knockdown alters dendritic spine/protrusion morphology, not density. *Journal of Comparative Neurology*, *522*, 1171–1190.

Hayashi, K., Ohshima, T., Hashimoto, M., and Mikoshiba, K. (2007). Pak1 regulates dendritic branching and spine formation. *Developmental Neurobiology*, *67*, 655–669.

Hayashi, S., Inoue, Y., Hattori, S., Kaneko, M., Shioi, G., Miyakawa, T., and Takeichi, M. (2017). Loss of X-linked Protocadherin-19 differentially affects the behavior of heterozygous female and hemizygous male mice. *Scientific Reports*, *7*, 1–15.

Hazlett, H.C., Poe, M.D., Gerig, G., Styner, M., Chappell, C., Smith, R.G., Vachet, C., and Piven, J. (2011). Early brain overgrowth in autism associated with an increase in cortical surface area before age 2 years. *Archives of General Psychiatry*, *68*, 467–476.

Heine-Suñer, D., Torres-Juan, L., Morlà, M., Busquets, X., Barceló, F., Picó, G., Bonilla, L., Govea, N., Bernués, M., and Rosell, J. (2003). Fragile-X syndrome and skewed X-chromosome inactivation within a family: A female member with complete inactivation of the functional X chromosome. *American Journal of Medical Genetics Part A*, *122A*, 108–114.

Herrup, K., and Kuemerle, B. (1997). The compartmentalization of the cerebellum. *Annual Review of Neuroscience*, *20*, 61–90.

Hettinger, J.C., Lee, H., Bu, G., Holtzman, D.M., and Cirrito, J.R. (2018). AMPA-ergic regulation of amyloid-β levels in an Alzheimer's disease mouse model. *Molecular Neurodegeneration*, *13*, 22.

Hirotsune, S., Takahara, T., Sasaki, N., Hirose, K., Yoshiki, A., Ohashi, T., Kusakabe, M., Murakami, Y., Muramatsu, M., Watanabe, S., et al. (1995). The

reeler gene encodes a protein with an EGF–like motif expressed by pioneer neurons. *Nature Genetics*, *10*, 77–83.

Homem, C.C.F., Repic, M., and Knoblich, J.A. (2015). Proliferation control in neural stem and progenitor cells. *Nature Reviews Neuroscience*, *16*, 647–659.

Hong, S.E., Shugart, Y.Y., Huang, D.T., Al Shahwan, S., Grant, P.E., Hourihane, J.O.B., Martin, N.D.T., and Walsh, C.A. (2000). Autosomal recessive lissencephaly with cerebellar hypoplasia is associated with human RELN mutations. *Nature Genetics*, *26*, 93–96.

Horlin, C., Falkmer, M., Parsons, R., Albrecht, M.A., and Falkmer, T. (2014). The cost of autism spectrum disorders. *PLoS ONE*, *9*, 106552.

Horn, S., Au, M., Basel-Salmon, L., Bayrak-Toydemir, P., Chapin, A., Cohen, L., Elting, M.W., Graham, J.M., Gonzaga-Jauregui, C., Konen, O., et al. (2019). De novo variants in PAK1 lead to intellectual disability with macrocephaly and seizures (Brain (2019)). *Brain*, *142*, 3351–3359.

Hoshina, N., Johnson-Venkatesh, E.M., Hoshina, M., and Umemori, H. (2021). Female-specific synaptic dysfunction and cognitive impairment in a mouse model of *PCDH19* disorder. *Science*, *372*, eaaz3893.

Hou, L., Antion, M.D., Hu, D., Spencer, C.M., Paylor, R., and Klann, E. (2006). Dynamic Translational and Proteasomal Regulation of Fragile X Mental Retardation Protein Controls mGluR-Dependent Long-Term Depression. *Neuron*, *51*, 441–454.

Hou, Q., Gilbert, J., and Man, H.Y. (2011). Homeostatic regulation of AMPA receptor trafficking and degradation by light-controlled single-synaptic activation. *Neuron*, *72*, 806–818.

Howell, B.W., and Smith, K.M. (2019). Synaptic structural protein dysfunction leads to altered excitation inhibition ratios in models of autism spectrum disorder. *Pharmacological Research*, *139*, 207–214.

Hsieh, H., Boehm, J., Sato, C., Iwatsubo, T., Tomita, T., Sisodia, S., and Malinow, R. (2006). AMPAR Removal Underlies Aβ-Induced Synaptic Depression and Dendritic Spine Loss. *Neuron*, *52*, 831–843.

Hu, Devlin, and Debski (2019). ASD Phenotype—Genotype Associations in Concordant and Discordant Monozygotic and Dizygotic Twins Stratified by Severity of Autistic Traits. *International Journal of Molecular Sciences*, *20*, 3804.

Hu, H., Qin, Y., Bochorishvili, G., Zhu, Y., Van Aelst, L., and Zhu, J.J. (2008). Ras

signaling mechanisms underlying impaired GluR1-dependent plasticity associated with fragile X syndrome. *Journal of Neuroscience*, *28*, 7847–7862.

Hu, W.F., Chahrour, M.H., and Walsh, C.A. (2014). The Diverse Genetic Landscape of Neurodevelopmental Disorders. *Annual Review of Genomics and Human Genetics*, *15*, 195–213.

Huang, N., Lee, I., Marcotte, E.M., and Hurles, M.E. (2010). Characterising and Predicting Haploinsufficiency in the Human Genome. *PLoS Genetics*, *6*, e1001154.

Huang, W., Zhou, Z., Asrar, S., Henkelman, M., Xie, W., and Jia, Z. (2011). p21-Activated Kinases 1 and 3 Control Brain Size through Coordinating Neuronal Complexity and Synaptic Properties. *Molecular and Cellular Biology*, *31*, 388–403.

Huber, K.M., Gallagher, S.M., Warren, S.T., and Bear, M.F. (2002). Altered synaptic plasticity in a mouse model of fragile X mental retardation. *Proceedings of the National Academy of Sciences of the United States of America*, *99*, 7746–7750.

Huguet, G., Ey, E., and Bourgeron, T. (2013). The Genetic Landscapes of Autism Spectrum Disorders. *Annual Review of Genomics and Human Genetics*, *14*, 191–213.

Hull, J. V., Jacokes, Z.J., Torgerson, C.M., Irimia, A., Van Horn, J.D., Aylward, E., Bernier, R., Bookheimer, S., Dapretto, M., Gaab, N., et al. (2017). Resting-state functional connectivity in autism spectrum disorders: A review. *Frontiers in Psychiatry*, *7*, 1.

Humeau, Y., and Choquet, D. (2019). The next generation of approaches to investigate the link between synaptic plasticity and learning. *Nature Neuroscience*, *22*, 1536–1543.

Huo, Y., Khatri, N., Hou, Q., Gilbert, J., Wang, G., and Man, H.-Y. (2015). The deubiquitinating enzyme USP46 regulates AMPA receptor ubiquitination and trafficking. *Journal of Neurochemistry*, *134*, 1067–1080.

Huppke, P., Maier, E.M., Warnke, A., Brendel, C., Laccone, F., and Gärtner, J. (2006). Very mild cases of Rett syndrome with skewed X inactivation. *Journal of Medical Genetics*, *43*, 814–816.

Hutsler, J.J., and Zhang, H. (2010). Increased dendritic spine densities on cortical projection neurons in autism spectrum disorders. *Brain Research*, *1309*, 83–94.

Iakoucheva, L.M., Muotri, A.R., and Sebat, J. (2019). Leading Edge Getting to the

Cores of Autism.

Idring, S., Lundberg, M., Sturm, H., Dalman, C., Gumpert, C., Rai, D., Lee, B.K., and Magnusson, C. (2015). Changes in Prevalence of Autism Spectrum Disorders in 2001–2011: Findings from the Stockholm Youth Cohort. *Journal of Autism and Developmental Disorders*, *45*, 1766–1773.

Iidaka, T., Kogata, T., Mano, Y., and Komeda, H. (2019). Thalamocortical hyperconnectivity and amygdala-cortical hypoconnectivity in Male patients with autism spectrum disorder. *Frontiers in Psychiatry*, *10*, 252.

Inuzuka, H., Gao, D., Finley, L.W.S., Yang, W., Wan, L., Fukushima, H., Chin, Y.R., Zhai, B., Shaik, S., Lau, A.W., et al. (2012). Acetylation-Dependent Regulation of Skp2 Function. *Cell*, *150*, 179–193.

Iossifov, I., Ronemus, M., Levy, D., Wang, Z., Hakker, I., Rosenbaum, J., Yamrom, B., Lee, Y. ha, Narzisi, G., Leotta, A., et al. (2012). De Novo Gene Disruptions in Children on the Autistic Spectrum. *Neuron*, *74*, 285–299.

Ishikawa, T., Miyata, S., Koyama, Y., Yoshikawa, K., Hattori, T., Kumamoto, N., Shingaki, K., Katayama, T., and Tohyama, M. (2012). Transient expression of Xpn, an XLMR protein related to neurite extension, during brain development and participation in neurite outgrowth. *Neuroscience*, *214*, 181–191.

Jackson, M.R., Loring, K.E., Homan, C.C., Thai, M.H.N., Määttänen, L., Arvio, M., Jarvela, I., Shaw, M., Gardner, A., Gecz, J., et al. (2019). Heterozygous loss of function of IQSEC2/Iqsec2 leads to increased activated Arf6 and severe neurocognitive seizure phenotype in females. *Life Science Alliance*, *2*.

Jacob, C.P., Koutsilieri, E., Bartl, J., Neuen-Jacob, E., Arzberger, T., Zander, N., Ravid, R., Roggendorf, W., Riederer, P., and Grünblatt, E. (2007). Alterations in expression of glutamatergic transporters and receptors in sporadic Alzheimer's disease. *Journal of Alzheimer's Disease*, *11*, 97–116.

Jacquemont, S., Coe, B.P., Hersch, M., Duyzend, M.H., Krumm, N., Bergmann, S., Beckmann, J.S., Rosenfeld, J.A., and Eichler, E.E. (2014). A higher mutational burden in females supports a "female protective model" in neurodevelopmental disorders. *American Journal of Human Genetics*, *94*, 415–425.

Jamain, S.S., Quach, H., Betancur, C., Råstam, M., Colineaux, C., Gillberg, C.C., Soderstrom, H., Giros, B., Leboyer, M., Gillberg, C.C., et al. (2003). Mutations of the X-linked genes encoding neuroligins NLGN3 and NLGN4 are associated with autism. *Nature Genetics*, *34*, 27–29.

Jaramillo, T.C., Speed, H.E., Xuan, Z., Reimers, J.M., Liu, S., and Powell, C.M.

(2016). Altered Striatal Synaptic Function and Abnormal Behaviour in Shank3 Exon4-9 Deletion Mouse Model of Autism. *Autism Research*, *9*, 350–375.

Jaramillo, T.C., Speed, H.E., Xuan, Z., Reimers, J.M., Escamilla, C.O., Weaver, T.P., Liu, S., Filonova, I., and Powell, C.M. (2017). Novel Shank3 mutant exhibits behaviors with face validity for autism and altered striatal and hippocampal function. *Autism Research*, *10*, 42–65.

Jarzylo, L.A., and Man, H.Y. (2012). Parasynaptic NMDA receptor signaling couples neuronal glutamate transporter function to AMPA receptor synaptic distribution and stability. *Journal of Neuroscience*, *32*, 2552–2563.

Jaworski, J., Spangler, S., Seeburg, D.P., Hoogenraad, C.C., and Sheng, M. (2005). Control of dendritic arborization by the phosphoinositide-3'-kinase-Akt-mammalian target of rapamycin pathway. *The Journal of Neuroscience : The Official Journal of the Society for Neuroscience*, *25*, 11300–11312.

Jeste, S.S., and Geschwind, D.H. (2014). Disentangling the heterogeneity of autism spectrum disorder through genetic findings. *Nature Reviews. Neurology*, *10*, 74–81.

Ji, J., Lee, H., Argiropoulos, B., Dorrani, N., Mann, J., Martinez-Agosto, J.A., Gomez-Ospina, N., Gallant, N., Bernstein, J.A., Hudgins, L., et al. (2015). DYRK1A haploinsufficiency causes a new recognizable syndrome with microcephaly, intellectual disability, speech impairment, and distinct facies. *European Journal of Human Genetics*, *23*, 1473–1481.

Jiang, Y., Wangler, M.F., McGuire, A.L., Lupski, J.R., Posey, J.E., Khayat, M.M., Murdock, D.R., Sanchez-Pulido, L., Ponting, C.P., Xia, F., et al. (2018). The phenotypic spectrum of Xia-Gibbs syndrome. *American Journal of Medical Genetics, Part A*, *176*, 1315–1326.

Joensuu, M., Lanoue, V., and Hotulainen, P. (2018). Dendritic spine actin cytoskeleton in autism spectrum disorder. *Progress in Neuro-Psychopharmacology and Biological Psychiatry*, *84*, 362–381.

Johnson, W.G. (1980). Metabolic interference and the + - heterozygote. A hypothetical form of simple inheritance which is neither dominant nor recessive. *American Journal of Human Genetics*, *32*, 374–386.

Jokiranta, E., Sourander, A., Suominen, A., Timonen-Soivio, L., Brown, A.S., and Sillanpää, M. (2014). Epilepsy among children and adolescents with autism spectrum disorders: A population-based study. *Journal of Autism and Developmental Disorders*, *44*, 2547–2557.

Ju, J., and Zhou, Q. (2018). Dendritic Spine Modifications in Brain Physiology. In Neuroplasticity - Insights of Neural Reorganization, (InTech), p.

Ju, W., Morishita, W., Tsui, J., Gaietta, G., Deerinck, T.J., Adams, S.R., Garner, C.C., Tsien, R.Y., Ellisman, M.H., and Malenka, R.C. (2004). Activity-dependent regulation of dendritic synthesis and trafficking of AMPA receptors. *Nature Neuroscience*, *7*, 244–253.

Just, M.A., Keller, T.A., Malave, V.L., Kana, R.K., and Varma, S. (2012). Autism as a neural systems disorder: A theory of frontal-posterior underconnectivity. *Neuroscience and Biobehavioral Reviews*, *36*, 1292–1313.

Kaas, J.H. (2013). The evolution of brains from early mammals to humans. *Wiley Interdisciplinary Reviews: Cognitive Science*, *4*, 33–45.

Kalashnikova, E., Lorca, R.A., Kaur, I., Barisone, G.A., Li, B., Ishimaru, T., Trimmer, J.S., Mohapatra, D.P., and Díaz, E. (2010). SynDIG1: An Activity-Regulated, AMPA- Receptor-Interacting Transmembrane Protein that Regulates Excitatory Synapse Development. *Neuron*, *65*, 80–93.

Kalueff, A. V., Stewart, A.M., Song, C., Berridge, K.C., Graybiel, A.M., and Fentress, J.C. (2016). Neurobiology of rodent self-grooming and its value for translational neuroscience. *Nature Reviews Neuroscience*, *17*, 45–59.

Kamenetz, F., Tomita, T., Hsieh, H., Seabrook, G., Borchelt, D., Iwatsubo, T., Sisodia, S., and Malinow, R. (2003). APP Processing and Synaptic Function. *Neuron*, *37*, 925–937.

Kana, R.K., Libero, L.E., Hu, C.P., Deshpande, H.D., and Colburn, J.S. (2014). Functional brain networks and white matter underlying theory-of-mind in autism. *Social Cognitive and Affective Neuroscience*, *9*, 98–105.

Katayama, Y., Nishiyama, M., Shoji, H., Ohkawa, Y., Kawamura, A., Sato, T., Suyama, M., Takumi, T., Miyakawa, T., and Nakayama, K.I. (2016). CHD8 haploinsufficiency results in autistic-like phenotypes in mice. *Nature*, *537*, 675–679.

Kato, M., and Dobyns, W.B. (2003). Lissencephaly and the molecular basis of neuronal migration. *Human Molecular Genetics*, *12*, R89–R96.

Kaushik, G., and Zarbalis, K.S. (2016). Prenatal neurogenesis in autism spectrum disorders. *Frontiers in Chemistry*, *4*, 12.

Keith, D., and El-Husseini, A. (2008). Excitation control: balancing PSD-95 function at the synapse. *Frontiers in Molecular Neuroscience*, *1*, 4.

Keller, T.A., Kana, R.K., and Just, M.A. (2007). A developmental study of the structural integrity of white matter in autism. *NeuroReport*, *18*, 23–27.

Kerstein, P.C., Nichol, R.H., and Gomez, T.M. (2015). Mechanochemical regulation of growth cone motility. *Frontiers in Cellular Neuroscience*, *9*, 244.

Khanna, R., Krishnamoorthy, V., and Parnaik, V.K. (2018). E3 ubiquitin ligase RNF123 targets lamin B1 and lamin-binding proteins. *The FEBS Journal*, *285*, 2243–2262.

Khatri, N., Gilbert, J.P., Huo, Y., Sharaflari, R., Nee, M., Qiao, H., and Man, H.-Y. (2018). The Autism Protein Ube3A/E6AP Remodels Neuronal Dendritic Arborization via Caspase-Dependent Microtubule Destabilization. *The Journal of Neuroscience : The Official Journal of the Society for Neuroscience*, *38*, 363–378.

Khayat, M.M., Li, H., Chander, V., Hu, J., Hansen, A.W., Li, S., Traynelis, J., Shen, H., Weissenberger, G., Stossi, F., et al. (2021). Phenotypic and protein localization heterogeneity associated with AHDC1 pathogenic protein-truncating alleles in Xia–Gibbs syndrome. *Human Mutation*, *42*, 577–591.

Kilinc, D. (2018). The Emerging Role of Mechanics in Synapse Formation and Plasticity. *Frontiers in Cellular Neuroscience*, *12*, 483.

Kim, H.J., Cho, M.H., Shim, W.H., Kim, J.K., Jeon, E.Y., Kim, D.H., and Yoon, S.Y. (2017). Deficient autophagy in microglia impairs synaptic pruning and causes social behavioral defects. *Molecular Psychiatry*, *22*, 1576–1584.

Kim, J., Jung, S.Y., Yeon, K.L., Park, S., Choi, J.S., Lee, C.J., Kim, H.S., Choi, Y.B., Scheiffele, P., Bailey, C.H., et al. (2008). Neuroligin-1 is required for normal expression of LTP and associative fear memory in the amygdala of adult animals. *Proceedings of the National Academy of Sciences of the United States of America*, *105*, 9087–9092.

Kim, J.H., Lee, H.K., Takamiya, K., and Huganir, R.L. (2003). The role of synaptic GTPase-activating protein in neuronal development and synaptic plasticity. *Journal of Neuroscience*, *23*, 1119–1124.

Kim, M.Y., Woo, E.M., Chong, Y.T.E., Homenko, D.R., and Kraus, W.L. (2006). Acetylation of estrogen receptor alpha by p300 at lysines 266 and 268 enhances the deoxyribonucleic acid binding and transactivation activities of the receptor. *Molecular Endocrinology (Baltimore, Md.)*, *20*, 1479–1493.

Kishi, N., and Macklis, J.D. (2004). MECP2 is progressively expressed in post-migratory neurons and is involved in neuronal maturation rather than cell fate decisions. *Molecular and Cellular Neuroscience*, *27*, 306–321.

Klingler, E., Francis, F., Jabaudon, D., and Cappello, S. (2021). Mapping the molecular and cellular complexity of cortical malformations. *Science*, *371*.

Knudsen, G.P.S., Neilson, T.C.S., Pedersen, J., Kerr, A., Schwartz, M., Hulten, M., Bailey, M.E.S., and Ørstavik, K.H. (2006). Increased skewing of X chromosome inactivation in Rett syndrome patients and their mothers. *European Journal of Human Genetics*, *14*, 1189–1194.

Köhling, R., and Wolfart, J. (2016). Potassium Channels in Epilepsy. *Cold Spring Harbor Perspectives in Medicine*, *6*, a022871.

Kohwi, M., and Doe, C.Q. (2013). Temporal fate specification and neural progenitor competence during development. *Nature Reviews Neuroscience*, *14*, 823–838.

Kolodkin, A.L., and Tessier-Lavigne, M. (2011). Mechanisms and molecules of neuronal wiring: A primer. *Cold Spring Harbor Perspectives in Biology*, *3*, 1–14.

Komiyama, N.H., Watabe, A.M., Carlisle, H.J., Porter, K., Charlesworth, P., Monti, J., Strathdee, D.J.C., O'carroll, C.M., Martin, S.J., Morris, R.G.M., et al. (2002). SynGAP Regulates ERK/MAPK Signaling, Synaptic Plasticity, and Learning in the Complex with Postsynaptic Density 95 and NMDA Receptor.

Kopec, C.D., Li, B., Wei, W., Boehm, J., and Malinow, R. (2006). Glutamate receptor exocytosis and spine enlargement during chemically induced long-term potentiation. *Journal of Neuroscience*, *26*, 2000–2009.

Kosugi, S., Hasebe, M., Tomita, M., and Yanagawa, H. (2009). Systematic identification of cell cycle-dependent yeast nucleocytoplasmic shuttling proteins by prediction of composite motifs. *Proceedings of the National Academy of Sciences of the United States of America*, *106*, 10171–10176.

Kouser, M., Speed, H.E., Dewey, C.M., Reimers, J.M., Widman, A.J., Gupta, N., Liu, S., Jaramillo, T.C., Bangash, M., Xiao, B., et al. (2013). Loss of predominant shank3 isoforms results in hippocampus-dependent impairments in behavior and synaptic transmission. *Journal of Neuroscience*, *33*, 18448–18468.

Krumm, N., Turner, T.N., Baker, C., Vives, L., Mohajeri, K., Witherspoon, K., Raja, A., Coe, B.P., Stessman, H.A., He, Z.-X., et al. (2015). Excess of rare, inherited truncating mutations in autism. *Nature Genetics*, *47*, 582–588.

Kubota, Y., Karube, F., Nomura, M., Gulledge, A.T., Mochizuki, A., Schertel, A., and Kawaguchi, Y. (2011). Conserved properties of dendritic trees in four cortical interneuron subtypes. *Scientific Reports*, *1*, 89.

Kuroda, Y., Ohashi, I., Naruto, T., Ida, K., Enomoto, Y., Saito, T., Nagai, J., Wada, T., and Kurosawa, K. (2015). Delineation of the KIAA2022 Mutation Phenotype: Two Patients with X-linked Intellectual Disability and Distinctive Features. *American Journal of Medical Genetics Part A*, *167*, 1349–1353.

Kwok, R.P.S., Liu, X.-T., and Smith, G.D. (2006). Distribution of co-activators CBP and p300 during mouse oocyte and embryo development. *Molecular Reproduction and Development*, *73*, 885–894.

Kwon, C.H., Luikart, B.W., Powell, C.M., Zhou, J., Matheny, S.A., Zhang, W., Li, Y., Baker, S.J., and Parada, L.F. (2006). Pten Regulates Neuronal Arborization and Social Interaction in Mice. *Neuron*, *50*, 377–388.

De La Torre-Ubieta, L., Won, H., Stein, J.L., and Geschwind, D.H. (2016). Advancing the understanding of autism disease mechanisms through genetics. *Nature Medicine*, *22*, 345–361.

Lai, M.-C., and Baron-Cohen, S. (2015). Identifying the lost generation of adults with autism spectrum conditions.

Lainhart, J.E., Piven, J., Wzorek, M., Landa, R., Santangelo, S.L., Coon, H., and Folstein, S.E. (1997). Macrocephaly in children and adults with autism. *Journal of the American Academy of Child and Adolescent Psychiatry*, *36*, 282–290.

Lainhart, J.E., Bigler, E.D., Bocian, M., Coon, H., Dinh, E., Dawson, G., Deutsch, C.K., Dunn, M., Estes, A., Tager-Flusberg, H., et al. (2006). Head circumference and height in autism: A study by the collaborative program of excellence in autism. *American Journal of Medical Genetics, Part A*, *140*, 2257–2274.

Lambert, M.P., Barlow, A.K., Chromy, B.A., Edwards, C., Freed, R., Liosatos, M., Morgan, T.E., Rozovsky, I., Trommer, B., Viola, K.L., et al. (1998). Diffusible, nonfibrillar ligands derived from Aβ1-42 are potent central nervous system neurotoxins. *Proceedings of the National Academy of Sciences of the United States of America*, *95*, 6448–6453.

Lambert, N., Dauve, C., Ranza, E., Makrythanasis, P., Santoni, F., Sloan-Béna, F., Gimelli, S., Blouin, J.-L., Guipponi, M., Bottani, A., et al. (2018). Novel NEXMIF pathogenic variant in a boy with severe autistic features, intellectual disability, and epilepsy, and his mildly affected mother. *Journal of Human Genetics*, *63*, 847–850.

Landa, R.J. (2008). Diagnosis of autism spectrum disorders in the first 3 years of life. *Nature Clinical Practice Neurology*, *4*, 138–147.

Lange, S.S., Tomida, J., Boulware, K.S., Bhetawal, S., and Wood, R.D. (2016). The Polymerase Activity of Mammalian DNA Pol ζ Is Specifically Required for Cell

and Embryonic Viability. *PLoS Genetics*, *12*.

de Lange, I.M., Helbig, K.L., Weckhuysen, S., Møller, R.S., Velinov, M., Dolzhanskaya, N., Marsh, E., Helbig, I., Devinsky, O., Tang, S., et al. (2016). De novo mutations of KIAA2022 in females cause intellectual disability and intractable epilepsy. *Journal of Medical Genetics*, *53*, 850–858.

De Lange, T. (2005). Shelterin: The protein complex that shapes and safeguards human telomeres. *Genes and Development*, *19*, 2100–2110.

Lasser, M., Tiber, J., and Lowery, L.A. (2018). The role of the microtubule cytoskeleton in neurodevelopmental disorders. *Frontiers in Cellular Neuroscience*, *12*, 165.

Lauterborn, J.C., Rex, C.S., Kramár, E., Chen, L.Y., Pandyarajan, V., Lynch, G., and Gall, C.M. (2007). Brain-derived neurotrophic factor rescues synaptic plasticity in a mouse model of fragile X syndrome. *Journal of Neuroscience*, *27*, 10685–10694.

Lauterborn, J.C., Palmer, L.C., Jia, Y., Pham, D.T., Hou, B., Wang, W., Trieu, B.H., Cox, C.D., Kantorovich, S., Gall, C.M., et al. (2016). Chronic Ampakine Treatments Stimulate Dendritic Growth and Promote Learning in Middle-Aged Rats. *The Journal of Neuroscience : The Official Journal of the Society for Neuroscience*, *36*, 1636–1646.

Lavelle, T.A., Weinstein, M.C., Newhouse, J.P., Munir, K., Kuhlthau, K.A., and Prosser, L.A. (2014). Economic burden of childhood autism spectrum disorders. *Pediatrics*, *133*, 520–529.

Lazaro, M.T., Taxidis, J., Shuman, T., Xu, X., Geschwind, D.H., and Correspondence, P.G. (2019). Reduced Prefrontal Synaptic Connectivity and Disturbed Oscillatory Population Dynamics in the CNTNAP2 Model of Autism.

Lee, E., Lee, J., and Kim, E. (2017). Excitation/Inhibition Imbalance in Animal Models of Autism Spectrum Disorders. *Biological Psychiatry*, *81*, 838–847.

Lee, J.E., Bigler, E.D., Alexander, A.L., Lazar, M., DuBray, M.B., Chung, M.K., Johnson, M., Morgan, J., Miller, J.N., McMahon, W.M., et al. (2007). Diffusion tensor imaging of white matter in the superior temporal gyrus and temporal stem in autism. *Neuroscience Letters*, *424*, 127–132.

Lee, K., Goodman, L., Fourie, C., Schenk, S., Leitch, B., and Montgomery, J.M. (2016). AMPA Receptors as Therapeutic Targets for Neurological Disorders. *Advances in Protein Chemistry and Structural Biology*, *103*, 203–261.

Lee, Y.W., Arora, R., Wischnewski, H., and Azzalin, C.M. (2018). TRF1 participates in chromosome end protection by averting TRF2-dependent telomeric R loops. *Nature Structural and Molecular Biology*, *25*, 147–153.

Lessard, J., Wu, J.I., Ranish, J.A., Wan, M., Winslow, M.M., Staahl, B.T., Wu, H., Aebersold, R., Graef, I.A., and Crabtree, G.R. (2007). An Essential Switch in Subunit Composition of a Chromatin Remodeling Complex during Neural Development. *Neuron*, *55*, 201–215.

Leterrier, C. (2018). The axon initial segment: An updated viewpoint. *Journal of Neuroscience*, *38*, 2135–2145.

Levy, D., Ronemus, M., Yamrom, B., Lee, Y. ha, Leotta, A., Kendall, J., Marks, S., Lakshmi, B., Pai, D., Ye, K., et al. (2011). Rare De Novo and Transmitted Copy-Number Variation in Autistic Spectrum Disorders. *Neuron*, *70*, 886–897.

Li, S., and Selkoe, D.J. (2020). A mechanistic hypothesis for the impairment of synaptic plasticity by soluble Aβ oligomers from Alzheimer's brain. *Journal of Neurochemistry*,.

Li, J., Park, E., Zhong, L.R., and Chen, L. (2019a). Homeostatic synaptic plasticity as a metaplasticity mechanism — a molecular and cellular perspective. *Current Opinion in Neurobiology*, *54*, 44–53.

Li, L., Liu, F., Salmonsen, R.A., Turner, T.K., Litofsky, N.S., Di Cristofano, A., Pandolfi, P.P., Jones, S.N., Recht, L.D., and Ross, A.H. (2002). PTEN in neural precursor cells: Regulation of migration, apoptosis, and proliferation. *Molecular and Cellular Neuroscience*, *20*, 21–29.

Li, N., Li, Y., Li, L.-J., Zhu, K., Zheng, Y., and Wang, X.-M. (2019b). Glutamate receptor delocalization in postsynaptic membrane and reduced hippocampal synaptic plasticity in the early stage of Alzheimer's disease. *Neural Regeneration Research*, *14*, 1037.

Li, S., Jin, M., Koeglsperger, T., Shepardson, N.E., Shankar, G.M., and Selkoe, D.J. (2011). Soluble Aβ oligomers inhibit long-term potentiation through a mechanism involving excessive activation of extrasynaptic NR2B-containing NMDA receptors. *The Journal of Neuroscience : The Official Journal of the Society for Neuroscience*, *31*, 6627–6638.

Lim, E.T., Raychaudhuri, S., Sanders, S.J., Stevens, C., Sabo, A., MacArthur, D.G., Neale, B.M., Kirby, A., Ruderfer, D.M., Fromer, M., et al. (2013). Rare Complete Knockouts in Humans: Population Distribution and Significant Role in Autism Spectrum Disorders. *Neuron*, *77*, 235–242.

Lima Caldeira, G., Peça, J., and Carvalho, A.L. (2019). New insights on synaptic dysfunction in neuropsychiatric disorders. *Current Opinion in Neurobiology*, *57*, 62–70.

Limoges, É., Mottron, L., Bolduc, C., Berthiaume, C., and Godbout, R. (2005). Atypical sleep architecture and the autism phenotype. *Brain*, *128*, 1049–1061.

Lin, A., Hou, Q., Jarzylo, L., Amato, S., Gilbert, J., Shang, F., and Man, H.-Y. (2011). Nedd4-mediated AMPA receptor ubiquitination regulates receptor turnover and trafficking. *Journal of Neurochemistry*, *119*, 27–39.

Lin, L., Liu, A., Li, H., Feng, J., and Yan, Z. (2019). Inhibition of Histone Methyltransferases EHMT1/2 Reverses Amyloid-β-Induced Loss of AMPAR Currents in Human Stem Cell-Derived Cortical Neurons. *Journal of Alzheimer's Disease*, *70*, 1175–1185.

Lin, Y.C., Frei, J.A., Kilander, M.B.C., Shen, W., and Blatt, G.J. (2016). A subset of autism-associated genes regulate the structural stability of neurons. *Frontiers in Cellular Neuroscience*, *10*.

Liu, X., Hebron, M.L., Mulki, S., Wang, C., Lekah, E., Ferrante, D., Shi, W., Kurd-Misto, B., and Moussa, C. (2019). Ubiquitin Specific Protease 13 Regulates Tau Accumulation and Clearance in Models of Alzheimer's Disease. *Journal of Alzheimer's Disease*, 1–17.

Llamosas, N., Arora, V., Vij, R., Kilinc, M., Bijoch, L., Rojas, C., Reich, A., Sridharan, B.P., Willems, E., Piper, D.R., et al. (2020). SYNGAP1 controls the maturation of dendrites, synaptic function, and network activity in developing human neurons. *Journal of Neuroscience*, *40*, 7980–7994.

Lledo, P.M., Zhang, X., Südhof, T.C., Malenka, R.C., and Nicoll, R.A. (1998). Postsynaptic membrane fusion and long-term potentiation. *Science (New York, N.Y.)*, *279*, 399–403.

Loomes, R., Hull, L., and Mandy, W.P.L. (2017). What Is the Male-to-Female Ratio in Autism Spectrum Disorder? A Systematic Review and Meta-Analysis. *Journal of the American Academy of Child and Adolescent Psychiatry*, *56*, 466–474.

Lord, C., Rutter, M., Goode, S., Heemsbergen, J., Jordan, H., Mawhood, L., and Schopler, E. (1989). Austism diagnostic observation schedule: A standardized observation of communicative and social behavior. *Journal of Autism and Developmental Disorders*, *19*, 185–212.

Lorenzo, M., Stolte-Dijkstra, I., van Rheenen, P., Smith, R.G., Scheers, T., and Walia, J.S. (2018). Clinical spectrum of *KIAA2022* pathogenic variants in males:

Case report of two boys with *KIAA2022* pathogenic variants and review of the literature. *American Journal of Medical Genetics Part A*, *176*, 1455–1462.

LoTurco, J.J., and Bai, J. (2006). The multipolar stage and disruptions in neuronal migration. *Trends in Neurosciences*, *29*, 407–413.

Lovero, K.L., Blankenship, S.M., Shi, Y., and Nicoll, R.A. (2013). SynDIG1 promotes excitatory synaptogenesis independent of AMPA receptor trafficking and biophysical regulation. *PloS One*, *8*, e66171.

Lu, S., Wang, J., Chitsaz, F., Derbyshire, M.K., Geer, R.C., Gonzales, N.R., Gwadz, M., Hurwitz, D.I., Marchler, G.H., Song, J.S., et al. (2020). CDD/SPARCLE: The conserved domain database in 2020. *Nucleic Acids Research*, *48*, D265–D268.

Lu, W.-Y., Man, H.-Y., Ju, W., Trimble, W.S., MacDonald, J.F., and Wang, Y.T. (2001). Activation of Synaptic NMDA Receptors Induces Membrane Insertion of New AMPA Receptors and LTP in Cultured Hippocampal Neurons. *Neuron*, *29*, 243–254.

Lundbye, C.J., Toft, A.K.H., and Banke, T.G. (2018). Inhibition of GluN2A NMDA receptors ameliorates synaptic plasticity deficits in the Fmr1−/y mouse model. *Journal of Physiology*, *596*, 5017–5031.

Lüscher, C., and Malenka, R.C. (2012). NMDA receptor-dependent long-term potentiation and long-term depression (LTP/LTD). *Cold Spring Harbor Perspectives in Biology*, *4*.

Lüscher, C., Xia, H., Beattie, E.C., Carroll, R.C., von Zastrow, M., Malenka, R.C., and Nicoll, R.A. (1999). Role of AMPA Receptor Cycling in Synaptic Transmission and Plasticity. *Neuron*, *24*, 649–658.

Lv, M., and Ma, Q. (2020). Autophagy in neurodevelopmental disorders. In Advances in Experimental Medicine and Biology, (Springer), pp. 171–182.

Lynch, G. (2006). Glutamate-based therapeutic approaches: Ampakines. *Current Opinion in Pharmacology*, *6*, 82–88.

Ma, T., and Klann, E. (2012). Amyloid β: linking synaptic plasticity failure to memory disruption in Alzheimer's disease. *Journal of Neurochemistry*, *120*, 140–148.

Maenner, M.J., Shaw, K.A., Baio, J., Washington, A., Patrick, M., DiRienzo, M., Christensen, D.L., Wiggins, L.D., Pettygrove, S., Andrews, J.G., et al. (2020). Prevalence of Autism Spectrum Disorder Among Children Aged 8 Years — Autism

and Developmental Disabilities Monitoring Network, 11 Sites, United States, 2016. *MMWR. Surveillance Summaries*, *69*, 1–12.

Magome, T., Hattori, T., Taniguchi, M., Ishikawa, T., Miyata, S., Yamada, K., Takamura, H., Matsuzaki, S., Ito, A., Tohyama, M., et al. (2013). XLMR protein related to neurite extension (Xpn/KIAA2022) regulates cell–cell and cell–matrix adhesion and migration. *Neurochemistry International*, *63*, 561–569.

Mak, A.B., Pehar, M., Nixon, A.M.L., Williams, R.A., Uetrecht, A.C., Puglielli, L., and Moffat, J. (2014). Post-Translational Regulation of CD133 by ATase1/ATase2-Mediated Lysine Acetylation. *J Mol Biol*, *426*, 2175–2182.

Makino, H., and Malinow, R. (2009). AMPA Receptor Incorporation into Synapses during LTP: The Role of Lateral Movement and Exocytosis. *Neuron*, *64*, 381–390.

Van Maldergem, L., Hou, Q., Kalscheuer, V.M., Rio, M., Doco-Fenzy, M., Medeira, A., de Brouwer, A.P.M., Cabrol, C., Haas, S.A., Cacciagli, P., et al. (2013). Loss of function of KIAA2022 causes mild to severe intellectual disability with an autism spectrum disorder and impairs neurite outgrowth. *Human Molecular Genetics*, *22*, 3306–3314.

La Malfa, G., Lassi, S., Bertelli, M., Salvini, R., and Placidi, G.F. (2004). Autism and intellectual disability: A study of prevalence on a sample of the Italian population. *Journal of Intellectual Disability Research*, *48*, 262–267.

Malinow, R., and Malenka, R.C. (2002). AMPA Receptor Trafficking and Synaptic Plasticity. *Annual Review of Neuroscience*, *25*, 103–126.

Mandel, J.L., and Chelly, J. (2004). Monogenic X-linked mental retardation: Is it as frequent as currently estimated? The paradox of the ARX (Aristaless X) mutations. *European Journal of Human Genetics*, *12*, 689–693.

Mandy, W., and Tchanturia, K. (2015). Do women with eating disorders who have social and flexibility difficulties really have autism? A case series. *Molecular Autism*, *6*, 6.

Mannion, A., and Leader, G. (2013). Comorbidity in autism spectrum disorder: A literature review. *Research in Autism Spectrum Disorders*, *7*, 1595–1616.

Marchetto, M.C., Belinson, H., Tian, Y., Freitas, B.C., Fu, C., Vadodaria, K.C., Beltrao-Braga, P.C., Trujillo, C.A., Mendes, A.P.D., Padmanabhan, K., et al. (2017). Altered proliferation and networks in neural cells derived from idiopathic autistic individuals. *Molecular Psychiatry*, *22*, 820–835.

Marco, E.J., and Skuse, D.H. (2006). Autism-lessons from the X chromosome.

Social Cognitive and Affective Neuroscience, *1*, 183–193.

Marder, E., and Goaillard, J.M. (2006). Variability, compensation and homeostasis in neuron and network function. *Nature Reviews Neuroscience*, *7*, 563–574.

Mariani, J., Coppola, G., Zhang, P., Abyzov, A., Provini, L., Tomasini, L., Amenduni, M., Szekely, A., Palejev, D., Wilson, M., et al. (2015). FOXG1-Dependent Dysregulation of GABA/Glutamate Neuron Differentiation in Autism Spectrum Disorders. *Cell*, *162*, 375–390.

Markram, H., Toledo-Rodriguez, M., Wang, Y., Gupta, A., Silberberg, G., and Wu, C. (2004). Interneurons of the neocortical inhibitory system. *Nature Reviews Neuroscience*, *5*, 793–807.

Martínez-Cerdeño, V. (2017). Dendrite and spine modifications in autism and related neurodevelopmental disorders in patients and animal models. *Developmental Neurobiology*, *77*, 393–404.

Di Martino, A., Kelly, C., Grzadzinski, R., Zuo, X.N., Mennes, M., Mairena, M.A., Lord, C., Castellanos, F.X., and Milham, M.P. (2011). Aberrant striatal functional connectivity in children with autism. *Biological Psychiatry*, *69*, 847–856.

Marttinen, M., Takalo, M., Natunen, T., Wittrahm, R., Gabbouj, S., Kemppainen, S., Leinonen, V., Tanila, H., Haapasalo, A., and Hiltunen, M. (2018). Molecular Mechanisms of Synaptotoxicity and Neuroinflammation in Alzheimer's Disease. *Frontiers in Neuroscience*, *12*.

Mash, L.E., Keehn, B., Linke, A.C., Liu, T.T., Helm, J.L., Haist, F., Townsend, J., and Müller, R.A. (2020). Atypical relationships between spontaneous EEG and fMRI activity in Autism. *Brain Connectivity*, *10*, 18–28.

Matson, J.L., and Shoemaker, M. (2009). Intellectual disability and its relationship to autism spectrum disorders. *Research in Developmental Disabilities*, *30*, 1107–1114.

Maximo, J.O., Cadena, E.J., and Kana, R.K. (2014). The implications of brain connectivity in the neuropsychology of autism. *Neuropsychology Review*, *24*, 16–31.

McAllister, A.K. (2002). Conserved cues for axon and dendrite growth in the developing cortex. *Neuron*, *33*, 2–4.

McBride, K.L., Varga, E.A., Pastore, M.T., Prior, T.W., Manickam, K., Atkin, J.F., and Herman, G.E. (2010). Confirmation study of PTEN mutations among individuals with autism or developmental delays/mental retardation and

macrocephaly. *Autism Research*, *3*, 137–141.

McCarthy, M.M., and Wright, C.L. (2017). Convergence of Sex Differences and the Neuroimmune System in Autism Spectrum Disorder. *Biological Psychiatry*, *81*, 402–410.

McClean, P.L., and Hölscher, C. (2014). Liraglutide can reverse memory impairment, synaptic loss and reduce plaque load in aged APP/PS1 mice, a model of Alzheimer's disease. *Neuropharmacology*, *76*, 57–67.

McFadden, K., and Minshew, N.J. (2013). Evidence for dysregulation of axonal growth and guidance in the etiology of ASD. *Frontiers in Human Neuroscience*, *7*.

McKernan, E.P., Russo, N., Burnette, C., and Kates, W.R. (2017). ASD concordance of twins across DSM-IV-TR and DSM-5 diagnostic criteria. *Research in Autism Spectrum Disorders*, *41–42*, 51–56.

Meikle, L., Talos, D.M., Onda, H., Pollizzi, K., Rotenberg, A., Sahin, M., Jensen, F.E., and Kwiatkowski, D.J. (2007). A mouse model of tuberous sclerosis: Neuronal loss of Tsc1 causes dysplastic and ectopic neurons, reduced myelination, seizure activity, and limited survival. *Journal of Neuroscience*, *27*, 5546–5558.

Migeon, B.R. (2020). X-linked diseases: susceptible females. *Genetics in Medicine*, *22*, 1156–1174.

Miles, J.H., Hadden, L.L., Takahashi, T.N., and Hillman, R.E. (2000). Head Circumference Is an Independent Clinical Finding Associated With Autism.

Miller, E.C., Teravskis, P.J., Dummer, B.W., Zhao, X., Huganir, R.L., and Liao, D. (2014). Tau phosphorylation and tau mislocalization mediate soluble Aβ oligomer-induced AMPA glutamate receptor signaling deficits. *European Journal of Neuroscience*, *39*, 1214–1224.

Miñano-Molina, A.J., España, J., Martín, E., Barneda-Zahonero, B., Fadó, R., Solé, M., Trullás, R., Saura, C.A., and Rodríguez-Alvarez, J. (2011). Soluble oligomers of amyloid-β peptide disrupt membrane trafficking of α-amino-3-hydroxy-5-methylisoxazole-4-propionic acid receptor contributing to early synapse dysfunction. *The Journal of Biological Chemistry*, *286*, 27311–27321.

Missler, M., Südhof, T.C., and Biederer, T. (2012). Synaptic cell adhesion. *Cold Spring Harbor Perspectives in Biology*, *4*, a005694.

Miyamae, T., Chen, K., Lewis, D.A., and Gonzalez-Burgos, G. (2017). Distinct physiological maturation of parvalbumin-positive neuron subtypes in mouse

prefrontal cortex. *Journal of Neuroscience*, *37*, 4883–4902.

Miyamoto, T., Kim, D., Knox, J.A., Johnson, E., and Mucke, L. (2016). Increasing the Receptor Tyrosine Kinase EphB2 Prevents Amyloid-β-induced Depletion of Cell Surface Glutamate Receptors by a Mechanism That Requires the PDZ-binding Motif of EphB2 and Neuronal Activity. *The Journal of Biological Chemistry*, *291*, 1719–1734.

Molnar, Z. (2013). Cortical Columns. In Neural Circuit Development and Function in the Healthy and Diseased Brain, J.L.R. Rubenstein, and P. Rakic, eds. (Academic Press), pp. 109–126.

Monteiro-Fernandes, D., Silva, J.M., Soares-Cunha, C., Dalla, C., Kokras, N., Arnaud, F., Billiras, R., Zhuravleva, V., Waites, C., Bretin, S., et al. (2020). Allosteric modulation of AMPA receptors counteracts Tau-related excitotoxic synaptic signaling and memory deficits in stress- and Aβ-evoked hippocampal pathology. *Molecular Psychiatry*, 1–13.

Moog, U., Kutsche, K., Kortüm, F., Chilian, B., Bierhals, T., Apeshiotis, N., Balg, S., Chassaing, N., Coubes, C., Das, S., et al. (2011). Phenotypic spectrum associated with CASK loss-of-function mutations. *Journal of Medical Genetics*, *48*, 741–751.

Moraes, B.J., Coelho, P., Fão, L., Ferreira, I.L., and Rego, A.C. (2020). Modified Glutamatergic Postsynapse in Neurodegenerative Disorders. *Neuroscience*,.

Moretti, P., Levenson, J.M., Battaglia, F., Atkinson, R., Teague, R., Antalffy, B., Armstrong, D., Arancio, O., Sweatt, J.D., and Zoghbi, H.Y. (2006). Learning and memory and synaptic plasticity are impaired in a mouse model of Rett syndrome. *Journal of Neuroscience*, *26*, 319–327.

Morleo, M., and Franco, B. (2008). Dosage compensation of the mammalian X chromosome influences the phenotypic variability of X-linked dominant male-lethal disorders. *Journal of Medical Genetics*, *45*, 401–408.

Morris-Rosendahl, D.J., and Crocq, M.A. (2020). Neurodevelopmental disorders-the history and future of a diagnostic concept. *Dialogues in Clinical Neuroscience*, *22*, 65–72.

Moseley, R.L., Ypma, R.J.F., Holt, R.J., Floris, D., Chura, L.R., Spencer, M.D., Baron-Cohen, S., Suckling, J., Bullmore, E., and Rubinov, M. (2015). Whole-brain functional hypoconnectivity as an endophenotype of autism in adolescents. *NeuroImage: Clinical*, *9*, 140–152.

Mouridsen, S.E., Rich, B., and Isager, T. (2011). A longitudinal study of epilepsy

and other central nervous system diseases in individuals with and without a history of infantile autism. *Brain and Development*, *33*, 361–366.

Moy, S.S., Nadler, J.J., Young, N.B., Nonneman, R.J., Grossman, A.W., Murphy, D.L., D'Ercole, A.J., Crawley, J.N., Magnuson, T.R., and Lauder, J.M. (2009). Social approach in genetically engineered mouse lines relevant to autism. *Genes, Brain and Behavior*, *8*, 129–142.

Moysés-Oliveira, M., Guilherme, R.S., Meloni, V.A., Di Battista, A., de Mello, C.B., Bragagnolo, S., Moretti-Ferreira, D., Kosyakova, N., Liehr, T., Carvalheira, G.M., et al. (2015). X-linked intellectual disability related genes disrupted by balanced X-autosome translocations. *American Journal of Medical Genetics Part B: Neuropsychiatric Genetics*, *168*, 669–677.

Moysés-Oliveira, M., Di-Battista, A., Zamariolli, M., Meloni, V.A., Bragagnolo, S., Christofolini, D.M., Steiner, C.E., Kosyakova, N., Liehr, T., Reymond, A., et al. (2019). Breakpoint mapping at nucleotide resolution in X-autosome balanced translocations associated with clinical phenotypes. *European Journal of Human Genetics*, 1.

Mukaetova-Ladinska, E.B., Arnold, H., Jaros, E., Perry, R., and Perry, E. (2004). Depletion of MAP2 expression and laminar cytoarchitectonic changes in dorsolateral prefrontal cortex in adult autistic individuals. *Neuropathology and Applied Neurobiology*, *30*, 615–623.

Müller, R.A., Shih, P., Keehn, B., Deyoe, J.R., Leyden, K.M., and Shukla, D.K. (2011). Underconnected, but how? A survey of functional connectivity MRI studies in autism spectrum disorders. *Cerebral Cortex*, *21*, 2233–2243.

Munno, D.W., and Syed, N.I. (2003). Synaptogenesis in the CNS: an odyssey from wiring together to firing together. *The Journal of Physiology*, *552*, 1–11.

Murdock, D.R., Jiang, Y., Wangler, M., Khayat, M.M., Sabo, A., Juusola, J., McWalter, K., Schatz, K.S., Gunay-Aygun, M., and Gibbs, R.A. (2019). Xia-Gibbs syndrome in adulthood: A case report with insight into the natural history of the condition. *Cold Spring Harbor Molecular Case Studies*, *5*.

Murray, A.L., Allison, C., Smith, P.L., Baron-Cohen, S., Booth, T., and Auyeung, B. (2017). Investigating diagnostic bias in autism spectrum conditions: An item response theory analysis of sex bias in the AQ-10. *Autism Research*, *10*, 790–800.

Nabavi, S., Fox, R., Proulx, C.D., Lin, J.Y., Tsien, R.Y., and Malinow, R. (2014). Engineering a memory with LTD and LTP. *Nature*, *511*, 348–352.

Namba, T., Funahashi, Y., Nakamuta, S., Xu, C., Takano, T., and Kaibuchi, K.

(2015). Extracellular and Intracellular Signaling for Neuronal Polarity. *Physiological Reviews*, *95*, 995–1024.

Nava, C., Lamari, F., Héron, D., Mignot, C., Rastetter, A., Keren, B., Cohen, D., Faudet, A., Bouteiller, D., Gilleron, M., et al. (2012). Analysis of the chromosome X exome in patients with autism spectrum disorders identified novel candidate genes, including TMLHE. *Translational Psychiatry*, *2*, e179.

Navarro-Pardo, E., López-Ramón, F., Alonso-Esteban, Y., Alcantud-Marín, F., and Es, F.A. (2021). Diagnostic tools for Autism Spectrum Disorders by sex: Analy-sis of current status and future lines.

Nelson, S.B., and Valakh, V. (2015). Excitatory/Inhibitory Balance and Circuit Homeostasis in Autism Spectrum Disorders. *Neuron*, *87*, 684–698.

Neniskyte, U., and Gross, C.T. (2017). Errant gardeners: glial-cell-dependent synaptic pruning and neurodevelopmental disorders. *Nature Publishing Group*, *18*.

Nicholas, J.S., Carpenter, L.A., King, L.B., Jenner, W., and Charles, J.M. (2009). Autism Spectrum Disorders in Preschool-Aged Children: Prevalence and Comparison to a School-Aged Population. *Annals of Epidemiology*, *19*, 808–814.

Nikolov, R.N., Bearss, K.E., Lettinga, J., Erickson, C., Rodowski, M., Aman, M.G., McCracken, J.T., McDougle, C.J., Tierney, E., Vitiello, B., et al. (2009). Gastrointestinal symptoms in a sample of children with pervasive developmental disorders. *Journal of Autism and Developmental Disorders*, *39*, 405–413.

Oddo, S., Caccamo, A., Shepherd, J.D., Murphy, M.P., Golde, T.E., Kayed, R., Metherate, R., Mattson, M.P., Akbari, Y., and LaFerla, F.M. (2003). Triple-transgenic model of Alzheimer's Disease with plaques and tangles: Intracellular Aβ and synaptic dysfunction. *Neuron*, *39*, 409–421.

Oliveira, B., Mitjans, M., Nitsche, M.A., Kuo, M.F., and Ehrenreich, H. (2018). Excitation-inhibition dysbalance as predictor of autistic phenotypes. *Journal of Psychiatric Research*, *104*, 96–99.

Opazo, P., Viana da Silva, S., Carta, M., Breillat, C., Coultrap, S.J., Grillo-Bosch, D., Sainlos, M., Coussen, F., Bayer, K.U., Mulle, C., et al. (2018). CaMKII Metaplasticity Drives Aβ Oligomer-Mediated Synaptotoxicity. *Cell Reports*, *23*, 3137–3145.

Orosco, L.A., Ross, A.P., Cates, S.L., Scott, S.E., Wu, D., Sohn, J., Pleasure, D., Pleasure, S.J., Adamopoulos, I.E., and Zarbalis, K.S. (2014). Loss of Wdfy3 in mice alters cerebral cortical neurogenesis reflecting aspects of the autism pathology. *Nature Communications*, *5*, 1–13.

Orrico, A., Galli, L., Buoni, S., Orsi, A., Vonella, G., and Sorrentino, V. (2009). Novel *PTEN* mutations in neurodevelopmental disorders and macrocephaly. *Clinical Genetics*, *75*, 195–198.

Oyrer, J., Maljevic, S., Scheffer, I.E., Berkovic, S.F., Petrou, S., and Reid, C.A. (2018). Ion channels in genetic epilepsy: From genes and mechanisms to disease-targeted therapies. *Pharmacological Reviews*, *70*, 142–173.

Ozkan, E.D., Creson, T.K., Kramár, E.A., Rojas, C., Seese, R.R., Babyan, A.H., Shi, Y., Lucero, R., Xu, X., Noebels, J.L., et al. (2014). Reduced cognition in Syngap1 mutants is caused by isolated damage within developing forebrain excitatory neurons. *Neuron*, *82*, 1317–1333.

Ozonoff, S., Young, G.S., Carter, A., Messinger, D., Yirmiya, N., Zwaigenbaum, L., Bryson, S., Carver, L.J., Constantino, J.N., Dobkins, K., et al. (2011). Recurrence risk for autism spectrum disorders: A baby siblings research consortium study. *Pediatrics*, *128*, e488.

Packer, A. (2016). Neocortical neurogenesis and the etiology of autism spectrum disorder. *Neuroscience and Biobehavioral Reviews*, *64*, 185–195.

Palop, J.J., and Mucke, L. (2010). Amyloid-B-induced neuronal dysfunction in Alzheimer's disease: From synapses toward neural networks. *Nature Neuroscience*, *13*, 812–818.

Pan, F., Aldridge, G.M., Greenough, W.T., and Gan, W.B. (2010). Dendritic spine instability and insensitivity to modulation by sensory experience in a mouse model of fragile X syndrome. *Proceedings of the National Academy of Sciences of the United States of America*, *107*, 17768–17773.

Pan, X., Chang, X., Leung, C., Zhou, Z., Cao, F., Xie, W., and Jia, Z. (2015). PAK1 regulates cortical development via promoting neuronal migration and progenitor cell proliferation. *Molecular Brain*, *8*, 9.

Panda, P.K., Sharawat, I.K., Joshi, K., Dawman, L., and Bolia, R. (2020). Clinical spectrum of KIAA2022/NEXMIF pathogenic variants in males and females: Report of three patients from Indian kindred with a review of published patients. *Brain and Development*, *42*, 646–654.

Paolicelli, R.C., Bolasco, G., Pagani, F., Maggi, L., Scianni, M., Panzanelli, P., Giustetto, M., Ferreira, T.A., Guiducci, E., Dumas, L., et al. (2011). Synaptic pruning by microglia is necessary for normal brain development. *Science*, *333*, 1456–1458.

Parameshwaran, K., Dhanasekaran, M., and Suppiramaniam, V. (2008). Amyloid

beta peptides and glutamatergic synaptic dysregulation. *Experimental Neurology*, *210*, 7–13.

Parato, J., and Bartolini, F. (2021). The microtubule cytoskeleton at the synapse. *Neuroscience Letters*, *753*, 135850.

Parenti, I., Rabaneda, L.G., Schoen, H., and Novarino, G. (2020). Neurodevelopmental Disorders: From Genetics to Functional Pathways. *Trends in Neurosciences*, *43*, 608–621.

Park, M., Penick, E.C., Edwards, J.G., Kauer, J.A., and Ehlers, M.D. (2004). Recycling endosomes supply AMPA receptors for LTP. *Science*, *305*, 1972–1975.

Park, M., Salgado, J.M., Ostroff, L., Helton, T.D., Robinson, C.G., Harris, K.M., and Ehlers, M.D. (2006). Plasticity-Induced Growth of Dendritic Spines by Exocytic Trafficking from Recycling Endosomes. *Neuron*, *52*, 817–830.

Parkinson, G.T., and Hanley, J.G. (2018). Mechanisms of AMPA receptor endosomal sorting. *Frontiers in Molecular Neuroscience*, *11*, 440.

Patel, P.A., Liang, C., Arora, A., Vijayan, S., Ahuja, S., Wagley, P.K., Settlage, R., LaConte, L.E.W., Goodkin, H.P., Lazar, I., et al. (2020). Haploinsufficiency of X-linked intellectual disability gene CASK induces post-transcriptional changes in synaptic and cellular metabolic pathways. *Experimental Neurology*, *329*, 113319.

Pathania, M., Davenport, E.C., Muir, J., Sheehan, D.F., López-Doménech, G., and Kittler, J.T. (2014). The autism and schizophrenia associated gene CYFIP1 is critical for the maintenance of dendritic complexity and the stabilization of mature spines. *Translational Psychiatry*, *4*, 374.

Paul, A., Nawalpuri, B., Shah, D., Sateesh, S., Muddashetty, R.S., and Clement, J.P. (2019). Differential regulation of syngap1 translation by FMRP modulates eEF2 mediated response on NMDAR activity. *Frontiers in Molecular Neuroscience*, *12*, 97.

Paula-Lima, A.C., Brito-Moreira, J., and Ferreira, S.T. (2013). Deregulation of excitatory neurotransmission underlying synapse failure in Alzheimer's disease. *Journal of Neurochemistry*, *126*, 191–202.

Payer, B. (2016). Developmental regulation of X-chromosome inactivation. *Seminars in Cell & Developmental Biology*, *56*, 88–99.

Peça, J., Feliciano, C., Ting, J.T., Wang, W., Wells, M.F., Venkatraman, T.N., Lascola, C.D., Fu, Z., and Feng, G. (2011). Shank3 mutant mice display autistic-like behaviours and striatal dysfunction. *Nature*, *472*, 437–442.

Pederick, D.T., Richards, K.L., Piltz, S.G., Kumar, R., Mincheva-Tasheva, S., Mandelstam, S.A., Dale, R.C., Scheffer, I.E., Gecz, J., Petrou, S., et al. (2018). Abnormal Cell Sorting Underlies the Unique X-Linked Inheritance of PCDH19 Epilepsy. *Neuron*, *97*, 59-66.e5.

Peñagarikano, O., Abrahams, B.S., Herman, E.I., Winden, K.D., Gdalyahu, A., Dong, H., Sonnenblick, L.I., Gruver, R., Almajano, J., Bragin, A., et al. (2011). Absence of CNTNAP2 leads to epilepsy, neuronal migration abnormalities, and core autism-related deficits. *Cell*, *147*, 235–246.

Peng, Y.J., He, W.Q., Tang, J., Tao, T., Chen, C., Gao, Y.Q., Zhang, W.C., He, X.Y., Dai, Y.Y., Zhu, N.C., et al. (2010). Trio is a key guanine nucleotide exchange factor coordinating regulation of the migration and morphogenesis of granule cells in the developing cerebellum. *Journal of Biological Chemistry*, *285*, 24834–24844.

Pengelly, R.J., Greville-Heygate, S., Schmidt, S., Seaby, E.G., Jabalameli, M.R., Mehta, S.G., Parker, M.J., Goudie, D., Fagotto-Kaufmann, C., Mercer, C., et al. (2016). Mutations specific to the Rac-GEF domain of TRIO cause intellectual disability and microcephaly. *Journal of Medical Genetics*, *53*, 735–742.

Penzes, P., Cahill, M.E., Jones, K.A., Vanleeuwen, J.E., and Woolfrey, K.M. (2011). Dendritic spine pathology in neuropsychiatric disorders. *Nature Neuroscience*, *14*, 285–293.

Persico, A.M., and Bourgeron, T. (2006). Searching for ways out of the autism maze: genetic, epigenetic and environmental clues. *Trends in Neurosciences*, *29*, 349–358.

Petzoldt, A.G., and Sigrist, S.J. (2014). Synaptogenesis.

Pfeiffer, B.E., Zang, T., Wilkerson, J.R., Taniguchi, M., Maksimova, M.A., Smith, L.N., Cowan, C.W., and Huber, K.M. (2010). Fragile X Mental Retardation Protein Is Required for Synapse Elimination by the Activity-Dependent Transcription Factor MEF2. *Neuron*, *66*, 191–197.

Phillips, M., and Pozzo-Miller, L. (2014). Dendritic spine dysgenesis in autism related disorders. *Neuroscience Letters*, *601*, 30–40.

Pinto, D., Pagnamenta, A.T., Klei, L., Anney, R., Merico, D., Regan, R., Conroy, J., Magalhaes, T.R., Correia, C., Abrahams, B.S., et al. (2010). Functional impact of global rare copy number variation in autism spectrum disorders. *Nature*, *466*, 368–372.

Pirozzi, F., Nelson, B., and Mirzaa, G. (2018). From microcephaly to megalencephaly: Determinants of brain size. *Dialogues in Clinical Neuroscience*,

20, 267–282.

Platt, R.J., Zhou, Y., Slaymaker, I.M., Shetty, A.S., Weisbach, N.R., Kim, J.A., Sharma, J., Desai, M., Sood, S., Kempton, H.R., et al. (2017). Chd8 Mutation Leads to Autistic-like Behaviors and Impaired Striatal Circuits. *Cell Reports*, *19*, 335–350.

Plenge, R.M., Stevenson, R.A., Lubs, H.A., Schwartz, C.E., and Willard, H.F. (2002). Skewed X-chromosome inactivation is a common feature of X-linked mental retardation disorders. *American Journal of Human Genetics*, *71*, 168–173.

Port, R.G., Oberman, L.M., and Roberts, T.P.L. (2019). Revisiting the excitation/inhibition imbalance hypothesis of ASD through a clinical lens. *British Journal of Radiology*, *92*.

Pozo, K., and Goda, Y. (2010). Unraveling mechanisms of homeostatic synaptic plasticity. *Neuron*, *66*, 337–351.

Prontera, P., Ottaviani, V., Toccaceli, D., Rogaia, D., Ardisia, C., Romani, R., Stangoni, G., Pierini, A., and Donti, E. (2014). Recurrent ~100 Kb microdeletion in the chromosomal region 14q11.2, involving CHD8 gene, is associated with autism and macrocephaly. *American Journal of Medical Genetics Part A*, *164*, 3137–3141.

Przanowski, P., Wasko, U., Zheng, Z., Yu, J., Sherman, R., Zhu, L.J., McConnell, M.J., Tushir-Singh, J., Green, M.R., and Bhatnagar, S. (2018). Pharmacological reactivation of inactive X-linked Mecp2 in cerebral cortical neurons of living mice. *Proceedings of the National Academy of Sciences of the United States of America*, *115*, 7991–7996.

Purves, D., and Lichtman, J.W. (1980). Elimination of synapses in the developing nervous system. *Science*, *210*, 153–157.

Quesnel-Vallières, M., Weatheritt, R.J., Cordes, S.P., and Blencowe, B.J. (2019). Autism spectrum disorder: insights into convergent mechanisms from transcriptomics. *Nature Reviews Genetics*, *20*, 51–63.

Rajmohan, R., and Reddy, P.H. (2017). Amyloid-Beta and Phosphorylated Tau Accumulations Cause Abnormalities at Synapses of Alzheimer's disease Neurons. *Journal of Alzheimer's Disease*, *57*, 975–999.

Rakic, P. (2008). Confusing cortical columns. *Proceedings of the National Academy of Sciences of the United States of America*, *105*, 12099–12100.

Rakic, P., Bourgeois, J.P., Eckenhoff, M.F., Zecevic, N., and Goldman-Rakic, P.S. (1986). Concurrent overproduction of synapses in diverse regions of the primate

cerebral cortex. *Science*, *232*, 232–235.

Ram Venkataraman, G., O'Connell, C., Egawa, F., Kashef-Haghighi, D., and Wall, D.P. (2017). De novo mutations in autism implicate the synaptic elimination network. In Pacific Symposium on Biocomputing, (World Scientific Publishing Co. Pte Ltd), pp. 521–532.

Raper, J., and Mason, C. (2010). Cellular strategies of axonal pathfinding. *Cold Spring Harbor Perspectives in Biology*, *2*.

Raymond, G. V., Bauman, M.L., and Kemper, T.L. (1995). Hippocampus in autism: a Golgi analysis. *Acta Neuropathologica*, *91*, 117–119.

Reddy, K.S. (2005). Cytogenetic abnormalities and fragile-x syndrome in Autism Spectrum Disorder. *BMC Medical Genetics*, *6*, 3.

Reiersen, A.M., and Todd, R.D. (2008). Co-occurrence of ADHD and autism spectrum disorders: phenomenology and treatment. *Expert Review of Neurotherapeutics*, *8*, 657–669.

Reinders, N.R., Pao, Y., Renner, M.C., da Silva-Matos, C.M., Lodder, T.R., Malinow, R., and Kessels, H.W. (2016). Amyloid-β effects on synapses and memory require AMPA receptor subunit GluA3. *Proceedings of the National Academy of Sciences of the United States of America*, *113*, E6526–E6534.

Reiner, O., Karzbrun, E., Kshirsagar, A., and Kaibuchi, K. (2016). Regulation of neuronal migration, an emerging topic in autism spectrum disorders. *Journal of Neurochemistry*, *136*, 440–456.

Reiserer, R.S., Harrison, F.E., Syverud, D.C., and McDonald, M.P. (2007). Impaired spatial learning in the APP Swe + PSEN1ΔE9 bigenic mouse model of Alzheimer's disease. *Genes, Brain and Behavior*, *6*, 54–65.

Ribeiro, M.C., and MacDonald, J.L. (2020). Sex differences in Mecp2-mutant Rett syndrome model mice and the impact of cellular mosaicism in phenotype development. *Brain Research*, *1729*, 146644.

Riccomagno, M.M., and Kolodkin, A.L. (2015). Sculpting Neural Circuits by Axon and Dendrite Pruning. *Annual Review of Cell and Developmental Biology*, *31*, 779–805.

Rietveld, L., Stuss, D.P., McPhee, D., and Delaney, K.R. (2015). Genotype-specific effects of Mecp2 loss-of-function on morphology of Layer V pyramidal neurons in heterozygous female Rett syndrome model mice. *Frontiers in Cellular Neuroscience*, *9*, 145.

Robinson, E.B., Lichtenstein, P., Anckarsäter, H., Happé, F., and Ronald, A. (2013). Examining and interpreting the female protective effect against autistic behavior. *Proceedings of the National Academy of Sciences of the United States of America*, *110*, 5258–5262.

Rodenas-Cuadrado, P., Ho, J., and Vernes, S.C. (2014). Shining a light on CNTNAP2: Complex functions to complex disorders. *European Journal of Human Genetics*, *22*, 171–178.

Rodrigues, E.M., Scudder, S.L., Goo, M.S., and Patrick, G.N. (2016). Aβ-Induced Synaptic Alterations Require the E3 Ubiquitin Ligase Nedd4-1. *The Journal of Neuroscience : The Official Journal of the Society for Neuroscience*, *36*, 1590–1595.

Romero-Garcia, R., Warrier, V., Bullmore, E.T., Baron-Cohen, S., and Bethlehem, R.A.I. (2019). Synaptic and transcriptionally downregulated genes are associated with cortical thickness differences in autism. *Molecular Psychiatry*, *24*, 1053–1064.

Ronemus, M., Iossifov, I., Levy, D., and Wigler, M. (2014). The role of de novo mutations in the genetics of autism spectrum disorders. *Nature Reviews Genetics*, *15*, 133–141.

Roselli, F., Tirard, M., Lu, J., Hutzler, P., Lamberti, P., Livrea, P., Morabito, M., and Almeida, O.F.X. (2005). Soluble β-amyloid1-40 induces NMDA-Dependent Degradation of Postsynaptic Density-95 at Glutamatergic Synapses. *Journal of Neuroscience*, *25*, 11061–11070.

Rotte, A., Bhandaru, M., Cheng, Y., Sjoestroem, C., Martinka, M., and Li, G. (2013). Decreased Expression of Nuclear p300 Is Associated with Disease Progression and Worse Prognosis of Melanoma Patients. *PLoS ONE*, *8*, e75405.

Roussignol, G., Ango, F., Romorini, S., Tu, J.C., Sala, C., Worley, P.F., Bockaert, J., and Fagni, L. (2005). Shank expression is sufficient to induce functional dendritic spine synapses in aspiny neurons. *Journal of Neuroscience*, *25*, 3560–3570.

De Rubeis, S., Pasciuto, E., Li, K.W., Fernández, E., DiMarino, D., Buzzi, A., Ostroff, L.E., Klann, E., Zwartkruis, F.J.T., Komiyama, N.H., et al. (2013). CYFIP1 coordinates mRNA translation and cytoskeleton remodeling to ensure proper dendritic Spine formation. *Neuron*, *79*, 1169–1182.

De Rubeis, S., He, X., Goldberg, A.P., Poultney, C.S., Samocha, K., Cicek, A.E., Kou, Y., Liu, L., Fromer, M., Walker, S., et al. (2014). Synaptic, transcriptional and chromatin genes disrupted in autism. *Nature*, *515*, 209–215.

Rubenstein, J.L.R., and Merzenich, M.M. (2003). Model of autism: Increased ratio of excitation/inhibition in key neural systems. *Genes, Brain and Behavior*, *2*, 255–267.

Russo, S., Marchi, M., Cogliati, F., Bonati, M.T., Pintaudi, M., Veneselli, E., Saletti, V., Balestrini, M., Ben-Zeev, B., and Larizza, L. (2009). Novel mutations in the CDKL5 gene, predicted effects and associated phenotypes. *Neurogenetics*, *10*, 241–250.

Rylaarsdam, L., and Guemez-Gamboa, A. (2019). Genetic Causes and Modifiers of Autism Spectrum Disorder. *Frontiers in Cellular Neuroscience*, *13*.

Ryoo, K., Hwang, S. gil, Kim, K.J., and Choi, E.J. (2015). RC3/neurogranin negatively regulates extracellular signal-regulated kinase pathway through its interaction with Ras. *Molecular and Cellular Biochemistry*, *402*, 33–40.

Sacai, H., Sakoori, K., Konno, K., Nagahama, K., Suzuki, H., Watanabe, T., Watanabe, M., Uesaka, N., and Kano, M. (2020). Autism spectrum disorder-like behavior caused by reduced excitatory synaptic transmission in pyramidal neurons of mouse prefrontal cortex. *Nature Communications*, *11*, 1–15.

Sacco, R., Militerni, R., Frolli, A., Bravaccio, C., Gritti, A., Elia, M., Curatolo, P., Manzi, B., Trillo, S., Lenti, C., et al. (2007). Clinical, Morphological, and Biochemical Correlates of Head Circumference in Autism. *Biological Psychiatry*, *62*, 1038–1047.

Della Sala, G., and Pizzorusso, T. (2014). Synaptic plasticity and signaling in rett syndrome. *Developmental Neurobiology*, *74*, 178–196.

Samanta, D., and Willis, E. (2020). KIAA2022-related disorders can cause Jeavons (eyelid myoclonia with absence) syndrome. *Acta Neurologica Belgica*, *120*, 205–207.

Samra, A., and Ramtahal, J. (2012). Recurrent subacute visual loss presenting in a 52-year-old Caucasian woman with chronic relapsing inflammatory optic neuropathy: a case report. *Brain*, *139*, 16–17.

Sánchez-Rodríguez, I., Djebari, S., Temprano-Carazo, S., Vega-Avelaira, D., Jiménez-Herrera, R., Iborra-Lázaro, G., Yajeya, J., Jiménez-Díaz, L., and Navarro-López, J.D. (2019). Hippocampal long-term synaptic depression and memory deficits induced in early amyloidopathy are prevented by enhancing G-protein-gated inwardly rectifying potassium channel activity. *Journal of Neurochemistry*, *153*, 362.

Sanders, S.J., Ercan-Sencicek, A.G., Hus, V., Luo, R., Murtha, M.T., Moreno-De-

Luca, D., Chu, S.H., Moreau, M.P., Gupta, A.R., Thomson, S.A., et al. (2011). Multiple Recurrent De Novo CNVs, Including Duplications of the 7q11.23 Williams Syndrome Region, Are Strongly Associated with Autism. *Neuron*, *70*, 863–885.

Sanders, S.J., Murtha, M.T., Gupta, A.R., Murdoch, J.D., Raubeson, M.J., Willsey, A.J., Ercan-Sencicek, A.G., Di Lullo, N.M., Parikshak, N.N., Stein, J.L., et al. (2012). De novo mutations revealed by whole-exome sequencing are strongly associated with autism. *Nature*, *485*, 237–241.

Sanders, S.J., He, X., Willsey, A.J., Ercan-Sencicek, A.G., Samocha, K.E., Cicek, A.E., Murtha, M.T., Bal, V.H., Bishop, S.L., Dong, S., et al. (2015). Insights into Autism Spectrum Disorder Genomic Architecture and Biology from 71 Risk Loci. *Neuron*, *87*, 1215–1233.

Satterstrom, F.K., Kosmicki, J.A., Wang, J., Breen, M.S., De Rubeis, S., An, J.Y., Peng, M., Collins, R., Grove, J., Klei, L., et al. (2020). Large-Scale Exome Sequencing Study Implicates Both Developmental and Functional Changes in the Neurobiology of Autism. *Cell*, *180*, 568-584.e23.

Scala, E., Ariani, F., Mari, F., Caselli, R., Pescucci, C., Longo, I., Meloni, I., Giachino, D., Bruttini, M., Hayek, G., et al. (2005). CDKL5/STK9 is mutated in Rett syndrome variant with infantile spasms. *Journal of Medical Genetics*, *42*, 103–107.

Schaaf, C.P., Sabo, A., Sakai, Y., Crosby, J., Muzny, D., Hawes, A., Lewis, L., Akbar, H., Varghese, R., Boerwinkle, E., et al. (2011). Oligogenic heterozygosity in individuals with high-functioning autism spectrum disorders. *Human Molecular Genetics*, *20*, 3366–3375.

Schmunk, G., and Gargus, J.J. (2013). Channelopathy pathogenesis in autism spectrum disorders. *Frontiers in Genetics*, *4*, 222.

Schubert, D., Kötter, R., and Staiger, J.F. (2007). Mapping functional connectivity in barrel-related columns reveals layer- and cell type-specific microcircuits. *Brain Structure and Function*, *212*, 107–119.

Schwarz, L.A., Hall, B.J., and Patrick, G.N. (2010). Activity-dependent ubiquitination of GluA1 mediates a distinct AMPA receptor endocytosis and sorting pathway. *The Journal of Neuroscience : The Official Journal of the Society for Neuroscience*, *30*, 16718–16729.

Schwede, M., Nagpal, S., Gandal, M.J., Parikshak, N.N., Mirnics, K., Geschwind, D.H., and Morrow, E.M. (2018). Strong correlation of downregulated genes related to synaptic transmission and mitochondria in post-mortem autism cerebral cortex. *Journal of Neurodevelopmental Disorders*, *10*, 18.

Sebat, J., Lakshmi, B., Malhotra, D., Troge, J., Lese-Martin, C., Walsh, T., Yamrom, B., Yoon, S., Krasnitz, A., Kendall, J., et al. (2007). Strong association of de novo copy number mutations with autism. *Science*, *316*, 445–449.

Sebti, S., Prébois, C., Pérez-Gracia, E., Bauvy, C., Desmots, F., Pirot, N., Gongora, C., Bach, A.S., Hubberstey, A. V., Palissot, V., et al. (2014). BAT3 modulates p300-dependent acetylation of p53 and autophagy-related protein 7 (ATG7) during autophagy. *Proceedings of the National Academy of Sciences of the United States of America*, *111*, 4115–4120.

Selkoe, D.J. (2002). Alzheimer's disease is a synaptic failure. *Science (New York, N.Y.)*, *298*, 789–791.

Selkoe, D.J., and Hardy, J. (2016). The amyloid hypothesis of Alzheimer's disease at 25 years. *EMBO Molecular Medicine*, *8*, 595–608.

Shang, Y., Wang, H., Mercaldo, V., Li, X., Chen, T., and Zhuo, M. (2009). Fragile X mental retardation protein is required for chemically-induced long-term potentiation of the hippocampus in adult mice. *Journal of Neurochemistry*, *111*, 635–646.

Shankar, G.M., Li, S., Mehta, T.H., Garcia-Munoz, A., Shepardson, N.E., Smith, I., Brett, F.M., Farrell, M.A., Rowan, M.J., Lemere, C.A., et al. (2008). Amyloid-β protein dimers isolated directly from Alzheimer's brains impair synaptic plasticity and memory. *Nature Medicine*, *14*, 837–842.

Sheng, M., Sabatini, B.L., and Südhof, T.C. (2012). Synapses and Alzheimer's disease. *Cold Spring Harbor Perspectives in Biology*, *4*, 10.

Shepherd, J.D., and Huganir, R.L. (2007). The Cell Biology of Synaptic Plasticity: AMPA Receptor Trafficking. *Annual Review of Cell and Developmental Biology*, *23*, 613–643.

Shi, D., Pop, M.S., Kulikov, R., Love, I.M., Kung, A.L., Kung, A., and Grossman, S.R. (2009). CBP and p300 are cytoplasmic E4 polyubiquitin ligases for p53. *Proceedings of the National Academy of Sciences of the United States of America*, *106*, 16275–16280.

Shi, Q., Chowdhury, S., Ma, R., Le, K.X., Hong, S., Caldarone, B.J., Stevens, B., and Lemere, C.A. (2017). Complement C3 deficiency protects against neurodegeneration in aged plaque-rich APP/PS1 mice. *Science Translational Medicine*, *9*, eaaf6295.

Shihab, H.A., Rogers, M.F., Campbell, C., and Gaunt, T.R. (2017). HIPred: an integrative approach to predicting haploinsufficient genes. *Bioinformatics*, *33*,

btx028.

Siegelbaum, S.A., and Kandel, E.R. (1991). Learning-related synaptic plasticity: LTP and LTD. *Current Opinion in Neurobiology*, *1*, 113–120.

Sikora, J., Leddy, J., Gulinello, M., and Walkley, S.U. (2016). X-linked Christianson syndrome: Heterozygous female Slc9a6 knockout mice develop mosaic neuropathological changes and related behavioral abnormalities. *DMM Disease Models and Mechanisms*, *9*, 13–23.

Da Silva, S.V., Haberl, M.G., Zhang, P., Bethge, P., Lemos, C., Gonçalves, N., Gorlewicz, A., Malezieux, M., Gonçalves, F.Q., Grosjean, N., et al. (2016). Early synaptic deficits in the APP/PS1 mouse model of Alzheimer's disease involve neuronal adenosine A2A receptors. *Nature Communications*, *7*.

Silverman, J.L., Yang, M., Lord, C., and Crawley, J.N. (2010). Behavioural phenotyping assays for mouse models of autism. *Nature Reviews Neuroscience*, *11*, 490–502.

Simonoff, E., Pickles, A., Charman, T., Chandler, S., Loucas, T., and Baird, G. (2008). Psychiatric disorders in children with autism spectrum disorders: Prevalence, comorbidity, and associated factors in a population-derived sample. *Journal of the American Academy of Child and Adolescent Psychiatry*, *47*, 921–929.

Smrt, R.D., Pfeiffer, R.L., and Zhao, X. (2011). Age-dependent expression of MeCP2 in a heterozygous mosaic mouse model. *Human Molecular Genetics*, *20*, 1834–1843.

Snijders Blok, L., Madsen, E., Juusola, J., Gilissen, C., Baralle, D., Reijnders, M.R.F., Venselaar, H., Helsmoortel, C., Cho, M.T., Hoischen, A., et al. (2015). Mutations in DDX3X Are a Common Cause of Unexplained Intellectual Disability with Gender-Specific Effects on Wnt Signaling. *American Journal of Human Genetics*, *97*, 343–352.

Sohal, V.S., and Rubenstein, J.L.R. (2019). Excitation-inhibition balance as a framework for investigating mechanisms in neuropsychiatric disorders. *Molecular Psychiatry*, *24*, 1248–1257.

Sokpor, G., Xie, Y., Rosenbusch, J., and Tuoc, T. (2017). Chromatin remodeling BAF (SWI/SNF) complexes in neural development and disorders. *Frontiers in Molecular Neuroscience*, *10*, 243.

Solso, S., Xu, R., Proudfoot, J., Hagler, D.J., Campbell, K., Venkatraman, V., Carter Barnes, C., Ahrens-Barbeau, C., Pierce, K., Dale, A., et al. (2016). Diffusion

tensor imaging provides evidence of possible axonal overconnectivity in frontal lobes in autism spectrum disorder toddlers. *Biological Psychiatry*, *79*, 676–684.

Song, I., and Huganir, R.L. (2002). Regulation of AMPA receptors during synaptic plasticity. *Trends in Neurosciences*, *25*, 578–588.

Sowers, L.P., Loo, L., Wu, Y., Campbell, E., Ulrich, J.D., Wu, S., Paemka, L., Wassink, T., Meyer, K., Bing, X., et al. (2013). Disruption of the non-canonical Wnt gene PRICKLE2 leads to autism-like behaviors with evidence for hippocampal synaptic dysfunction. *Molecular Psychiatry*, *18*, 1077–1089.

Spence, E.F., and Soderling, S.H. (2015). Actin out: Regulation of the synaptic cytoskeleton. *Journal of Biological Chemistry*, *290*, 28613–28622.

Spence, S.J., and Schneider, M.T. (2009). The role of epilepsy and epileptiform eegs in autism spectrum disorders. *Pediatric Research*, *65*, 599–606.

Spencer, C.M., Alekseyenko, O., Hamilton, S.M., Thomas, A.M., Serysheva, E., Yuva-Paylor, L.A., and Paylor, R. (2011). Modifying behavioral phenotypes in Fmr1KO mice: Genetic background differences reveal autistic-like responses. *Autism Research*, *4*, 40–56.

Spruston, N. (2008). Pyramidal neurons: Dendritic structure and synaptic integration. *Nature Reviews Neuroscience*, *9*, 206–221.

Stamberger, H., Hammer, T.B., Gardella, E., Vlaskamp, D.R.M., Bertelsen, B., Mandelstam, S., de Lange, I., Zhang, J., Myers, C.T., Fenger, C., et al. (2020). NEXMIF encephalopathy: an X-linked disorder with male and female phenotypic patterns. *Genetics in Medicine*, *0*.

Steinberg, J., Honti, F., Meader, S., and Webber, C. (2015). Haploinsufficiency predictions without study bias. *Nucleic Acids Research*, *43*, 101.

Stone, J.L., Merriman, B., Cantor, R.M., Yonan, A.L., Conrad Gilliam, T., Geschwind, D.H., and Nelson, S.F. (2004). Evidence for sex-specific risk alleles in autism spectrum disorder. *American Journal of Human Genetics*, *75*, 1117–1123.

Stoner, R., Chow, M.L., Boyle, M.P., Sunkin, S.M., Mouton, P.R., Roy, S., Wynshaw-Boris, A., Colamarino, S.A., Lein, E.S., and Courchesne, E. (2014). Patches of Disorganization in the Neocortex of Children with Autism. *New England Journal of Medicine*, *370*, 1209–1219.

Storch, E.A., Arnold, E.B., Jones, A.M., Ale, C.M., Wood, J.J., Ehrenreich-May, J., Lewin, A.B., Mutch, P.J., and Murphy, T.K. (2012). The Role of Co-Occurring Disruptive Behavior in the Clinical Presentation of Children and Adolescents with

Anxiety in the Context of Autism Spectrum Disorders. *Child Psychiatry & Human Development*, *43*, 734–746.

Strauss, K.A., Puffenberger, E.G., Huentelman, M.J., Gottlieb, S., Dobrin, S.E., Parod, J.M., Stephan, D.A., and Morton, D.H. (2006). Recessive Symptomatic Focal Epilepsy and Mutant Contactin-Associated Protein-like 2. *New England Journal of Medicine*, *354*, 1370–1377.

Sturman, O., Germain, P.L., and Bohacek, J. (2018). Exploratory rearing: a context- and stress-sensitive behavior recorded in the open-field test. *Stress*, *21*, 443–452.

Stuss, D.P., Boyd, J.D., Levin, D.B., and Delaney, K.R. (2012). MeCP2 Mutation Results in Compartment-Specific Reductions in Dendritic Branching and Spine Density in Layer 5 Motor Cortical Neurons of YFP-H Mice. *PLoS ONE*, *7*, e31896.

Styr, B., and Slutsky, I. (2018). Imbalance between firing homeostasis and synaptic plasticity drives early-phase Alzheimer's disease. *Nature Neuroscience*, *21*, 463–473.

Sultan, K.T., and Shi, S.H. (2018). Generation of diverse cortical inhibitory interneurons. *Wiley Interdisciplinary Reviews: Developmental Biology*, *7*.

Sun, H., Liu, M., Sun, T., Chen, Y., Lan, Z., Lian, B., Zhao, C., Liu, Z., Zhang, J., and Liu, Y. (2019). Age-related changes in hippocampal AD pathology, actin remodeling proteins and spatial memory behavior of male APP/PS1 mice. *Behavioural Brain Research*, *376*, 112182.

Sungur, A.Ö., Vörckel, K.J., Schwarting, R.K.W., and Wöhr, M. (2014). Repetitive behaviors in the Shank1 knockout mouse model for autism spectrum disorder: Developmental aspects and effects of social context. *Journal of Neuroscience Methods*, *234*, 92–100.

Sutton, M.A., Ito, H.T., Cressy, P., Kempf, C., Woo, J.C., and Schuman, E.M. (2006). Miniature Neurotransmission Stabilizes Synaptic Function via Tonic Suppression of Local Dendritic Protein Synthesis. *Cell*, *125*, 785–799.

Swanson, G.T. (2009). Targeting AMPA and kainate receptors in neurological disease: therapies on the horizon? *Neuropsychopharmacology : Official Publication of the American College of Neuropsychopharmacology*, *34*, 249–250.

Tabuchi, K., Blundell, J., Etherton, M.R., Hammer, R.E., Liu, X., Powell, C.M., and Südhof, T.C. (2007). A neuroligin-3 mutation implicated in autism increases inhibitory synaptic transmission in mice. *Science*, *318*, 71–76.

Taherian, M., Maghsoudi, H., Bidaki, K., and Taherian, R. (2016). The Relationship between Skewed X-chromosome Inactivation and Neurological Disorders Development. *International Clinical Neuroscience Journal*,.

Takata, A., Ionita-Laza, I., Gogos, J.A., Xu, B., and Karayiorgou, M. (2016). De Novo Synonymous Mutations in Regulatory Elements Contribute to the Genetic Etiology of Autism and Schizophrenia. *Neuron*, *89*, 940–947.

Takeuchi, K., Gertner, M.J., Zhou, J., Parada, L.F., Bennett, M.V.L., and Zukin, R.S. (2013). Dysregulation of synaptic plasticity precedes appearance of morphological defects in a Pten conditional knockout mouse model of autism. *Proceedings of the National Academy of Sciences of the United States of America*, *110*, 4738–4743.

Talebizadeh, Z., Bittel, D.C., Veatch, O.J., Kibiryeva, N., and Butler, M.G. (2005). Brief report: Non-random X chromosome inactivation in females with autism. *Journal of Autism and Developmental Disorders*, *35*, 675–681.

Tan, A.P., Chong, W.K., and Mankad, K. (2018). Comprehensive genotype-phenotype correlation in lissencephaly. *Quantitative Imaging in Medicine and Surgery*, *8*, 673–693.

Tan, S.S., Faulkner-Jones, B., Breen, S.J., Walsh, M., Bertram, J.F., and Reese, B.E. (1995). Cell dispersion patterns in different cortical regions studied with an X-inactivated transgenic marker. *Development*, *121*, 1029–1039.

Tanaka, H., Sakaguchi, D., and Hirano, T. (2019). Amyloid-β oligomers suppress subunit-specific glutamate receptor increase during LTP. *Alzheimer's and Dementia: Translational Research and Clinical Interventions*, *5*, 797–808.

Tang, G., Gudsnuk, K., Kuo, S.H., Cotrina, M.L., Rosoklija, G., Sosunov, A., Sonders, M.S., Kanter, E., Castagna, C., Yamamoto, A., et al. (2014). Loss of mTOR-Dependent Macroautophagy Causes Autistic-like Synaptic Pruning Deficits. *Neuron*, *83*, 1131–1143.

Tavazoie, S.F., Alvarez, V.A., Ridenour, D.A., Kwiatkowski, D.J., and Sabatini, B.L. (2005). Regulation of neuronal morphology and function by the tumor suppressors Tsc1 and Tsc2. *Nature Neuroscience*, *8*, 1727–1734.

Thapar, A., and Rutter, M. (2015). Neurodevelopmental disorders. In Rutter's Child and Adolescent Psychiatry: Sixth Edition, (John Wiley and Sons Ltd), pp. 31–40.

Thion, M.S., and Garel, S. (2018). Microglia Under the Spotlight: Activity and Complement-Dependent Engulfment of Synapses. *Trends in Neurosciences*, *41*, 332–334.

Thomas, G.H. (1996). High male:female ratio of germ-line mutations: An alternative explanation for postulated gestational lethality in males in X-linked dominant disorders. *American Journal of Human Genetics*, *58*, 1364–1368.

Thomas, M.H., Paris, C., Magnien, M., Colin, J., Pelleïeux, S., Coste, F., Escanyé, M.C., Pillot, T., and Olivier, J.L. (2017). Dietary arachidonic acid increases deleterious effects of amyloid-β oligomers on learning abilities and expression of AMPA receptors: Putative role of the ACSL4-cPLA2 balance. *Alzheimer's Research and Therapy*, *9*, 69.

Thorns, V., Mallory, M., Hansen, L., and Masliah, E. (1997). Alterations in glutamate receptor 2/3 subunits and amyloid precursor protein expression during the course of Alzheimer's disease and Lewy body variant. *Acta Neuropathologica*, *94*, 539–548.

Tian, Y., Yang, C., Shang, S., Cai, Y., Deng, X., Zhang, J., Shao, F., Zhu, D., Liu, Y., Chen, G., et al. (2017). Loss of FMRP impaired hippocampal long-term plasticity and spatial learning in rats. *Frontiers in Molecular Neuroscience*, *10*, 269.

Tick, B., Bolton, P., Happé, F., Rutter, M., and Rijsdijk, F. (2016). Heritability of autism spectrum disorders: a meta-analysis of twin studies. *Journal of Child Psychology and Psychiatry*, *57*, 585–595.

Till, S.M., Asiminas, A., Jackson, A.D., Katsanevaki, D., Barnes, S.A., Osterweil, E.K., Bear, M.F., Chattarji, S., Wood, E.R., Wyllie, D.J.A., et al. (2015). Conserved hippocampal cellular pathophysiology but distinct behavioural deficits in a new rat model of FXS. *Human Molecular Genetics*, *24*, 5977–5984.

Ting, J.T., Kelley, B.G., Lambert, T.J., Cook, D.G., and Sullivan, J.M. (2007). Amyloid precursor protein overexpression depresses excitatory transmission through both presynaptic and postsynaptic mechanisms. *Proceedings of the National Academy of Sciences of the United States of America*, *104*, 353–358.

Towbin, K.E., Pradella, A., Gorrindo, T., Pine, D.S., and Leibenluft, E. (2005). Autism Spectrum Traits in Children with Mood and Anxiety Disorders. *Journal of Child and Adolescent Psychopharmacology*, *15*, 452–464.

Tramutola, A., Triani, F., Di Domenico, F., Barone, E., Cai, J., Klein, J.B., Perluigi, M., and Butterfield, D.A. (2018). Poly-ubiquitin profile in Alzheimer disease brain. *Neurobiology of Disease*, *118*, 129–141.

Travers, B.G., Adluru, N., Ennis, C., Tromp, D.P.M., Destiche, D., Doran, S., Bigler, E.D., Lange, N., Lainhart, J.E., and Alexander, A.L. (2012). Diffusion Tensor Imaging in Autism Spectrum Disorder: A Review. *Autism Research*, *5*, 289–313.

Tremblay, R., Lee, S., and Rudy, B. (2016). GABAergic Interneurons in the Neocortex: From Cellular Properties to Circuits. *Neuron*, *91*, 260–292.

Trinchese, F., Liu, S., Battaglia, F., Walter, S., Mathews, P.M., and Arancio, O. (2004). Progressive age-related development of Alzheimer-like pathology in APP/PS1 mice. *Annals of Neurology*, *55*, 801–814.

Tropea, D., Giacometti, E., Wilson, N.R., Beard, C., McCurry, C., Dong, D.F., Flannery, R., Jaenisch, R., and Sur, M. (2009). Partial reversal of Rett Syndrome-like symptoms in MeCP2 mutant mice. *Proceedings of the National Academy of Sciences of the United States of America*, *106*, 2029–2034.

Trubanova, A., Donlon, K., Kreiser, N.L., Ollendick, T.H., and White, S.W. (2014). Underidentification of Autism Spectrum Disorder in Females: A Case Series Illustrating the Unique Presentation of this Disorder in Young Women. *Scandinavian Journal of Child and Adolescent Psychiatry and Psychology*, *2*, 66–76.

Trzepacz, P.T., Cummings, J., Konechnik, T., Forrester, T.D., Chang, C., Dennehy, E.B., Willis, B.A., Shuler, C., Tabas, L.B., and Lyketsos, C. (2013). Mibampator (LY451395) randomized clinical trial for agitation/aggression in Alzheimer's disease. *International Psychogeriatrics*, *25*, 707–719.

Tsai, N.P., Wilkerson, J.R., Guo, W., Maksimova, M.A., Demartino, G.N., Cowan, C.W., and Huber, K.M. (2012). Multiple autism-linked genes mediate synapse elimination via proteasomal degradation of a synaptic scaffold PSD-95. *Cell*, *151*, 1581–1594.

Tuchman, R., Cuccaro, M., and Alessandri, M. (2010). Autism and epilepsy: Historical perspective. *Brain and Development*, *32*, 709–718.

Tukiainen, T., Villani, A.C., Yen, A., Rivas, M.A., Marshall, J.L., Satija, R., Aguirre, M., Gauthier, L., Fleharty, M., Kirby, A., et al. (2017). Landscape of X chromosome inactivation across human tissues. *Nature*, *550*, 244–248.

Tuoc, T.C., Boretius, S., Sansom, S.N., Pitulescu, M.E., Frahm, J., Livesey, F.J., and Stoykova, A. (2013). Chromatin Regulation by BAF170 Controls Cerebral Cortical Size and Thickness. *Developmental Cell*, *25*, 256–269.

Turner, K.C., Frost, L., Linsenbardt, D., McIlroy, J.R., and Müller, R.A. (2006). Atypically diffuse functional connectivity between caudate nuclei and cerebral cortex in autism. *Behavioral and Brain Functions*, *2*, 1–12.

Turrigiano, G. (2012). Homeostatic synaptic plasticity: local and global mechanisms for stabilizing neuronal function. *Cold Spring Harbor Perspectives in*

Biology, *4*, a005736.

Turrigiano, G.G., and Nelson, S.B. (2004). Homeostatic plasticity in the developing nervous system. *Nature Reviews Neuroscience*, *5*, 97–107.

Twigg, S.R.F., Babbs, C., Van den elzen, M.E.P., Goriely, A., Taylor, S., Mcgowan, S.J., Giannoulatou, E., Lonie, L., Ragoussis, J., Akha, E.S., et al. (2013). Cellular interference in craniofrontonasal syndrome: Males mosaic for mutations in the x-linked EFNB1 gene are more severely affected than true hemizygotes. *Human Molecular Genetics*, *22*, 1654–1662.

Tye, C., Runicles, A.K., Whitehouse, A.J.O., and Alvares, G.A. (2019). Characterizing the Interplay Between Autism Spectrum Disorder and Comorbid Medical Conditions: An Integrative Review. *Frontiers in Psychiatry*, *9*, 751.

Ueda, S., Fujimoto, S., Hiramoto, K., Negishi, M., and Katoh, H. (2008). Dock4 regulates dendritic development in hippocampal neurons. *Journal of Neuroscience Research*, *86*, 3052–3061.

Uhlmann, E.J., Wong, M., Baldwin, R.L., Bajenaru, M.L., Onda, H., Kwiatkowski, D.J., Yamada, K., and Gutmann, D.H. (2002). Astrocyte-specific TSC1 conditional knockout mice exhibit abnormal neuronal organization and seizures. *Annals of Neurology*, *52*, 285–296.

Uzunova, G., Pallanti, S., and Hollander, E. (2016). Excitatory/inhibitory imbalance in autism spectrum disorders: Implications for interventions and therapeutics. *World Journal of Biological Psychiatry*, *17*, 174–186.

Vacca, M., Della Ragione, F., Scalabrì, F., and D'Esposito, M. (2016). X inactivation and reactivation in X-linked diseases. *Seminars in Cell & Developmental Biology*, *56*, 78–87.

Varcin, K.J., and Jeste, S.S. (2017). The emergence of autism spectrum disorder: Insights gained from studies of brain and behaviour in high-risk infants. *Current Opinion in Psychiatry*, *30*, 85–91.

Varga, E.A., Pastore, M., Prior, T., Herman, G.E., and McBride, K.L. (2009). The prevalence of PTEN mutations in a clinical pediatric cohort with autism spectrum disorders, developmental delay, and macrocephaly. *Genetics in Medicine*, *11*, 111–117.

Vargas, J.Y., Fuenzalida, M., and Inestrosa, N.C. (2014). In vivo activation of Wnt signaling pathway enhances cognitive function of adult mice and reverses cognitive deficits in an Alzheimer's disease model. *Journal of Neuroscience*, *34*, 2191–2202.

Vazquez, L.E., Chen, H.J., Sokolova, I., Knuesel, I., and Kennedy, M.B. (2004). SynGAP regulates spine formation. *Journal of Neuroscience*, *24*, 8862–8872.

Verma, V., Paul, A., Vishwanath, A.A., Vaidya, B., and Clement, J.P. (2019). Understanding intellectual disability and autism spectrum disorders from common mouse models: Synapses to behaviour. *Open Biology*, *9*.

Villa, C., and Combi, R. (2016). Potassium Channels and Human Epileptic Phenotypes: An Updated Overview. *Frontiers in Cellular Neuroscience*, *10*, 81.

Vissers, M.E., X Cohen, M., and Geurts, H.M. (2012). Brain connectivity and high functioning autism: A promising path of research that needs refined models, methodological convergence, and stronger behavioral links. *Neuroscience and Biobehavioral Reviews*, *36*, 604–625.

Vitriol, E.A., and Zheng, J.Q. (2012). Growth Cone Travel in Space and Time: The Cellular Ensemble of Cytoskeleton, Adhesion, and Membrane. *Neuron*, *73*, 1068–1081.

De Vries, B.B.A., Wiegers, A.M., Smits, A.P.T., Mohkamsing, S., Duivenvoorden, H.J., Fryns, J.P., Curfs, L.M.G., Halley, D.J.J., Oostra, B.A., Van Den Ouweland, A.M.W., et al. (1996). Mental status of females with an FMR1 gene full mutation. *American Journal of Human Genetics*, *58*, 1025–1032.

Vyas, Y., Montgomery, J.M., and Cheyne, J.E. (2020). Hippocampal Deficits in Amyloid-β-Related Rodent Models of Alzheimer's Disease. *Frontiers in Neuroscience*, *14*.

Waites, C.L., Craig, A.M., and Garner, C.C. (2005). MECHANISMS OF VERTEBRATE SYNAPTOGENESIS. *Annual Review of Neuroscience*, *28*, 251–274.

Wakabayashi, K., Narisawa-Saito, M., Iwakura, Y., Arai, T., Ikeda, K., Takahashi, H., and Nawa, H. (1999). Phenotypic down-regulation of glutamate receptor subunit GluR1 in Alzheimer's disease. *Neurobiology of Aging*, *20*, 287–295.

Walsh, D.M., Klyubin, I., Fadeeva, J. V., Cullen, W.K., Anwyl, R., Wolfe, M.S., Rowan, M.J., and Selkoe, D.J. (2002). Naturally secreted oligomers of amyloid β protein potently inhibit hippocampal long-term potentiation in vivo. *Nature*, *416*, 535–539.

Wang, C.-C., Held, R.G., and Hall, B.J. (2013). SynGAP Regulates Protein Synthesis and Homeostatic Synaptic Plasticity in Developing Cortical Networks. *PLoS ONE*, *8*, e83941.

Wang, D., Yuen, E.Y., Zhou, Y., Yan, Z., and Xiang, Y.K. (2011a). Amyloid β peptide-(1 - 42) induces internalization and degradation of β 2 adrenergic receptors in prefrontal cortical neurons. *Journal of Biological Chemistry*, *286*, 31852–31863.

Wang, G., Li, S., Gilbert, J., Gritton, H.J., Wang, Z., Li, Z., Han, X., Selkoe, D.J., and Man, H.-Y. (2017). Crucial Roles for SIRT2 and AMPA Receptor Acetylation in Synaptic Plasticity and Memory. *Cell Reports*, *20*, 1335–1347.

Wang, S., Tan, N., Zhu, X., Yao, M., Wang, Y., Zhang, X., and Xu, Z. (2018a). Sh3rf2 Haploinsufficiency Leads to Unilateral Neuronal Development Deficits and Autistic-Like Behaviors in Mice. *Cell Reports*, *25*, 2963-2971.e6.

Wang, X., McCoy, P.A., Rodriguiz, R.M., Pan, Y., Je, H.S., Roberts, A.C., Kim, C.J., Berrios, J., Colvin, J.S., Bousquet-Moore, D., et al. (2011b). Synaptic dysfunction and abnormal behaviors in mice lacking major isoforms of Shank3. *Human Molecular Genetics*, *20*, 3093–3108.

Wang, Y., Zeng, C., Li, J., Zhou, Z., Ju, X., Xia, S., Li, Y., Liu, A., Teng, H., Zhang, K., et al. (2018b). PAK2 Haploinsufficiency Results in Synaptic Cytoskeleton Impairment and Autism-Related Behavior. *Cell Reports*, *24*, 2029–2041.

Ward, S.E., Bax, B.D., and Harries, M. (2010). Challenges for and current status of research into positive modulators of AMPA receptors. *British Journal of Pharmacology*, *160*, 181–190.

Wasser, C.R., and Herz, J. (2017). Reelin: Neurodevelopmental architect and homeostatic regulator of excitatory synapses. *Journal of Biological Chemistry*, *292*, 1330–1338.

Webster, R., Cho, M.T., Retterer, K., Millan, F., Nowak, C., Douglas, J., Ahmad, A., Raymond, G.V., Johnson, M.R., Pujol, A., et al. (2017). *De novo* loss of function mutations in *KIAA2022* are associated with epilepsy and neurodevelopmental delay in females. *Clinical Genetics*, *91*, 756–763.

Wegiel, J., Kuchna, I., Nowicki, K., Imaki, H., Wegiel, J., Marchi, E., Ma, S.Y., Chauhan, A., Chauhan, V., Bobrowicz, T.W., et al. (2010). The neuropathology of autism: Defects of neurogenesis and neuronal migration, and dysplastic changes. *Acta Neuropathologica*, *119*, 755–770.

Weiner, J.A. (2006). Protocadherins and synapse development. In Molecular Mechanisms of Synaptogenesis, (Springer US), pp. 137–150.

Weiner, D.J., Wigdor, E.M., Ripke, S., Walters, R.K., Kosmicki, J.A., Grove, J., Samocha, K.E., Goldstein, J.I., Okbay, A., Bybjerg-Grauholm, J., et al. (2017).

Polygenic transmission disequilibrium confirms that common and rare variation act additively to create risk for autism spectrum disorders. *Nature Genetics*, *49*, 978–985.

Weng, S.M., McLeod, F., Bailey, M.E.S., and Cobb, S.R. (2011). Synaptic plasticity deficits in an experimental model of rett syndrome: Long-term potentiation saturation and its pharmacological reversal. *Neuroscience*, *180*, 314–321.

Werling, D.M., and Geschwind, D.H. (2013). Sex differences in autism spectrum disorders. *Current Opinion in Neurology*, *26*, 146–153.

Werling, D.M., Parikshak, N.N., and Geschwind, D.H. (2016). Gene expression in human brain implicates sexually dimorphic pathways in autism spectrum disorders. *Nature Communications*, *7*.

Weston, M.C., Chen, H., and Swann, J.W. (2014). Loss of mTOR repressors Tsc1 or Pten has divergent effects on excitatory and inhibitory synaptic transmission in single hippocampal neuron cultures. *Frontiers in Molecular Neuroscience*, *7*, 1.

Wezenberg, E., Jan Verkes, R., Ruigt, G.S.F., Hulstijn, W., and Sabbe, B.G.C. (2007). Acute Effects of the Ampakine Farampator on Memory and Information Processing in Healthy Elderly Volunteers. *Neuropsychopharmacology*, *32*, 1272–1283.

Whitehouse, A.J.O., Bishop, D.V.M., Ang, Q.W., Pennell, C.E., and Fisher, S.E. (2011). CNTNAP2 variants affect early language development in the general population. *Genes, Brain and Behavior*, *10*, 451–456.

Wible, C.G. (2013). Hippocampal physiology, structure and function and the neuroscience of schizophrenia: A unified account of declarative memory deficits, working memory deficits and schizophrenic symptoms. *Behavioral Sciences*, *3*, 298–315.

Wieland, I., Jakubiczka, S., Muschke, P., Cohen, M., Thiele, H., Gerlach, K.L., Adams, R.H., and Wieacker, P. (2004). Mutations of the ephrin-B1 gene cause craniofrontonasal syndrome. *American Journal of Human Genetics*, *74*, 1209–1215.

Wisniewski, M.L., Hwang, J., and Bahr, B.A. (2011). Submicromolar Aβ42 reduces hippocampal glutamate receptors and presynaptic markers in an aggregation-dependent manner. *Biochimica et Biophysica Acta - Molecular Basis of Disease*, *1812*, 1664–1674.

Won, H., Mah, W., and Kim, E. (2013). Autism spectrum disorder causes, mechanisms, and treatments: focus on neuronal synapses. *Frontiers in Molecular*

Neuroscience, *6*, 19.

Wong, C.T., Bestard-Lorigados, I., and Crawford, D.A. (2019). Autism-related behaviors in the cyclooxygenase-2-deficient mouse model. *Genes, Brain and Behavior*, *18*, e12506.

Wong, C.W., Wang, Y., Liu, T., Li, L., Cheung, S.K.K., Or, P.M.Y., Cheng, A.S.L., Choy, K.W., Burbach, J.P.H., Feng, B., et al. (2020). Autism-associated PTEN missense mutation leads to enhanced nuclear localization and neurite outgrowth in an induced pluripotent stem cell line. *FEBS Journal*, *287*, 4848–4861.

Woodward, N.D., Giraldo-Chica, M., Rogers, B., and Cascio, C.J. (2017). Thalamocortical Dysconnectivity in Autism Spectrum Disorder: An Analysis of the Autism Brain Imaging Data Exchange. *Biological Psychiatry: Cognitive Neuroscience and Neuroimaging*, *2*, 76–84.

Wu, D., Ji, C., Chen, Z., and Wang, K. (2020). Novel NEXMIF gene pathogenic variant in a female patient with refractory epilepsy and intellectual disability. *American Journal of Medical Genetics, Part A*, *182*, 2765–2772.

Wu, G.Y., Zou, D.J., Rajan, I., and Cline, H. (1999). Dendritic dynamics in vivo change during neuronal maturation. *The Journal of Neuroscience : The Official Journal of the Society for Neuroscience*, *19*, 4472–4483.

Wu, H., Luo, J., Yu, H., Rattner, A., Mo, A., Wang, Y., Smallwood, P.M., Erlanger, B., Wheelan, S.J., and Nathans, J. (2014). Cellular resolution maps of X chromosome inactivation: implications for neural development, function, and disease. *Neuron*, *81*, 103–119.

Wurzman, R., Forcelli, P.A., Griffey, C.J., and Kromer, L.F. (2015). Repetitive grooming and sensorimotor abnormalities in an ephrin-A knockout model for Autism Spectrum Disorders. *Behavioural Brain Research*, *278*, 115–128.

Xia, F., Bainbridge, M.N., Tan, T.Y., Wangler, M.F., Scheuerle, A.E., Zackai, E.H., Harr, M.H., Sutton, V.R., Nalam, R.L., Zhu, W., et al. (2014). De novo truncating mutations in AHDC1 in individuals with syndromic expressive language delay, hypotonia, and sleep apnea. *American Journal of Human Genetics*, *94*, 784–789.

Xiao, Y., Peng, Y., Wan, J., Tang, G., Chen, Y., Tang, J., Ye, W.C., Ip, N.Y., and Shi, L. (2013). The atypical guanine nucleotide exchange factor Dock4 regulates neurite differentiation through modulation of Rac1 GTPase and actin dynamics. *Journal of Biological Chemistry*, *288*, 20034–20045.

Xu, G., Strathearn, L., Liu, B., O'Brien, M., Kopelman, T.G., Zhu, J., Snetselaar, L.G., and Bao, W. (2019). Prevalence and Treatment Patterns of Autism Spectrum

Disorder in the United States, 2016. *JAMA Pediatrics*, *173*, 153–159.

Xu, Q., Liu, Y.Y., Wang, X., Tan, G.H., Li, H.P., Hulbert, S.W., Li, C.Y., Hu, C.C., Xiong, Z.Q., Xu, X., et al. (2018). Autism-associated CHD8 deficiency impairs axon development and migration of cortical neurons. *Molecular Autism*, *9*, 1–17.

Yabut, O., Renfro, A., Niu, S., Swann, J.W., Marín, O., and D'Arcangelo, G. (2007). Abnormal laminar position and dendrite development of interneurons in the reeler forebrain. *Brain Research*, *1140*, 75–83.

Yan, J., and Kurgan, L. (2017). DRNApred, fast sequence-based method that accurately predicts and discriminates DNA-and RNA-binding residues. *Nucleic Acids Research*, *45*, e84.

Yan, Z., Kim, E., Datta, D., Lewis, D.A., and Soderling, S.H. (2016). Synaptic actin dysregulation, a convergent mechanism of mental disorders? In Journal of Neuroscience, (Society for Neuroscience), pp. 11411–11417.

Yang, X. (2020). Characterizing spine issues: If offers novel therapeutics to Angelman syndrome. *Developmental Neurobiology*, *80*, 200–209.

Yang, M., Bozdagi, O., Scattoni, M.L., Wöhr, M., Roullet, F.I., Katz, A.M., Abrams, D.N., Kalikhman, D., Simon, H., Woldeyohannes, L., et al. (2012). Reduced excitatory neurotransmission and mild Autism-Relevant phenotypes in adolescent shank3 null mutant mice. *Journal of Neuroscience*, *32*, 6525–6541.

Yang, Y., Li, S., Wang, Y., Ma, Z., Wong, K.-C., and Li, X. (2021). Identification of haploinsufficient genes from epigenomic data using deep forest. *Briefings in Bioinformatics*,.

Yasuda, R.P., Ikonomovic, M.D., Sheffield, R., Rubin, R.T., Wolfe, B.B., and Armstrong, D.M. (1995). Reduction of AMPA-selective glutamate receptor subunits in the entorhinal cortex of patients with Alzheimer's disease pathology: a biochemical study. *Brain Research*, *678*, 161–167.

Yi, F., Danko, T., Botelho, S.C., Patzke, C., Pak, C., Wernig, M., and Südhof, T.C. (2016). Autism-associated SHANK3 haploinsufficiency causes Ih channelopathy in human neurons. *Science*, *352*, aaf2669.

Yokota, Y., Ring, C., Cheung, R., Pevny, L., and Anton, E.S. (2007). Nap1-Regulated Neuronal Cytoskeletal Dynamics Is Essential for the Final Differentiation of Neurons in Cerebral Cortex. *Neuron*, *54*, 429–445.

Yoo, H. (2015). Genetics of Autism Spectrum Disorder: Current Status and Possible Clinical Applications. *Experimental Neurobiology*, *24*, 257–272.

Young, J.I., and Zoghbi, H.Y. (2004a). X-Chromosome Inactivation Patterns Are Unbalanced and Affect the Phenotypic Outcome in a Mouse Model of Rett Syndrome. *American Journal of Human Genetics*, *74*, 511–520.

Young, J.I., and Zoghbi, H.Y. (2004b). X-Chromosome Inactivation Patterns Are Unbalanced and Affect the Phenotypic Outcome in a Mouse Model of Rett Syndrome. *The American Journal of Human Genetics*, *74*, 511–520.

Yu, W., and Lu, B. (2012). Synapses and dendritic spines as pathogenic targets in Alzheimer's disease. *Neural Plasticity*, *2012*.

Yu, T.W., Chahrour, M.H., Coulter, M.E., Jiralerspong, S., Okamura-Ikeda, K., Ataman, B., Schmitz-Abe, K., Harmin, D.A., Adli, M., Malik, A.N., et al. (2013). Using Whole-Exome Sequencing to Identify Inherited Causes of Autism. *Neuron*, *77*, 259–273.

Zafeiriou, D.I., Ververi, A., and Vargiami, E. (2007). Childhood autism and associated comorbidities. *Brain and Development*, *29*, 257–272.

Zhabotinsky, A.M., Camp, R.N., Epstein, I.R., and Lisman, J.E. (2006). Role of the neurogranin concentrated in spines in the induction of long-term potentiation. *Journal of Neuroscience*, *26*, 7337–7347.

Zhang, A., Li, J., Zhang, Y., Jin, X., and Ma, J. (2019a). Epilepsy and Autism Spectrum Disorder: An Epidemiological Study in Shanghai, China. *Frontiers in Psychiatry*, *10*, 658.

Zhang, B., Li, Y., Liu, J.-W., Liu, X.-W., Wen, W., Cui, Y., and Huang, S.-M. (2019b). Postsynaptic GluR2 Involved in Amelioration of Ab-Induced Memory Dysfunction by KAIXIN-San Through Rescuing Hippocampal LTP in Mice. *Rejuvenation Research*, *22*.

Zhang, D., Hou, Q., Wang, M., Lin, A., Jarzylo, L., Navis, A., Raissi, A., Liu, F., and Man, H.Y. (2009). Na, K-ATPase activity regulates AMPA receptor turnover through proteasome-mediated proteolysis. *Journal of Neuroscience*, *29*, 4498–4511.

Zhang, J., Yin, Y., Ji, Z., Cai, Z., Zhao, B., Li, J., Tan, M., and Guo, G. (2017). Endophilin2 Interacts with GluA1 to Mediate AMPA Receptor Endocytosis Induced by Oligomeric Amyloid- β. *Neural Plasticity*, *2017*.

Zhang, S., Zhu, Y., Cheng, J., and Tao, J. (2019c). Ion Channels in Epilepsy: Blasting Fuse for Neuronal Hyperexcitability. In Epilepsy - Advances in Diagnosis and Therapy, (IntechOpen), p.

Zhang, X., Li, Y., Ma, L., Zhang, G., Liu, M., Wang, C., Zheng, Y., and Li, R. (2020a). A new sex-specific underlying mechanism for female schizophrenia: accelerated skewed X chromosome inactivation. *Biology of Sex Differences*, *11*, 1–11.

Zhang, Y., Kurup, P., Xu, J., Anderson, G.M., Greengard, P., Nairn, A.C., and Lombroso, P.J. (2011). Reduced levels of the tyrosine phosphatase STEP block beta amyloid-mediated GluA1/GluA2 receptor internalization. *Journal of Neurochemistry*, *119*, 664–672.

Zhang, Y., Guo, O., Huo, Y., Wang, G., and Man, H.-Y. (2018). Amyloid-B Induces AMPA Receptor Ubiquitination and Degradation in Primary Neurons and Human Brians of Alzheimer's Disease. *Journal of Alzheimer's Disease*, *62*, 1789–1801.

Zhang, Y., Li, N., Li, C., Zhang, Z., Teng, H., Wang, Y., Zhao, T., Shi, L., Zhang, K., Xia, K., et al. (2020b). Genetic evidence of gender difference in autism spectrum disorder supports the female-protective effect. *Translational Psychiatry*, *10*, 4.

Zhao, L.-X., Chen, M.-W., Qian, Y., Yang, Q.-H., Ge, Y.-H., Chen, H.-Z., and Qiu, Y. (2019). M1 Muscarinic Receptor Activation Rescues β-Amyloid-Induced Cognitive Impairment through AMPA Receptor GluA1 Subunit. *Neuroscience*, *408*, 239–247.

Zhao, M.G., Toyoda, H., Ko, S.W., Ding, H.K., Wu, L.J., and Zhuo, M. (2005). Deficits in trace fear memory and long-term potentiation in a mouse model for fragile X syndrome. *Journal of Neuroscience*, *25*, 7385–7392.

Zhao, W.-Q., Santini, F., Breese, R., Ross, D., Zhang, X.D., Stone, D.J., Ferrer, M., Townsend, M., Wolfe, A.L., Seager, M.A., et al. (2010). Inhibition of calcineurin-mediated endocytosis and alpha-amino-3-hydroxy-5-methyl-4-isoxazolepropionic acid (AMPA) receptors prevents amyloid beta oligomer-induced synaptic disruption. *The Journal of Biological Chemistry*, *285*, 7619–7632.

Zhong, L., and Gerges, N.Z. (2010). Neurogranin and synaptic plasticity balance. *Communicative & Integrative Biology*, *3*, 340–342.

Zhou, Y., Kaiser, T., Monteiro, P., Zhang, X., Van der Goes, M.S., Wang, D., Barak, B., Zeng, M., Li, C., Lu, C., et al. (2016). Mice with Shank3 Mutations Associated with ASD and Schizophrenia Display Both Shared and Distinct Defects. *Neuron*, *89*, 147–162.

Zhu, J., and Tsai, N.P. (2020). Ubiquitination and E3 Ubiquitin Ligases in Rare Neurological Diseases with Comorbid Epilepsy. *Neuroscience*, *428*, 90–99.

Zhu, X., Li, M., Pan, H., Bao, X., Zhang, J., and Wu, X. (2010). Analysis of the parental origin of de novo MECP2 mutations and X chromosome inactivation in 24 sporadic patients with Rett syndrome in china. *Journal of Child Neurology*, *25*, 842–848.

Ziats, M.N., and Rennert, O.M. (2016). The Evolving Diagnostic and Genetic Landscapes of Autism Spectrum Disorder. *Frontiers in Genetics*, *7*, 65.

Zikopoulos, B., Barbas, H., Amaral, D., Schumann, C., Nordahl, C., Bachevalier, J., Loveland, K., Barbas, H., Barbas, H., Barbas, H., et al. (2010). Changes in prefrontal axons may disrupt the network in autism. *The Journal of Neuroscience : The Official Journal of the Society for Neuroscience*, *30*, 14595–14609.

Zipper, R., Baine, S.D., Genizi, J., Maoz, H., Levy, N.S., and Levy, A.P. (2017). Developmental progression of intellectual disability, autism, and epilepsy in a child with an IQSEC2 gene mutation. *Clinical Case Reports*, *5*, 1639–1643.

Ziv, N.E., and Fisher-Lavie, A. (2014). Presynaptic and postsynaptic scaffolds: Dynamics fast and slow. *Neuroscientist*, *20*, 439–452.

Zoghbi, H.Y. (2003). Postnatal Neurodevelopmental Disorders: Meeting at the Synapse? *Science*, *302*, 826–830.

Zoghbi, H.Y., and Bear, M.F. (2012). Synaptic dysfunction in neurodevelopmental disorders associated with autism and intellectual disabilities. *Cold Spring Harbor Perspectives in Biology*, *4*.

Zweier, C., Kraus, C., Brueton, L., Cole, T., Degenhardt, F., Engels, H., Gillessen-Kaesbach, G., Graul-Neumann, L., Horn, D., Hoyer, J., et al. (2013). A new face of Borjeson-Forssman-Lehmann syndrome? De novo mutations in PHF6 in seven females with a distinct phenotype. *Journal of Medical Genetics*, *50*, 838–847.

CURICULUM VITAE

